The Role of MAP Kinase Cascade in Neonatal Brain Response to Hypoxia-Ischemic Insult

Laura Jacqueline Thei
University College London

A thesis submitted for the degree of
Doctor of Philosophy (Neuroscience)
to University College London
2014

DECLARATION

I, Laura Thei, confirm that the work presented in this thesis is my own. Where information has been derived from other sources, I confirm that this has been indicated in the thesis.

Signed: Date:

Word Count: **67,372**

Abstract

Babies that are born more than 8 weeks premature or those deprived of oxygen during the perinatal period are susceptible to brain injury, particularly in conjunction with maternal or fetal infection, leading to neurological deficits later in life. Multiple studies have shown that even brief exposure to hypoxic conditions will cause rapid and selective increase in specific mitogen-activated protein kinases including extracellular signal-related kinase 1 and 2 (ERK1/2) and C-Jun N-terminus Kinases 1 to 3 (JNK1-3) as well as the JNK downstream effector: C-Jun.

To gain insight into the *in vivo* function of some of these intracellular pathways that contribute to neuronal damage in ischemic postnatal brains, we examined the effects of global or cell type specific as single or combined deletions of ERK 1 and 2 and both cell type specific or functional deletions of C-Jun. In addition, ERK phosphorylation was prevented by the administration of the selective MEK inhibitor SL327. This was observed with both pre- and post -injury application. Lastly, to explore the effect of endotoxin as a sensitising agent prior to neonatal hypoxia ischemia: lipopolysaccharide given to neonatal mutant mice, with sensitising effects noted at a dosage of 0.6mg/kg of LPS and a time interval between endotoxin administration and hypoxia-ischemia of 12hr. The Rice-Vannucci mouse model is a well-established experimental paradigm for hypoxic ischemic injury, providing insights into molecular signals that determine both white and grey matter tissue loss.

Normal pERK is detectable in periventricular white matter axons (15-45min post HI), followed by white and grey matter glia and cortical neurons (1-4h post HI), returning to normal by 8hr. Mice with double mutation of global ERK1 and neuronal ERK2 deletion showed a lack of pERK expression through the forebrain following HI. In LPS-sensitised HI, we observed a strong decrease in infarct size, histological brain injury and microglial activation in cortex, striatum, and thalamus. A more discreet effect was seen in subcortical white matter and hippocampus. ERK1 deletion attenuated the effect of neuronal ERK2 deletion. These results were reproduced following severe HI insult alone. Astrocytic ERK

mutation exhibited a polar response with a 3-4fold increase in microglia activation and the number of dying cells within grey matter regions.

Global inactivation of ERK, through pharmacological ERK inhibitor SL327 significantly reduced cell death, and associated microglial activation in both grey and white matter at 48h following HI insult. Application of SL327 even as late as 1hr post insult significantly reduced brain damage induced by mild HI exposure. Systemic administration 1hr after severe HI dramatically increased the survival rate of pups at 48hr post insult by 80% compared to sham-treated controls.

Deletion of C-Jun in all neural-epithelial lineage cells resulted in a strong increase in injury following severe and LPS-sensitised insult. In contrast, neuron-specific deletion of C-Jun resulted in neuroprotection. Tunel positive cell death was significantly reduced compared to control groups, in white matter, cortex and thalamus. Microglial activation, and infarct volume loss was more discreetly decreased with a notable effect in cortex. C-Jun expression in astrocytes is not a major contributor to ischemic damage response, with very mild reduction in markers for cell death and microglia recruitment following severe hypoxia, and no change observed between mutants and controls after endotoxin-sensitised HI.

Replacement of the four JNK-dependent C-Jun phosphorylation sites (jun4A) resulted in a mild decrease in cell death and microglial activation compared to littermate controls, which did not reach the level of statistical significance.

Overall, the data points to an important role of neuronal ERK and C-Jun in both a cellular and biochemical response to HI in the neonatal cerebral brain, but also argues against the involvement of JNK-dependent C-Jun phosphorylation in mediating neural damage. In addition, inhibition of ERK via pharmaceutical agents shows promise in decreasing morbidity and mortality caused by mild to moderate HI exposure. Lastly, neuroepithelial C-Jun expression appears to be a critical factor in normal cortical development and employment of endogenous neuroprotective mechanisms against postnatal insult.

Acknowledgements

First, I would like to thank Professor Gennadij Raivich, for giving me the opportunity to do my PhD in his laboratory. I am grateful to him for his guidance, patience and supervision and for teaching me how to critically evaluate research, an invaluable skill for a scientist. I am equally indebted to my supervisors, Professor Donald Peebles and Dr Mariya Hristova, where without their advice and support this project could not have come to completion. Particularly I would like to thank Dr Mariya Hristova for constantly being there as a mentor, a teacher and a friend despite her own busy schedule. From teaching me how to perform surgeries to labelling thousands of slides for days on end, you have always been there to offer a hand and sage advice and at times- a coffee and cake and shoulder to cry on. Thank you.

To the most fantastic fellow PhD students – Alejandro Acosta-Saltos, Carolina Acosta-Saltos, Eridan Rocha Ferreira, and Smriti Patodia – thank you for the best of company whether at 6am or 10 at night we have had the best of times and have always helped each other smile and laugh. Thank you for scientific discussions, and moral support when presenting work and applying for scholarships. I am grateful for your positivity, willingness to help, and friendship. I look forward to seeing the church of celebrations continue beyond our office.

I would like to thank the many BSc and MSc students that I have been privileged to supervise and see grow as scientists. Lidia Bartoszewicz, Naomi Gostelow, Megan Galloway, Afiqah Latip, Matilde Picard, Matilde Kerling, Kian Sabsevari and Despina Peyioti – Thank you for your contribution in various experiments and for bringing out the teaching skills in me.

I would also like to thank Dr Nick Tuner for his advice and help in formatting and the gift of Endnote, Gary Landreth for the ERK2-flox mice, and Axel Behrens for the C-Jun floxed, Jun4A, and Syn: Cre mice. To my graduate tutors Siobhan Sengupta and Suzy Buckley for their academic advice and guidance; to Angela Poulter, Nadine Mogford and Christina Alfors for all the administrative support; to Nick Davies, Richard Pugh, Nicole, Claire, Angie and the girls in the animal house for taking good care of our mice. Lastly, to SPARKS and to Wellcome

Trust for funding my research, as well as to the Jean Ginsburg Memorial Foundation scholarship for funding the last stage of my PhD.

To my wonderful family and friends – thank you for your love, laughter, moral support, patience and many boxes of tissues and chocolate over the years. Thank you to my parents, John and Sandra Thei and my sisters Ruth and Judith- I cannot express my eternal gratitude to you! I am where I am today only because of your unconditional love, sacrifice and encouragement. Whilst we have not prevented all the storms, we have at least learnt to dance in the puddles together. I am so lucky and proud to have you as my family, and I hope I have made you equally proud. To my Booba Dina, whose own worth she will never see. I have learnt so much about how to be mensch, and to fight for what I believe to be right from you. To work hard and acknowledge the achievements that comes from this. Your love for your family, for your friends and for living your life is an inspiration to us all.

Finally, to my wonderful partner (in crime), my better half, my best friend, Ed Gray - Your love and support has been a rock over the last five years. I am both fortunate and honoured to have you in my life, and I could not have done this without you.

Thank you all.

Table of Contents

Index of Figures

Index of Tables

Index of Abbreviations

AACP- American academy for cerebral palsy

ADC- apparent diffusion coefficient

AEEG- amplitude electroencephalography

AMPA- α-Amino-3-hydroxy-5-methyl-4-isoxazolepropionic acid

AP-1- activation protein 1

APAF-1- apoptotic protease activating factor 1

ATP- adenosine 5-triphosphate

BBB- blood brain barrier

BNPP- basal nuclei predominant pattern

BW- birth weight

COX2- cyclooxygenase 2

CP- cerebral palsy

CROC- carotid artery occlusion

CTC- cytochrome C

DAMP- damage-associated molecule pattern

DUSP- dual specificity MAPK phosphatases

DWI- diffusion weighted images

EEG- electroencephalography

EGF- epidermal growth factor

EPO- erythropoietin

ERK- extracellular signal-related kinase

FR- free radicals

GA- gestational age

G-CSF- granulocyte colony-stimulating factor

GFAP- glial fibrillary acidic protein

GM- grey matter

GMFCS- gross motor function classification system

HI- hypoxia ischemia

HIE- hypoxia ischemia encephalopathy

HIF- hypoxia-inducible factor

ICAM-1- intercellular adhesion molecule 1

IEG- immediate early gene

IL- interleukin

IP- intraperitoneal

JIP- JNK-interacting protein

JNK- C-Jun N-terminus kinase

KO- knocked out

LPS- lipopolysaccharide

MAPK- mitogen-activated protein kinase

MHC- major histocompatibility complex

MRI- magnetic resonance imaging

MRS- magnetic resonance spectroscopy

MSC- mesenchymal stem cells

NAA- N-acetytlaspartate

NAC- N-acetylcysteine

NF-κB- nuclear factor kappa-light-chain-enhancer of B cells

NHE- N^+/K^+ exchanger

NICHD- national institute of child's health and human development

NMDA- N-Methyl-D-aspartic acid

NO- nitric oxide

NOS- nitric oxide synthase

ODC- oligodendrocyte

OS- oxidative stress

P7- postnatal day 7

PAMP- pathogen-associated molecular pattern

PARP- Poly (ADP-ribose) polymerase

PERK- phosphorylated ERK

PLoIC- Periventricular leukomalacia

PRR- pattern recognition receptor

PVL- Periventricular leukomalacia

RIP1- receptor-interacting protein 1

ROCK1- Rho-associated kinase 1

ROS- reactive oxygen species

SAPK- stress activated protein kinase

SOD- superoxide dismutase

TGFβ- transforming growth factor β

TLR- toll-like receptor

TNF- tumour necrosis factor

TOR- target of rapamycin

TRIF- TIR-domain containing adapter inducing interferon β

VEGF- vascular endothelial growth factor

WM- white matter

WSPP- watershed predominant pattern.

Introduction

Cerebral hypoxia ischemia (HI) is one of the leading causes of neurological deficits in neonates. Hypoxic/Ischemic complications during the perinatal period, 24th week pregnancy to 4 weeks following birth, occur in 1 in every 500 births worldwide. The consequences of HI in the neonatal brain are highly debilitating behavioural and neurological disorders (Dixon et al., 2002; Lindstrom et al., 2008). The most common of which is cerebral palsy. Other associated conditions include impairment of speech, hearing, vision and memory. Long term effects can include epilepsy, learning difficulties, altered behavioural and emotional problems, for example: hyperactivity and anxiety issues (Marlow et al., 2005). Persistent and severe HI eventually leads to death (Vannucci, 1990; Vannucci and Hagberg, 2004) .

Impaired cerebral blood flow is a major source of HI in the perinatal brain. The causes of which are many, including: placental insufficiency; umbilical cord disruption; birth asphyxia; amniotic infection; and uterine rupture (Higgins and Shankaran, 2009; Vincer et al., 2006). The immature brain is especially vulnerable to HI; the subcortical white matter (WM) is still unmyelinated and predominantly populated with oligodendrocyte precursor cells that are highly susceptible to exogenous free radicals due to a lack of antioxidants, high concentrations of unbound iron and insufficient scavenging mechanisms (Ferriero et al., 1996; Volpe, 2001). Pattern of damage seen is dependent on the type of trauma, its duration, the neonates' age and other aforementioned factors. The exact mechanisms that give rise to hypoxia/ ischemia are incredibly complex and highly variable between individuals.

Autoregulation of cerebral blood flow and pressure in neonates and infants is easily compromised as the dynamic range of blood pressure is much narrower than that in the adult (10-20mmHg compared to 40mmHg) (Greisen, 2005; Panerai et al., 1995). It is hypothesised that hypoxia causes a reflexive increase in systemic blood pressure resulting in cerebral blood pressure being beyond its normal range (Niijima et al., 1988; Vannucci, 1990). This results in injury along vascular watershed zones between anterior and middle cerebral arteries, and between posterior and middle

cerebral arteries. Lesions formed from ischemia affect white matter and cortex regions of the forebrain. When a more acute insult occurs, infarction occurs in the central grey nuclei, cortex around the central sulcus and the hippocampus.

After which, the foetus is initially more able to adapt by redistributing cardiac output, decreasing brain metabolism and utilising various energy substrates in addition to glucose, including ketone bodies, lactate, pyruvate, glutamate, and glutamine. Ketone bodies converts acetyl coA into long chain fatty acids that cannot otherwise pass the BBB (Prins, 2007). Alternatively, neurons can efficiently use lactate as an energy substrate with a preference for lactate over glucose when both substrates are present. This way, cerebral tissue can acquire vital nutrients, but only for a finite time (de Vries and Jongmans, 2010). Once a critical threshold occurs, cellular mechanisms fail, ending in two phases of damage: primary energy failure, followed by secondary neuronal cell death.

Primary energy failure ensues when cells can no longer sustain activity due to reduced nutrient and adenosine 5-triphosphate (ATP) supply. This leads to multiple failures of cell regulation, causing cell depolarisation, cation influx and cell lysis. The use of high energy phosphate reserves results in anaerobic respiration which, if allowed to continue, gives rise to an increase in lactic acid causing pH fluctuation and the formation of free radicals leading to oxidative stress (Higgins and Shankaran, 2009; Vannucci and Hagberg, 2004). The loss of cellular homeostasis results in cell death, either directly (necrosis) or via apoptotic signalling that will reduce damage to surrounding cells. Key elements of apoptosis include caspase3, caspase12 and Bax (Zhu et al., 2005), all of which are up-regulated in immature cerebral tissue compared to adult, leaving the perinatal brain more susceptible to neuronal death (Yager et al., 1992).

After initial insult, reperfusion gives a transient restoration of energy resources (Gilland et al., 1998) before secondary cell injury occurs (Blumberg et al., 1997). Whether reperfusion leads to resolution of ischemia,

and restoration of homeostasis, or whether secondary neuronal injury occurs is dependent on the duration and severity of primary energy failure.

Secondary neuronal cell death is the outcome of multiple molecular imbalances, instigated by excitotoxicity, oxidative stress and mitochondrial failure (Budd, 1998; Mori et al., 2004). A breakdown in astroglia glutamate uptake in addition to an increase of glutamate release into the synaptic cleft leads to a disruption of the finely tuned balance of transmitter concentration. This results in an accumulation of α-Amino-3-hydroxy-5-methyl-4-isoxazolepropionic acid (AMPA), an analogue of glutamate, especially at the N-Methyl-D-aspartic acid (NMDA) receptor. Activation of NMDA receptors lead to an influx of Ca^{2+} into the cell to abnormally high levels. This, exacerbated by internal Ca^{2+} release, becomes toxic instigating up-regulation of lipases, proteases and endonucleases. Oxidative stress is due to an increase in free radicals formed by the activation of enzymes such as cyclooxygenase, xanthine oxidase and lipooxidase. Furthermore Ca^{2+} activation of neuronal nitric oxide synthase (NOS) leads to a toxic level of nitric oxide and the free radicals: O^{-}, OH^{-}, OHOO (Ferriero et al., 1996). As cells undergo oxidative stress, so this reflects on their mitochondria. Mitochondria, under continuous ROS release, lose outer membrane stability. Neuronal loss by HI is regulated by different mechanisms, and can be a direct result of the stress or of the compensatory mechanisms. This is beneficial while the compensatory mechanisms themselves are tightly regulated, or pathological, when the control of protective mechanisms is lost.

The mitogen activated protein kinases (MAPK) are a complex group of serine-threonine kinases, serving as secondary messenger systems required to transfer extracellular signals from the cell surface throughout the cell to the nucleus (Lu and Xu, 2006). Upregulation of all four subfamilies of the MAPK cascade are observed in the cerebral cortex under hypoxic ischemic conditions. Following HI, multiple stimuli of MAPK are released including growth factors, cytokines, glutamate and FR. Indirect activation and phosphorylation can occur due to ischemic loss of cell integrity and dysfunction (Ho et al., 2008; Irving and Bamford, 2002; Jin et al., 2002).

Whether the activation of these pathways is due to cell loss or whether they actually regulate the mechanism underlying HI insult remains unclear.

This introductory chapter aims to provide a background of the recognition and clinical management of infants subject to hypoxic-ischemic insult during the perinatal period. It will also explore the pathology and cellular responses of the injured brain. Lastly, there is conflicting evidence of whether the MAPK family members ERK and JNK play a regulatory role in the brains response to HI. This review will highlight current theories as to their pro-survival and pro-death function in the ischemic brain.

Perinatal Brain Injury

Prevalence of perinatal encephalopathy

In developed countries, cerebral hypoxic ischemic (HI) insult affects 1-6 per 1000 live births as a result of peripartum asphyxia (Robertson et al., 2007; Vannucci and Vannucci, 1997). In developing countries, the chance of incidence is 10 fold higher. 10-60% of affected infants will die within the newborn period. Those suffering mild encephalopathy, the rate of mortality is 2%, increasing to 19% with moderate insult and 63% with severe. Of the global 4million neonatal deaths per year, nearly a quarter are due to birth asphyxia. For patients that survive, 25% go on to have permanent neurological defects including motor, sensory and cognitive impairments.

HI is still one the major causes of neurodevelopmental disorders at term. The foremost sequela of perinatal asphyxia is hypoxia ischemia encephalopathy (HIE). Moderate HIE will result in a 10% risk of death, 30% risk of disability with an increased chance of cognitive impairment (Robertson et al., 2007; Vannucci, 1990; Vannucci and Vannucci, 1997; Vannucci and Hagberg, 2004). HI is a major factor of cerebral palsy, responsible for 3-25% of all cases (Colver et al., 2000). Of these, 80% are considered dyskinetic (Paneth, 2008). A population based study in Sweden showed 0.7% of all infants born in 1985 had neonatal encephalopathy. Forty-three individuals were identified with moderate injury on an Apgar score less than seven. Wechsler Intelligence Scale for Children (3rd edition) was performed at adolescence (15-19 years) to determine long-term neurological outcomes. In the moderate group, 30% had developed cerebral palsy. Of the remaining 70%, 71% had definite cognitive dysfunction and 18% had a hearing impairment. Only 8% remained unaffected (Lindström et al., 2006).

The severity of outcome is dependent on a dose response of worsening HI insult and a maturation dependent susceptibility of the developing brain. Other factors such as a gestational age <30 weeks, birth weight <2100g and clinical risk factors such as pre-eclampsia and infection also contribute to an increased risk of mortality and morbidity (Peebles and Wyatt, 2002; Pharoah et al., 1998;

Wu et al., 2004). Lastly, there is a broad suggestion that gender may also play a role with males affected more than females (Skiöld et al., 2014; Streja et al., 2013).

Studies such as these indicate that intrapartum hypoxia ischemia gives rise to significant encephalopathy, which in turn has long-term impact on neuro-developmental repercussions.

Susceptibility of the Neonatal Brain

The brain has a greater pre-disposition to oxidative stress (OS) in the perinatal period compared to the mature adult brain. OS occurs at birth because of the hyperoxic challenge that occurs at the transition from intrauterine to extrauterine life. During normal labour, the fetus has metabolic and haemodynamic compensatory mechanisms with which to counter oxygen demand. Some OS is required for normal embryonic and fetal growth, where it is implicated in follicular development, ovulation, embryogenesis and placental differentiation (Peebles and Hanson, 2002). Paradoxically OS is also a major contributor to pregnancy related disorders including miscarriage, pre-eclampsia, fetal growth restriction and pre-term labour (Blair and Stanley, 1993; Greenwood et al., 2005).

Oxidative stress occurs when the production of free radicals (FR) exceed the capability of antioxidant defences (Volpe, 2001). Sources of FRs included inflammation, hyperoxia, hypoxia, and ischemia, all resulting in reperfusion of the cerebral cortex, neutrophil and macrophage activation, increased excitotoxic glutamate, and the release of unbound iron (Fe^{2+}) a FR in its own right, reactive oxygen species (ROS), nitric oxide (NO) and nitric oxide synthase (NOS) which mediate redox signals (Dugan and Choi, 1994; Kaur and Ling, 2009; Perrone et al., 2013; Vexler and Ferriero, 2001).

The newborn, particularly pre-term, brain has a greatly reduced number of anti-oxidant defences due to insufficient levels of superoxide dismutase (SOD), catalase, glutathione peroxidase and an insufficient scavenging system to mop up FRs and Fe^{3+} ions leaving greater concentrations of both (Noshita et al., 2002). In addition, there is evidence to suggest a greater number of

glutaminergic synapses (Lesuisse and Martin, 2002). Because of these two factors, the developing brain is highly receptive to excitotoxicity. The consequences of which are an increase in FRs, hyper-perfusion of cerebral vascular beds and eventually depletion of ATP leading to primary energy failure and cell death (Dugan and Choi, 1994). ATP diminution results in damage to multiple cellular components including proteins, lipids, polysaccharides, DNA (through fragmentation, apoptosis, strand breaks and base modulation) and organelles- particularly mitochondria but also cell membrane and Golgi apparatus (Northington et al., 2011; Thornton et al., 2012). In the developing brain, the cerebral metabolic rates of glucose, oxygen and ATP are much higher than the mature brain (Peebles and Hanson, 2002). Cell consumption is regulated by modifications to the mitochondrion structure, its functional activity, the number of mitochondria per cell, its release of proteins and respiratory enzymes, and matrix density (Deng, 2010; Johnston et al., 2001). Normally, ATP production is equivalent to its utilisation. An interruption to ATP generation leads to long lasting and irreversible damage.

Cerebral blood flow is also higher in the neonatal brain. An increase in oxygen demand caused by hypoxia leads to greater cardiac output to the brain, heart and adrenal glands, regulated by the sympathetic adrenergic nervous system. When demand exceeds output capacity, a reduction in blood gas exchange can transpire- exacerbating hypoxia and subsequent hypercapnia (Bax and Nelson, 1993; Vannucci et al., 2001). This leads to cerebral hypo-perfusion and decreased high energy phosphate metabolism, instigating a cellular and molecular response cascade concluding in neural cell death (Gunn et al., 1992; Niijima et al., 1988).

During fetal development, the cerebral white matter (WM) remains relatively unmyelinated due to the myelin-producing cells: oligodendrocytes (ODC) being in their immature precursor form. ODC precursors are particularly sensitive to FR induced cell death (Cowan et al., 2003; Liu et al., 2002; Volpe, 2001). In addition, FRs can attach to myelin sheaths resulting in lipid peroxidation, where lipid peroxide is a FR. Furthermore, the cerebral WM contains high concentrations of unsaturated fatty acids, constituting the cells lipid membranes.

These, as with myelin, are highly vulnerable to FR toxicity, resulting in a greater risk of WM damage (Dewar et al., 2003; Kaur and Ling, 2009).

Lastly, when injury accompanies systemic inflammation, the neonatal brain becomes hypersensitive to HI, contributing to sustained CNS inflammation. Bacterial invasion of the chorio-decidual space leads to the production of endotoxins and cytokines by the deciduous and fetal membranes. These excitotoxic cytokines include interleukin (IL) -1α, IL-1β, IL-8, tumour necrosis factor α (TNFα), and granulocyte colony-stimulating factor (G-CSF) (Chock and Giffard, 2005; Dugan and Choi, 1994; Gehrmann et al., 1995; Sadeghi et al., 2007). Cytokine release results in the synthesis of prostaglandins which in turn stimulates uterine contraction, cervical softening and eventual rupture of the chorioamniotic membranes- potentiating labour (Goldenberg et al., 2000).

Causes of injury

Identifying risk factors of neonatal brain injury remains a considerable challenge due to the variable response between one infant and another to the same insult. It is essential that we are able to recognise potential risk newborns to predict accurately the long-term outcomes as well as apply and evaluate emerging therapeutic strategies to reduce damage. An example is the use of systemic or selective cerebral hypothermia.

Whilst epidemiologically, hypoxia is responsible for only a small proportion of infant neuronal disabilities, it remains the single most important cause of perinatal brain injury. The aetiology of neonatal encephalopathy can be identified into three causal groups: maternal and idiopathic congenital; perinatal; and postnatal (Baxter et al., 2004).

Antenatal origins of HI are vast, and include existing maternal disease, pre-eclampsia, premature placental rupture, bleeding at >20 weeks, gestational or pre-existing diabetes, maternal substance abuse, induced conception, raised α-fetoprotein, and intrauterine growth restriction (Vincer et al., 2006). 48% of UK cerebral palsy cased showed at least one of these impediments (Gaffney et al., 1994). In HI induced neonatal encephalopathy, antenatal factors account for the majority of causes whilst intrapartum factors, such as labour and delivery

trauma, make up the minority. Postnatal factors are due to complications such as post-birth trauma, infection prolonged seizures and inborn metabolic errors.

When HI is severe enough to induce damage, it is often hand in hand with other organ malfunction, predominantly the heart, liver and kidneys. This pattern of multi-organ failure occurs in cases of cerebral dysgenesis, metabolic disorders, fetal bradycardia, fetal stroke and maternal hypertension, all of which can result in perinatal encephalopathy (Heinz and Provenzale, 2009; Lindstrom et al., 2008).

Other than HI, the next major perinatal risk factor for pre-term labour and subsequent encephalopathy is feto/maternal inflammatory response (Aziz et al., 2008; Goldenberg et al., 2000; Hagberg et al., 2012). Antenatal infection plays a sensitising role of the fetus to HI induced brain injury. A maternal intrapartum fever of >38°C persisting for longer than an hour is a clinical indicator of chorioamnionitis (Costeloe et al., 2000). Infection sensitises HI by increasing the permeability of the blood brain barrier (BBB), leaving the neonatal brain more vulnerable to secondary insult (Impey et al., 2001). There is surprisingly little correlation between clinical and histological chorioamnionitis, however perinatal infection strongly ties into later brain injury. Markers of inflammation in women at pre-term labour, or in the umbilical cord at term, were associated with the development of periventricular leukomalacia and cerebral palsy (Duggan et al., 2001; Varner and Esplin, 2005; Yoon et al., 1996).

Patterns of cerebral brain damage

Advances in MR imaging have led to the detection of two major patterns of brain damage resulting from neonatal HI. The first is watershed predominant pattern (WSPP) usually due to prolonged partial asphyxia. WSPP involves the cerebral white matter (WM) that lies along the vascular watershed zones between the anterior and cerebral arteries, and between the posterior and middle cerebral arteries. If HI is severe enough, this damage extends into the cortical grey matter. The second pattern observed is the basal nuclei predominant pattern (BNPP), caused by acute profound asphyxia. BNPP affects the deep grey nuclei, the rolandic cortex and hippocampus (Francisco and Linda, 2005). The emergence of these patterns, as well as the selectivity of

specific regions affected, are predictive of distinct neurodevelopmental outcome. WSPP leads to a predominantly cognitive dysfunction with minimal motor impairment, although this is not immediately detectable. Indeed a delay of >2yrs can be applicable. Both cognitive and motor defects associate with BNPP, evident within the first 12months of life (Cowan et al., 2003; Vries and Groenendaal, 2010).

Watershed predominant pattern

Rudolph Virchow, using post mortem specimens, first described WM damage in 1867. He observed the presence of macroscopic pale soft areas of degeneration in the periventricular region. This he termed as congenital encephalomytis. Periventricular leukomalacia (PVL) was not coined until as late as 1962. Similarly, from post mortem studies, microscopic lesions of necrosis were seen in the subcallosal white matter, superior fronto-occipital and superior longitudinal fascule, and in the external and internal sagittal strata of both the temporal and the occipital horns of the lateral ventricle. These lesions were surrounded by areas of liquification and had an increased vascular periphery (Baxter et al., 2004).

Pathology of WM damage is due to a combination of both the incomplete development of vascular supply to the cerebral brain and a maturation-dependent impairment of cerebral blood flow regulation. Autoregulation of cerebral blood flow and pressure in neonates and infants is susceptible to compromise, as the dynamic range of blood pressure is much narrower than that in the adult (10-20mmHg compared to 40mmHg). One hypothesis is that hypoxia causes a reflexive increase in systemic blood pressure resulting in a cerebral blood pressure beyond its normal range. This disrupts the autoregulation of cerebral blood flow, leading to pressure-passive cerebral circulation. This means the cerebral blood flow is set to copy systemic flow, so when systemic pressure falls, so does the cerebral (Greisen, 2005; Panerai et al., 1995). Reduction in blood flow eventually leads to ischemia and subsequent reperfusion of the cerebral vasculature- key factors underlying WSPP. It can also result in apnoea. The foremost outcome from WSPP is focal cystic PVL which gives rise to spastic diplegic cerebral palsy (CP) due to a disruption to the corticospinal tracts within the posterior limb of the internal capsule (PLoIC)

(Volpe, 2001). A more diffuse WM damage is responsible for cognitive and behavioural abnormalities.

WSPP is associated to both a reduction in gestational age and birth weight (Greenwood et al., 2005). Between gestational ages 23-32 weeks, the cerebral WM is especially sensitive to damage due to its pre-myelinated state. WM at this stage in development is largely populated with ODC precursors which, along with neuronal axons, are susceptible to cell death induced by FR formation, cytokines and glutamate excitotoxicity (Kaur and Ling, 2009; Liu et al., 2002). Periventricular leukomalacia in the pre-term occurs due to haemorrhage of the germinal matrix, the zone of cells lining the walls of the lateral ventricles, and not due to ischemia of watershed zones (Huang and Castillo, 2008). Contrary to previous paradigms, WSPP is not solely associated to premature birth. Term and pre-term foetuses will both respond to HI in a qualitatively similar manner. Fetal response to mild-moderate HI is different to term but the overall pattern of cerebrovascular response in severe HI is similar. In pre-term fetus, there is progressive failure of combined ventricular output with a fall in both central and peripheral perfusion, associated with decreased pressure (Gunn and Bennet, 2009). At term blood is prioritised to vital structures such as brainstem, thalami, basal ganglia and hippocampus at the expense of less metabolically active regions such as cortex and white matter. As such watershed zones become hypo perfused. White matter restriction is most pronounced in parasagittal territories (Huang and Castillo, 2008). A 2003 study of 173 term infants, subject to moderate HI, showed a mixture of both WSPP and BNPP by MRI. Interestingly, WSPP was observed in 45% of cases whilst BNPP accounted for just 30% (Cowan et al., 2003). Opinions are emerging that HI at term will result in a mixture or even atypical patterns of damage.

Basal nuclei predominant pattern

Alternatively known as the basal ganglia/thalamus pattern, BNPP is recognisable by three lesion patterns by MRI- differentiated by the severity of HI. With mild insult, lesions transpire in the nucleus lentiformis and the ventro-lateral thalamus only. Intermediate insult will affect these regions, plus the rolandic cortex. Severe HI affects the nucleus lentiformis, the rolandic cortex, complete thalamus and the hippocampus (Johnston et al., 2002; SilVerstein et

al., 1984). Additionally severe case lesions are often atrophic, leading to total brain injury and potentially death.

BNPP pathology is due to neuronal cell death owing to mitochondrial oxidative stress. Even when insult is not enough to instigate immediate cell death, it can promote a neurotoxic cascade, disrupting cellular mechanisms, and changes in intracellular pH (Thornton et al., 2012). These modulations will, in turn, further neuronal loss through necrosis, apoptosis and autophagy mechanisms.

Outcome from BNPP is often poor, resulting in death, developmental impairment, reduced head growth and brain weight, and cerebral palsy (de Vries and Jongmans, 2010; Dixon et al., 2002). The extent of outcome directly correlates with the severity of BNPP; Mild lesion patterns give rise to dyskinetic CP in comparison to intermediate and severe lesion patterns with dyskinetic-spastic CP. The extend of HI and BNPP associates with a number of other clinical manifestations including intensive resuscitation at birth, increased encephalopathy and an increase in severity of seizures (Blair and Stanley, 1993; Dixon et al., 2002).

BNPP is more common at term because of perinatal HI and shock. Neuro-metabolic disorders have no correlation to BNPP, implicating HI as the key underlying factor. Ensuing motor impairment is evident within the first few months of life, and though cognitive development is variable, disorders due to BNPP are observed in the first 30 months (Cowan et al., 2003; Himpens et al., 2008)). These damage patterns underline the need for early detection and diagnosis of injury as a vital process for predicting and preventing detrimental outcome.

Outcome: Hypoxia Ischemia Encephalopathy (HIE)

Birth asphyxia is a condition of impaired blood gas exchange, which if persistent, results in hypoxemia, hypercapnia and hypoxia. The most common outcome of birth asphyxia is hypoxia (a reduction in oxygen content) –ischemia (restriction in blood supply) encephalopathy. Encephalopathy is the consequence of oxidative stress due to an increase in FR, ROS and excitotoxic cytokine formation. These affect multiple cell components leading to deregulation and cell death. There are two notable forms of injury seen after

birth asphyxia: severe total hypoxia- seen, for example, with abrupt placenta, and prolonged partial hypoxia- in cases of extended labour. Both forms give rise to a specific pattern of brain damage, as described later in this study.

In nearly all cases, hypo-perfusion of the fetal circulation accompanies hypoxia (Gunn and Bennet, 2009). Decreased blood flow to the middle cerebral arteries results in periventricular white matter infarction. Modulators of blood flow include cyclooxygenase 2 (COX2) and prostaglandins. COX2 promotes the production of and release of vascular endothelial growth factor (VEGF) which in turn promotes vasculo- and angio-genesis (Streja et al., 2013). However, like both inflammatory cytokines and NO, excessive VEGF will incite the disruption of tight junctions in the BBB, leading to increased permeability and microglia activation (Feng et al., 2008). The BBB has a critical role in communication between the brain and peripheral body. Separation of tight junctions prompts a detachment of endothelial cells from the basement membrane, resulting in endothelial blebbing and necrosis. Reactive microglia release FR that further damage endothelial cells. This damage propagates an inflammatory response via the loss of normal endothelial NO production.

Energy failure after HI may go on to promote further injury via glutamate excitotoxicity. Compared to the adult brain, there are a higher number of glutaminergic synapses in the neonatal brain (Sie et al., 2000). After HI, there is a transient increase in glutamate receptor activation. This activation can go on to depress mitochondrial respiration, inducing cell death (Johnston et al., 2002; Kitagawa, 2012; Perrone et al., 2013). In addition, the neonate has a greatly reduced production of glutathione and glutathione peroxidases. Glutathione is a powerful antioxidant with the dual action of being able to compete with glutamate receptor ligands, preventing excitotoxicity. Excessive glutamate at the synapse prevents the uptake of cysteine, a building block of glutathione, further reducing the antioxidant defences available to the brain (Northington et al., 2011). In an UK study of 90 newborns with a gestational age >32 weeks and varying degrees of HIE, an attenuation of glutathione peroxidase activity was seen within the first 48hr and neuron-specific endolase (a brain damage marker) was seen at 72hr (Zhu et al., 2005). Decrease in glutathione

peroxidase directly correlated with the clinical stage of HIE as well as neurodevelopmental outcome.

Outcome: Cerebral Palsy (CP)

Cerebral palsy is defined as a permanent disorder of voluntary movement or posture due to defects or non-progression lesions within the immature brain (Baxter et al., 2004).This is the most cited definition of CP, coined by Bax in 1964. A more specific definition of CP remains in contention due its variability of form and severity as well as the spacio-temporal influences of insult. That it is a clinical manifestation of multiple and interacting pathologies may explain the apparent complexities to define it shown in scientific literature. CP affects 1 in 400 live births; meaning that globally, 1800 infants are diagnosed. It remains the most common cause of severe physically disability in childhood.

Cerebral palsy, or as it was termed-cerebral paresis, was first described by the English orthopaedic surgeon William Little in 1843 as part of a series of lectures entitled “Deformities of the Human Frame”. Little’s lectures focused on joint contractures ad deformities resulting from long-standing spasticity and paralysis (Little, 1843). Here, Little indicated that the cause was often damage to the brain during infancy. In a second set of lectures in 1862, he expounded this theory to implicate pre-term birth and asphyxia. Initially there was no published work further exploring the mechanism of CP. However in 1920 Winthrop Phelps, pioneered a more modern approach to the physical management of CP. Phelps had four treatment goals: To improve locomotion; to encourage self-help and reliance; to establish coherent speech; and to improve the quality of general appearance. It was not until 1997, when the gross motor function classification system (GMFCS) was introduced in response to the pressing need for a standardised allocation of the severity of movement disability amongst CP patients (Jones et al., 2007; Kavčič and Vodušek, 2005; Panteliadis et al., 2013).

GMFCS remains the principle method to describe motor disability in children with CP. In 2004, an international workshop met, founded by the united cerebral palsy research and educational foundation (USA) and the Castang foundation

(UK) in order to revisit CP classification. This was in light of technologically advances in brain imaging and their correlation to clinical symptoms, and the changing paradigms of the underlying neurobiology of CP. Participants agreed that CP describes “a group of permanent disorders of the development of movement and posture, causing activity limitation, that are attributed to non-progressive disturbances of the fetal or infant brain” (Baxter et al., 2004; Paneth, 2008).

Whilst there is no single given cause of CP, two risk factors are implicated in its incidence: Gestational age (GA) and birth weight (BW). Greenwood, in 2005 found that 15% of CP cases were born between 33 weeks and 36 weeks and that 54% were born at 37 weeks or more. When added to population data it was extrapolated that CP occurs in 42 in 1000 live births at 32 weeks GA, 6 in 1000 between 33 weeks and 36 weeks GA, and 1 in 1000 at 37 weeks or more. Infection and hypoxia were shown as markers that correlated with an increased risk in CP, both at pre-term and term, antenatal complications such as pre-eclampsia only increased the risk of CP in term infants (Greenwood et al., 2005).

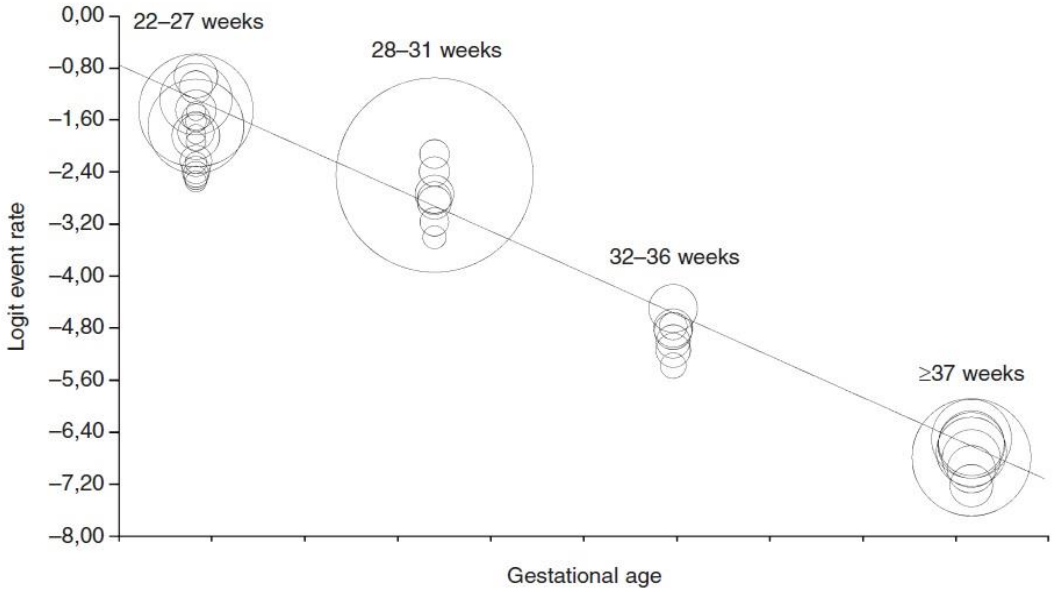

Figure 1.1 Regression of gestational age measured on a Logit event rate. Reproduced with permission (E. Himpens et al. 2008).

A 2008 meta-analysis looked to determine a relationship between GA and the prevalence, type and severity of CP. The review included 28 studies between 1985 and 2005. They affirmed that an incidence of CP significantly reduces with

an increase in GA. In extreme pre-term (GA <28 weeks), 14.6% infants were positively diagnosed. In severe pre-term (GA between 28- 32 weeks) this was 6.4%, moderate pre-term (GA between 32- 36 weeks) – 0.4- 0.7%, and at term (GA> 36 weeks) – 0.1%. This is illustrated in figure 1.1. The occurrence of CP only began to decrease after 27 weeks until term (Himpens et al., 2008).

Other research groups have focused on birth weight (BW) as a deciding factor in both incidence and severity of CP. Pharaoh et al. used a cohort of CP registers covering Scotland and six England counties between 1984 and1989. When apportioned by BW, a significant increase in CP cases were observed in patients with a BW <1000g, at 7.8% compared to 0.1% with a BW <2500g (Pharoah et al., 1998). Colver et al. in 2000 found a complimentary trend looking at a northeast England cohort over a 30 year period (1964- 1993). They found that newborns with a BW ≥2500g had neither an increased risk of CP nor severity whereas a BW ≤2500g gave a higher prevalence of CP and increased severity (Colver et al., 2000).

These studies show that both GA and BW contribute to an increased chance of developing CP, but these patients are a highly heterogeneous group and so not easily defined.

Outcome: Long term cognitive impairments

This thesis has already established that of the surviving infants from HI insult, 25% go on to acquire prominent neurodevelopmental disorders. Between 3-25% are functionally diagnosed with CP, and cognitive impairments are common, both alone and in combination to CP. Those infants who suffer mild HI have, in general, a good prognosis for outcome, whereas, moderate and severe insult proves more heterogeneous.

Cerebral white matter damage, as a consequence of HI can be due to hypo-perfusion of the cerebral arteries vascular bed and the susceptibility of myelin and its generating cells: oligodendrocyte precursors to FR and oxidative stress. A lack of myelinated axons in addition to glutamate activation of ion channels in the neuron results in hyper-synchronous generation of action potentials. This deregulation of electrical impulses along the neuron is an underlying cause of seizures and consequentially epilepsy. Seizures can occur early after birth with

frequency increasing within 24-48hr after onset (Lieberman et al., 2000; Wu et al., 2004). In addition, white matter damage is an indicator of HI and inflammation induced mental retardation. Other physical traits associated with HI are sensory-neural hearing loss, and cortical visual impairment.

Skills underlying learning and memory are key focal points in long-term assessment of infants with HIE. Robertson and Finer in 1989 and more recently Marlow et al. in 2005 both followed up case studies of CP at the ages of 15-19yr and 7-9yr respectively. At these age points, differential abilities in CP children are more apparent by the higher demand for complexities required at school. Both studies showed that severe HI lead to difficulties in language, reading, spelling and arithmetic in CP patients compared to their peers. Moderate HI on the other hand showed cognitive abilities within normal range, although these were still lower when compared to peers (Marlow et al., 2005; Robertson et al., 1989).

The developing brain is pre-disposed to insult due to the vulnerability of ODC precursors and a lack of anti-oxidant and FR scavenger defences. Antenatal factors are most likely to contribute to the cause of neonatal HI, although a correlation in birth weight to severity of outcome is also prevalent. The pattern of damage seen is dependent on the type of trauma, its duration, the neonates' age as well as other factors. The severity of outcome is dependent on the regions of the brain affected by HI. This shows that the exact mechanisms that give rise to hypoxia-ischemia to be incredibly complex and highly variable between individual.

Animal models of neonatal HI brain injury

Due to the multiple differences between the neonatal and adult brain, correlating data from human adults, in cases such as stroke, to newborns is limited. As such, the development of animal models has proved a vital tool for the study of developing brain and its response to injury, as well as testing the therapeutic efficacy of emerging treatments. This is due to the ability of such models to mimic clinical entities such as biomarkers, aEEG and pH (Faulkner et al., 2011; Robertson et al., 1999; Robertson et al., 2013).

New models are still arising, as are the adaptations of existing ones. In the 1970s Dobbing and Sands led the way in establishing neurodevelopmental parallels being humans and other species based on the rate of brain growth (Dobbing and Sands, 1978). Studies that are more recent have focused on models with an origin in the histological and functional maturity of individual brain regions and neural systems. To date, the most widely used model of neonatal development is the P7 rat, whose maturity is accepted to equate to the human early third trimester. Other popular species include primates, the fetal sheep, lambs, piglets, rabbits, and other rodents. An analysis of 292 animal studies of term neonates with HIE conducted between 1955 and1997 indicated that rodents were used in 26%, piglets in 23% and sheep in 22%. A time point of 24-48hr proved optimal for analysis of damage (Hagberg et al., 2002a; Northington, 2006).

Whilst no single model is ideal, each provides a preferential advantage depending on the research question and materials used. Primates have a phylogenic proximity closer to humans than any other animal. They are well suited for long-term studies of neurological development and behaviour. However, their use is limited by expense and ethical considerations. Piglets and sheep have an extensive history of research to back their use, mostly focused on cerebral metabolic outcome and physical endpoints. However, litter sizes are small and their postnatal maturation is fast, leaving the timing of an experimental window critical. Rodents also have a good baseline of data to back them and have the advantage of large litter sizes. They are utilised for histological findings after injury as well as long term behavioural outcome. However due to their small size, multiple organ monitoring as well as some *in vivo* imaging techniques are limited.

A number of these species have aided our understanding of the pathology underlying WM damage induced by either HI alone or in combination to other exacerbating factors such as endotoxin or excitotoxic glutamate. A pre-term sheep model of LPS and HI gave rise to transient hypoxemia and hypotension, a fall in arterial pH and a rise in lactate (Gunn et al., 1992). All predictors of HIE in humans. WM damage was seen in the LPS treated group. A P1 rat model of ischemic insult used bilateral carotid artery occlusion. Here ventriculomegaly

and a reduction of density in the corpus callosum were observed by a decrease in myelin basic protein expression. AMPA agonists introduced to P7 HI rats proved protective against the damage of ODC precursors and WM. Lastly, global KO of IL-18 in mice proved neuroprotective against HI insult compared to littermate controls (Hedtjärn et al., 2002; Northington, 2006; Roohey et al., 1997).

In 1981, Rice and Vannucci modified an adult rat model of stroke, described by Levine in 1960. Levine's model saw brain damage occur due to ischemia-induced neuronal alterations in forebrain regions ipsilateral to artery occlusion (Levine, 1960). Rice and Vannucci used 25 P7 rats and occluded the left common carotid artery (CROC). They were recovered for 4-8hr before subject to 8% oxygen at 37°C for 3.5hr. After hypoxia, the pups were returned to dams and monitors over a 50hr period. Experimental animals were compared to CROC alone and naïve littermates. In 92% of experimental animals, injury included neuronal changes and damage to the ipsilateral cerebral cortex, corpus striatum, hippocampus, and thalamus. Fifty-six percent of these also had tissue infarct in regions surrounding the middle cerebral artery. Unlike Levine's model, necrosis of the subcortical WM was greater in the ipsilateral hemisphere and spreading from myelinated foci.

To this study, Rice and Vannucci added 22 more animals. They were subject to CROC and HI, and observed for cerebral water content. This significantly increased in the ipsilateral hemisphere (0.6-3.3%) suggesting that edema is a consequence of ischemic damage and not a cause. Later studies by this and other collaborative groups have shown that glucose, α-ketoglutarate, phosphocreatine, ATP and adenine levels to be lower in this model. Other groups have also made their own modifications including bilateral CROC plus 6.5% O_2 for 1hr. The result of which was severe and homogenous cortical lesions in 89% of animals. Another example is the adaptation of the model to one of extreme immaturity at P1- P2. The experimenters found that in these animals a longer and more severe degree of HI was required to induce a response. However, when it did there was an elevated degree of damage to the subcortical WM. This is believed to be a consequence of ODC precursor and sub plate neuronal cell death (Rice et al., 1981).

During the 1990s, The Rice Vannucci model was tailored to mice with modifications to the length of hypoxia being the most changeable factor. Mice have the advantage of there being a high number of commercially available genetically modified strains including global or conditional knockouts (KO) of target genes. It is for this reason that we have employed this model in our laboratory. It is important to note that in mice there is a strain dependent response, even amongst wild type animals. As such, the choice of background is important. P7 CD1 mice showed a 4fold increase in sensitivity to 30min HI compared to 129SVJ. C57/Bl6 lie in the middle, although closer to CD1 (Sheldon et al., 1998).

In the following thesis, we have utilised the P7 mouse model of either HI injury, HI alone in moderate (30 min exposure to 8% O2) or severe (60 min exposure) form, or with sensitisation by LPS at 12hr prior to insult. Details of the methodology and strains employed are shown in chapter 2.

Clinical Management

Identifying risk infants

Neonatal encephalopathy is associated with an increased risk of morbidity and mortality in the neonatal period. Perinatal indicators of fetal stress include abnormal heart rate, meconium stained amniotic fluid, umbilical cord pH of 7.0/7.1, and a delayed onset of spontaneous respiration- leading to the need for resuscitation and ventilation. A low Apgar score of <6 or 7 at 5min is also common (Paneth, 2008). Advances in magnetic resonance imaging (MRI), such as MR spectroscopy (MRS) and diffusion-weighted images (DWI) provide novel perspectives on the neonate's brain metabolisms and connectivity's.

Clinical biomarkers

Assessment of the foetal condition is aided by the measurement of fetal blood pH, CO_2 content, and base (alkaline) deficit or excess. These values can be taken either at late stage of delivery from fetal scalp blood, or immediately after birth from the umbilical cord vessels (Paco et al., 2011). Metabolic acidosis and subsequent rebound alkalosis both have strong links to neurodevelopmental outcome. Indicators of acidosis are a cord pH of 7.0 or 7.1 and/or a base deficit threshold of 12mMol/l or more. Brain pH can also be measured using whole

brain ^{31}P MR spectroscopy during the sub-acute phase after birth (Kendall et al., 2011b; Low et al., 1997).

Magnetic resonance spectroscopy (MRS) is an analytical method that provides a spectroscopic indication of the metabolic activity of the brain. The metabolites of interest following neonatal HI include choline, creatine, lactate and N-acetytlaspartate (NAA). Under normal circumstances, infants have their highest concentration of brain NAA in neurons, with this level increasing with brain maturation.

In the event of HI, a lactate peak is commonly observed within the first 48hr after injury, peaking at 5days. An increase in lactate occurs due to a disturbance in cerebral energy substrates and oxygen metabolism. Ratios of one metabolite to another are altered to various degrees depending on insult. These changes in ratio are often predictive of outcome. Under HI: lactate/creatine; lactate/choline; lactate/NAA; and NAA/creatine all increase, whereas NAA/choline will decrease (Bartha et al., 2006; Chau et al., 2009).

With the development of imaging techniques such as MRI, recognising injured infants has become both faster and more accurate. A combination of MRI with other detection methods, such as MR spectroscopy leads to an enhancement of efficacy in both distinguishing risk infants, and predicting the regional pattern and extends of damage. This can provide an improved insight into neonatal brain injury.

Pathophysiology of neonatal HI brain injury

During neonatal HI insult, once a critical threshold is reached, cellular mechanisms begin to fail due to an insufficiency in ATP supply leading to a two-phase neurotoxic cascade, summarised in figure 1.2. Principally primary energy failure-resulting in immediate and necrotic cell death, followed by a latent period of up to 6hr in which reperfusion occurs. The length of this respite is dictated by the severity of the primary energy failure. Afterwards, a secondary neuronal cell death stage occurs due to multiple molecular imbalances instigated by excitotoxic oxidative stress and mitochondria failure. This secondary phase can last up to 24hr after the initial insult and is considered most responsible for neuronal loss and abnormal neurological outcome (Sanders et al., 2010).

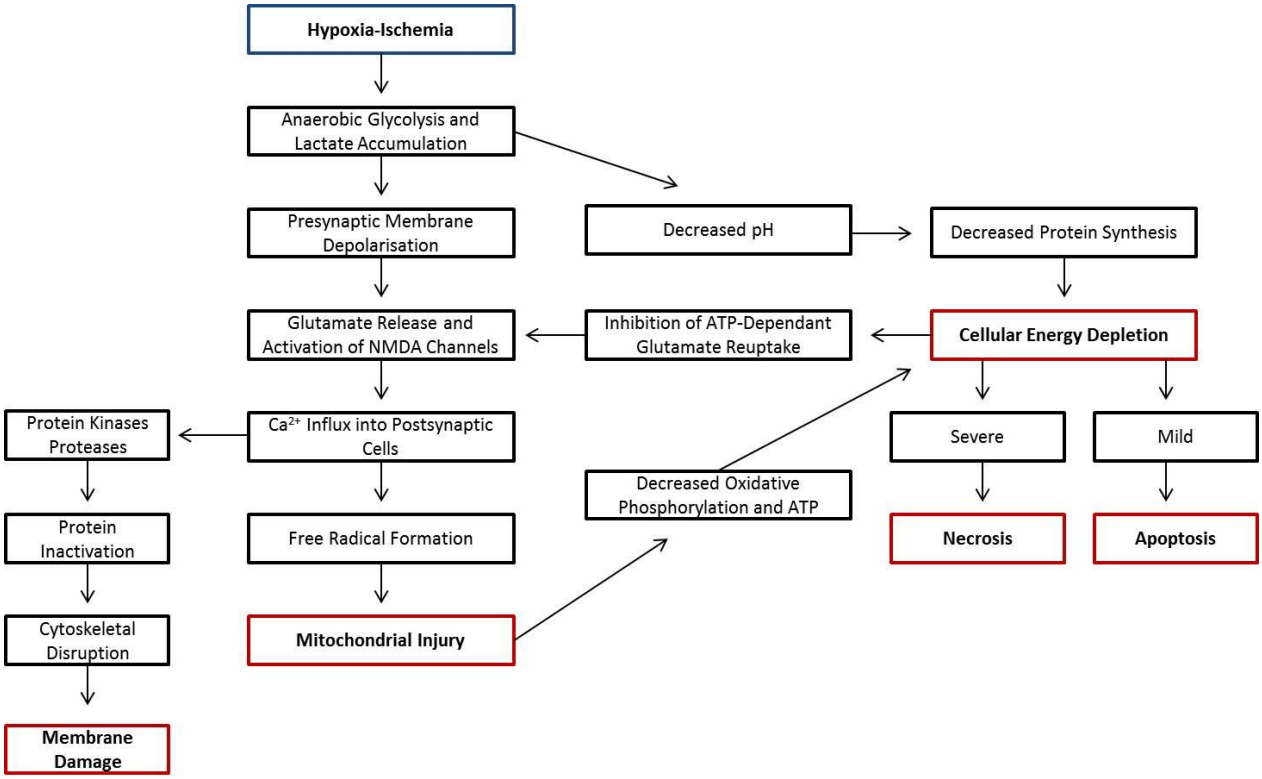

Figure 1.2 Mechanisms of energy failure and subsequent cell death following hypoxia-ischemic insult. Modified from Huang, B. Y. et al. Radiographics 2008.

Primary energy failure occurs within minutes of having loss of cerebral oxygen supply and is when the cells in the brain can no longer meet the nutrient and ATP demand of HI and its ensuing oxidative stress. This leads to the cells accessing and employing high-energy phosphate reserves. Once completely depleted, respiration switches to anaerobic, increasing lactic acid build up, pH fluctuations and eventual free radical (FR) formation. FR typically takes the form

of reactive oxygen species (ROS) which in turn further exacerbates the oxidative stress on the cells (Johnston et al., 2002; Kendall et al., 2011b).

Oxygen and ATP depletion triggers the switch from aerobic to anaerobic respiration. Consequentially, mitochondria initiate the glycolysis of pyruvate into lactate in order to provide additional ATP. While this compensatory mechanism restores some ATP stores, there is still a lack of scavenging mechanisms for H^+ ions from the resulting ATP hydrolysis. Accumulation of protons will eventually induce intracellular acidosis. One defence mechanism for low pH is the activation of N^+/K^+ exchanger (NHE) ion channels. NHE activation removes H^+ ions from the cell, normalising the intracellular pH (Faulkner et al., 2011). Rebound alkalosis can occur if these channels fail to switch off after normalisation. An increase in pH can be equally as detrimental as low pH. Indeed, a more severe phenotype from HI is seen in infants with the most alkaline intracellular pH (Kendall et al., 2011b). This rise in pH can lead to elevated NMDA receptor activation of phospholipases and proteases.

ATP depletion leads to the failure of cell regulation and integrity causing dysfunction of membrane bound ATP-dependent ion channels and exchangers, notably Na^+/K^+ pumps and Ca^{2+} transporters. As a result, the cell depolarises and/or lyses, prompting neurotransmitter, such as glutamate, release into the extracellular space. At the same time, Na^+ and Ca^{2+} cations and water enter the cell via passive diffusion gradients. Too much water entry and cytotoxic edema can occur. Excessive increase in intracellular Ca^{2+} initiates a series of nuclear and cytoplasmic events which if sustained conclude in tissue damage. Damage occurs by the activation of phospholipid, protein and DNA modifications, and the over excitation of enzyme systems including proteases, lipases, endonucleases and protein kinases. These contribute to the degradation of cytoskeletal proteins and the uncoupling of mitochondrial oxidative phosphorylation fundamental to FR, superoxide and other ROS formation, membrane, DNA and mitochondria damage and the initiation of both pro- and anti- apoptotic pathways including autophagy and activation of death receptor/ligands (Higgins and Shankaran, 2009; Vannucci and Hagberg, 2004).

Glutamate, one of the 22-proteinogenic amino acids, is the most abundant excitatory neurotransmitter in the brain. It is stored in synaptic vesicles until

stimulus releases it into the synaptic cleft. From here, it can act on dedicated receptors present on the post-synaptic cell. These receptors are namely N-methyl-D-aspartic acid (NMDA) and α-aminio-3-hydroxy-5-methyl-4-isoxazole propionic acid (AMPA) receptors. Glutamate is rapid removed from the extracellular space by dedicated transporters present on both neuronal and glial membranes (Dugan and Choi, 1994).

During primary energy failure, a surplus of extracellular glutamate amasses due to increased Ca^{2+} influx, prompting its release from the cell. In addition, malfunction of its dedicated ATP-dependent transporters results in a failure to remove it. Under stress, these transporters may act in reverse, increasing glutamate release. This is due to the loss of an electrochemical ion gradient, leaving passive motion of ions only. Ionic gradients give a direction cue for glutamate movement. Inter-synaptic glutamate accumulation can be 10fold higher after HI resulting in excitotoxicity of the tissue.

Excitotoxicity occurs when excessive glutamate over stimulates NMDA and AMPA receptors leading to transmembrane influx of Ca^{2+} into the cell, lipid peroxidation, decrease of anti-oxidant enzyme catalase, and release of nitric oxide synthase (NOS). NMDA receptors are particularly sensitive targets of glutamate action due to their increased number in the neonate compared to adult. NMDA receptors in the immature brain open more readily and stay open longer due to the prevalence of their NR2B subunit. Increased expression of NMDA receptor numbers leaves the brain more susceptible to excitotoxic damage (Dugan and Choi, 1994; Northington et al., 2011; Vexler and Ferriero, 2001). In addition, brief activation of kainate (KA) receptors by glutamate is able to sensitise ODCs to complement toxicity both in vitro and freshly isolated optic neurons, suggesting a role for KARs in the vulnerability of ODCs to glutamate induced excitotoxicity. Kainate as an analogue of glutamate is also an agonist for AMPA receptors (Vincent and Mulle, 2009) . Non-neuronal cells also express glutamate receptors. In particular ODCs which have a prevalence of AMPA and KARs. Acute activation of either AMPA or KA receptors was toxic to ODCs however expose to agonists of NMDA and metabotropic glutamate receptors did not impair cell viability (Sánchez-Gómez et al., 1999). Lastly, glutamate binds to metabolic glutamate receptors (mGluR). mGluR are transiently and increasingly

expressed in ODC precursors but down regulated in mature ODC. Activation of group 1 mGluRs attenuates ODC excitotoxicity by inhibition of ROS, and intracellular glutathione loss (Deng et al., 2003a).

NOS production increases the release of NO both within the cell and in the extracellular space. Nitric oxide will intensify various components of cell damage. Firstly, it can act in a feedback loop with glutamate by its modification of the glycine bonding sites of NMDA receptors causing their sustained activation and subsequent Ca^{2+} influx. In addition, NO reacts with superoxide (O_2^-) to produce peroxynitrate ($ONOO^-$), a toxic hydroxyl radical that directly peroxidises both lipids of plasma membranes and DNA. Lastly, NO is a trigger for pro-apoptotic cell death pathways via the disruption of mitochondrial respiration (Rousset et al., 2012).

A latent period follows these cytotoxic mechanisms, due to the reperfusion of cerebral blood flow once HI stimulus is removed. At this point, the opportunity to restore cellular homeostasis arises. Cerebral circulation, glucose utilisation, ATP production and oxygen restoration can take place. This leads to a reduction in metabolic acidosis, cell swelling and edema, and excitotoxic amino acid accumulation. However, reperfusion brings its own dangers as micro-vascular dysfunction, a result of too many rapid changes overwhelming the circulatory mechanisms, enhances fluid filtration. This promotes the release of pro-inflammatory mediators and subsequent formation of O^- and NO. NO formation activates iNOS production in astrocytes and microglia, further sustaining NO production and instigating the cell damage mechanisms that contribute to second phase of neuronal death (Blumberg et al., 1997; Gilland et al., 1998).

A secondary decrease in high-energy phosphate and glucose metabolism incites neuronal cell death by the deregulation and dysfunction of mitochondria and their ability to modulate oxidative phosphorylation and energy metabolism. Initiation of cell death is via mitochondrial release of pro-apoptotic factors into the cytosol. This secondary energy failure is detectable in the clinic by changes in energy metabolism. MRS shows a reduction in the ratio of phosphocreatine to inorganic phosphates and ATP, and an increase in lactate. Infants displaying these biomarker changes go on to develop poor neurological outcomes (Faulkner et al., 2011; Kendall et al., 2006).

As with primary energy failure, secondary damage emerges from excitotoxic glutamate release, increased intracellular calcium, ROS, and NO formation. The accumulation of insult not only activates cytotoxic mechanism but can both directly and detrimentally affects the mitochondria, leading to mitochondrial swelling and increased membrane permeability. This results in a loss of trophic support, inflammatory response and recruitment of BCL-2 pro- and anti-apoptotic family members. Mitochondria in the neonatal brain are unable to cope with increased FR due to insufficient production of the endogenous anti-oxidant glutathione peroxidase. In addition, they release ROS, which targets polyunsaturated fatty acids present in lipid and organelle membranes (Budd, 1998; Rousset et al., 2012). Break down of lipid membranes gives rise to an increase in unbound iron (Fe^{3+}). Fe^{3+} reacts with reduced oxygen intermediates to produce oxidative FR. These can then positively feedback on ferritin, unbinding more Fe^{3+} ions (Jatana et al., 2006; Martin et al., 1988).

Impairment of mitochondria function induces greater permeability via two routes. Firstly, by means of outer membrane permeability due to Bax influx from the cytosol interacting with its fellow BCL-2 member Bid to form pores in the outer membrane. Through these pores, proteins may easily move in and out. Secondly, a transition pore can form at the point that the inner and outer membranes are closest. Here it is the inner membrane that is permeabilised leading to mitochondrial depolarisation. The pro-apoptotic tumour suppressor protein P53 is implicated in aiding transition pore formation. Depolarisation results in the cessation of ATP production, and FR and ROS formation. Increased permeability leads to cytosolic translocation of pro-death proteins cytochrome C (CTC), apoptosis-inducing factor (AIF), endonuclease G, and Smac/Diablo. CTC binds to APAF-1 (apoptotic protease activating factor 1) to produce an apoptosome that in turn binds pro-caspase 9 resulting in caspase 3 activation. Smac/Diablo will also increase caspase activity whereas AIF interacts with Cytophilin A in a caspase independent apoptotic manner. The resulting complex locates to the nuclease where it incites DNA fragmentation. Apoptosis is the principle, but not singular, mechanism of cell death in ODC and neurons undergoing injury (Bambrick et al., 2004; Hagberg et al., 2009; Infante et al., 2013; Rousset et al., 2012; Thornton et al., 2012).

Mechanisms of cell death

Excitotoxic and oxidative injury accompanying energy failure is followed by a wave of 'programmed cell death', or apoptosis. Apoptosis is required in normal development in aid of reducing the number of redundant neurons and regulating appropriate neural networks. After HI, the apoptotic component is pathogenic and usually secondary to loss of synaptic connectivity, trophic support, inflammatory cytokine accumulation and mitochondria impairment. Alternative forms of cell death are modifiers of neuronal loss after HI. These include necrosis, autophagy and para-apoptosis. Para-apoptosis is where there is a controlled death process, which lacks some of the defining features of classic apoptosis. For example, apoptotic body formation. Activation of apoptosis is due to both caspase dependent and independent pathways. HI induces two regional aspects of cell death: an ischemic core directly formed by the lack of oxygen and nutrients, here necrosis is dominant, and the penumbra, which is the area surrounding infarct where apoptosis is dominant (Northington et al., 2011).

Apoptosis

Apoptosis is a programmed form of cell death activated by signalling cascades defined by cellular and nuclear morphological changes. Phenotypically, apoptotic cell nuclei show DNA fragmentation (pyknosis) and chromatin condensation (karyorrhexis). Dying cells also undergo plasma membrane blebbing and shrinkage although the cytosolic organelles remain normal size. This is so that apoptotic bodies can form during later stages in cell death, where the organelles retain their potentially harmful or inflammatory contents whilst the cell is degrading. Apoptosis is initiated by mitochondrial translocation of Bax and subsequent release of CTC into the cytosol. Induction occurs by either intrinsic or extrinsic mechanisms both of which converge downstream at the level of the mitochondria. As such, mitochondrial release of CTC is a focus for therapeutic prevention of neuronal loss after HI (Druilhe et al., 2003; Hagberg et al., 2009; Hong et al., 2004; Infante et al., 2013).

Caspases that play a key role in apoptosis and inflammation are broadly separated into three categories: initiator caspases 2, 8, 9, and 10; effector caspases 3, 6, and 7; and inflammatory caspases 1, 4, 5, 11, and 12. Effector caspases are activated by initiator caspases that are themselves activated by

multiple upstream regulators depending on insult. Effector caspases cleave cellular substrates including Poly (ADP-ribose) polymerase (PARP), lamin, fodrin, and Rho-associated kinase 1 (ROCK1) resulting in DNA fragmentation, membrane blebbing and cell shrinkage (Velier et al., 1999; Zhu et al., 2005).

The intrinsic pathway includes the formation of the CTC/APAF-1 (apoptotic protease activating factor 1) complex, which activates caspase 9, which in term activates the initiator caspase 3. The extrinsic pathway involves the activation of death receptors through FAS, TNFα and caspase 8. Ligand binding to death receptors requires caspase 8 dependent adapter proteins to form a death-invoking signalling complex. This leads to the dimerisation and activation of caspase 8 that in turn cleaves and activates downstream effector caspases. FAS, TNFα, and TRAIL all contain death domains within their intracellular component, allowing them to interact with death receptors. Once caspase 8 is stimulated, it will in turn activate effector caspases or cleave cytosolic Bid into its truncated form. Truncated Bid translocates to the mitochondria initiating CTC release and subsequent intrinsic pathway activation (Cagnol and Chambard, 2010; Matsumoto et al., 2007; Niu et al., 2012).

In neonatal HIE, caspase 3 is particularly active in neuronal cell bodies and processes (Lesuisse and Martin, 2002). In the P7 rat model of HI, Caspase 3 expression is seen in the striatum and hippocampus at 12-18hr following insult, co-labelling with markers for neurons and ODC precursors (Back et al., 2002; Liu et al., 2002; Manabat et al., 2003).

Necrosis

Necrosis is unorganised and spontaneous cell death. It is the cellular response to dramatic disruptions in homeostasis. Cytoplasmic swelling, chromatin disintegration (karyolysis), and lysis of cell membranes and organelles morphologically define it. Necrosis will lead to further damage of neighbouring cells through the release of toxic substances and enzymes from the lysed organelles (Chavez-Valdez et al., 2012).

Autophagy

Autophagy is a catabolic process in which cells degrade and recycle their own cytoplasm and organelles. Degradation occurs due to the lysosomal system in order to maintain cellular homeostasis. Under critical stress conditions

autophagy results in non-apoptotic programmed cell death. Autophagy is distinguishable by the accumulation of autophagic vacuoles. These form from autophagosomes originating in the endoplasmic reticulum and plasma membrane. PI3K and target of rapamycin (TOR) kinase activity direct autophagosome formation. Once formed, they fuse to cytosolic lysosomes, within which they degrade their contents via lysosomal hydrolase (Nair et al., 2013; Northington et al., 2011).

Cross talk between autophagy and apoptosis may exist in a temporal manner in response to HI. In the neonatal mouse, inhibition of autophagy prior to injury saw a shift from apoptotic to necrotic in the damaged cells. It may be that early on in HI, autophagy is required to conserve energy stores at an adequate level long enough for apoptosis to commence. Conversely, later inhibition of autophagy proved neuroprotective, i.e. once all reserves of ATP are used autophagy is now pro-death. This indicates synergy between autophagy and apoptosis is early stage and for a limited period only (Zhu et al., 2005).

Cross talk can also exist between necrosis and apoptosis via receptor-interacting protein 1 (RIP1). Apoptosis induced by FAS and TNF receptor leads to active caspase 8 that in turn cleaves RIP1 a negative regulator of necrosis. However, inhibition of RIP1 results in TNF and FAS ligand induced cell death being switched to necrosis (Kim et al., 2006; Tran et al., 2001).

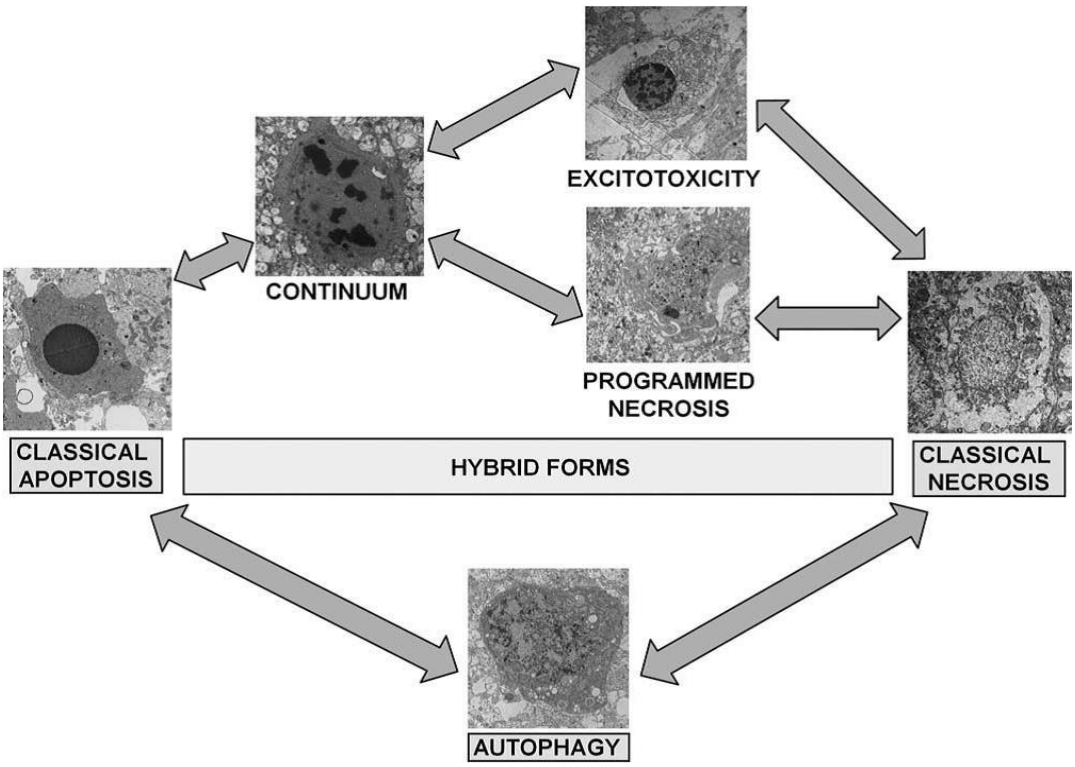

Figure 1.3 The cell death continuum. Cell death following HI brain injury exists as a continuum of classical apoptosis and necrosis at opposite ends and hybrid forms in between. Reproduced with permission (Northington et al., 2011).

Synergy of inflammation and HI in neonatal brain injury

Mechanisms of inflammatory response to HI

Inflammation is a key factor in acute CNS injury in both the adult and neonatal brain. Infection and inflammation are common causes of pre-term birth, especially prior to GA 30weeks (Goldenberg et al., 2000; Peebles and Wyatt, 2002). Children with CP consistently show elevated levels of pro-inflammatory cytokines in the blood and cerebral spinal fluid at birth compared to uninjured infants. High concentrations of IL-1, -6, -8, and TNFα are particularly associated to spastic diplegia CP (Hagberg et al., 2012).

Causes of neonatal infection include chorioamnionitis and intra-partum fever. Here bacterial invasion of the choriodecidual space propagates infection from the chorioamniotic membranes into the amniotic fluid where it can enter the fetal circulation. This results in the release of pro-inflammatory cytokines including IL-1α, IL-1β, IL-8, TNFα, and G-CSF (Goldenberg et al., 2000). Infection increases the risk of brain damage by cytokine activity on the BBB leading to increased permeability and basement membrane degradation- exposing the brain to secondary insult (Wang et al., 2012b). In the case of systemic infection, this is problematic due to chemotaxis of bacteria entering the brain along with peripheral immune cells recruited to help the brain cope with the initial infection (Hagberg and Mallard, 2005).

Non-infectious exposure to excitotoxic HI by itself will induce inflammatory responses that can hypersensitise the neonatal brain to insult. Inflammation induces the up-regulation of both pro- and anti- toxic cytokines and chemokines in activated microglia and astrocytes. The balance of these pro- and anti-mechanisms modulates injury and repair over the extent of HI insult. The immune system of the developing brain consists of a dedicated subset of cells-glia and microglia, which along with the BBB will prevent the entry of peripheral antigens. Unfortunately, this privileged environment becomes a constriction once an inflammatory response is initiated. Unless damage is severe enough to disrupt the BBB, there is little aid from the peripheral immune system. Typically peripheral granulocytes are not present in the brain parenchyma, but entry into the damaged nervous system is a common observation in many brain

pathologies. Their protease and cytotoxic functions aid the phagocytic removal of cellular debris and pathogens (Bohatschek et al., 2001).

The cells responsible for CNS immune response are predominately microglia and parenchyma derived macrophages, but also leukocytes, mast cells, endothelia of the blood brain barrier and astroglia (Bailey et al., 2006; Bohatschek et al., 2001). During the early inflammatory phase of HI, microglia release factors such as platelet-aggregating factor, TNFα, IL-1β, IL-18, caspase 1 and complement Clq into the extracellular space (Chock and Giffard, 2005). TNFα, IL-1β and interferon- γ have a direct and toxic effect on both neurons and ODC precursors. Additionally, they auto-regulate microglia and astrocytes resulting in further activation and release of cytokines. In addition to cyto- and chemo-kine release, the activated microglia will produce the FR NO and O_2^- and up-regulate iNOS, COX2 and ROS. This exacerbates insult by the deregulation of mitochondria (Dommergues et al., 2003; Kaur and Ling, 2009). Inhibition of microglial pro-inflammatory signals reduces brain injury in animal models of inflammation. Pre and post- HI treatment with IL-1 antagonists, deletion of IL-18, and deletion of IL-18 plus IL-1β all significantly reduce lesion size (Hedtjärn et al., 2002; Hedtjärn et al., 2005; Liu et al., 1999).

Some studies indicate that pro-inflammatory microglia can undergo transition to anti-inflammatory. During excitotoxicity, microglia release anti-inflammatory cytokines, producing a neuroprotective affect. These include IL-10 and transforming growth factor β1 (TGF- β1) (Raivich et al., 1999). IL-10 reduces the production of IL-1 and TNFα, whereas TGF- β1 is an immuno-suppressor, directly inhibiting microglial activation via receptor-ligand binding (Suzumura et al., 1993). Conversely perinatal systemic infection, induced by IL-1β injection, sensitises the brain to secondary excitotoxicity via inhibition of IL-10 production (Vincent et al., 1997). Interestingly, in animal studies of endotoxin induced inflammation neither IL-10 nor TGF- β1 were up-regulated (Xiao et al., 1996), suggesting that these pro-survival cytokines modulate non-infectious inflammation.

Microglia can be activated by endotoxin via microbial products binding to antigen sensing receptors on the cell surface. Receptor binding leads to the activation of transcription factor NF-κB, a known regulator of further cytokine

release, gene expression and cell survival (Chock and Giffard, 2005). Receptors responsible for mediating inflammation-activation of microglia and macrophages are a group known as pattern recognition receptors (PRR). PRRs are predominately on the cell surface of microglia. Differentiated dendritic cells of the meninges and choroid plexus also express them. PRRs identify and response to pathogen-associated molecular pattern (PAMP) molecules from micro-organisms, for example, endotoxin from bacteria, or to damage-associated molecule patterns (DAMP) from injured cells (Gorina et al., 2011; Lehnardt et al., 2003; Sadeghi et al., 2007).

Multiple PRRs have been identified in the brain, the most numerous of which are toll-like receptors (TLR). PRRs also include nucleotide-binding oligomerisation domain proteins, scavenger receptors, and components of the compliment system. TLR are transmembrane proteins. There are 11 family members all with extracellular immunoglobulin domains. Interaction of TLR and PAMP instigates NF-κB activation via the binding of MYD88 (myeloid differentiation primary response protein 88) (Gorina et al., 2011; Wang et al., 2009). TLR can have opposing roles. In the adult mouse hippocampus, TLR2 enhanced neurogenesis whilst TLR4 inhibited neuronal differentiation.

Endotoxin induced inflammation

Lipopolysaccharide (LPS) is found on the outer membrane of gram-negative bacteria where it plays a vital role in maintaining structural integrity. LPS is a known endotoxin, inducing an inflammatory response by binding to the CD14/TLR4/MD2 receptor complex. This mediates the release of cytokines and subsequent nuclear transport of NF-κB leading to the downstream activation of other transcription factors (Figure 1.4). LPS has been extensively used in animal models and research due to its consistent ability to incite inflammation (Hagberg and Mallard, 2005).

In neonatal studies, LPS injection led to an up-regulation of pro-inflammatory cytokines and neuronal death (Hagberg et al., 2002b; Kendall et al., 2011a; Mallard et al., 2003). Systemic injection of 1mg/kg LPS into P9 mice saw a reduction in the number of hippocampal neurons and astrocytes when observed at 32 days post injection. However cell proliferation and behavioural outcome

remained unaffected (Järlestedt et al., 2013). When the fetal brains were observed at birth, a reduction in myelin formation and a marked increase in activated microglia and astrocytes were seen (Cai et al., 2000).

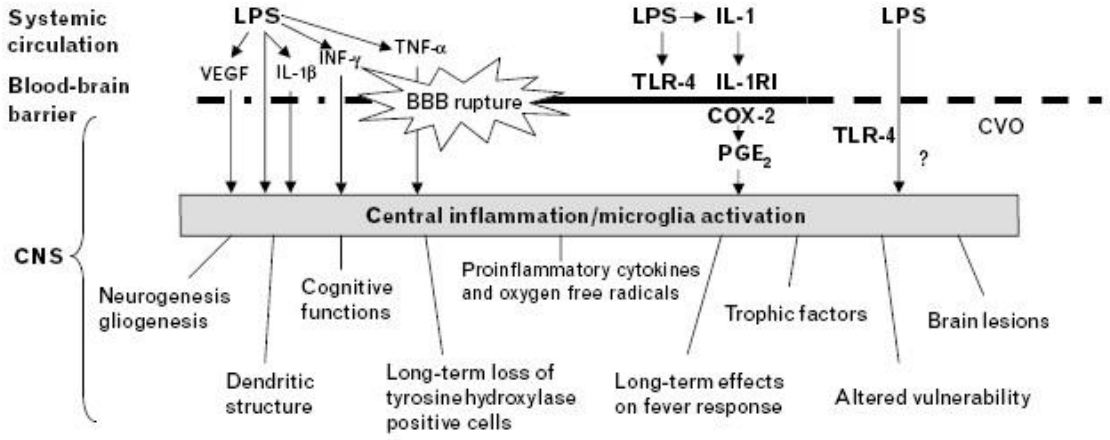

Figure 1.4 Lipopolysaccharide-induced systemic inflammation is transferred to the brain across an intact barrier via receptor-mediated prostaglandin production, areas with an incomplete barrier and through rupture of the blood–brain barrier (BBB). Central inflammation and microglia activation elicit a cytokine/ trophic factor response, affect central nervous system (CNS) functions, structure, cellular proliferation and vulnerability, and can produce brain lesions. Reproduced with permission (Hagberg and Mallard, 2005).

Synergy of endotoxin and HI injury

Multiple studies have combined LPS and HI in neonatal models, where a synergy of injury occurs. LPS injected either intraperitoneal (Eklind et al., 2001; Yang et al., 2004) or into the subarachnoid cisternae (Coumans et al., 2003) increased lesion size in the P7 rat when administered immediately after HI. Similarly, another study saw LPS injected IP into pregnant rats at E17 and HI performed on the newborn pups at P1. Significant increase to the extent of cortical lesions was observed (Girard et al., 2009).

This synergistic nature of LPS to HI has the same underlying mechanisms to produce WM and GM lesions as those seen in humans with infection and HIE. Previous work in our laboratory and in others indicates microglia activation and their release of pro-inflammatory markers are responsible for the increase in lesion size. These effects transmit through TLR4 present on the blood vessel endothelia and microglia. TLR4 activation occurs through the Myd88 adapter protein and/or through TRIF (TIR-domain containing adapter inducing interferon β) (Gorina et al., 2011; Hagberg and Mallard, 2005; Sadeghi et al., 2007). TLR4$^{-/-}$ mice failed to develop brain injury following HI, whereas Myd88$^{-/-}$ mice lose

sensitivity to LPS aggravated HI, although not to HI alone(Wang et al., 2009). Our laboratory looked upstream to microglia activation and showed that global deletion of the TNF cluster of genes- including TNFα, lymphotoxin α and lymphotoxin β, nullified the sensitising effect of LPS in the P7 mouse (Kendall et al., 2011a). Here LPS was administered 12hr prior to moderate HI.

This work gives credence to an alternative form of synergy where cytokines enhance HI insult by their actions at the BBB. The integrity of the BBB is reduced in the presence of TNFα and IL-1β as a consequence of their up-regulation of ICAM-1. ICAM-1 leads to an increase in permeability of the BBB, allowing peripheral chemotoxins to enter the brain (Kendall et al., 2011a). In adult mice, IP injection of LPS results in an influx of granulocytes into the parenchyma (Bohatschek et al., 2001). Granulocytes have an implied role in stroke and trauma due to containing high concentrations of cytotoxic molecules and proteases.

Overall there is the suggestion that synergy can occur when the fetal inflammatory response attenuates normal compensatory mechanisms to HI insult.

Non-neuronal components in injury response to HI

Microglia

Microglia constitute the majority of immunocompetent cells in the brain. They are the most abundant form of brain macrophage, making up 20% of the non-neuronal population (Hickey et al., 1992; Raivich, 2005). In the neonatal brain they show an elevated level of activation due to an increased expression of MHCII, CD40, and CD86, markers of antigen presenting cells that aid in cellular response to external stimuli (Kaur and Ling, 2009). Perivascular macrophages are short lived. However, their role as phagocytes and immune responders are vital. Recent studies by Ginhoux et al. have shown that unlike peripheral macrophages, microglia do not derive from the bone marrow as expected but instead from primitive myeloid progenitors within the yolk sac during embryonic development (E8) prior to blood circulation. In addition postnatal microglia are maintained independently by local precursors that colonise the brain prior to birth. Microglia invade the brain through the pia surface and fourth ventricle,

spreading into the cephalic mesenchyme where their role in neurodevelopment includes neuronal pruning and tissue modelling (Ginhoux et al., 2010). Unlike peripheral macrophages, microglia are of a finite number. Microglia contribute to secondary brain injury after HI through the production of pro-inflammatory cytokines, proteases, compliment factors, excitotoxic amino acids and free radicals (Hagberg et al., 2002b; Hristova et al., 2010; Streit, 1993).

Microglia in their resting state are highly ramified with tiered arborisation of projections that survey large areas surrounding the cells. In vivo imaging has shown that whist the cell body, at rest, is static the elaborate ramifications are continually extending and contracting in order to sample the extracellular environment. Activation of microglia occurs as a result of injury stimuli and tissue disruption. This leads to a rapid recruitment of microglia to the injured area at which the arborized projections surround the damaged tissue in a sphere of branches, effectively walling it off from undamaged tissue (Raivich, 2005).

Phenotypic differentiation of systemic macrophages to resident microglia is a major immunohistochemical issue due to multiple shared markers of expression. There is close homology between microglia and monocytes/macrophages via expression of markers including F4/80, Fcγ Receptor and CD11b (Ginhoux et al., 2013; Raivich et al., 1999). No single specific marker for microglia with the exception of morphology under SEM. In postnatal rat brains, microglia are observed to be spiny in contrast to the smooth surfaced macrophages (Guillemin and Brew, 2004). However expense and technical variability makes this an insecure marker to go with.

Following trauma microglia, become activated in a stereotypic and graded response as illustrated in figure 1.5. Activation occurs in the same sequence independent of insult type (Raivich et al., 1999). The extent of damage correlates with the level of activation seen (Gehrmann et al., 1995; Kreutzberg, 1996). Stages of microglia activation can be visualised by an increase in expression of the microglia antibody αMβ2, where the morphological changes of microglia occur in response to injury. Many cell adhesion molecules co-regulate with αMβ2, such as αXβ2 integrin, whose expression is only present in phagocytic microglia. This combination of markers allows the stages of

microglia activation to be determined. Previous work by this group have shown that strong expression of the antigen marker αM is typical of early activated microglia and provides a valuable tool for immuno-labelling of such cells during hypoxia (Hristova et al., 2010; Kendall et al., 2011a).

The up-regulation of cell adhesion molecules facilitates the migration of microglia to the injury site, aided by the expression of MHCI and MHCII (major histocompatibility complex 1 and 2) enzymes that degrade the extracellular matrix. Microglia also act as antigen presenting cells, releasing cytokines, in order to recruit other immuno cells to the injured region.

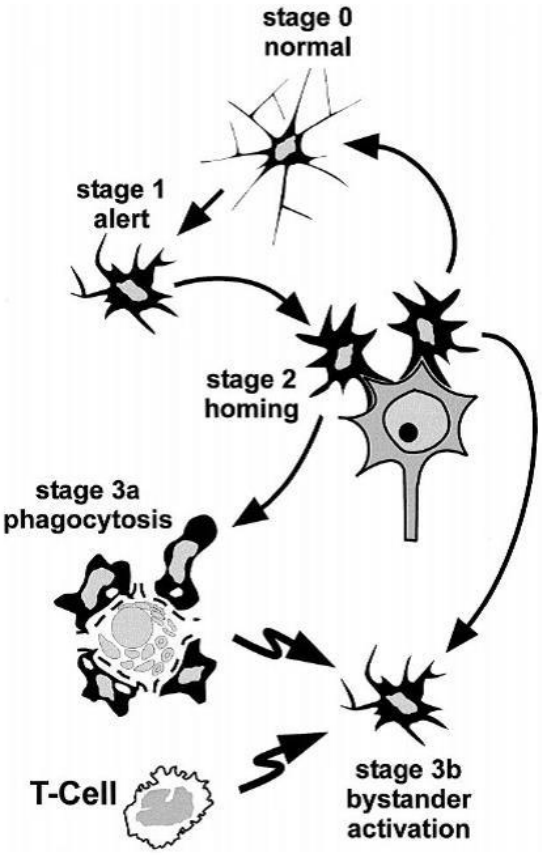

Figure 1.5 Schematic summary of microglia activation. Activated microglia proceed through a series of morphological changes. In resting state is highly ramified (stage 0). Following neuronal injury, ramified microglia transformed to a more de-ramified form (stage 1) which home on injured neurons (stage 2). If no further damage occurs, it returns to the resting state (stage 0) whereas if cell death occurs, microglia are further transformed into phagocytic cell (stage 3). These phagocytic foci also activate the adjacent, non-phagocytic microglia (stage 3b). (Raivich et al., 1999)

Activation of microglia is seen in neonatal post mortem samples and animal models of periventricular leukomalacia, excitotoxicity and HIE. Injection of NMDA into the cortex of P7 rats induces microglia activation in areas undergoing subsequent neural degeneration (Acarin et al., 1996). The presence

of microglia is a good indication of damaged regions by their migration to these areas. Importantly, their immediate response to changes in the microenvironment often precedes that of histological damage, providing an early detection system for tissue injury (Gehrmann et al., 1995). In the cerebral infarct zone, activated microglia adopt a phagocytic phenotype. These differ morphologically to resting ramified glia by retracted processes and a rounded appearance (Kaur and Ling, 2009; Polazzi and Monti, 2010).

Microglia evidence an important role in immune surveillance, cytokine production, compliment activation and phagocytosis within the CNS. The mechanism of their actions in perinatal brain repair and protection remain not fully understood.

Astrocytes

Astrocytes or astroglia are the most abundant cell population of the brain. They are easily characterised by their star shape and play an important role, both mechanically and metabolically, in supporting neurons. Histologically they are recognised by the expression of glial fibrillary acidic protein (GFAP). Astrocytes can contribute to brain pathology by glial scarring in areas of tissue loss. This occurs due to astrocyte accumulation at these sites (Sen and Levison, 2006). Here astrocytes form a web of their membrane protrusions, similar to microglia, which fills in the infarct space. Neighbouring neuronal outgrowth is prevented by the release of modifiers of extracellular matrix, laminin, fibronectin, and proteoglycans (Emsley et al., 2004; Nieto-Sampedro, 1999). Lastly, astrocytes have the potential to release FR, TNFα as well as anti-inflammatory TGF-β via the activation of neurotransmitter transporters at their plasma membranes (Shu Zhen and Takashima, 1999).

Astrocytes show a duality in response to injury. Under oxidative stress they can be protective by the production of anti-inflammatory factors and glutathione as well as uptake of glutamate (Arai and Lo, 2010). However, once these mechanisms are overwhelmed or depleted, astrocytes have the potential to be detrimental via the release of IL-1, ROS and glutamate onto neighbouring cells (Bambrick et al., 2004).

In post mortem samples of neonatal HIE, astrogliosis increases between 15-40%. Whether astrocytes contribute to HI remains unclear (Rezaie and Dean,

2002). Nor is it certain that their activation during HI is due to damage to themselves or in response to neuronal and ODC injury, or both.

In adult mouse models, the role of astrocytes shows conflicting evidence. GFAP null mice show a decrease in infarct volume following middle cerebral occlusion; however, the same mice show a decrease in later neuronal regeneration of retinal transplants (Kinouchi et al., 2003; Li et al., 2007). In neonatal models astrocytes activation is common. Interestingly, whilst microglia are active within hours of insult, returning to a resting state in a matter of days, astrocytes are not active until 72-96hr post-insult, but remain in an active state for weeks after (Dommergues et al., 2003; Northington, 2006; Olson and McKeon, 2004; Raivich et al., 1999; Thornton et al., 2012). This implies that their recruitment to the injury site by microglia, possibly through the release of IL-1.

Cellular response to oxidative stress is biphasic with the critical loss of ATP and anti-oxidant defences, glutamate-induced excitotoxicity and initiation of inflammatory response. These factors culminate in neuronal loss. Microglia are the main immune cells of the brain. Their accumulation and activation at an ischemic region is an early marker of damage. In addition, they can recruit neighbouring astrocytes in order to limit the extent of injury. Whether these non-neuronal factors ultimately help or hinder the brains resistance to HI is still to be determined.

Pharmacological Therapies for HIE

Understanding the brains cell specific and differential response to HI is vital in establishing a therapeutic window for treatment. The pathology and cell mechanisms behind damage dictate the timing and application of new therapeutics and pharmaceutical interventions. It has been noted that global yet reversible HI-induced neuronal death is biphasic. When insult is severe enough, immediate cell death occurs due to cellular hypoxia and depletion of high energy ATP leading to cell exhaustion. This is categorised as primary energy failure. Following this first phase is a latent period of around 6hr or more, in which reperfusion of the cerebral blood flow can occur. In MRI studies of both pre-term and term infants this was established as the optimal interval for therapeutic intervention in order to prevent or at least diminish the subsequent secondary energy failure (Bartha et al., 2006; de Vries and Jongmans, 2010; Rutherford et al., 2006; Shah et al., 2006). This secondary phase of neuronal loss is multi-factorial, namely hyperaemia leading to cytotoxic edema, mitochondria dysfunction, FR formation, NOS production, endotoxin accumulation and glutaminergic excitotoxicity. Secondary energy failure is the stage of HI insult most associated to the appearance of encephalopathy, increase in seizures, and lesion size (Blumberg et al., 1997; Johnston et al., 2002; Perrone et al., 2013).

Current treatments in the clinics are mostly palliative, for example botulinum toxin for seizure control and physiotherapy, or hypothermia. Two models of hypothermia are currently in use: whole body cooling or selective head cooling (Gluckman et al., 2005; Jacobs, 2005; Shankaran et al., 2005). The rationale behind the latter is that newborns produce 70% of their total body heat in their brain. In addition, an unhealthy neonate will be more susceptible to the physiological side effects of systemic hypothermia. Theoretical modelling of this system suggests that to decrease the temperature of deep brain regions, a core body temperature of 35°C is required.

Hypothermia protects neurons by reducing the cerebral metabolic rate. This prevents the release of excitotoxic amino acids, glutamate, and dopamine as well as reducing NO and FR formation. Several pre-term and term models have

shown that a brain temperature reduction of 2-4°C, immediately after HI, will give a decrease in energy expenditure and histological loss. Other studies in the neonatal piglet show that hypothermia for 2hr following HI resulted in a reduction of apoptosis, though necrotic cell death was unaffected. It is noted that hypothermia does not offer complete protection, resulting in a 40% reduction in injury. When insult is extreme, cell loss is unrecoverable (Iwata et al., 2005). This has been faithfully replicated in animal models of both neonatal and adult HIE (Dickey et al., 2011).

This limited efficacy of hypothermia has given rise to other promising therapies, most of which have not yet reached the clinics but all offer the potential to aid in the protection against HIE, either alone or in combination. Different interventions target early pathways of injury- such as inflammation, apoptosis and oxidative stress, or later pathways of growth factor deprivation, glutamate excitotoxicity and secondary cell death. Figure 1.6 indicates current pharmaceutical agents and their optimal timing for use currently under investigation with the purpose to be clinical treatments for HIE.

Hypothermia

Hypothermia has been a recognised treatment for hypoxic ischemic encephalopathy since the 1940s after studies in the neonatal guinea pig model showed a significant increase in survivability after exposure to 10°C. optimisation of hypothermia, using animal models, showed that with moderate cooling, whole body temperature decrease of 2-4°C immediately after HI, there is a preservation of cerebral energy metabolism and a reduction in cellular edema (Fan et al., 2010; Higgins and Shankaran, 2009). Since then many other groups have used randomised trials of hypothermia for risk infants with HIE. Three trials, CoolCap, NICHD, and TOBY, measured neurological outcome at 18 months after birth and show that there is a significant benefit in cooling that correlates to a decreased risk of death and neurodevelopmental disability. Combined they have treated 767 infants.

Alternative and future therapies

Both animal and pilot clinical studies have looked into alternative therapies in neonatal HIE. Each is designed based on the current knowledge of the spacio-temporal pathology of injury. They include preventative treatments, such as pre-conditioning, early possibilities that target primary energy failure via antioxidants and vasodilators, and later possibilities that target secondary neuronal death using anti-apoptotic agents, FR scavengers and anti-inflammatories. Lastly, delayed therapies, such as stem cell administration, have the potential to regenerate the neurons lost following HI (figure 1.6).

Stage of HI Insult	Cause of Injury	Therapeutic Treatment
Baseline	None	Pre-conditioning
Hypoxia-Ischemia	Primary Energy Failure	Melatonin, Allopurinol, Statins
Reperfusion/Latent Phase	Inflammation/ Apoptosis	Hypothermia, $MgSO_4$, Xenon, Argon, Melatonin
Secondary Energy Failure	Loss of trophic factors/ Cell Death	NAC, Melatonin, EPO,
Post Insult	Cell Death	EPO, Stem Cells

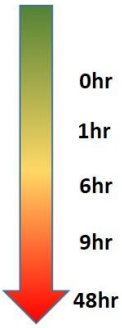

Figure 1.6 Therapeutic possibilities and their optimal time to start, according to their mechanisms of action. Up to now, hypothermia is the only standard therapy for full-term neonates with moderate to severe hypoxic-ischemic encephalopathy. Melatonin and statins could have neuroprotective effects when administrated prophylactically. Hypothermia and antioxidant strategies are optimal within the first 6 hours after reperfusion/re-oxygenation. Anti-inflammatory and anti-apoptotic strategies should equally start early and no later than 9hr after reperfusion/re-oxygenation. Trophic factors and stem cells are still plausible therapies up to 48hr, after reperfusion/re-oxygenation. Modified from (Perrone et al., 2012; Sanders et al., 2010)

Pre-conditioning

Pre-conditioning involves brief non-lethal episodes of hypoxia to protect against subsequent periods of lethal HI. Animal studies show promise in the prevention of secondary energy failure. Although primary energy failure is the ideal target, it is harder to predict the timing of its onset. Pre-condition is of particular interest in preparing the foetus for hypoxia insults during the peri-partum period of labour. P7 rats were subject to 8% oxygen for 3hr prior to pathological HI 24hr later. The animals were then assessed 8weeks post insult. The treated group showed an 80% increase in neuroprotection compared to control littermates. In addition there was a significant reduction in apoptosis and an improvement in functional behaviour recovery (Sanders et al., 2010).

Pre-conditioning works by the activation of HIF resulting in downstream expression of protective vascularisation factors including VEGF and erythropoietin (EPO). Pre-conditioning also incites an increase in endogenous anti-oxidants and glycogen which in turn regulates high energy phosphate production (Kitagawa, 2012).

Targets of early cell death

In order to prevent the energy depletion caused by oxidative stress, research groups have focused on the use of anti-oxidants through xanthine oxidase inhibitors, NMDA receptor antagonists, Nobel gases and statins.

Allopurinol, a xanthine oxidase inhibitor, and its metabolite oxypurinol are structural isomers of the endogenous purine hypoxanthine. Inhibition of xanthine oxidase results in a reduction of superoxide formation, especially at the reperfusion phase following HI. High doses can scavenge FR and bind free iron. Oxypurinol, more so than allopurinol, can cross the BBB. Three pilot studies in humans showed that when given 3hr post HI in term neonates, there was a significant reduction in FR formation (Benders et al., 2006). A meta-analysis of both human and animal studies indicated that overall there is no significant change in primary outcome following treatment.

Magnesium is administrated in the form of $MgSo_4$. It is a known inhibitor of NMDA receptors as well as a modulator in mitochondrial function. In a neonatal rat model, Magnesium infusion gave an increase in cerebral blood flow and a decrease in infarct volume (Cetinkaya et al., 2011; Perrone et al., 2013). Higher doses further supplemented neuroprotection, but there was the additional risk of hypertension.

Xenon: Studies in both rats and piglets have looked to the therapeutic benefits of xenon due to its antagonistic nature against NMDA. Xenon is a noble gas already routinely used in the clinics as a general anaesthesia. It rapidly crosses the BBB and can induce aesthesia in a manner both protective to neurons and myocardial tissue. In addition to antagonising NMDA, xenon can inhibit AMPA and kainate receptors leading to a reduction of neurotransmitter release and action of excitotoxic glutamate. Treatment with xenon resulted in the stabilisation of blood pressure, inhibition of Ca^{2+}/calmodulin dependent PKII,

inactivation of anti-apoptotic BclxL and Bcl-2, and the induction of HIF1α, EPO and VEGF (Fan et al., 2010). Xenon looks highly promising in the treatment of HIE, but its limits are its cost, availability and method of regulating administration. An alternative is proposed in the form of argon which is cheaper, more available and ubiquitous. It has been used in rat adult models of focal cerebral ischemia, delivered at 1hr post insult. A reduction in infarct volume was observed but no change in survival (Brücken et al., 2013). More studies on argon are required to establish its efficacy in neonates.

Statins are inhibitors of HMG-CoA (3 hydrozy-3-methylglutaryl co-enzyme A) reductase, and are used clinically to lower cholesterol. In the neonatal rat, cerebral injection of simvastatin alleviated HI induced ODC injury, microglial activation and decreased the number of pyknotic neurons. In the adult rat model, simvastatin reduced ischemia-induced mRNA expression of the pro-inflammatory markers: IL-1β, TNFα and ICAM-1. Cell survival also increased via the activation of the Akt/CREB pathway (Runchel et al., 2011; Sanders et al., 2010).

Targets of secondary neuronal loss

Later approaches look at the latent period between both intervals of cell death as a window for therapies targeting the second excitotoxic neuronal injury. These therapies focus on anti-inflammatories, FR scavengers and anti-apoptotic factors.

Erythropoietin (EPO). Endogenous EPO is a glycoprotein hormone essential to the regulation of red blood cells and protection of their proteins. It is also a vasoconstrictor and initiator of angiogenesis. Under hypoxic conditions, EPO is a strong neuroprotective agent via its activation of anti-oxidant enzymes. This leads to a decrease in excitotoxic damage by upregulation of anti-apoptotic and anti-inflammatory agents, and a decrease in lipid peroxidation. In the neonatal mouse model, EPO treatment prior to HI insult gave a reduction of apoptosis in the cortex through the up-regulation of Bcl-2 and down regulation of BCL2, Bax and IL-1β. Leukocyte recruitment was attenuated (Fan et al., 2011).

Recombinant EPO (rEPO) is neuroprotective in rodents. Inhibition of LPS-activated pro-inflammatory cytokines in the WM of neonatal rats, and ODC genesis, neurogenesis and reduced WM damage in mice was observed. In both cases, rEPO was injected immediately following HI. However in clinical studies there is issue with the efficacy of systemic administration as only 2% crosses the BBB (Elmahdy et al., 2010). EPO can also offer later stage trophic support. In a neonatal rat model of HI, EPO increased the re-vascularisation of the ipsilateral hemisphere leading to an enhanced uptake of oxygen, neurogenesis in the subventricular zone, and migration of neuronal progenitor cells into the ischemic cortex and striatum (Shen et al., 2009).

Melatonin is another endogenous hormone, secreted by the pineal gland in response to environmental light-dark cycles. It easily crossed multiple physiological barriers. Its function include defence against oxidative stress, regulation of energy metabolism, FR scavenging and enhancement of immune function. Melatonin acts through G-protein coupled receptors in the plasma membrane. In addition, it can interact with orphan nuclear receptors and calmodulin in the cytosol. Lastly, melatonin and its metabolites are able to detoxify ROS (Cetinkaya et al., 2011; Robertson et al., 2013).

In an adult rat model of stroke, delayed injection of melatonin showed an increase in electrophysiological and neurobehavioral recovery. In addition, there was a decrease in cortex and striatum infarction and a reduction in cerebral inflammatory response (Kondoh et al., 2002; Torii et al., 2004). In neonates, a fetal sheep model showed decreased inflammation and WM damage when melatonin was administered to them directly or via their ewes (Miller et al., 2005; Welin et al., 2007). In the neonatal rat, melatonin was administered before HI and then repeated three times after at 0hr, 12hr and 48hr. by 24hr after insult there was a reduction in free Fe^{3+}, Fe^{2-}, and Fe^{4-} indicating FR scavenging role (Signorini et al., 2009).

N-acetylcysteine (NAC) is a synthesised drug derivative of cysteine and a nutrient supplement. It is a precursor to the anti-oxidant glutathione and as such acts as a FR scavenger. NAC has low toxicity and easily crosses both the placenta and BBB. However its efficacy in neonatal HIE requires a high dosage. In adult rat focal cerebral ischemia, NAC restored glutathione levels, attenuated

reperfusion injury and reduced both inflammation and NO production (Jiang-Qin Liu et al., 2010). In the neonatal rat, NAC proved superior to melatonin in decreasing infarct damage in LPS sensitised HI. When administered both prior and immediately following insult, brain injury was decreased by 78%. Administration after HI alone reduced damage by 41% (Jatana et al., 2006). NAC has been clinically used in one randomised trial for extreme lung disorder due to pre-mature birth. One hundred and ninety-four extreme low BW newborns received NAC by continuous infusion for the first 6days of life. Though no effect was seen on chronic lung disease, a 39% decrease in periventricular leukomalacia was observed in the treated group (Ahola et al., 2003).

Post injury treatment

Post injury therapies incorporate the use of neuronal stem cells in order to induce neurogenesis and astrocytes formation once HI induced cell death has already occurred. Although some endogenous regeneration mechanisms exist in the brain, these are only partially able to restore HI damage. Mesenchymal stem cells (MSC) are easily recoverable from bone marrow, placental tissue, umbilical cord stroma and blood without current ethical issue. MSC secrete trophic factors such as colony-inducing factor, VEGF, basic fibroblast growth factor, neural growth factor and bone-derived neurotrophic factor.

Neonatal rats, where MSC injected intracranially at 3-10days post insult, showed a reduction in histological damage and improved long-term behavioural outcome. In addition, P9 mice were subject to 10% oxygen for 45min before injection of bone-derived MSC into the ipsilateral hemisphere. At day 3, and day 21 post-insult the ipsilateral cortex exhibited BrdU positive proliferating cells. MSC increased neurogenesis and ODC production. Lesion size was significantly reduced in the dendrite gyrus at day 10 and in the cortex at day 21. Functional behaviour outcome was also markedly improved (van Velthoven et al., 2010).

Combined therapies

There is accumulating pre-clinical evidence that some of these therapies can be synergistic in the enhancement of neuroprotection by reduction of cell injury and

the encouragement of endogenous repair mechanisms. Most combined therapy studies focus on adjunctive therapies to hypothermia. As such, they are agents that also target secondary neuronal loss. These include xenon, melatonin and NAC.

Xenon and hypothermia synergy has been observed in both rodent and piglet models of neonatal HI. In rats, sub-therapeutic xenon (20%) and 33°C hypothermia were given at 4hr post insult for duration of 90min. Synergistic neuroprotection was observed via the attenuation of intrinsic apoptotic pathways. Combined treatment proved effective still when administered 10hr post insult. In addition, myocardial response was also protected (Ma et al., 2005). In a piglet study, 36 newborn piglets were recruited and placed into one of four treatment groups following transient cerebral HI: normothermia; normothermia plus 80% inhaled xenon for 24hr; 33.5°C hypothermia for 24hr; and hypothermia and inhaled xenon. Both hypothermia alone and the combined group showed decreased ratios of phosphocreatine to exchangeable phosphate pool compared to the other two groups (Faulkner et al., 2011).

The same group looked at hypothermia and melatonin. Here 17 newborn piglets were recruited and subject to either hypothermia (33.5°C) alone, maintained for 2-24hr post resuscitation, or to hypothermia plus iv injection of 5mg/kg/h melatonin for 10min-6hr post resuscitation. A second dose of melatonin was then given 24hr post resuscitation. Combined treatment gave an improved aEEG pattern as well as a significant reduction in lactate/NAA and lactate/creatine ratios in deep grey matter regions. The number of Tunel positive nuclei was decreased in the thalamus, hippocampus, internal capsule, putamen, and caudate compared to hypothermia alone (Robertson et al., 2013).

Addition of NAC to systemic cooling (30°C) reduced infarct volume and increased myelin expression 48hr in P7 rat HI. Behavioural outcome was additionally improved (Jatana et al., 2006). In a model of spinal cord ischemia, NAC or hypothermia alone did little to improve outcome. Combined therapy significantly increased spinal cord function (Cakir et al., 2003).

Hypothermia has been a recognised treatment for hypoxic ischemic encephalopathy since the 1940s after studies in the neonatal guinea pig model

showed significant increase in survivability after exposure to 10°C. Hypothermia is currently used in the clinic where it has proven to reduce cerebral damage as well as increase survivability. More recent studies have indicated that combining hypothermia with pharmacological agents, such as ameliorates, modulators of brain pH, or allopurinol- a xanthine-oxidase inhibitor may result in a reduction of damage and lesion size. In addition, xenon, an inert noble gas and NMDA inhibitor, in combination with hypothermia could potentially reduce damage further. There is the growing impression that optimum neuroprotection will involve the use of more than one therapy, targeting different parts of the neurotoxic cascade.

The mitogen activated protein kinases (MAPK) signalling cascade

The mitogen activated protein kinases (MAPK) are a complex group of serine-threonine kinases, serving as secondary messenger systems required to transduce extracellular signals from the cell surface throughout the cell to the nucleus. The MAPK cascade is tightly conserved from yeast to multicellular complex organisms. There are over 20 MAPK in mammalian cells, all of which receive and integrate upstream signals. Upon activation, MAPK regulate key cellular events in the cytoplasm by phosphorylation of membrane associated and cytoplasmic proteins and by interactions with other kinases and cytoskeletal elements. This response results in growth differentiation, inflammation or apoptosis depending on which MAPK is recruited. Specificity of response is determined by factors that affect the spacio-temporal activity of MAPK, such as the density and rate of internalisation of cell surface receptors, desensitisation of receptors and formation of scaffold complexes (Plotnikov et al., 2011).

Four major MAPK subfamilies have been identified, the C-Jun N-terminal Kinases (JNK) 1-3, the stress activated protein kinases (SAPK) p38 α, β, γ, and δ, extracellular signal-regulated kinases 1 and 2 (ERK1/2) and extracellular signal-regulated kinase 5 (ERK5). Each will respond to a plethora of signals and execute multiple cellular responses. ERK 3, 7, and 8 are recognised as MAPK-like molecules although their functions are not well understood. Activated kinases can act on a number of cytoplasmic substrates or translocate to the nucleus where they initiate the desired cellular response. MAPK nuclear targets are generally transcription factors and include ELK1, CMyc, protein kinases and C-JUN. Downstream targets include MAPK-activated protein kinases (MAPK-APK) including RSL 3 and 4, mitogen stress activated (MSK), MAPK interacting kinase (MNK) and MAPK-APK 3 and 5.

MAPK activation occurs through a canonical three to five tiered cascade of phosphorylation, as shown in figure 1.7. This originates from upstream signals, such as growth factors, stress, GPCR, and cytokine activation of sensors including RAS, RAP1, PKCs, and protein tyrosine kinases, leading to the phosphorylation of MAPK kinase kinases (MAP3K). These then phosphorylate MAPK kinases (MAP2K) which in turn phosphorylate the MAPKs themselves.

All MAPKs contain the signature activation sequence TXY where T- threonine, Y- tyrosine and X- glutamate, proline or glycine respective to ERK, JNK and P38. Phosphorylation of both threonine and tyrosine is essential for the activation of MAPK with phosphorylation of threonine having to precede that of tyrosine. Although the phosphorylation of both is required, they can have selective or overlapping substrates, and may be phosphorylated independently.

MAP3K is the most diverse stage of the cascade and includes A-, B-, and C-RAF, MOS, TPl2, TAK, DLK, MEKK 1-4, ASK, and map3k. The large presence of MAP3K implies that combinations of stimuli and cross over between the four pathways are required for optimal stimulation and tight regulation of the signal. The MAP2Ks are more conserved. MEK1 and 2 are selective for ERK 1/2, MKK 3, 4 and 6 for P38, MKK 4 and 7 for JNK, and MEK5 for ERK5. Another MAP2K was found- P43-MEK1b; however it is believed to be catalytically inactive (Bodart, 2010; Bogoyevitch and Court, 2004; Bogoyevitch et al., 2010).

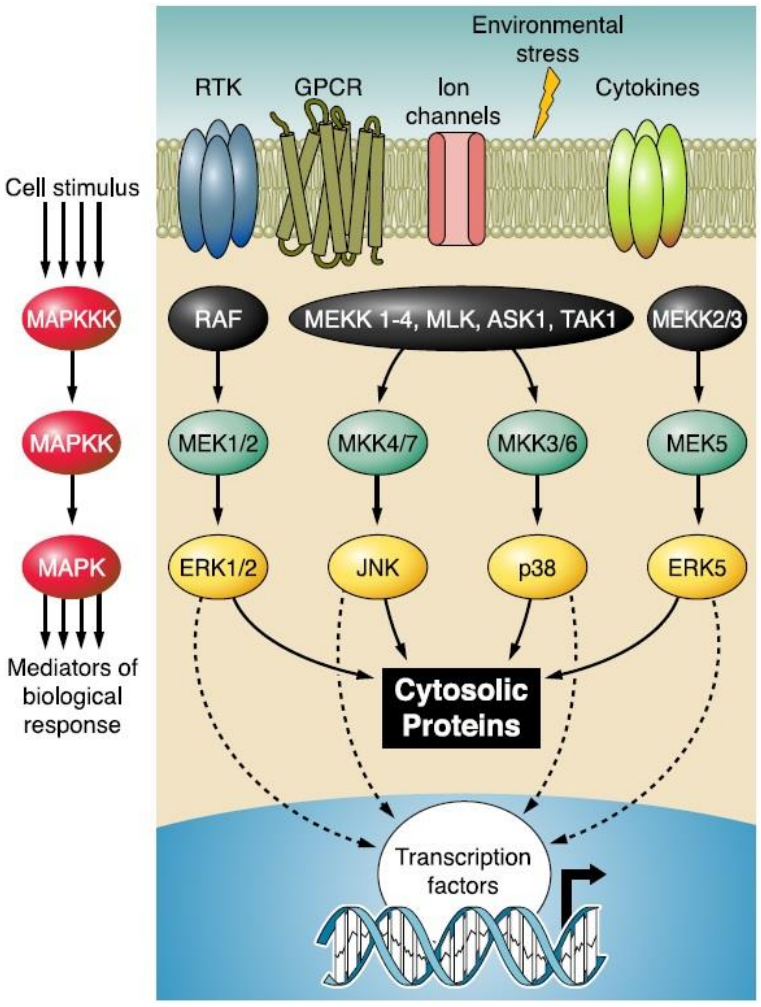

Figure 1.7 Serial activation cascade of mitogen-activated protein kinase (MAPK) signalling. MAPK are activated by canonical three-tiered phosphorylation events that transmit upstream signals from MAPKKK (MAP3K), through MAPKK (MAP2k) phosphorylation, leading ultimately to activate MAPK. Mammalian MAPK family consists of four sub-families. C-Jun N-terminal kinase (JNK), the stress activated protein kinase (SAPK) P38, and the extracellular signal-regulated kinases (ERK1/2) and ERK5. Multiple steps may exist between the cell stimulus and activation of the MAPKKK and between activation of the MAPK and the biological response. The effects include cell migration, proliferation, differentiation or apoptosis (Rose, 2010).

Proper signal specificity and faster kinetics for signal transmission is regulated by the recruitment of scaffold proteins. These are non-enzyme associated components, which bring together activators and their appropriate targets (Shaul and Seger, 2007; Weston and Davis, 2002). They also help the cascade to perform multiple functions in response to one or more stimuli. Scaffolds can prevent the dephosphorylation, and thus inactivation of MAPK, by binding to them directly. One example of this is kinase suppressor of Ras (KSR) which binds to MEK 1 and 2, leaving it constitutively active (Pouysségur and Lenormand, 2003).

For a substrate to bind and phosphorylate a MAPK, they interact first at specific docking domains present in the non-catalytic region of MAPK. These docking grooves are hydrophobic, negatively charged regions that recognise the MAPK docking, or D- motifs on the given substrate. D-motifs are positively charged amino acids followed by a hydrophobic residue and are usually located on the c-terminal upstream to the phosphorylation site (Tanoue et al., 2000).

Negative regulation or deactivation of MAPK occurs via the dephosphorylation of the TXY residues. This is controlled by tyrosine phosphatases and/or dual specificity MAPK phosphatases (DUSP) also known as MAPK phosphatases (MKP). There are 10 DUSPs, of which three regulate MAPK after injury: MKP1, MKP 5 and DUSP2 (also known as PAC1).

MKP1 anchors to the nucleus via its n-terminus and preferentially dephosphorylates P38 and JNK over ERK. Studies in MKP1 null mice showed that MKP1 is a negative regulator of TLRs after endotoxin stimulation. Here an increase in p38, JNK and cytotoxic cytokines occurs. Interestingly, MKP1 have a number of post-translational modifications that optimise its binding ability. These modifications are ERK dependent. MKP5 is found in both cytosol and nucleus and is also selective to P38 and JNK (Bermudez et al., 2010). After injury, its upregulation is associated to a decrease in AP-1 activity. DUSP2 is located in the nucleus. $DUSP^{-/-}$ cells had a decrease in inflammatory cytokine release, decreased ERK activation and increased JNK. Selective inhibition of JNK restored ERK expression in these cells (Jeffrey et al., 2006).

Crosstalk between ERK and JNK signalling pathways

ERK, JNK and P38 can all activate common downstream transcription factors. All four of C-Jun's phosphorylation sites can be directly, to a larger or lesser degree, targeted by ERK (Junttila et al., 2008). In addition, ERK can indirectly increase C-Jun activity. GSK3 and CK11 both phosphorylate thr239 at C-Jun's c-terminus, retaining it in a non-DNA binding state (Raivich, 2008). ERK activates P70 s6 kinase that in turn phosphorylates GSK at ser21. Deactivated GSK unbinds C-Jun and thus increases C-Jun's DNA binding activity (Leppä et al., 1998). Another indirect activation of C-Jun by ERK is through phosphorylation of the co-activator P300, which in turn acetylates lysine 268, 271 and 273 of the C-Jun base region (Vries et al., 2001; Wang et al., 2006). This forms a DNA binding complex, enhancing C-Jun's transduction function. C-Jun activity is only regulated by sustained, not transient ERK activity. During prolonged pERK expression, C-Jun transcription and stability is maintained via CREB and GSK3 activity. This results in C-Jun activation of RACK1 and cyclinD1. Negative crosstalk can also occur between JNK and ERK in TNFα stimulated cells. Here prolonged JNK activity causes the uncoupling of MEK from ERK in a C-Jun dependent manner (Nijboer et al., 2009).

MAPK in neonatal HI injury

Accumulating evidence suggests that all four subfamilies of MAPK cascades to associate to cerebral upregulation under hypoxic ischemic conditions. The relationship of MAPK to ischemic response started with studies in the heart and kidneys in the early 1990s (Armstead et al., 2008). Following HI, multiple stimuli of MAPK are released including growth factors, cytokines, glutamate and FR. Indirect activation and phosphorylation can occur due to ischemic loss of cell integrity and dysfunction (Irving and Bamford, 2002). Whether the activation of these pathways is due to cell loss or whether they actually regulate the mechanism underlying HI insult remains unknown.

ERK has shown a dichotomy of response to HI. It is upregulated in the ischemic core of HI lesions and co-expresses with markers of apoptosis. Inhibition of ERK has both resulted in a reduction of neuronal loss and a prevention of BDNF induced neuronal survival (Almeida et al., 2005). The JNK and P38

pathways are weakly activated by mitogens but are strongly upregulated by stress stimuli. LPS and cytokines IL-1 and TNFα result in the altered transcription, translation and activation of JNK and P38 (Hambleton et al., 1996). JNK inhibition after HI results in reduced neuronal death in by the prevention of AP-1 assembly. However variable differences in infarct volume were seen in neonatal models of HI (Ferrer et al., 2003).

Owing to their extensive control over normal cell function, the MAPK kinases have a potential role in the induction of cell death resulting from hypoxic conditions. This study focuses on two of the major MAPK pathways: ERK 1 and 2, and JNK. Both are upregulated following neonatal HI in animal models. However, whether they are neuroprotective remains unclear, as does their cell specific actions. This study aims to elucidate the answer to these questions.

Extracellular signal-regulated kinases (ERK) 1 and 2

ERK 1/2 is essential for cell growth via nucleotide synthesis, activation of gene transcription via transcription factors including CREB and ELK1 and chromatin phosphorylation, protein synthesis, and the formation of cyclinD (CDK4) which rate limits cell growth (Lu and Xu, 2006). The multiplicity of this cascade's substrates includes transcription factors, protein kinases, cytoskeletal elements and regulators of apoptosis.

Extracellular stimuli such as growth factors, hormones and neurotransmitters interact with complimentary receptors in the target cell membrane. The activation of receptor linked tyrosine kinases through extracellular mitogens stimulates signal transduction through the G-protein complex Ras that activates downstream Raf. MEK 1/2, a dual specificity kinase, is consequently upregulated-phosphorylating ERK 1/2. Upstream activation steps of ERK have few substrates, whereas ERK itself will phosphorylate a diverse amount, over 200, of substrates at serine (ser) and threonine (thr) residues. These targets are present in all cell compartments including the plasma membrane, cytosol, organelles and nucleus (Mebratu and Tesfaigzi, 2009; Nishimoto and Nishida, 2006; Roskoski, 2012). The spacio-temporal activation of ERK dictates which substrate it will phosphorylate and as such the biological outcome.

ERK1, or mapk p44, was the first to be cloned in 1991, purified as a 43kDa insulin-stimulated MAP2 (microtubule associated protein 2). It genetically relates most to two yeast kinases- Kss1 and Fus3 that are regulators of cell cycle. ERK2, mapk p42, was subsequently cloned 2years later by the same group (Boulton et al., 1991). It is a 42.1kDa protein with fewer residues at the N-terminus preceding the catalytic domain. ERK1 and 2 are co-expressed in virtually all tissue. Their relative abundance is highly variable between locations. In the brain, ERK2 is the most abundant. They have extensive amino acid identity (84%) between them, as well as spacio-temporal regulation (Vantaggiato et al., 2006). As such, the general viewpoint is one of them being functionally identical. ERK 5 (or Big MAPK) is the next nearest kinase with 67% identity of the C-terminal amino acid sequence. Though its N-terminal contains the TEY motif of ERK 1 and 2, ERK 5 is phosphorylated by MEK 5 and not MEK 1/2 (Nishimoto and Nishida, 2006).

ERK1 and 2 are essential for mesoderm formation. ERK2 and MEK1 are particularly required for embryonic development. Null mice for either kinase are embryonically lethal at E11.4-E13 due to placental and mesodermal defects. In contrast, ERK1 and MEK2 mice are fully viable suggesting redundancy of function between them. Some studies show an opposing role of ERK 1 and 2 after Ras signalling, where ERK1 antagonises ERK2 signalling. In fibroblasts and neurons from ERK1 KO mice, stimulus activation of ERK2 was 2fold higher than in WT cells (Lefloch et al., 2008), with an additional increase of early transcription factors and proliferation. Initially these experiments led to ERK2 being thought of as the sole contributor to cell proliferation. However, when ERK2 expression is reduced, ERK1 can functionally compensate.

The kinetics of ERK activation is biphasic with a rapid and transient burst of immediate activity by phosphorylation at the thr and tyrosine (Tyr) residues of the TXY motif. For ERK1 this is thr202, glu203, tyr204, and for ERK2 it is thr183, glu184, tyr185 (where glu is glutamate). Following is a second more stable activation that can last for hours (Bromberg-White et al., 2012). Non-mitogen stimulation results in transient ERK phosphorylation, less than 15min, which is not long enough for entry to cell cycle. Mitogenic stimuli will induce cell proliferation by long-term (more than 6hr) activation of ERK.

Scaffold proteins ensure spacio-temporal fidelity. Inactive ERK and MEK will interact with each other either directly or via scaffold proteins at protein-interaction motifs. MEK contains a basic and hydrophobic D-motif within the N-terminus. ERK has multiple binding sites, including a CRS/CD domain; N-terminal domain; kinase insert domain; and the presence of residues at the C-terminus whose phosphorylation incites conformational change to enhance ERKs catalytic activity. The detachment of ERK from MEK leads to independent translocation of both to the nucleus. ERK remains here between minutes and hours whereas MEK rapidly moves back to the cytosol via the nuclear export domain in its N-terminal. Duration and intensity of response is also partially due to the compartmentalisation of signal molecules. For example, growth factors promote the nuclear accumulation and persistent activation of ERK1 and 2. This retention relies on the synthesis of short-term nuclear anchoring proteins (Roberts and Der, 2007). As such, the nucleus represents the site for ERK activation, accumulation, and signal termination.

Whilst phosphorylated ERK (pERK) has an established role in proliferation, differentiation and cell cycle progression, its function in cell survival or, on the contrary, cell death is still a matter of controversy.

A number of studies have shown that the greatest discrepancy between ERK 1 and 2 expressions occurs in the brain and spinal cord (Chung et al., 2005; Di Benedetto et al., 2007; Nadjar et al., 2005; Ortiz et al., 1995). Some regions show very little ERK1 to ERK2, 13 times less in the superficial cortex for example, whereas in others they are more on par. There is an apparent rostral-caudal gradient of ERK1 to ERK2 relative expression (See figure 1.8). In each region the levels of phosphorylated ERK1 and 2 match the relative abundance of inactive protein (Ortiz et al., 1995). This selective expression of ERK in the CNS suggests a role in function and adaptive response. Studies in regeneration of the nigro-striatal pathway saw that increased neuronal firing was associated with elevated ERK activity. In addition, ERK1 and 2 are phosphorylated in the hippocampus after electroconvulsive shock-induced seizures. Isolation of the hippocampal neurons showed that pERK was the result of EGF and glutamate release (Chen et al., 2009).

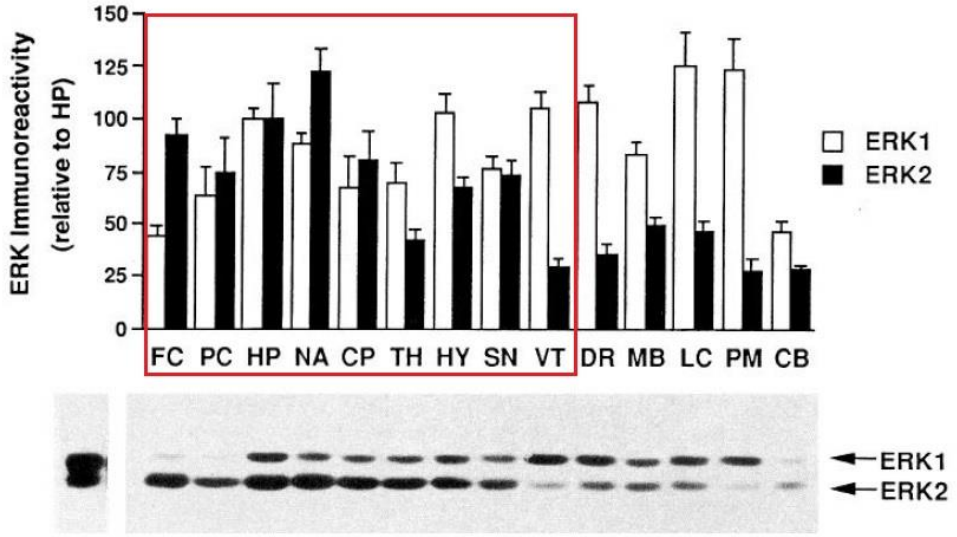

Figure 1.8 Regional distributions of ERK l and ERK 2 in rat brain. FC, frontal cortex; PC, parietal cortex; HP, hippocampus; NA, nucleus accumbens; CP, caudate/putamen; TH, thalamus HY, hypothalamus; SN, substantia nigra; VT, ventral tegmental area; DR, dorsal raphe; MB, midbrain; LC, locus coeruleus; PM, pans/medulla; CB, cerebellum. Outlined areas encompass the regions of the forebrain. (Ortiz et al. 1995)

ERK expression however is not limited to the neurons, as it is also present in microglia and astrocytes. Using co-immunofluorescence with cell specific markers, a model of spinal nerve ligation and inflammation indicated a sequential activation of ERK in these cells. Immediately after insult, 93% of all cells expressing ERK were neurons. By 48hr, only 3% of expressing cells were neurons, whereas 93% were microglia and 3% were astrocytes. At 21days: 2% were neurons, 16% microglia and 76% were astrocytes. In this model, both pERK1 and pERK2 were upregulated in equal measure. Within the cell compartments, ERK1 and ERK2 were highest in the nuclear and mitochondria, both in the outer membrane and intramembrane space, fractions. Expression of ERK1 and ERK2 did not change, indicating that the presence of ERK in the mitochondria was not due to cytosolic movement (Zhuang et al., 2005). As such, it is theorised that ERK can be downstream from ROS but upstream from mitochondria dysfunction in stress conditions.

Role of ERK 1 and 2 in cell death

Several groups have identified ERK as having opposing roles in protection against cell injury and in the instigation of cell death signalling. The first implication of ERK in cell death was in vitro ODC cultures. On stimulation with

peroxide ERK, JNK, and P38 were all activated (Bhat and Zhang, 1999). The ensuing cell death was prevented by treatment with the MEK 1/2 inhibitor PD98059, whereas inhibition of JNK or P38 showed no difference. In the same cells, glutamate induced cell death was also attenuated with an analogue of PD98059- UO126 (de Bernardo et al., 2004). Here glutathione depletion was replenished, and ROS activated ERK prevented. In a mouse macrophage line, ERK inhibition was associated with increased survival and diminished necrotic cell death but no change in caspase expression or DNA fragmentation. In addition, CA^{2+} inhibitors attenuated pERK, mitochondrial depolarisation and caspase activation. In contrast, cadmium cell toxicity was unaffected by the inhibitors (Martin and Pognonec, 2010). In untreated cells, ROS activity resulted in activation of RAS and degradation of DKP3 resulting in sustained ERK activity suggesting a role in protection.

In HT22 cells, dominant negative MEK1 decreased glutathione depletion-induced cell death via the inactivation of transient pERK. Equally when this initial pERK was blocked with mGLUR1 antagonists, the cells became more sensitive to sub-threshold glutamate. Constitutively active ERK2 showed no effect (Luo and DeFranco, 2006). Transient ERK activation by insulin-like growth factor (ILGF) 1 prevented its own sustained activation in cerebellum granular neurons. These studies indicate that the biphasic pattern of ERK response dictates when it is pro-survival or pro-death. Transient activation is associated with pro-survival, whereas sustained activity results in cell death by a ROS dependent manner (Anastassiadis et al., 2013).

Oxidants induce phosphorylation of ERK through Ca^{2+} channel activation or directly via Src-tyrosine kinase. Sustained ERK translocates to the nucleus where it can promote cell death via its regulation of transcription factors. Whether ERK directly incites cell death pathways or regulates pro-death gene expression profiles remains undefined. However, the nuclear location of ERK suggests the latter (Shaul and Seger, 2007). When ERK returns to the cytosol neuronal cell death does not occur (Chen et al., 2009). This too can be contended as, in non-neuronal cells, cytoplasmic retention of ERK is required for death-associated protein kinase (DAPK) activation via phosphorylation at ser735 (Cagnol and Chambard, 2010). NO produced by iNOS in macrophages

will initiate apoptosis following traumatic spinal cord injury. Both an increase in pERK and pro-inflammatory cytokines occurred. Inhibition of ERK reduced IL-1 and was protective in cortical neurons. Cytoplasmic ERK 1/2 was seen in microglia adjacent to injury. Inhibition of ERK reduced neuronal loss at the site of lesions. However, ERK inhibition was not completely neuroprotective, possibly due to its duality of roles in survival in neurons (Xu et al., 2006). Cytosolic retention of ERK denies access for transcription factor substrates that are responsible for mitogenic response. This potentiates the catalytic activity of some pro-apoptotic proteins including DAPK. PEA-15 and SEF are MEK specific scaffold proteins that reside in the Golgi of astrocytes. They preferentially complex ERK to cytoplasmic substrates over nuclear due to their nuclear export sequence. When bound to ERK, nuclear Elk1/C-Fos/IL-1 activation is attenuated (Jiang et al., 2002). Separating ERKs activity in a cell specific manner would lead to greater understanding on the therapeutic benefit of ERK inhibition after injury.

ERK can participate in both the intrinsic and extrinsic pathways of apoptotic cell death via the increase of mitochondria CTC release, caspase 8 activation, cell cycle arrest, or autophagic vacuolisation. This is illustrated in figure 1.9. All are associated with sustained pERK in specific subcellular compartments (Castro-Obregón et al., 2004; Chu et al., 2004). Compartmentalised activity is regulated by DUSP-2,-4 and -6 all of which provide negative feedback loops to prevent Ras/Raf/ERK signalling. In tumour cell lines B-Raf promotes cell survival by activation of anti-apoptotic BclxL, Mcl-1 and Bcl-2 which in turn inhibit Bad and BIM (Luca et al., 2012). ERK will upregulate Caspase 8, via DAPK, by interacting with the death receptor ligands-TNFα, FAS and FASL. Cytoplasmic ERK activates FOXO3a which induces apoptosis via Bim and FASL (Tran et al., 2001). ERK can directly activate RSK, which translocates to the nucleus where it phosphorylates BAD. ERK can also mediate the upregulation of P53 by direct phosphorylation at ser15 or by phosphorylation of CMyc at ser62. This in turn activates P53 (Persons et al., 2000; Sawe et al., 2008). In Hela and renal cells, inhibition of ERK prevents mitochondrial depolarisation, CTC release and subsequent caspase 3 activation. Interestingly ERK inhibition prevented caspase3 activation independently of CTC release suggesting it can have a

downstream role to CTC. Bax expression was also reduced (Whelan et al., 2012).

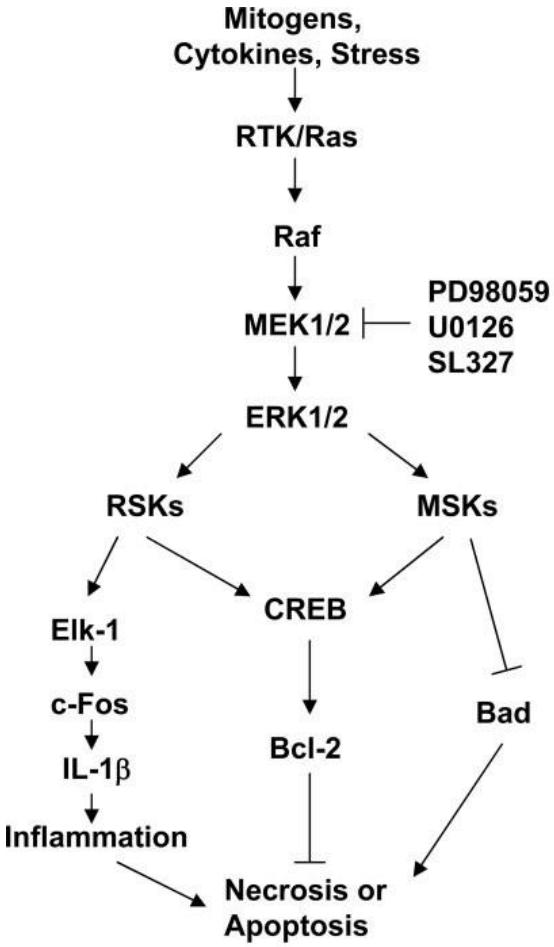

Figure 1.9 Diagram showing the primary elements of the ERK pathway involved in ischemic stroke. ERK activity may exaggerate inflammation by up-regulating interleukin 1b thus leading to necrosis. ERK activity may also block apoptosis by enhancing the level of the anti-apoptotic protein Bcl-2 or blocking the pro-apoptotic protein Bad. RTK, receptor tyrosine kinase; MEK, MAPK kinase; PD 98059, U0126, and SL 327, MEK inhibitors; ERK, extracellular-regulated kinase; RSK, p90 ribosomal S6 kinase; MSK, mitogen-and stress-activated kinases; CREB, cAMP-response element binding protein; Elk-1, ets-like gene-1; IL-1b, interleukin-1b. Reproduced with permission (Sawe et al. 2008).

Implication of ERK 1 and 2 in HI insult

In vitro studies show that both immature neuronal cultures and HT22 cells, subject to oxidative stress, were protected from cell death with the addition of MEK inhibitors. These cells lack NMDA receptors resulting in glutathione depletion via glutamate action on co-transporters (Luo and DeFranco, 2006). In mixed neuron and glia cell culture, PD98059 and UO126 both reduced NO induced cell death following glutathione withdrawal. Increased pERK was seen to near exclusively co-label with astrocytes. On removal of astrocytes, neurons recovered from NO associated injury. NO initiated the nuclear translocation of

ERK in astrocytes, glia and ODC progenitors (Stanciu, 2000). In vivo, inhibition of tyrosine phosphorylation during cerebral ischemia in adult rats resulted in decreased release of excitotoxic amino acid and neurotransmitter release. ERKs ability to phosphorylate tyrosine aids glutamate and aspartate release as well as the activation of cytosolic phospholipase A_2 ($cPLA_2$). In $cPLA_2^{-/-}$ mice, a reduction in infarct volume is observed following focal ischemia (Saluja et al., 1999). Other studies of adult rat focal cerebral and global ischemia show that SOD protects against ROS induced neuronal death by the prevention of CTC release from mitochondria. Phosphorylated ERK co-localised with cells producing ROS. Expression of pERK was reduced in SOD1 tg (over expression of SOD1) mice compared to WT controls. O_2^- production was similarly decreased. SOD1 actions on ERK are via the P13K/AKT pathway (Noshita et al., 2002). ERK has also been implicated in models of Alzheimer's disease where tau hyper-phosphorylation and subsequent neuronal loss is regulated by ERK (Krägeloh-Mann et al., 2002; Pei et al., 2002).

Alessandrini et al. were the first to look at ERK inhibition in adult mouse model of asphyxia. In mice subject to middle cerebral artery occlusion, PD98059 was applied 30min prior to insult. A 55% reduction in infarct was observed at 24hr and 36% at 72hr post insult, compared to untreated littermate controls. In untreated mice, pERK is immediately and transiently upregulated in cortical neurons following occlusion with a constant increase up to 2hr post insult. Neuroprotection by PD98059 was accompanied by a reduction in neurobehavioral defects. In addition, PD98059 had no adverse effects on respiratory or cardiovascular parameters, temperature or pH (Alessandrini et al., 1999). Using the same model, other groups have shown that neurokinin receptor antagonists gave a decrease in infarct and an increase in functional recovery. These actions were mediated by preventing ERK activation of the orphan nuclear receptor NUR77, also called NGF-1B, which in turn modulates neurokinin receptor activity. NUR77 can also act as a transcription factor in the nucleus or translocates to the mitochondria where it incites CTC release and upregulation of pro-apoptotic Bax and caspase 3 (Castro-Obregón et al., 2004). Alessandrini's group also looked at an adult gerbil model of ischemia, specifically at reperfusion following HI. During reperfusion, an increase in pERK2 was observed in the hippocampus. An IV injection of UO126 protected

the hippocampus from ischemic damage, with a decrease in infarct seen 3hr post insult. In mice, UO126 pre-treatment decreased infarct by 42% at 24hr and improved neurobehavioral outcome. When injected 1hr post insult, UO126 was still neuroprotective. However, injection at 3hr post insult showed no significant effect. Another group introduced UO126 10min prior to reperfusion following 3hr middle cerebral artery occlusion. Infarct was reduced by 41% at 24hr post insult. In addition, they confirmed that pERK 2 was reduced by 27% and total pERK by 90% (Namura et al., 2001).

In the neonatal rat model, pERK positive neurons were seen at 8hr, 24hr and 72hr post insult. These were located at the core of infarct and at the border zones to undamaged tissue. PERK positive border cells showed signs of DNA damage and calpain induced fodrin degradation. By 72hr, pERK was also observed in microglia at the border zones and in astrocytes and ODC within the white matter of both hemispheres (Wang et al., 2004a). In P7 Mice, intracerebroventricular administration of BDNF gave a rapid increase in pERK and in P13K/AKT. When ERK, but not P13k/AKT, was inhibited; BDNF mediated neuroprotection was lost. In this model, pERK is near exclusively nuclear bound and expression was localised to the cortex, subventricular zone, dendrite gyrus and thalamus. In untreated mice, 8hr after HI, pERK expressing neurons were smaller and condensed compared to non-expressing neurons. By 14hr, these cells were pyknotic. At 48hr, 40% of pERK expressing cells were microglia (Han and Holtzman, 2000).

Lastly, one study has suggested that ERK could contribute to neuroprotective effect of hypothermia in treatment of ischemic insult. In adult rats subject to mild post-ischemia hypothermia (33°C) an increase in pERK and decrease in pJNK is observed. Increased pERK corresponded to an increase in BDNF and tyrosine phosphorylation of the growth factor receptor TrkB (D'Cruz et al., 2005).

C-Jun N-terminal kinases (JNK) 1-3

The JNK proteins are an evolutionary conserved subfamily of the MAP kinases. JNK/C-Jun signalling is initiated through a number of extracellular stimuli including growth factors, inflammatory cytokines, UV radiation, and oncogenic

stress. Their major downstream target is AP-1, mediated by the phosphorylation of C-Jun. JNK, also known as SAPK was first described in the early 1990's. These early discoveries identified three mammalian JNK genes: JNK 1-3, also named SAPK γ, α, and β respectively. These three loci have multiple isoforms due to alternative splicing (Weston and Davis, 2002). Dual phosphorylation at tyr and thr residues of the TXY motif is required for full activation of JNK. The downstream convergence point for all three JNKs is C-Jun. Following JNK phosphorylation, C-Jun is activated as an immediate early gene (IEG) following cell injury. IEGs encode for transcription factors that are important in signal transduction. They include C-Jun, C-Fos, JunB, knox-20, and zif-268 (Bogoyevitch et al., 2010; Herdegen et al., 1997).

In 1987, Lee et al. found a DNA binding protein that was able to initiate gene transcription and named it activation protein 1 (AP-1). The encoded gene was not identified at that time. AP-1 has the binding sequence TGA (C/Q) TCA. This was found to be the identical site of a yeast protein GCN4 (Lee et al., 1987). Also in 1987, Maki et al. cloned the Jun oncogene from avian sarcoma virus 17. Jun showed sequence homology to GCN4; as such AP-1 was concluded to be Jun (Maki et al., 1987). After these discoveries, several DNA binding proteins, including Jun and FOS were found to contain a protein dimerisation domain- the leucine zipper domain. Other members of these basic zipper families of transcription factors are JunB and JunD of the Jun family, and FosB, Fra1 and Fra2 of the Fos family (Raivich, 2008). Dimerisation of C-Jun is essential for its DNA binding. C-Jun can form either hetero or homodimers whereas FOS can only form heterodimers. The heterodimerization partner C-Jun gets can determine the DNA binding specificity. JNK has just over 50 substrates that regulate various processes from cell death to movement. Two features underlie JNK substrate recognition: firstly, JNK are proline directed serine/threonine kinases; and secondly, substrate interaction occurs at defined JNK binding motifs that connect to the CD docking site in JNKs c-terminal (Wagner and Nebreda, 2009; Weston and Davis, 2002).

JNK 1 and 2 are ubiquitously expressed throughout the body whereas JNK 3 is restricted to neural and cardiac cells. JNKs 1-3 are activated by the MAP2Ks MKK 4 and 7, which phosphorylate JNKs T-loop. Upstream to MKK 4 and 7 are

multiple MAP3Ks including MEKK 1-4, apoptosis signal related kinases (ASK) 1 and 2, and mixed lineage kinases (MLK) 2 and 3. Signal specificity is mediated through scaffold proteins. JNK interacting protein (JIP) provides a scaffold for the MLK3/MKK2/JNK1 complex after excitotoxic stress in neurons, resulting in C-Jun activation (Centeno et al., 2007).

Some MAP3Ks can act as scaffolds too- MEKK2 mediates the complex formation of MEKK2/MKK7/JNK1. Following JNK phosphorylation, activation and nuclear localisation occurs of a host of transcription factors such as C-Jun, JunD, ATF3, P311, SOX11, and stat3. In addition, there is a deregulation of islet-1, ATF2 and NF-κB (Bogoyevitch et al., 2010). JNK binds to C-Jun at a delta-docking domain present in C-Jun's N-terminus (figure 1.10). From here JNK then phosphorylates C-Jun at ser63, plus ser73, and thr91 and 93 in the N-terminal in the transduction domain (Morton et al., 2003; Vries et al., 2001).

Phosphorylation of C-Jun results in its dimerization and therefore activation of transcription factor complexes, allowing them to bind to specific DNA sequences. These target DNA sequences are the 12-O-tetradecanoylphorbol-13-acetate (TPA) Response Elements, otherwise known as the TRE and consists of the palindromic sequence 5' –TGAGCTCA – 3'. Once bound, AP-1 acts as transcriptional regulator of target genes downstream to the TRE such as those involved in cell proliferation, death and survival. The AP-1 transcription complex is a well-characterised regulator of neural development. It consists of either homo- or heterodimer complexes between Jun, C-Fos, or ATF/CREB family members (Dérijard et al., 1994; Raivich et al., 2004). Deactivation of C-Jun occurs via dephosphorylation of thr239 leading to ubiquitination and degradation or via C-terminal lysine acetylation near amino acids 257-276 (figure 1.10) (Raivich, 2008; Vries et al., 2001).

JNK1, 2, and 3 knockout mice are all viable with no obvious phenotypes. However, JNK1 and 2 double mutants are lethal at embryonic day 11.5 due to defects in neural tube closure. Double mutants with JNK 3 were still viable with normal phenotype. C-Jun null mice are lethal between E10.5-15.5 (Davies and Tournier, 2012; Kuan et al., 2003; Pirianov et al., 2007). So as to study C-Jun's role in injury, a functional KO was created. JunAA have ser63 and 73 converted into alanine, preventing their phosphorylation by JNK. These mice were both

viable and had no developmental defects. In kainate induced excitotoxicity, JunAA mice had greater neuroprotection then WT controls, that was on par with JNK $3^{-/-}$ mice (Behrens et al., 1999). It may be that removal of all four phosphorylation sites (ser63 and 73, and thr91 and 93) will produce even greater neuroprotection (Aguilera et al., 2011).

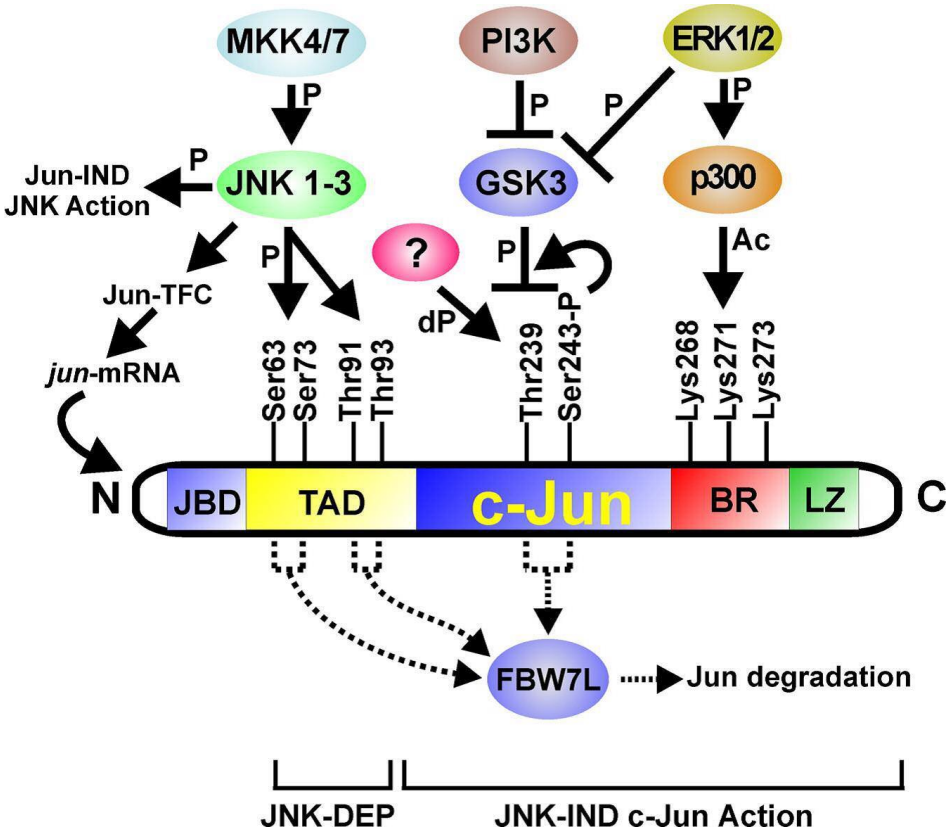

Figure 1.10 An overview of key pathways involved in C-Jun activation. N-terminal phosphorylation via JNK, GSK3 phosphorylation of Thr 239 and p300 acetylation of lysine residues along the C-terminal provide the major routes of C-Jun induction. (Raivich 2008)

JNK1 and 2 can have opposing roles. In MEF cultures, JNK1 phosphorylates C-Jun to increase proliferation, whereas JNK2 phosphorylated C-Jun resulting in cell degradation via a negative feedback loop (Dérijard et al., 1994). Targeted disruption of JNK3 protects neurons from excitotoxic injury, whereas inhibition of JNK1 and 2 gave no effect (Kuan et al., 2003). There is also evidence that JNK can localise to the mitochondria and microtubules in addition to its role in regulating nuclear gene expression (Zhao and Herdegen, 2009). In the mitochondria, JNK can be pro-survival through the phosphorylation, and subsequent deactivation of Smac/Diablo (Hagberg et al., 2009). Although JNK and C-Jun evidence multiple roles in cellular response to insult, there are still many outstanding questions on the function and regulation of its signalling.

Studies using target gene deletion or pharmaceutical inhibition show a three-part role of C-Jun in neural degeneration, inflammation and repair. In the nervous system, JNK/C-Jun signalling is mostly associated with regulation of apoptosis. C-Jun mediates apoptosis through the upregulation of FASL and pro-apoptotic Bcl-2 members: BIM and dp5 (Kuan et al., 2003). Previous work in our laboratory has shown that neuron specific deletion of C-Jun strongly reduces the speed of axonal regeneration and target re-innervation following facial nerve axotomy in the adult mouse. Here a decrease in gene expression occurred in conjunction to a loss of trophic support by BDNF, GDNF and GAP43. A local application of the trophic factors BDNF and artemin recovered regeneration defect (Fontana et al., 2012). In this same model, complete neuronal JNK knockout saw a decrease in caspase dependent neuronal cell death. JNK1$^{-/-}$ and JNK3$^{-/-}$ mice had delayed functional recovery, whereas JNK 2$^{-/-}$ saw no effect. In sympathetic neurons, dominant negative C-Jun mutants show an attenuation of AP-1 activity and apoptosis following extreme nerve trauma (Raivich et al., 2004; Ruff et al., 2012). In addition, recruitment of lymphocytes and activation of local microglia was reduced. Dominant negative C-Jun attenuates cell death in PC12 cell cultures that occurs due to NGF withdrawal. Conversely, MEFs with C-Jun ablation were unable to avoid apoptosis under UV stress. Here, an increase in P53 and P21 led to cell cycle arrest (Dérijard et al., 1994; Herdegen et al., 1998).

C-Jun is implicated in mediating the cells response to pro-inflammatory cytokines such as TNFα and IL-1β. Cytokine receptor activation results in the prolonged induction of C-Jun expression and AP-1 activity. TNF receptor recruits FADD and TRAF2 to initiate apoptosis in association to increased C-Jun and c-fos. Interestingly, cells treated with TNF saw an activation of MKK7 but not 4 (Adiseshaiah et al., 2006). Phosphorylation of C-Jun by JNK 3 triggers the transcription of death genes including BIM, TNFR and FAS. NGF withdrawal incites BIM$_{\varepsilon L}$ expression that in turn causes Bax-induced release of CTC from mitochondria (Hidding et al., 2002; Kaminska et al., 2009). In addition, studies in Hela cells have shown that JNK can activate caspase 8 independent of the cleavage of Bid into J-Bid, this results in the preferential release of Smac/Diablo over CTC from the mitochondria (Deng et al., 2003a). JNK can also be a regulator of autophagy. JNK inhibition sees a decrease in the formation of

autophagosomes via the post-translational modification of Bcl2. JNK 1 mediates Bcl2 phosphorylation by interfering with its binding to the pro-autophagy protein beclin-1 (Wang et al., 2012a). This disassociate of beclin-1 is an initiator of autophagy.

JNK/C-Jun signalling in HI injury

JNK activation precedes cell death in multiple cell types including neurons. Increased activation of JNK is observed in brain following ischemic stress. C-Jun is consequently rapidly phosphorylated. JNK is believed to mediate NMDA induced excitotoxicity during cerebral ischemia (Pirianov et al., 2007). JNK $3^{-/-}$ mice were resistant to ischemic apoptosis and to dopaminergic neuronal loss after MPTP treatment (Pan et al., 2009). C-Jun activation is linked to a loss of neurons in ALS, Alzheimer's and Parkinson's disease (Brecht et al., 2005). However, the role of JNK and C-Jun in neonatal brain injury is still to be established.

The neonatal brain shows increased susceptibility to HI damage due to presence of immature and thus vulnerable ODC precursor cells. JNK upregulation is seen in ODC precursors after apoptotic stimuli in addition the immature brain has a seven fold increase in C-Jun expression and a distinct pattern of JNK activation compared to the adult brain (Wang et al., 2012a). In neonatal rats, upregulation of C-Jun and C-Fos occurs in the striatum, cortex and hippocampus following HI insult. In a model of mild HI in the neonatal gerbil, a modest yet prolonged activation of C-Jun and AP-1 binding was observed in both the striatum and thalamus (Sommer et al., 1995). Strong C-Jun immunoreactivity co-labelled with apoptotic but not necrotic cells following HI and focal ischemia in P9 rats (Akaji et al., 2003; Ginet et al., 2009).

Targeting JNK in cerebral ischemia has so far been done by the use of small peptide inhibitors. JIP-1 derived JNK inhibitory peptide- D-JNKi is a powerful inhibitor of JNK. It consists of 31 D-amino acids giving it increased protease resistance. L-JNKi is the L-form equivalent. Both have shown neuroprotection in vitro studies of excitotoxicity and in vivo models of cerebral hypoxia-ischemia. D-JNKi penetrates both normal and ischemic brain regions by use of a FITC tag

(Repici et al., 2007; Zhao et al., 2012). Although D-JNKi shows efficacy in improving outcome, it failed to reduce infarct volume, despite a decrease in the activation of pro-death proteases, calpain and caspase 3 (Ginet et al., 2009). In both adult and juvenile (P16) rats, D-JNKi gave a reduction in injury following 10% oxygen. Neither MKK 4 and MKK 7 or C-Jun activity was affected in these mice. C-Jun was rapidly upregulated following insult in both treated and untreated groups, suggesting that in these models C-Jun activation can be independent of JNK (Repici et al., 2009).

In one neonatal rat model, D-JNKi reduced calpain activation at 6hr and caspase and autophagosome production at 24hr. However lesion size was unchanged (Ginet et al., 2009). Another group, also using the neonatal rat, saw that L-JNKi's inhibition of JNK and subsequent AP-1 activity resulted in a decrease of neuronal death. In this model, AP-1 activity immediately increased after insult, and peaks at 3-6hr. injection of L-JNKi straight after injury completely ablated AP-1 expression. When L-JNKi was injected within 3hr of injury, infarct volume was reduced by 30%. No change in cytokine expression was seen, caspase 3 and Smac/Diablo were decreased. At 14weeks post insult, both white matter and grey matter damage had a 50% reduction in the treated animals versus non-treated littermates. L-JNKi injection at 6hr post insult saw a loss of its neuroprotective effects (Nijboer et al., 2010). This same group re-visited D-JNKi activity when injected immediately after HI in P7 rats. They saw an 85% reduction of damage with a therapeutic window of 6hr. In addition, cognitive and motor function was restored at 9weeks post-insult. D-JNKi attenuated the phosphorylation of nuclear C-Jun and AP-1 activity as well as cytokine production at both 3hr and 24hr after HI. Nuclear C-Jun is activated by cytosolic or nuclear JNK phosphorylation. Surprisingly, neither nuclear, nor cytosolic JNK was upregulated in the untreated group following HI. However mitochondrion JNK was. This increase in mitochondria JNK was completely blocked by D-JNKi, preventing the ability for Bcl-2 and BclxL to be upregulated. Neuroprotection was lost when a double injection of D-JNKi was given at 0hr plus 3hr, whilst administration at either time point was still effective. Using a mitochondrial JNK specific inhibitor- Sabkini at 0hr post HI, a 55% reduction in damage was observed throughout the ipsilateral hemisphere. In addition, cytokine mRNA expression saw a decrease in the levels of TNFα, IL-1β, IL-8

and MIP2 (Nijboer et al., 2013)). The therapeutic potential of commercially available D-JNKi is very promising. D-JNKi treatment associates to the preservation of mitochondria integrity, evidenced by the prevention of HI induced ATP depletion, reduction of ROS production and cytosolic translocation of mitochondria proteins.

To summarise, while there is evidence for the therapeutic potential of ERK1/2 and/or JNK inhibition, there are also reasons to expect that blocking these MAPK could be detrimental. Different levels and temporal patterns of expression suggest that there might be a therapeutic window where inhibition could be beneficial while outside this window it could be of no effect or even harmful. If it were possible to localize and optimize the levels of inhibition and to target the therapeutic window, pro-death effects of pERK and JNK post-HI could be diminished, significantly improving the outcomes.

Project Aims

As outlined, all four major branches of the MAP kinase-signalling cascade are implicated in the neonatal brain response to ischemic injury. Transcription factors often act as the driving forces of regeneration, regulating the expression of a complex web of target genes simultaneously. This thesis aims to investigate the likely role of two MAPK family members: ERK1 and 2, and C-Jun in promoting neuronal survival after hypoxic-ischemic insult to the postnatal day 7 (P7) mouse brain in vivo. Both molecules are known to be strongly and immediately upregulated following injury with sustained activation correlating to severity of insult. Given the time constraints to conduct this study, in addition to the already extensive literature on in neonatal HI, we will not be considering the role of P38 in our model at this time. Cell-type specific deletions of the individual genes will be used to characterise the unambiguous roles of these molecules in HI response.

The work will be undertaken in the Rice-Vannucci neonatal mouse paradigm - a reliable and highly reproducible model of HI insult equivalent, in respect to regional damage observed, to term human infants. It enabled assessment of the effects on the non-neuronal cell (microglia and astrocyte) activation and recruitment to areas of damage, cellular response and neuronal survival, resulting from conditional alteration of these proteins.

Extracellular Signal-Related Kinase

Specifically, MEK-dependent inhibition of ERK phosphorylation and ensuing activation protects against cell damage resulting from focal cerebral ischemia. Preliminary studies in our group present several lines of evidence in favour of MEK and ERK involvement in neonatal hypoxic ischemic insult. Neuronal over expression of Ras resulted in increased damage 48hr following 30min exposure to 8% O_2 (Appendix 2A-C). In addition, a dominant negative isoform of MEK1 (DN MEK), with a neuron-specific tubulin alpha 1 promoter, causes considerable reduction in lesion size following severe hypoxic ischemic insult (Appendix 2D). Inhibition of the Na^+/H^+ exchanger, a downstream target of MEK and ERK, with amiloride also causes a massive reduction in hippocampal and cortical tissue loss following neonatal hypoxic ischemic insult.

Based on the data described above, we propose the following related hypotheses:

- Neuronal and/or astrocytic ERK activation causes phosphorylation of downstream targets that play a role in mediating neonatal cerebral brain damage.
- Endotoxin will act synergistically and enhance potential for damage, at time points where shortened HI insult alone will not cause axonal or glial injury. Here, glial and axonal may act in concert, due to the effects of ERK in glial synthesis and release of proinflammatory cytokines (e.g. IL1, TNF), NO and oxygen radicals.
- Direct and prompt pharmacological inhibition of active ERK will block the appearance of axonal pERK during and shortly after HI insult and inhibit the resulting white matter damage, particularly in axons. In addition, in view of MEK/ERK function in inflammation-mediated oligodendroglia cell death, non-neuronal effects will be reduced following inactivation of glial ERK.

ERK Objectives

To further verify involvement or non-involvement ERK1 and 2 we will use transgenic mice, with homozygous deletion of ERK1 and insertion of lox P sites surrounding the ERK2 gene, abbreviated as $ERK2^{f/f}$ or 22, which can be used to cut out both copies of ERK2 with a recombinase cre via a cell type specific promoter. In the current case, we will use the synapsin promoter (synapsin-cre) and GFAP promoter (GFAP-cre) in order to delineate the role of neuronal or glial ERK expression following insult. Mutant mice and their littermate controls will be subject to moderate (30min) or severe (60min) hypoxic-ischemic insult alone or moderate insult in combination with systemic injection of lipopolysaccharide (LPS). For pharmaceutical intervention, we will use the specific MEK inhibitor SL327.

C-Jun

The AP1 transcription factor C-Jun is rapidly upregulated and activated by Jun N-terminal kinase (JNK) phosphorylation following hypoxic-ischemic (HI) insult, trauma or neuronal axotomy, which has suggested that this protein could serve

as a master switch of the degeneration program in a variety of injured neuronal and glial cells.

The proposed project will explore this hypothesis by examining the role of C-Jun and its specific phosphorylation by JNK following hypoxic-ischemic insult, using transgenic mouse mutants carrying cell type-specific and functional transgenic C-Jun mutations to determine their effects on white and grey matter damage and on functional recovery after HI insult. If this mechanism can be fully understood, then further strategies for primary prevention may be identified and, hence, the incidence and severity of brain injury reduced. To build on previous studies, a number of hypotheses were formulated as the basis for the current study:

- C-Jun activation of AP-1 and the subsequent downstream factors results in upregulation of pro-apoptotic targets in response to cerebral ischemia in the neonatal brain.

- C-Jun is involved in mediating the synergy between infectious and HI stimuli and the resultant injury to the neonatal cerebral brain. In vitro, many of the effects of lipopolysaccharide (LPS), mimicking bacterial infection, such as upregulation of cytokines and chemokines including TNFα, IL-6, and COX-2 are dependent on JNK and Jun activation. In vivo, brain synthesis of the TNF cluster of cytokines is strongly upregulated by very moderate amounts of systemically applied. Studies from our group show that the synergistic, damage-enhancing effects of LPS, injected 12h before the HI insult are completely abolished in mice lacking both copies of the TNF cluster.

- Upregulation of JNK and C-Jun activity following insult is due to both complimentary and parallel pathways in opposed to direct interaction. We will assess, whether these effects require or do not require JNK-dependent Jun phosphorylation by utilising transgenic mutants where all four N-terminus phosphor-acceptor sites by JNK (ser63/73 and thr91/93) are converted to alanine (Jun4A).

C-Jun Objectives

To determine the full scale of C-Jun effects on white and grey matter damage following HI this project will use neural deletion of floxed Jun gene with nestin driven cre recombinase. In addition, we propose to identify, which of the C-Jun expressing cells (neurons or astrocytes) act as a pacemaker, in mediating C-Jun dependent HI brain damage, using cell-type specific promoters for cre recombinase (synapsin-cre, GFAP-cre). Mutant mice and their littermate controls will be subject to moderate (30min) or severe (60min) hypoxic-ischemic insult alone or moderate insult in combination with systemic injection of lipopolysaccharide (LPS).

Understanding the molecular mechanisms underlying neonatal hypoxic-ischemic injury and association of specific MAP kinases and their signalling components will improve the success of neuronal protection, as well enhance the therapeutic intervention required to prevent poor neurological outcome following insult.

Materials and Methods

Animals

Legislation

All experiments and techniques were carried out in accordance with the UK Animals (Scientific procedures) Act 1986, as authorised by the Home Office. The mice were bred *in house* at the UCL Cruciform Biological Services Unit. Initial genetically engineered strains, used in these studies, were independently sourced from a number of laboratories, as summarised in table 2.1. Mice are widely available commercially and genotyping by PCR is a proven method for each transgenic strain.

All mice were kept under standard conditions with a 12-hour light/dark cycle at 21-23°C, and an average humidity of 60%. They had access to pelleted laboratory chow and water ad libitum.

Modified Genetic Mutation Strain	Acronym	Strain Background	Sourced From
Synapsin Cre	**S**	C57/Bl6	Axel Behrens Cancer Research, UK
GFAP Cre	**G**	FVB	Jackson Laboratories, USA
Nestin Cre	**N**	C57/Bl6	Axel Behrens Cancer Research, UK
ERK1 Neo	**11**	C57/Bl6	Gary Landreth Case Western Reserve University, Cleveland Ohio, USA
ERK2 Floxed	**22**	C57/Bl6	Gary Landreth Case Western Reserve University, Cleveland Ohio, USA
C-Jun Floxed	**JJ**	C57/Bl6	Axel Behrens Cancer Research, UK
C-Jun 4A	**44**	C57/Bl6	Axel Behrens Cancer Research, UK
C57/Bl6	**WT**	C57/Bl6	Charles River, UK

Table 2. 1: Summary of the genetically modified animals used for these studies

Breeding Strategies

Cell specific cre recombinase deletions- ERK2 and C-Jun were selectively deleted in specific cell types, including neurons, neuroepithelium derived cells (neurons, oligodendroglia and astrocytes), and astroglia. Cell specific conditional mutants were utilised due to global deletion of these genes resulting in embryonic lethality.

Cre recombinase acts as a catalyst to excise gene sequences by recognising them when flanked (floxed) by two forward facing LoxP sites. A cell selective deletion occurs by introducing Cre into the promoter region of cell-type specific markers, in these studies: synapsin for neurons; nestin for neuroepithelium lineage cells; and glial fibrillary acidic protein (GFAP) for astroglia. Developmental expression of the promoter gene allowed for endogenous cre excision of the floxed target. Floxed genes were ablated only in cells expressing these markers, at the point of expression whilst retaining wildtype gene transcription elsewhere. Synapsin is expressed at E12, GFAP at E16 and nestin at E7.5.

Animals with the floxed genes are bred homozygously so that both alleles of the gene will be excised. These homozygous animals were then bred against mice heterozygous for cre, creating cell selective homozygous null as well as cre-absent, wildtype gene expression, littermate controls.

Global deletion of ERK1- ERK1 was ablated in all endogenously expressing cells, as previously described by Nekrasova et al, in 2005. In brief, exons 1 to 6 of the ERK1 protein coding sequence were replaced with a neomycin resistance cassette. These constructs were electroporated into the 129 SVJ-derived embryonic stem cells. Chimeras were generated by injecting two targeted clones into CD1 blastocysts (Nekrasova et al., 2005). Homozygous mutants were obtained by re-crossing the successful chimeras with wildtype C57/Bl6 mice for two generations until on a uniform background.

For our experiments, the ERK1 animals were bred in a heterozygous manner with C57/Bl6 wildtypes to produce homozygous null mutants ($ERK1^{-/-}$) and wildtype controls ($ERK1^{+/+}$).

Jun4A; modification of C-Jun's phosphorylation sites- the most direct activation of C-Jun is via JNKs phosphorylation of 4 selective sites in the N-terminus. In Jun4A animals these sites- Serine 63 and 73 (Ser63&73) and Threonine 91 and 93 (Thr91&93) are substituted by Alanine. This renders C-Jun as functionally null by JNK activation.

Jun4A mice were bred heterozygously to produce both homozygotes and wildtype littermate controls. A summary of these breeding strategies can be seen below.

Mutation	Breeding Strategy	Outcome Genotypes
S1122	Heterozygous	22, S22, 1122, S1122
G1122	Homozygous	1122, G1122
SJJ	Homozygous	JJ, SJJ
GJJ	Homozygous	JJ, GJJ
NJJ	Homozygous	JJ, NJJ
Jun4A	Heterozygous	WT, 44

Table 2.2: Breeding strategies and their required outcome strains for use in these experiments

Genotyping

Individual animals were identified by an ear-notch system. To genotype, a ≤5mm section of tail was biopsied and the DNA extracted through the addition of 20μl of Proteinase K (20μg/ml, Promega UK) and 750ul of extraction buffer (20% 0.5M EDTA, 5% 1M TRIS, 3.4% 3M NaCl, and 1% SDS). Each sample was pulse-vortexed before incubating at 55°C overnight in a shaker water bath. On the second day, samples were placed on ice for 10min and subsequently centrifuged at 16,900g for 10min. The supernatant was separated out and inversion-mixed with 600μl isopropanol (VWR, UK). DNA was elicited by centrifuging for a further 15min at 11000g, producing a pellet of supercoiled DNA which was then washed in 70% EtOH (VWR, UK) and centrifuged at 11000g for 5min before being air dried for 1hr. Lastly the DNA was re-suspended in 50μl TRIS-EDTA (TE buffer, Promega UK) and stored at 4°C until required.

Polymerase Chain Reaction (PCR) verified the genotypes of each sample. A 25μl reaction mix was created with 2.5μl 10xbuffer, 5μl Q solution, 0.25μl 25mM dNTPs, 0.125μl of each primer and 0.2μl Taq polymerase (Taq DNA Polymerase Kit, Qiagen UK). This mix was made to a total volume of 24μl with DEPC-treated water (Life Technologies) and 1μl of the DNA sample (made to a 1:20 dilution in DEPC water) was added. Table 2.3 shows a list of primers used in this study.

PCR conditions were optimised on a T-Gradient PCR machine (biometra, Germany). The products were separated via electrophoresis on a 2% agarose (Eurogenics)/1x TRIS-Acetate-EDTA (TAE) gel containing 0.5% Ethidium Bromide (10mg/ml solution, Sigma), alongside a positive control and 100bp DNA Ladder (NEB, UK). Each gel was run in a TAE running buffer for 40min at a constant voltage of 100V. The resulting bands were visualised in an ultraviolet transilluminator (BioDoc-it 200 imaging system, UVP).

Target Gene	Forward Primer	Reverse Primer	Band Size
Generic Cre	**LCK Cre Fwd**	**LCK Cre Rev**	
	5'-CGGTCGATGCAACGAGTGATGAGG-3'	*5'-CCAGAGACGGAAATCCATCGCTCG-3'*	600bp
ERK1 Neo	**Neo Cassette Fwd**	**Neo Cassette Rev**	
	5'-CTTGGGTGGAGAGGCTATTC-3'	*5'-AGGTGAGATGACAGGAGATC-3'*	280bp
ERK1 WT	**WT Fwd**	**WT Rev**	
	5'-CCAGGAGGACCTTAATTGCATCATT-3'	*5'-TTAGGGGCCCTCTGGCGCCCCTGGCTG-3'*	700bp
ERK2 Flox	**E2F-L**	**E2F-U**	350bp FLOX
	5'-AGCCAACAATCCCAAACCTG-3'	*5'-GGCTGCAACCATCTCACAAT-3'*	275bp WT
C-Jun Flox	**LOX5**	**LOX6**	350bp FLOX
	5'-CTCATACCAGTTCGCACAGGCGGC-3'	*5'-CCGCTAGCACTCACGTTGGTAGGC-3'*	300bp WT
Jun4A	**4A Fwd**	**4A Rev**	248bp 44
	5'-AGAACTTGACTGGTTGCGACA-3'	*5'-AGTCCATCGTTCTGGTCGCGC-3'*	198bp WT

Table 2.3: PCR Products, primer sequences and their subsequence band size for the genetically modified mice tail DNA samples.

Surgery

Hypoxia-Ischemia (HI) Insult

The Rice-Vannucci model of HI injury in neonatal rodents was modified from Levine (1960) which had been originally generated to study stroke conditions in adult rats. Rice et al. found that an ischemic insult was required in addition to hypoxia to result in a significant increase in damage to both the adult and neonatal brain. In this revised model, tissue loss was observed in the cerebral cortex, striatum, thalamus and hippocampus, faithfully imitating Levine's adult model (Rice et al., 1981). However, in addition, the neonatal rat brain also exhibited lesions in white matter region- the external capsule.

Model of Brain Injury

In order to study perinatal brain injury, multiple animal models have been used. These have been performed in various animals and often use bacteria, endotoxin, viruses, excitotoxins or hypoxia-ischemia. Research has begun to use combinations of such insults to better study how other factors influence the outcome following hypoxia-ischemia (Coumans et al., 2003; Eklind et al., 2001; Yang et al., 2004). The most commonly used rodent model of perinatal hypoxia-ischemia is the Rice-Vannucci model. The initial model involved permanent carotid occlusion and timed exposure to hypoxia in a 7 day old rat. Individually, carotid occlusion or hypoxia is not sufficient to cause histological damage. However, in combination, carotid occlusion followed by hypoxia led to histological evidence of brain injury in 90% of animals and an infarct in 56% (Rice et al., 1981). From a neurological perspective, the seven day-old mouse or rat is considered to be a reasonable representation of the human neonate at term; specifically due to a lack of prenatal myelination (Hagberg et al., 2002a). Mice and rats are born pre-myelination, but undergo rapid myelin production in the first postnatal week. As such the pattern of brain injury in the 7 day-old rodent model is similar to that seen in the term neonate following hypoxia-ischemia with damage to the ipsilateral cerebral cortex, thalamus, striatum, hippocampus as well as subcortical and ventricular white matter. It is clear that in animal models and human neonates, hypoxia ischemia and/or inflammation can, if severe enough, result in permanent brain injury. However, it has been indicated that much milder combinations of these insults, not sufficient alone to cause injury, may result in permanent brain injury (Peebles and Wyatt, 2002).

Carotid Artery Occlusion

At P7, mouse pups were anaesthetised with isoflurane/oxygen (1L/min, Abbott) with a 5% induction and 1.5% maintenance. Following midline incision, left common carotid artery was occluded by ligation using an 8-0 polypropylene suture (Ethicon). The incision was closed with tissue glue and the pups recovered in an aerated warm chamber (36°C) before being returned to their dams for 1.5hr. Post recovery the animals were placed in a sealed 36°C hypoxia chamber and exposed to humidified 8% oxygen balanced with nitrogen. Hypoxia lasted for 30min- generating a mild insult, or 60min-severe insult. Lastly, the animals recovered in the aerated chamber for further 10min prior to

returning to the dams until point of death. The pups were sacrificed between 0-96hr post-injury.

Endotoxin-Sensitisation and HI

In addition to a pure HI model, these studies have explored the synergistic interaction between LPS induced inflammation and HI injury to the neonatal brain. Previous work by this group show that when LPS was administered prior to unilateral carotid occlusion and 30min HI, the observed tissue loss was exacerbated compared to either LPS or HI alone (Kendall et al., 2006). In these initial experiments, a titration of LPS was performed and a dosage of 0.3μg/gBW was found to be optimal. For these experiments, a new stock of LPS was acquired that was of a different batch than that used in these original experiments. As such, a titration was performed by Dr Mariya Hristova and an improved dosage of 0.6μg/gBW was found.

P6 mouse pups were injected intraperitoneally (i.p) with LPS/0.9% sterile saline (Escherichia Coli, Serotype, 055; B5, Fluka). A dose of 0.6μg LPS/saline in 10μl/gBW was administered 12hr prior to surgery and 30min hypoxia. Surgery, hypoxia and recovery were performed as described above. All pups subject to LPS were sacrificed at 48hr, a time point previously examined by this group (Kendall et al., 2011a).

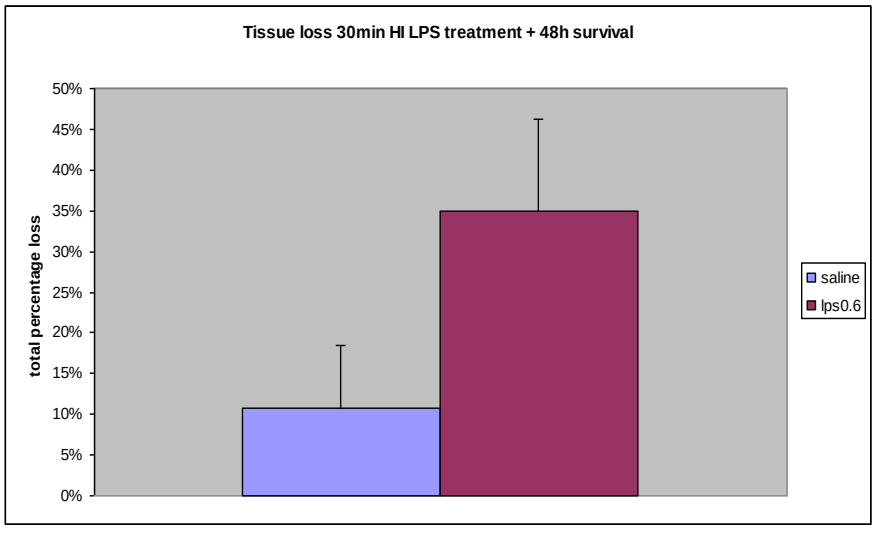

Figure 2.1: Compared to saline treated control animals (n=8), animals sensitised with 0.6 μg/g of LPS (n=6) displayed significant increase in infarct volume as estimated by NISSL staining and volume measurement (p<0.05). Dr Mariya Hristova (unpublished)

Perfusion

Animals were anaesthetised by i.p injection of 40μl pentobarbitone sodium (0.2μg/μl Euthatal, Merial). Paw withdrawal reflex was used to determine deep anaesthesia. The thoracic cavity was exposed and the pups perfused intracardially with 4% paraformaldehyde (PFA, sigma) in 0.1M phosphate buffer saline (PBS). A 26-gauge needle was attached to a perfusion pump (Gilson, UK) and inserted at the heart apex and into the left ventricle. Four percent PFA was perfused through the pump for 2.5min at a flow rate of 0.02L/min.

Fixation

Following perfusion, the brain was removed and post-fixed for 1hr in 4% PFA, on a rotator (8RPM) at 4°C. The fixed brains were then cryoprotected for 48hr in a phosphate-buffered 30% sucrose solution (Fluka, UK). Forebrains were mounted onto Whatman paper and frozen on dry ice (BOC, UK). All samples were kept at - 80°C (New Brunswick U535 Freezer) until required.

Cryosectioning

Frozen forebrains were cut on a Leica CM 1900 cryostat into 50 sequential sections at a thickness of 40μm. Samples were mounted into a chuck with OCT compound (Tissue Tek, Netherlands) and secured into the cryostat with the chuck head temperature at -15°C and ambient temperature set to -20°C. Coronal sections were taken, starting at the level of corpus callosum fusion, and collected onto double-gelled 0.5% gelatine (Merck, UK) coated slides (Thermo Scientific, UK). Slides were then frozen on dry ice and stored at - 80°C until required.

Light Microscopy

Immunohistochemistry (IHC)

IHC required a two-day protocol for AlphaM (CD11b), AlphaX (CD11c), GFAP, and phosphorylated C-Jun. Five sections- 400μm apart were selected for each stain. Frozen cryosectioned slides were rehydrated with distilled water (dH_2O) and spread flat onto the slides under a dissecting microscope and using fine brushes. Samples were allowed to air-dry at room temperature (RT) for 1hr before being bounded with pap-pen (Dako, Cambridgeshire UK). These were

then fixed in a solution of 4% PFA (Sigma, UK) for 5min and recovered in 0.1M phosphate buffer (PB).

Antigen retrieval was achieved by acetone (VWR) de-fatting. Here slides were submerged into cuvettes holding 50% acetone/H_2O, 100% acetone, 50% acetone/H_2O for 2min each. This was immediately followed by two washes in 0.1M PB. Finally, slides were rested in a cuvette containing 0.1M PB/0.1% bovine serum albumin (PB/BSA) (BSA: Sigma, UK). Sections were then individually removed and dab-dried using laboratory tissue. They were placed into humidified staining trays and non-specific antigen binding was blocked for 30min at RT with 90μl of 5% goat serum (Sigma, UK) in 0,1M PB. Block solution was removed by pipette and 90μl primary antibody, made to the appropriate dilution in PB/BSA, was added. Slides were incubated at 4°C overnight (O/N). Dilutions of primary antibodies were optimised via titration staining's. These are summarised in table 2.4.

The corresponding biotinylated secondary antibodies were incubated with mouse serum at 37°C for 30min before being diluted 1:100 in PB/BSA. Slides were washed in 0.1M PB and PB/BSA and 90μl of secondary antibody was applied for 1hr at RT. Sections were then washed in 0.1M PB. Avidin-Biotinylated horseradish peroxidase complex (ABC, Vectastain Kit- Peroxidase Standard PK-4000; Wiesbaden, Germany) was prepared at a 1:100 dilution and 90μl applied to each slide for 1hr at RT.

In order to allow for visualisation of the target antigens, sections were washed in 10mM PB and placed into a filtered (Size 4 filter, Whatman) solution of diaminobenzidine (DAB, Sigma, UK) and hydrogen peroxide (H_2O_2). This reactive solution consisted of 0.5g/l DAB in 10mM PB and a 1:3000 dilution of H_2O_2. Reaction lasted between 2-6min determined by monitoring under a light microscope. It was stopped in dH_2O.

The slides stained for AlphaX and TUNEL (see below) were visualised with DAB/H_2O_2 enhanced with 0.25g/l cobalt sulphate ($CoSO_4$) and 0.2g/l nickel chloride ($NiCl_2$). Sections were subsequently re-spread flat onto the slides and allowed to air-dry O/N at RT. Lastly, sections were passed through three

cuvettes containing xylene (VWR, UK), covered using DePex mounting media (BDH, UK) and left to adhere O/N.

Marker	Primary Antibody	Manufacturer	Code	Optimal Dilution	Secondary Antibody	Manufacturer	Code	Optimal Dilution
Alpha M CD11b	Rat anti-Mouse igG	Serotec	SECD11b	1 in 5000	Goat anti-Rat igG	Vector	BA-9400	1 in 100
AlphaX CD11c	Hamster anti-Mouse igG	Pierce Endogen	MA11C5	1 in 400	Goat anti-Hamster igG	Vector	BA-9100	1 in 100
GFAP	Rabbit anti-Mouse igG	Dako	70334	1 in 6000	Goat anti-Rabbit igG	Vector	BA-1000	1 in 100
C-Jun	Rabbit anti-mouse	Santacruz Biotechnology	SC-1694	1 in 200	Goat anti-Rabbit igG	Vector	BA-1000	1 in 100
Monoclonal pERK	Mouse anti-Mouse igG	Cell Signalling Systems	9106L	1 in 400	Poly-HRP anti-Mouse igG	Millipore	2702	1 in 250
Polyclonal pERK		Cell Signalling Systems	9101	1 in 100	Goat anti-Rabbit igG	Vector	BA-1000	1 in 200
SERA								
Goat Serum	Sigma	G9023	1 in 20					
Mouse Serum	Serotec	C115A	1 in 50					

Table 2.4: Summary of Primary and Secondary Antibodies and Sera used in IHC

IHC- Free Floating Method

This technique was utilised to stain for phosphorylated ERK due to the polyclonal primary antibody's sensitivity to dehydration. Sections were selected as above, rehydrated in PBS and placed into a sieved 12-well plate. They were washed twice in PBS on a rotating shaker at 8RPM for 2min. Endogenous peroxidases were blocked using 3% H_2O_2 in dH_2O for 10min at RT. Antigen retrieval was achieved using 0.3% triton (triton X-100, Bio-Rad, UK) in a 5% Goat serum/PBS solution for 30min. Sections were then washed again in PBS before being placed into wells containing 2.5ml polyclonal pERK primary antibody was diluted 1:100 in 5% Goat serum/PBS, and incubated with the sections O/N at 4°C.

Second day, samples were washed three times in PBS at RT than incubated for 1hr with 2.5ml secondary goat-anti-rabbit antibody. This was followed by three more PBS washes. ABC was prepared as before and added to the wells for 1hr at RT. The stain was visualised with DAB/H_2O_2 and the correct intensity measured under a light microscope. The reaction was stopped in dH_2O. Lastly, the brains were spread flat onto 0.5% gelatinised slides and allowed to air-dry O/N. Coverslips were affixed as described above.

Fluorescent immunochemistry

Fluorescence double labelling was carried out for pERK and C-Jun with GFAP, α- M and NG2. When preparing the antibody dilutions, a mixture of both antibodies was first made before vigorous mixing and application to the slide. The antibody dilutions were prepared as shown in table 2.5. Day one was carried out as described above for IHC, with 5% donkey serum used as block. For day 2, slides were washed in PB/BSA and 0.1M PB before 90μl of the corresponding fluorophore-conjugated secondary antibody was applied for 1hr at RT. Sections were washed again in PB/BSA and 0.1M PB followed by application of the same fluorophore labelled tertiary antibody as used for secondary. This was for 1hr incubation in a staining tray at RT. Slides were washed a final three times in 10mM PB before covered with DAPI containing mounting media (VectaShield) and protective glass coverslips. Slides were sealed and stored at 4°C for confocal analysis.

Primary Antibody	Secondary Antibody	Manufacturer	Code	Optimal Dilution	Tertiary Antibody	Manufacturer	Code	Optimal Dilution
pERK	Poly-HRP anti- Mouse igG	Millipore	2702	1:250	Avidin Texas Red	Molecular Probes	A-820	1:200
C-Jun	Donkey anti-Rabbit IgG	Immuno-research	711-005-152	1:100	Streptavidin 555 Alexafluor	Invitrogen	S-32355	1:1000
GFAP	Goat anti-Rabbit Alexa 488	Molecular Probes	A-11008	1:200	Donkey anti Goat Alexafluor 488	Molecular Probes	A-11055	1:200
Alpha M	Goat anti-Rat Alexa 488	Molecular Probes	A-11006	1:200	Donkey anti Goat Alexafluor 488	Molecular Probes	A-11055	1:200
NG2	Goat anti-Guinea Pig IgG	Molecular Probes	A-18773	1:200	Donkey anti Goat Alexafluor 488	Molecular Probes	A-11055	1:200
SERA								
Donkey Serum		Sigma	D9663	1 in 20				

Table 2.5 Additional secondary and tertiary antibodies required for fluorescent immunochemistry

TUNEL- Terminal Transferase-Mediated dUTP Nick End Labelling

Sections were selected, rehydrated, spread and fixed as mentioned in IHC protocol. Endogenous peroxidases were blocked by immersion of slides into a solution of 3% H_2O_2/Methanol (VWR, UK) for 15min at RT. They were recovered in 0.1M PB. Antigen retrieval was performed by acetone followed by the washes described above.

Slides were dab-dried and 100μl TUNEL enzyme solution (TdT and dUTP Kits, Roche, UK) was added to incubate in a 37°C chamber for 2hr. TUNEL solution consisted of 0.1% TdT, 0,15% 1mM dUTP and 1% cacodylate buffer diluted in dH_2O. After 2hr, the reaction was stopped in TUNEL Stop solution (300mM NaCl, 30mM sodium citrate) for 10min before 0.1M PB and PB/BSA washes. ABC was prepared as described above and 90μl applied to each slide for 1hr at RT. The staining was visualised with DAB/H_2O_2/$CoSO_4$/$NiCl_2$. Reaction was stopped and the slides subsequently processed and covered as above.

Nissl- Cresyl Violet Histology Stain

Sections were selected, rehydrated, spread and dried as mentioned in IHC protocol. These were fixed in 4% formaldehyde (FA, BDH, UK) made up in 0.1M PB. The slides were kept in 4% FA overnight at RT, followed by immersing the sections in 70% EtOH overnight at RT. A 1% cresyl violet solution was prepared by adding 4g cresyl violet (BDH, UK) to 40ml 100% EtOH and mixed for 15min. Cresyl violet/EtOH mixture was then added to 360ml heated dH_2O and filtered O/N (Whatman filter: Size 4).

Slides were submerged in 1% cresyl violet solution for 6min, after which excess solution was cleared completely using free-flowing water. Sections were then dehydrated through sequential washes of increasing concentrations of EtOH (70%, 90%, 95%) before de-stained in 95% EtOH containing 12drops (~600μl) glacial acetic acid. Optimal de-staining was established by monitoring colour intensity under a light microscope. Reaction was stopped and the slides further dehydrated by being placed in 100% EtOH, followed by isopropanol. Coverslips were affixed as described above.

Quantifications

Regions of Interest

Neonatal forebrain regions for assessment of hypoxic ischemic damage included external capsule, cerebral cortex, striatum, pyriform cortex, hippocampus and thalamus. Each region was assessed over five equal distance slides for each brain on both the ipsilateral, hypoxia-ischemic insult hemisphere and the contralateral, hypoxia alone hemisphere. For cell counts, 3 fields at 20x magnification were assessed per region of interest. Semi-quantitative scores were examined under a 10x magnification and assessed over the whole region. Infarct volume was measured over the whole region at 1x magnification with luminosity, a measure of density, of ipsilateral regions, taken as a percentage of its contralateral counterpart.

Controls

Each experiment included control animals subject to sham surgery no hypoxia, or left carotid artery occlusion but no hypoxia. In addition for each experimental animal the contralateral hemisphere acts as an intracranial control for hypoxia alone due to the presents of sufficient blood flow to these regions. Multiple

controls were required to minimise any false responses due to either technical error or by one damage type alone. In the Rice-Vannucci model of neonatal hypoxia ischemia it has been well established that both hypoxia and ischemia are required to induce insult (Hagberg et al., 2002a). When examined, the levels of expression for markers of damage, listed herein, were unchanged between control groups. As such only contralateral, hypoxia alone, controls are used to illustrate changes in response to the ipsilateral hypoxia-ischemic forebrain regions.

Positive Antigen-Expressing Cell Counts

Number of activated phagocytic microglia (AlphaX), dying cells (TUNEL) and pERK immunoreactive cells were quantified by counting the number of cells positively stained for these respective markers. Counts were performed under a Zeiss Axiolab light microscope (Zeiss, UK) at a 20x magnification. Our regions of interest were the external capsule, striatum, pyriform cortex, cerebral cortex, hippocampus and thalamus. Total counts were taken over three eye-fields for each region. Numbers were obtained for both the ipsilateral and contralateral hemispheres in relation to the carotid occlusion. For each experimental cohort, the average of all total counts was taken as a representing number of positive cells observed in that group.

Semi-Quantitative Scoring

Microglial activation (AlphaM) and neuronal cell loss (Nissl) were scored using a semi-quantitative scoring system, previously established in this laboratory (Kendall et al., 2006) under a 10x magnification. A grade between 0-4 was assigned to each section where 0 was where neither focal activation of microglia nor tissue loss were observed, and 4 represented widespread activation and total tissue. The breakdown of each score grading is given in table 2.6.

All 6 region were assed for AlphaM, and all except external capsule (due to lack of Nissl bodies present outside of neuronal soma) for Nissl. A score was assigned for both the ipsilateral and contralateral areas.

A total tissue injury score was obtained for all regions by combining the average scores allocated to each experimental cohort. All slides were assessed blindly.

Score	Alpha-M Staining	Score	Nissl (Cresyl Violet) Staining
0	No activation	**0**	No damage
1	Focal activation	**1**	Minimal evidence of damage without evidence of infarct
2	Mild diffuse activation, occasional phagocytic macrophages	**2**	Small infarct, ≤ 50% of the affected region
3	Widespread activation, predominant phagocytic macrophages	**3**	Large infarct, ≥ 50% of the affected region
4	Tissue loss	**4**	Total neuronal loss

Table 2.3: Injury scoring system for AlphaM and Nissl. Adapted from Kendall et al., 2006

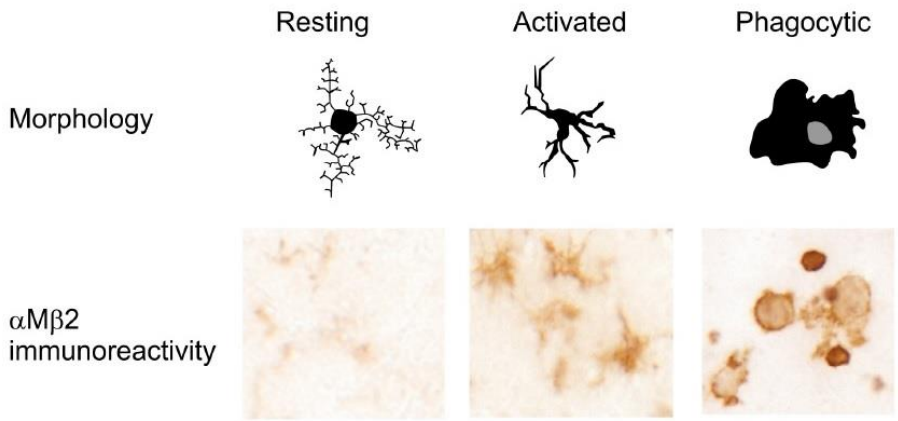

Figure 2.2 Stages of activation of microglia. In resting microglia there is very low alphaM expression and highly branched (ramified) dendrites. At the activated or alert phenotype, alphaM expression is increased and there is a reduction in complexity of branching. Phagocytic microglia are deramified cells with an amoeboid morphology. AlphaM staining is moderate to strong. Modified by Dr Giles Kendall from (Raivich et al., 1999)

Infarct Volumes

Both severe HI (60min hypoxia) and LPS-sensitised HI resulted in large areas of tissue loss, known as damage infarct sites. To quantify these lesions, Nissl stained slides were photographed using a Sony 3CCD colour video camera (AVT-Horn, Aachen, Germany). 8-bit RBG images for each section were captured at a 1x magnification and the images were imported into Optimas v6.5 image analysis software (MediaCybernetics, Bothell, WA). All 6 regions of interest were bounded using a free-hand tool and the total pixel count per area calculated by a histogram tool. This count was then converted into mm using

Excel. The volumes were acquired as the percentage of area loss in the ipsilateral regions compared to the corresponding contralateral-intracranial control regions.

Time Course of Cellular Changes in HI-damaged Mouse Forebrain

In order to determine which time points would be optimal to study the effects of pharmacological inhibition and genetic deletion of ERK or C-Jun, a time course for damage markers was generated between 0-96hr post HI insult in the P7 C57/Bl6 mouse (figure 2.3). Cell death associated with DNA fragmentation showed a sharp peak in the ipsilateral striatum and cortex. A prolonged expression of TUNEL positivity was observed only in the hippocampus; the contralateral side was unaffected. 60 min HI insult was associated with a much a higher level of cell death, but also a later onset (24hr), than 30 min (16hr). Interestingly, the periventricular white matter showed a high intrinsic level, with a slight elevation on the ipsilateral side only at 24h following 60 min HI insult (figure 2.3C).

In contrast to TUNEL, assessment of microglial activation (figure 2.3B) and histological tissue loss (nissl) based on the scoring system noted in table 2.6, revealed a very robust and similar time course. Following a 60 minute HI insult, significant microglial activation was already observed at 8 hours across the different white and grey matter regions, reaching persistently high levels in the following hours and days. A milder increase, with a peak at 16-24h followed the moderate, 30 min insult. The same pattern of expression was observed using cresyl violet as a histological marker for neuronal cell loss (figure 2.3A). As a fourth marker, we also evaluated the appearance and density of phagocytic, alphaX beta2 integrin+ brain macrophages (figure 2.3D). This was generally a late onset event, and only became pronounced 3-4 days after the severe, 60 min, HI insult. Although alphaX+ macrophages are thus a sensitive marker of phagocytosis, in the current model they only become useful biomarkers at comparatively late stages of the degenerative process.

Time points

Overall, the current data reconfirm a 48h time point as the first base point to assess the effects of mutations, deletions and pharmacological inhibition. This is particularly true for studying later effects of HI including the presence of

infarct and phagocytosis of cell debris. Equally, as 48hr was the time point used in previous studies in our laboratory, by using it in the experiments herein we are able to draw comparisons. Lastly, by looking at peak expression of early damage markers including alphaM integrin and tunel labelled dying cells, the data suggests using the additional cell death and early activation data points at 16h for the moderate, and 24h for the severe forms of HI insult.

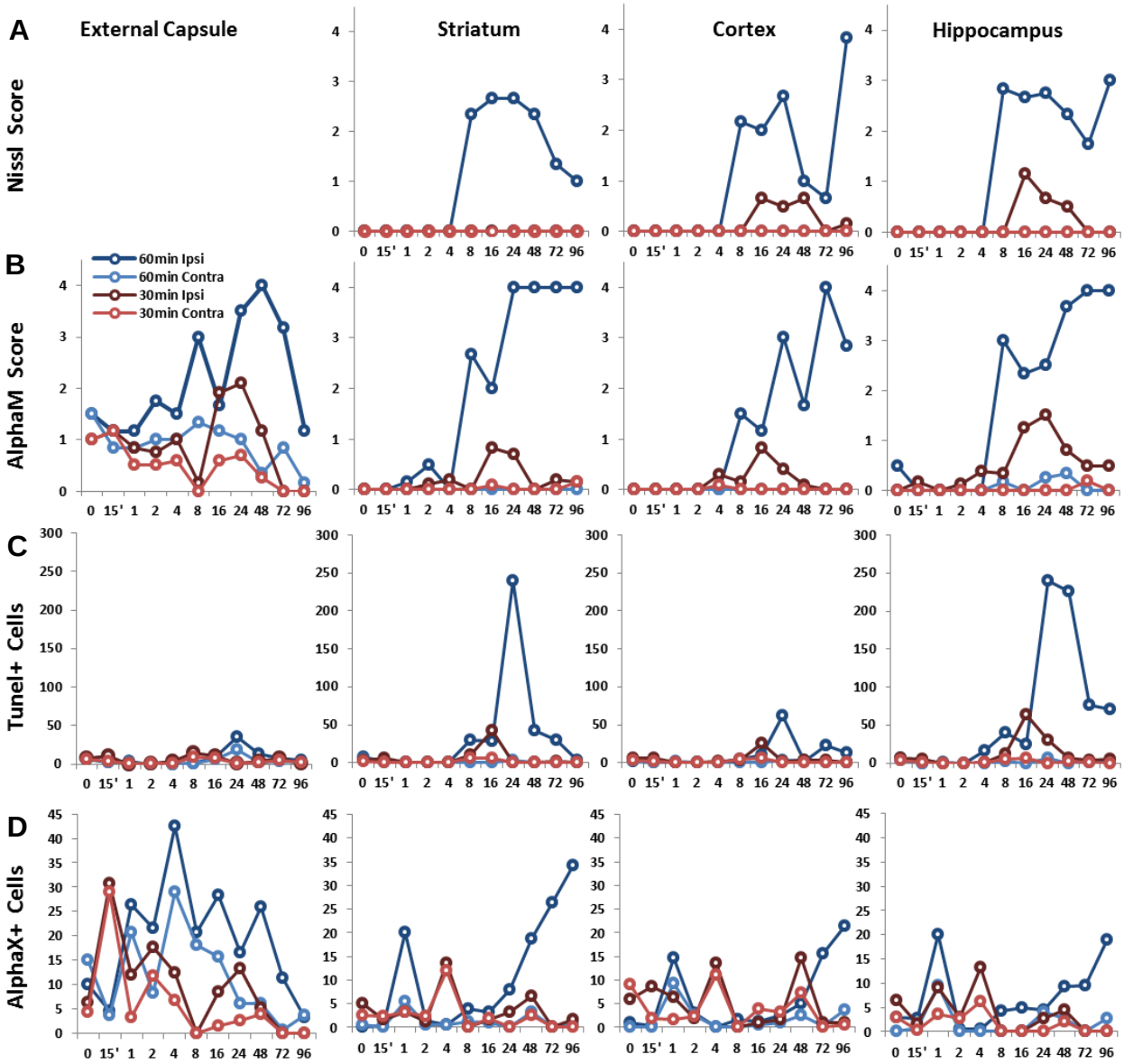

Figure 2.3 Neuronal cell loss, microglia activation and cell death time course following hypoxic/ischemic exposure for 30min (red) or 60min (blue) where n=3/time point. Filled circles indicate the hemisphere regions ipsilateral to carotid artery occlusion, whereas empty circles are contralateral regions. Neuronal cell loss and microglia activation based on staining for Nissl and alphaM/beta2 integrin respectively using blindly scored tissue sections. All 4 regions show a very similar time course, with strong onset of persistent tissue damage and microglia activation at 8hr following 60min HI and a milder activation at 16hr following 30min HI. The appearance of phagocytic, alphaX brain macrophages is a late stage occurrence, particularly pronounced 3-4days after 60min HI. TUNEL histochemistry was used to detect nuclear DNA fragmentation, number per 20x eye field (mean plus SEM over 3 fields). Sharp peak in ipsilateral striatum and cortex and a prolonged time course in hippocampus; contralateral hemisphere remains unaffected. There are intrinsically high levels of TUNEL+ dying cells in external capsule with only a slight elevation on ipsilateral side at 24hr following 60min HI.

Luminosity

GFAP, a marker for activated astrocytes, was assessed by mean optical luminosity where less light projected through a region on the glass slide, correlates with a higher intensity of staining and thus a greater number of activated astrocytes in that area.

The AVT-Horn camera, as above, was used to capture three 8-bit RBG images of each of our regions of interest under a 20x magnification. Images were then imported into the Optimas v6.5 Software. Each image was run against an Excel algorithm to obtain the mean and standard deviation (SD) of luminosity through that region.

For each image, the SD was subtracted from the mean, and this resulting value further subtracted from the mean optical luminosity of the sham glass slide. This provides a specific Optical Luminosity Value (OLV). OVLs were obtained for both the ipsilateral and contralateral hemispheres.

Statistical Analysis

For all Tunel and AlphaX positive cell counts, AlphaM and Nissl scores, infarct volume and GFAP luminosity data, the mean ± standard error of the mean (SEM) were calculated using Excel. Analysis was done to compare values between the injured and non-injured hemispheres of both mutant and control cohorts. A standard two-tailed Students T-Test was executed to determine significance between groups. A p value <5% was considered to represent a significant difference.

Where more than two groups were compared, ANOVA with posthoc Tukey was used. Results were considered significant when the p-value was less than 0.05 on both tests, run consecutively.

Photographs

Bright field micrographs were acquired in Optimas v6.5. Each image was corrected for background by condensing two 8-bit images of the sham glass slide and subtracting those from the images of the forebrain sections. This was utilised to remove microscopic artefacts. Examples can be seen in figure 2.4.

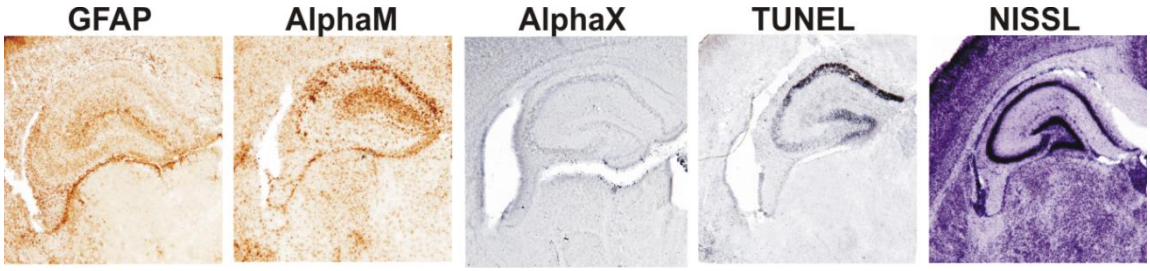

Figure 2.4: Examples of micrographs taken at 4x magnification of a selection of stains used in these studies. Namely GFAP for astrocytes, AlphaM and AlphaX for microglia activation, TUNEL for cell death, and Nissl for neuronal cell loss and infarct volume.

Cell Specific Deletion of ERK 1 and 2 Results

Extracellular signal-related kinases ERK 1 (MAPK 44) and ERK 2 (MAPK 42) are members of the mitogen activated protein kinases superfamily involved in multiple cell regulatory functions, including proliferation, differentiation and cell cycle progression (Boulton et al., 1991; Luca et al., 2012; Luo and DeFranco, 2006; Napoli et al., 2012; Ortiz et al., 1995; Plotnikov et al., 2011; Rosenblum et al., 2002; Shaul and Seger, 2007). Whilst these are well-established outcomes of ERK activation, involvement in cell survival remains uncertain. Following ischemic insult in adult mice, phosphorylated, and thus activated, ERK (pERK) was observed immediately after insult with constant increase up to 2hr (Alessandrini et al., 1999). In a neonatal rat model of HI: pERK positive neurons were observed at 8hr, 24hr, 48hr and 72hr after insult. PERK also co-labelled to markers of microglia and astrocytes from 48hr onward with all pERK positive cells located in or at the borders of ischemic lesions (Wang et al., 2004a). In both models studies have shown that pre-application of a selective MEK 1/2 inhibitor gives rise to partial neuroprotection indicating ERK to have a role in the brains response to HI damage (Alessandrini et al., 1999; D'Cruz et al., 2005; Jones and Bergeron, 2004; Li et al., 2008; Namura et al., 2001).

Since global deletion of ERK2 is embryonically lethal, neuron- and astrocyte-selective deletion of ERK2, in combination with global ERK1$^{-/-}$ has been used in order to investigate the role of both kinases in cell death, infarct size and the recruitment of non-neuronal cells to the site of injury.

Mapping out the activation of ERK in the neonatal forebrain following mild hypoxia-ischemic insult

To study the interaction of ERK activation and HI, a time course was undertaken. Here phosphorylated ERK expression was recorded at 0hr, 15min, 1hr, 4hr, 16hr, 24hr and 48hr following mild hypoxia.

Sixty-four C57/bl6 mouse postnatal day 7 (P7) pups underwent unilateral left carotid artery occlusion (CROC), of which half went on to be exposed to 8% O_2 for 30min. The remaining 32 pups served as CROC-alone controls. Four pups were sacrificed at each time point following HI, along with four control animals. At sacrifice, the pups were perfused and the brains extracted and processed as

previously described. Five equal distance sections were taken per brain and stained for pERK via a free-floating immunohistochemistry technique. For each brain, seven forebrain regions were assessed: striatum; hippocampus; thalamus; pyriform cortex; dorsal cortex; mid-dorsal cortex and ventral cortex. PERK positive cells were counted under a 20x magnification. The hemispheres ipsilateral to CROC were compared to contralateral hemisphere (i.e. hypoxia alone) and CROC-alone control brains.

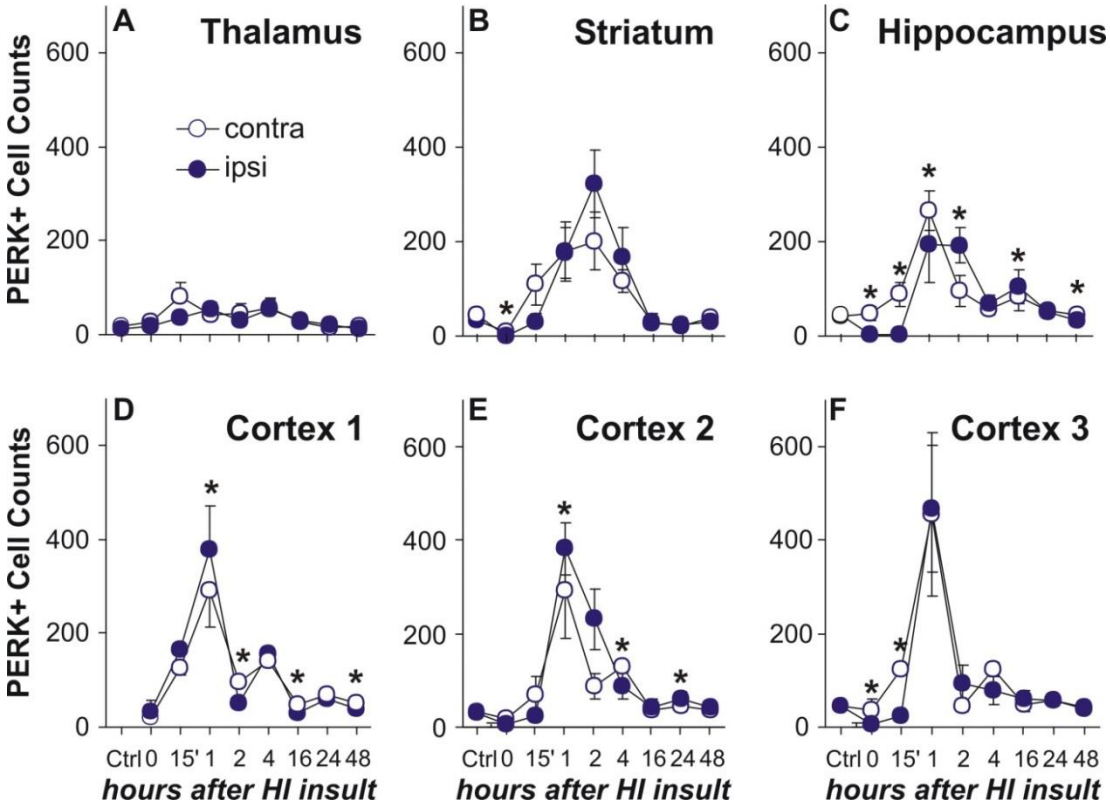

Figure 3.1 Phosphorylated ERK immunoreactive cells following HI insult. Blue circles are indicative of hemisphere regions ipsilateral to carotid artery occlusion. White circles indicate contralateral regions. Positive cell counts were assessed over 3 fields per region at a magnification of 20x and analysed as mean ± SEM, n=4 animals per time point. In thalamus (A), striatum (B), hippocampus (C), and in dorsal (D), mid-dorsal (E) and mid-ventral (F) regions of cerebral cortex. HI insult induces drastic changes in ERK phosphorylation in postnatal mouse forebrain, first causing a blanking out on the ipsilateral side (0-15min) and then a bilateral peak expression at 1-2hr. *P<0.05 in paired student t-test for ipsilateral versus contralateral hemispheres.

Controls showed no change in pERK expression at any time point (noted as CTRL on graphs of figure 3.1). In experimental animals, two prominent changes in ERK activation were observed. Firstly, ipsilateral pERK is rapidly and significantly attenuated immediately following HI (0hr to 15min) compared to the contralateral hemisphere, particularly in striatum (P=0.05), hippocampus (P=0.003), mid-dorsal cortex (Cortex 2) (P<0.001), ventral cortex (Cortex 3) (P<0.001), and in the neurons of the pyriform cortex (P<0.001). This followed by

a large and transient increase of expression, mostly bilateral, in all regions bar thalamus where ERK activation was relatively unaffected by injury, between 1-2hr. PERK levels decline to baseline levels by 4hr.The highest expression of activated ERK was in Cortex 3 with 403.7±44.5 positive cells at 1hr. Pyriform pERK immunoreactivity showed the same trend as other regions with a decrease until 15min and then an increase to 1hr. However unlike other regions, pERK expression is sustained until 48hr. Interestingly the morphology of pERK positive cells at 1hr differed from those at 15min in hippocampus, cortex and pyriform cortex (figure 3.2).

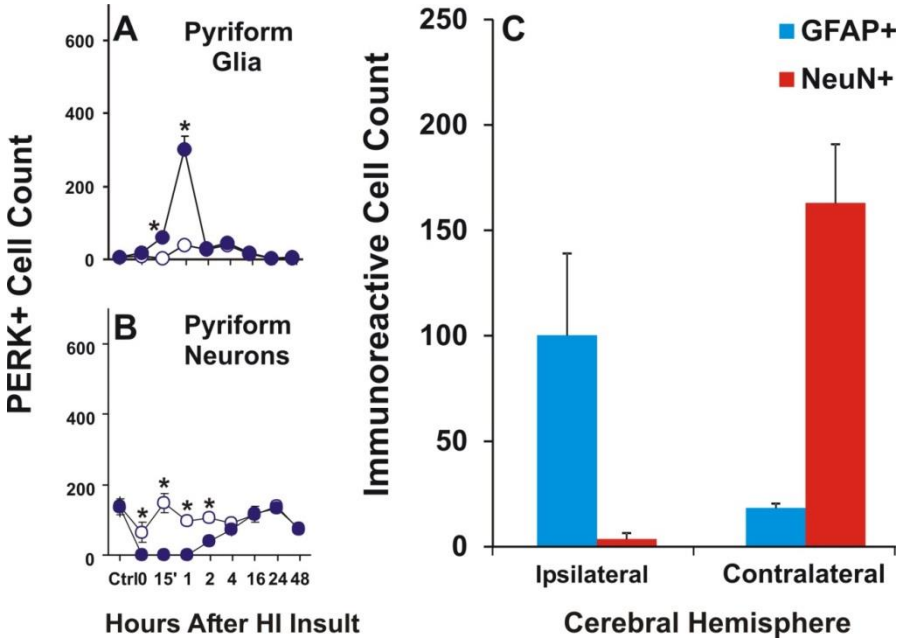

Figure 3.2 Phosphorylated ERK immunoreactive cells in pyriform cortex following HI insult. Blue circles are indicative of hemisphere regions ipsilateral to carotid artery occlusion. White circles indicate contralateral regions. Positive cell counts were assessed over 3 fields per region at a magnification of 20x and analysed as mean ± SEM, n=4 animals per time point. Positive cells were observed in both glia (A) and neurons (B). C indicates number of pERK positive cells co-expressing with markers of neurons (NeuN) and astrocytes (GFAP) in the pyriform region at 15min following 30min HI insult. Unlike other grey matter regions pERK positive glia are observed soon after insult whereas neuronal expression was suppressed. Glial pERK shows a peak at 1hr that returns to baseline levels by 2hr where there is a switch to neuronal expression until 24hr. *P<0.05 in paired student t-test for ipsilateral versus contralateral hemispheres.

The pyriform is a region of large soma neurons easily and histologically differentiated from neighbouring small soma glia. Consequently pERK positive cells were counted in terms of neurons and glia individually. Neuronal pERK expression was inhibited from 0-1hr following insult on the ipsilateral side. After which, there was a gradual increase until 16hr where bilateral expression plateaued until 48hr (figure 3.2B. In glia, expression was again inhibited until 15min, followed by a sharp increase a peak of expression at 1hr, returning to

baseline at 2hr (figure 3.2A). Contralateral glial expression is unchanged after HI.

ERK activation within the subcortical white matter (WM), an area strongly affected in periventricular leukomalacia, utilised electron microscopy to assess expression within neuronal axons. Between 0hr and 15min, no ERK activation was observed. At 15min, pERK was present within the axonal tracts of the periventricular corpus callosum, cingulum, fornix and internal capsule (figure 3.3B). Staining with silver/gold revealed that pERK clusters 200-500nM in size, occur in 1-2μM long segments within central axons. The segments of pERK expression within axons run parallel with neighbouring axonal segments within the WM (figure 3.3C and D, black arrows). Neuronal expression is gone by 1hr when it is superseded by glia immunoreactivity between 2-4hr. pERK positive glia extend throughout the external and internal capsules and the fornix.

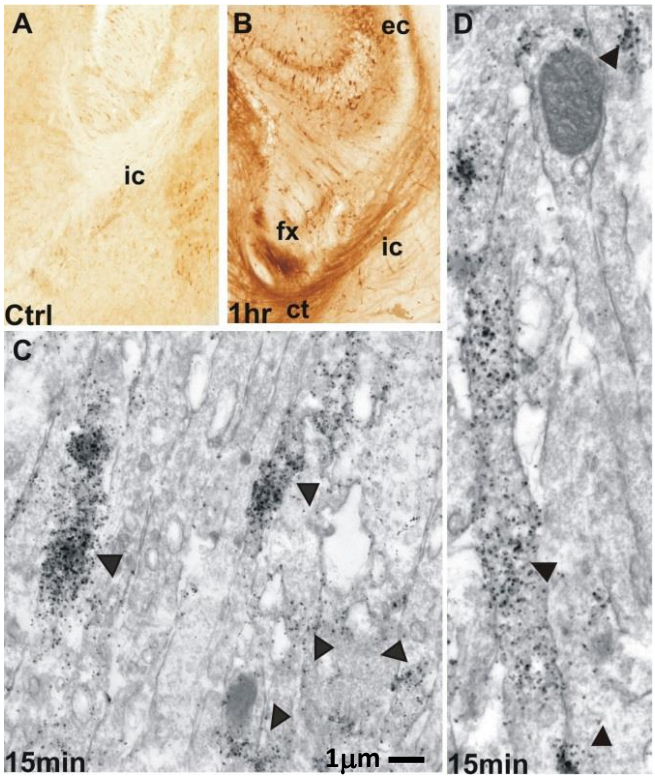

Figure 3.3 Schematic summary of white matter pERK expression with 30min hypoxia-ischemic insult. no pERK is seen at 0hr (A, Control), however by 1hr (B) there is a strong increase of expression in forebrain nerve fibre tracts within the external capsule (ec), fornix (fx), cortico-thalamic fibres (ct), and descending tracts of the internal capsule (ic). C, D: electron microscopy of the internal capsule. Early pERK reactivity is located to the axons only. Arrows point to pERK positive clusters within adjacent neurons.

In view of the critical function of ERK in regulating cell death, survival and activation, these separate windows of neuronal and glial expression provide a clear route in order to target one cell type or the other.

Generation of mutant mice lacking ERK 1 and neuronal ERK 2

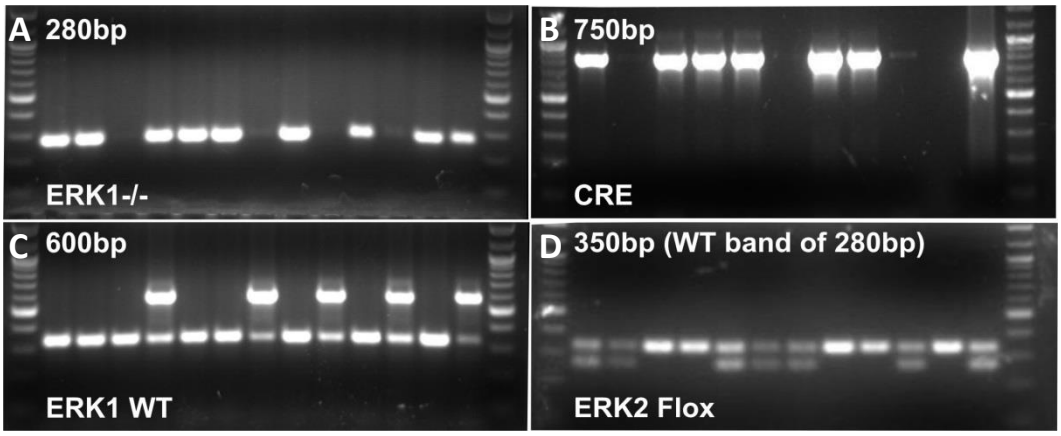

Figure 3.4 Generation of ERK mutant mice. Neuron-specific deletion of ERK 2 was achieved using Syn-Cre excision of floxed ERK 2 combined with global deletion of ERK 1. Agarose gel electrophoresis of PCR products were visualised to detect ERK 1 -/WT allele at 280bp/600bp respectively (A and B), ERK 2 floxed/wild type at 350bp and 280bp respectively (D), and Syn-Cre allele at 750bp (C). Whilst all animals with homozygous ERK2 floxed will show the appropriate bands, only those positive for Cre are mutants for neuronal ERK 2 deletion.

To examine cell type specific involvement of ERK, the cre-recombinase system was employed. Global deletion of ERK1 and 2 is impossible due to the embryonic lethality of $ERK2^{-/-}$. As such neuronal deletion of ERK was achieved by crossing mice with global ERK1 knock out ($ERK1^{-/-}$) with mice with ERK 2 flanked by LoxP sites (Floxed: $ERK2^{Fl/Fl}$). The offspring were further bred against animals expressing cre recombinase under the control of the synapsin promoter (Syn-Cre) which targets ERK2 excision specifically to neurons. Both global ERK1 and neuronal ERK2 deletion were confirmed by PCR and immunohistochemistry. Mice heterozygous for ERK 1 gave rise to a 280bp band for the null deletion and a 600bp band for the wild type (WT) allele. Though both $ERK2^{Fl/Fl}$ animals will show ERK2 to be floxed by a positive band of 350bp (and absence of non-floxed band at 280bp), only Syn-Cre: $ERK2^{Fl/Fl}$ mutants, with a positive band for cre, result in the removal of ERK2 from the neurons.

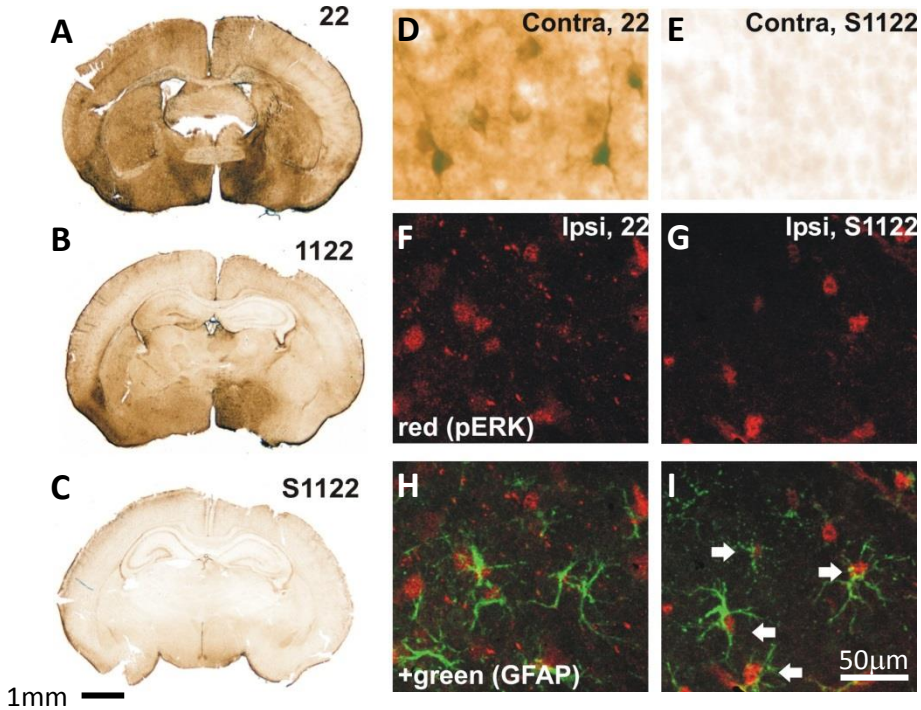

Figure 3.5 Effects of global ERK1 (11) and neuronal ERK2 deletion (S22) on pERK immunoreactivity following 30min HI insult and 15min recovery. A-C: A-shows a control (22) animal, B- mouse with global deletion of ERK1 (11), C-global deletion of ERK1 and neuronal deletion of both ERK2 copies (S22) at a 64x magnification. Note the reduction in pERK immunoreactivity in B and its almost complete disappearance following deletion of both copies of ERK1 and ERK2. In A-C, occluded hemisphere is on the right. D-I: Distribution of pERK at 64x magnification. PERK staining in the pyriform cortex. D, E: strong neuronal reactivity on the largely unaffected contralateral side, note the prominent dendritic staining in the wild type and its disappearance in S1122. F-I: residual immunoreactivity on the ipsilateral side, F, G: pERK alone. H, I: double labelling with GFAP. This co-localisation in astrocytes is particularly pronounced in S1122 (white arrows).

Further, ERK1$^{-/-}$ animals resulted in partial deletion of pERK activity after 30min HI whereas ERK1 and neuronal ERK2 deletion were associated with a near complete disappearance (90%) of activated ERK (figure 3.5A-C). Interestingly, animals with both ERK1 and neuronal ERK2 deletion saw an increased number of pERK positive glia compared to controls. This increase was confirmed by immunofluorescence co-labelling with GFAP, a marker of activated astrocytes (figure 3.4I). Mutant animals could not be bred homozygously due to the triple mutants becoming lethal at day 14 (See figure 3.11). As such, heterozygous breeding gave rise to four distinct genotypes: ERK2$^{Fl/Fl}$ alone (22) which were functionally wild type; Syn-Cre and ERK2$^{Fl/Fl}$ where neurons lacked ERK2 but ERK1 is expressed as normal (S22); global deletion of ERK1 and ERK2$^{Fl/Fl}$ (1122); and Syn-Cre plus ERK2$^{Fl/Fl}$ plus ERK1$^{-/-}$ (S1122) where ERK1 is homozygously knocked out in all cells and both alleles of ERK2 is deleted in neurons alone.

Neuronal deletion of ERK reduces microglial activation following mild hypoxia-ischemic insult

Following HI is an increase in neuronal cell death, and the recruitment of both microglia and astrocytes to the injury site, all of which contribute to increased infarct and lesion volume. Activation of cell death occurs within the first 48hr of insult, though other events such as phagocytosis of cell debris by microglia are later stage (>72hr). Previous work by this group has shown that whilst there is relatively little neuronal death following mild HI, damage can still be seen due to injury of the axons and oligodendrocyte precursors. In addition strong microglia activation occurs, as does their migration to the damaged white matter and surrounding grey matter (GM) regions. An event that often precedes the presence of dying cells in these areas.

To understand whether activated ERK is responsible for mediating cellular response to HI, we examined the expression of damage markers following exposure of mutant mouse pups to 30min 8% O_2. These include microglia activation and phagocytic phenotype via immunostaining for the integrin's alphaM (αM) and alphaX (αX) respectively, TUNEL positive cell death, and cresyl violet histology staining which also shows morphological changes such as shrinkage of Nissl bodies- itself an indicator of neuronal chromatolysis.

In total 35 pups at P7 were subject to 30min HI with a survival time of 48hr. Eleven animals died either at hypoxia or between hypoxia and 48hr. There was no discernable genotypic cause. Of those that survived, the brains were perfused and post-fixed as previously described. The animals were genotyped, resulting in 5x 22 animals, 5x S22 animals, 6x 1122, and 8x S1122. For each brain, five sections were retrieved per stain. The 22 pups, which have endogenous expression of both ERK1 and ERK2, are the controls for this experiment.

Activation of microglia after HI is a hallmark feature of regional sensitivity to insult, often appearing just prior to neuronal damage or cell death markers. Its quantification is via a scoring system of 0 to 4, where zero is non-stained fully ramified microglia, and four is amoeboid morphology as well as physical tissue damage. When the different forebrain regions were analysed independently, a

decrease in αM was observed in all GM regions (striatum, pyriform cortex, cortex, hippocampus, and thalamus) of S22 pups compared to 22 controls. Global deletion of ERK 1 (1122) aggravated the extent of microglia activation by an average of 30%, reaching 60% in hippocampus. This increase was insignificance by 2-way ANOVA and posthoc TUKEY (P>0.1). Damage exhibited by 1122 animals is muted in the presence of neuronal ERK 2 deletion (S1122) by up to 73% in the striatum. Again though, significance was not seen (P>0.09) (figure 3.7A). External capsule (WM) exhibited increased activated microglia in S22 (0.76±0.22), 1122 (1.50±0.63), and in S1122 (1.29±0.31) compared to 22 littermates (0.59±0.24).

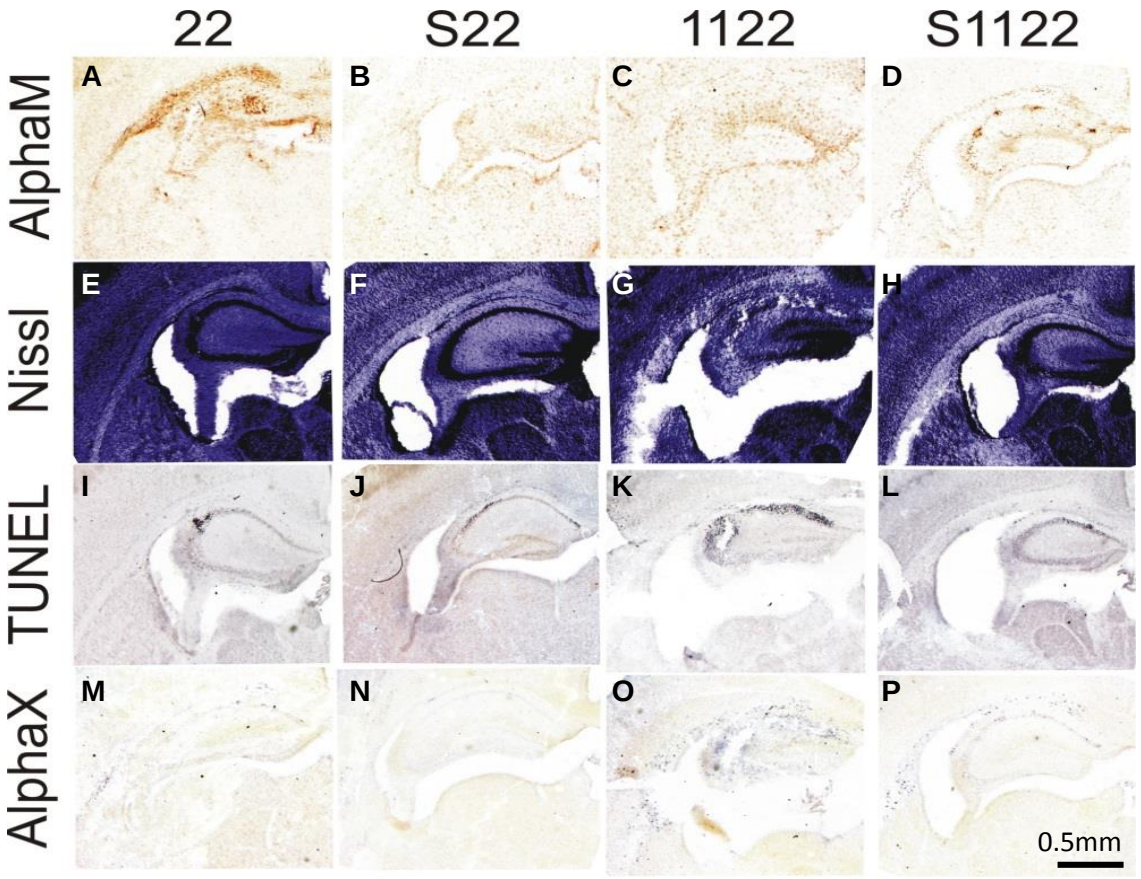

Figure 3.6 Illustrative response of the ipsilateral hemisphere in P7 mice to 30min HI. Transgenic mutant mice with combine global ERK1 deletion (11) and neuronal specific ERK2 deletion (S22) using the cre-recombinase system. Mice were bred to give four mutant variations: wild type (22), neuronal ERK2 deletion only (S22), Global ERK1 deletion only (1122), and global ERK1 deletion plus neuronal ERK2 deletion (S1122). Forebrain sections were analysed for microglia activation (A-D), neuronal loss (E-H), Tunel+ cell death (I-L) and phagocytic microglia (M-P). CTX (Cortex), STR (Striatum), EC (External Capsule), HIP (Hippocampus), THAL (Thalamus).

Neuronal loss, measured as an injury score (where 0 is no damage and 4 is extensive tissue loss) using cresyl violet histology of nissl body formation, and TUNEL positive cell death saw a more variable response than αM. Assessment for histological brain injury was performed by combining microglial activation

score to neuronal loss. S22, 1122, and S1122 mutants all had higher levels than 22 (figure 3.7C). 1122 were the most responsive to damage with hippocampus being the hardest hit region with a neuronal loss of 3.63±1.38, and Tunel count of 257.61±134.70. The dampening effect of S1122 was still evident in cortex, striatum, and hippocampus (figure 3.7E).

When the whole ipsilateral hemisphere was analysed, it was evident that single global deletion of ERK1 is highly detrimental following HI injury in the P7 mouse, with a strong significant increase of brain injury compared to control littermates where 2-way ANOVA and posthoc TUKEY gave a P value of 0.001. This is partially and significantly recovered when combined with neuronal deletion of ERK2 (S1122), P=0.005. The same differentiation of response between cohorts was observed with Tunel immunoreactivity, where 1122 animals had a significant increase in dying cell numbers (P=0.01) which was diminished in double mutants for ERK (p=0.04)

Similarly, phagocytic microglia increased in number in all forebrain regions of S22, 1122, and S1122 mutants. Deletion of ERK2 in neurons, either alone (S22) or in combination with $ERK1^{-/-}$ (S1122) gave rise to elevated numbers of phagocytic microglia within the external capsule (3fold) and hippocampus (2fold) when compared to 22 and 1122 animals respectively (figure 3.7G).

The contralateral hemisphere evidenced a baseline level of dying cells within the external capsule, striatum, cortex, hippocampus and thalamus, with an average of 8.66±0.93. Regionally these did not differ between the experimental groups (figure 3.7F) however, when taken over the whole hemisphere S22 animals exhibited significantly more dying cells than the wildtype littermates (P=0.001) which is in contrast to the neuroprotective nature of neuronal ERK2 deletion after combined hypoxia-ischemic insult. Lastly, external capsule showed low levels of both activated and phagocytic microglia with no specificity to genotype (figure 3.7H).

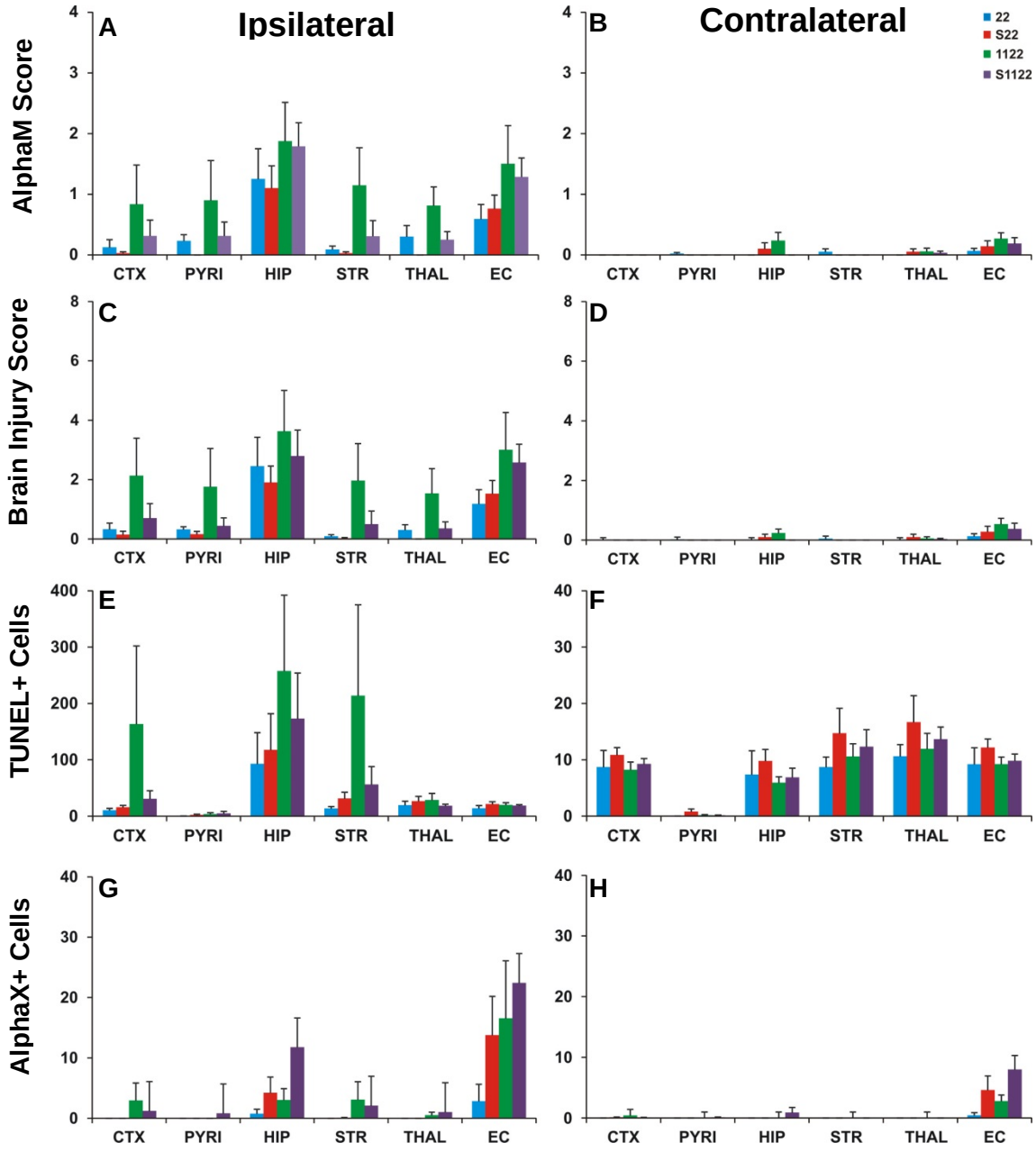

Figure ***3.7 Transgenic mutant mice were created to combine global ERK1 deletion (11) and neuronal specific ERK2 deletion (S22) using the cre-recombinase system. Four mutant variations were compared: wild type (22, blue), neuronal ERK2 deletion only (S22, red), Global ERK1 deletion only (1122, green), and global ERK1 deletion plus neuronal ERK2 deletion (S1122, purple). Forebrain sections were analysed for microglia activation (A-B), changes in brain injury (C-D), Tunel+ cell death (E-F) and phagocytic microglia (G-H). Analysis at 20x eye field (mean plus SEM over 3 fields) and student t-test used where significance is p<0.05. A-H: analysis of forebrain regions for damage markers. Regions include external capsule (EC), striatum (STR), pyriform cortex (PYR), cortex (CTX), hippocampus (HIP), and thalamus (THAL). A: microglia activation is reduced in the presence of neuronal ERK2 deletion (S22). Global ERK1 deletion (1122) causes a rise in immunoreactivity, however this is less so where neuronal ERK2 is also present (S1122). C-H: Tunel+ dying cells and recruitment of phagocytic microglia remain unchanged between groups. B, D, F, H: Contralateral hemisphere to carotid occlusion (hypoxia alone intracranial control). Baseline levels of active and phagocytic microglia are seen in the white matter (B and H). Developmental cell death occurs in all regions bar pyriform with no difference between groups (F). Significance was analysed using ANOVA and posthoc TUKEY.***

Neuronal deletion of ERK2 alone is insufficient to reduce damage with 60min HI

In order to verify the neuroprotective effect of neuronal ERK deletion, the above experiment was repeated with an increased severity of hypoxia. Previous work within this group have shown that exposure to 60min hypoxia leads to an almost complete loss of hippocampal neurons and severe tissue damage in cortex, thalamus and basal ganglia, as well as in the subcortical white matter. In addition, an elevated level of microglia activation occurs in comparison to milder insult. S22 animals (n=10) were compared to 22 (n=11) littermate controls when assessed for microglia activation (figure 3.8A-D, M), neuronal loss (figure 3.8E-H, N), Tunel positive dying cells (figure 3.8I-L, O) and the extent of resulting infarct volume (figure 3.8P).

Infarct volume is assessed by measuring the areas of intact cresyl violet staining, bilaterally for each forebrain region, and calculating the ipsilateral regions as percentages of the contralateral (uninjured) hemisphere.

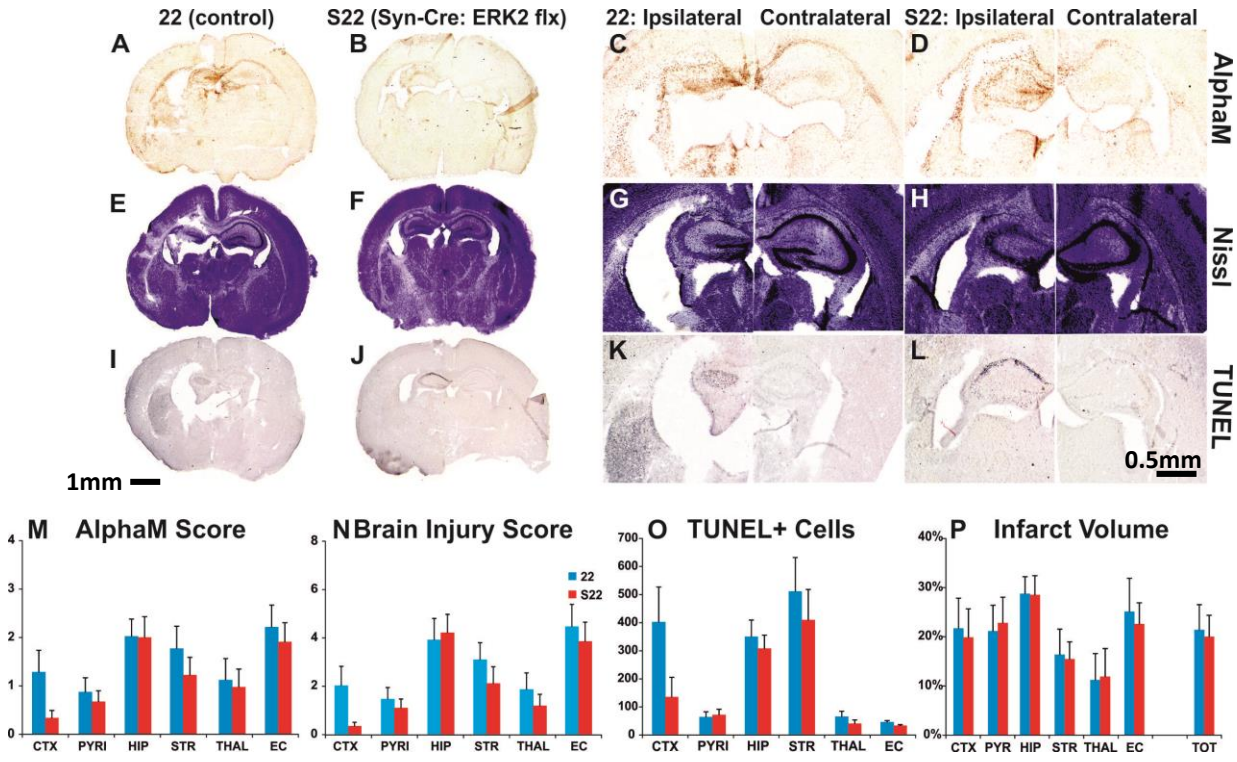

Figure 3.8 Effect of 60min hypoxia on P7 mutant mice with neuronal deletion of ERK 2 compared to littermate controls. At 48hr post insult, the animals were assessed for microglia activation (AlphaM, A, E, and F), neuronal loss (Nissl score, B, G, and H), dying cells (TUNEL, C, I, and J), and infarct volume (Nissl histology, D, G, and H). A trend decrease in each marker was observed in S22 animals but not to a significant extent.

Whilst all forebrain regions were individually assessed, an overall trend of a decrease in damage was observed in S22 animals compared to 22 controls.

The cortex was the area with greatest reduction of activated microglia, brain injury, and dying cells. However this was not significantly so with P=0.07, 0.06, 0.08 respective with the three markers. The reduction of injury was not reflected in the extent of infarction where there was no difference between groups in each region, nor in combined total area (TOT in figure 3.8D).

Glial deletion of ERK 2 is highly detrimental to the neonatal mouse brains response to mild hypoxic insult

ERK activation in astrocytes is implicated following oxygen deprivation in vitro. In mixed cell cultures of neurons and glia, pERK expression was near exclusively upregulated in astrocytes (co-labelling with GFAP) after NO toxicity and/or glutathione depletion (de Bernardo et al., 2004; Jiang et al., 2002). The ensuing neuronal cell death was recovered on application of MEK 1/2 selective inhibitors. In vivo studies of the P7 rat model of cerebral ischemia, 40% of pERK expressing cells were glia at 48hr following exposure to 2.5hr 8% O_2 (Wang et al., 2004a). Other models of neuronal injury verify this finding. For example, models of severe spinal cord trauma showed pERK expression in microglia and astrocytes adjacent to injury (Xu et al., 2006). Inhibition of ERK reduced neuronal loss at the site of injury. This indicates that glial ERK activity not only is an effect of HI, but also actively modulates the response of nearby neurons to insult.

To investigate this supposed role further ERK was deleted in astrocytes by the breeding of globally knocked out ERK1 ($ERK1^{-/-}$) mice with those that have ERK2 floxed ($ERK2^{Fl/Fl}$) to create the same 1122 mutants described previously. These were then further bred to mice expressing cre recombinase under the control of the GFAP (glial fibrillary acidic protein- a cell specific marker of astrocytes) promoter. Animals expressing both cre and $ERK2^{Fl/Fl}$ saw ERK2 deletion selective to astrocytes. Heterozygous breeding allowed for the generation of both 1122 and G1122 experimental groups. 22 (wildtype expression of ERK) controls were added to the experiment. P7 mouse pups were subject to 30min O_2 before returning to their dams for 48hr. At sacrifice, the brains were perfused and fixed in 4% PFA then cryoprotected in saturated sucrose solution. After which the brains were frozen, cryosectioned and stored at -80°C until required. At perfusion, the genotypes were ascertained, resulting

in 9 controls (22), and 10 each for the 1122 and G1122 groups. The brains were assessed for activated microglia, neuronal loss and number of TUNEL positive dying cells. Five sections per brain were retrieved for each immunostaining.

As with neuronal ERK deletion studies, single and global deletion of ERK1 resulted in exacerbation of the neonatal brains response to hypoxia-ischemia when compared to 22 controls.

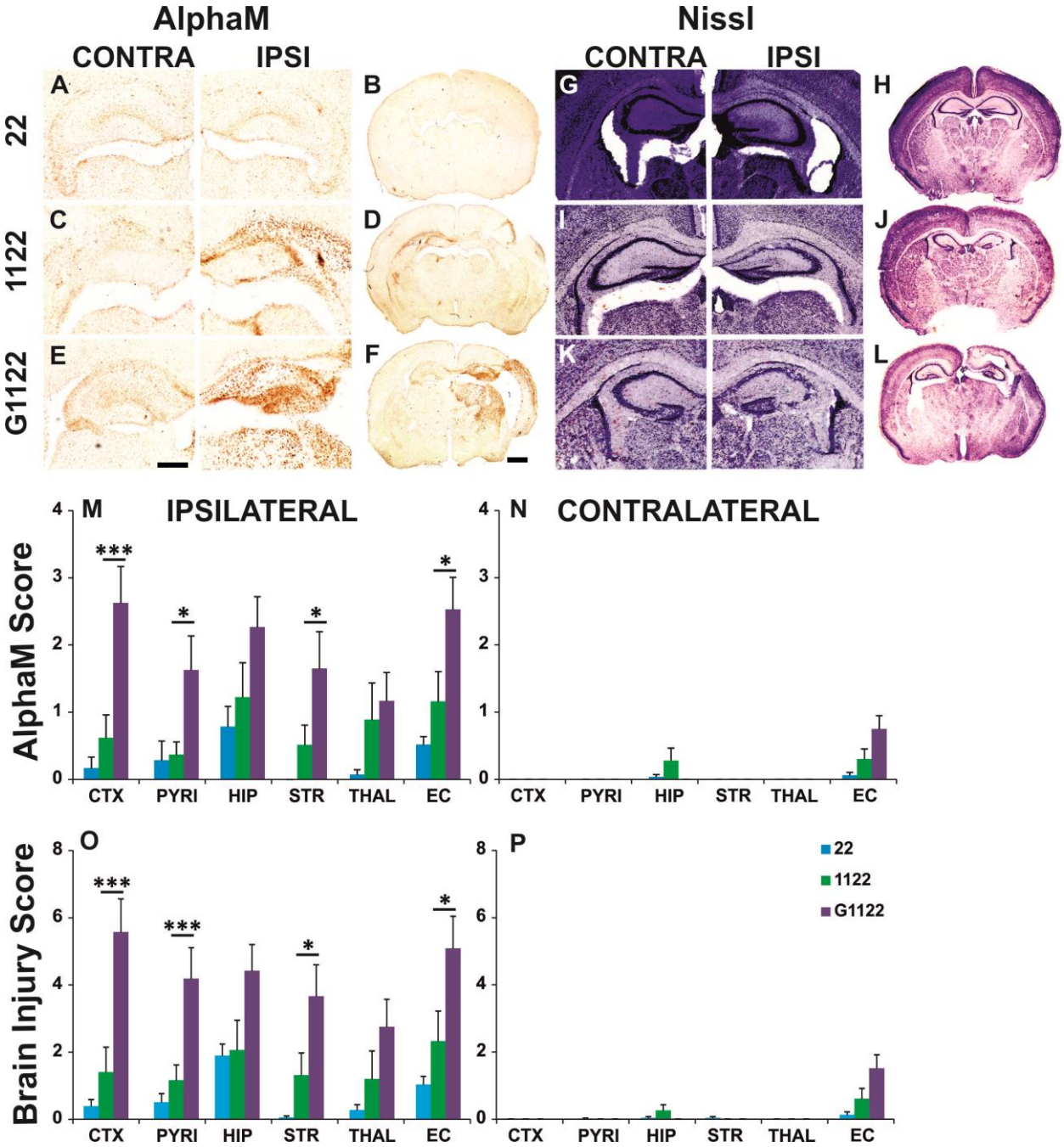

*Figure 3.9 microglia activation (A:F) and neuronal loss (G-L) in P7 transgenic mutant mice with global deletion of ERK 1 and astrocytic deletion of ERK 2, following 30min exposure to 8% oxygen. At 48hr post insult, a strong increase in microglial activation was observed, using αM immunostaining, in the ipsilateral hemispheres of both 1122 and G1122 groups compared to controls (M). This pattern of response was replicated in brain injury score, a combined score for microglial activation and neuronal loss (O). Black arrow indicates the CA1 region of hippocampus, area most affected by HI insult in this experiment. Scale bars indicate 0.5mm and 1mm respectively. *P= 0.05, ***P< 0.001 Using ANOVA and posthoc TUKEY.*

This was identified by increased microglial activation in all forebrain regions in addition to a higher score awarded for brain injury within the striatum, pyriform cortex, cortex, and thalamus. The number of TUNEL positive cells remained relatively unchanged between these two groups with the exception of striatum counts. Here the 1122 group showed an average number of dying cells at 133±61.8 compared to 45±27.6 in controls. The capacity of ERK 1 to sensitise damage response was not significant.

What provides a striking contrast to the neuronal ERK study is that a double mutation of $ERK1^{-/-}$ and astrocytic deletion of ERK2 (G1122) significantly intensifies the neonatal brains damage response to mild hypoxia.

AlphaM immunostaining was 24-76% higher in G1122 compared to 1122. Cortex, pyriform cortex, striatum and external capsule were significantly increased with a P value of 0.002, 0.02, 0.05, and 0.03 respectively (figure 3.8B, C, and G). The extent of brain injury proved even more effected. 1122 group showed elevated scores compared to 22 controls, uniform across the forebrain regions, with an average score of 1.58±0.74 (figure 8E and I). G1122 gave rise to a heightened response with significance in external capsule (p= 0.03), pyriform cortex (p= 0.04), striatum (p= 0.03) and cortex (p= 0.01) (figure 3.8F and I). The G1122 pyriform cortex and cortex were the most sensitive to injury with average scores of 4.17±0.92 and 5.54±0.92 respectively.

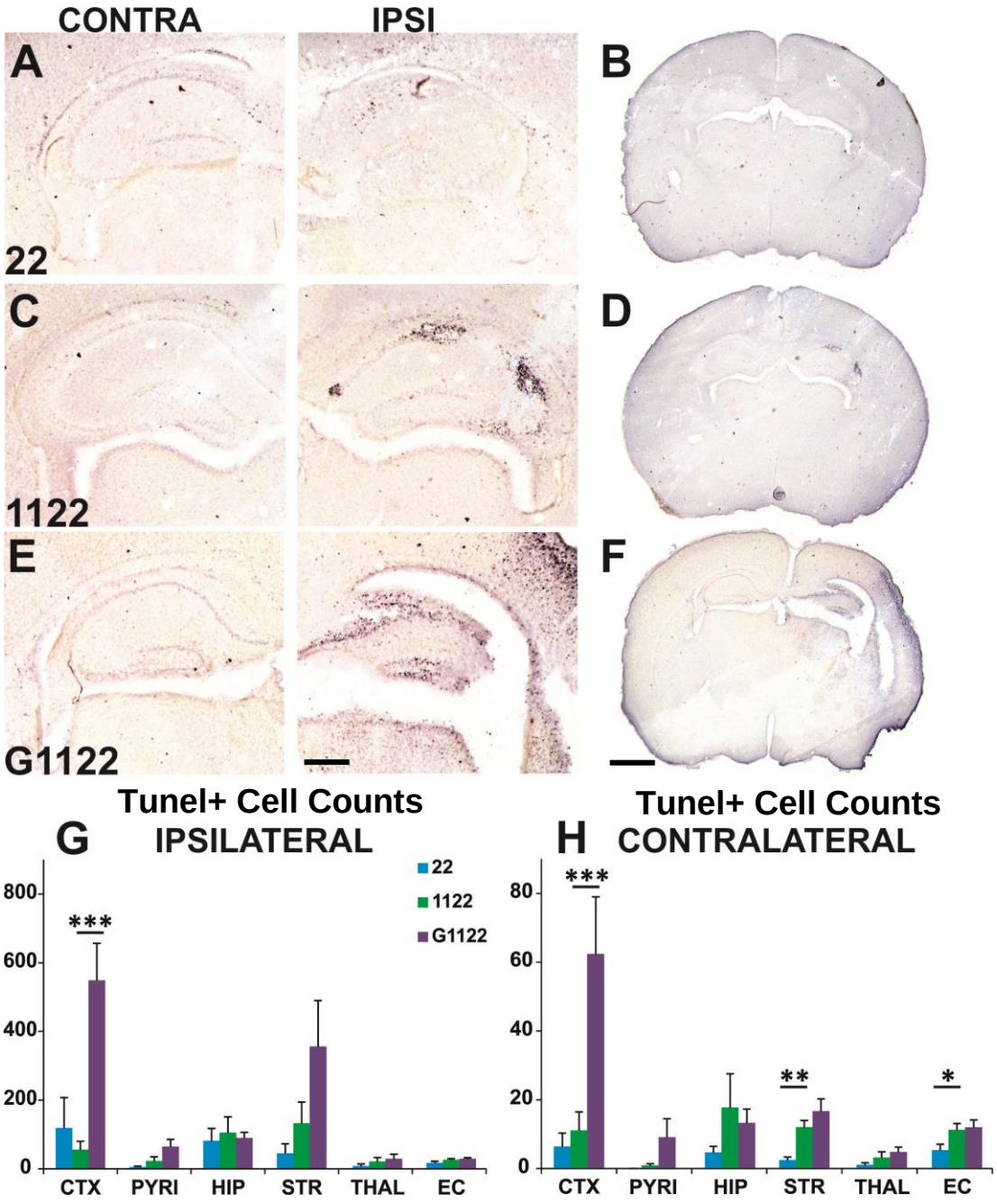

Figure 3.10 number of Tunel positive dying cells in P7 transgenic mutant mice with global deletion of ERK 1 and astrocytic deletion of ERK 2. Wild type controls (A) showed little increase in dying cells in either hypoxic or experimental hemispheres (D, E: Blue). Global deletion of ERK1 (1122) gave an increase in TUNEL expression in the hemisphere ipsilateral to carotid occlusion (B, D: Green). Global ERK 1 deletion in conjunction to deletion of ERK 2 in astrocytes (G1122) exacerbates damage further, particularly in thr cortex of both hemispheres (C: E Purple). Scale bar indicates 0.25mm and 1mm respectively. *P= 0.05, **P= 0.01. ***P< 0.01 by ANOVA with posthoc TUKEY.

Despite this evident tissue loss, Tunel positive cell death was not so clearly different between groups (figure 3.10). The number of dying cells remained at low levels for all three groups in external capsule, pyriform cortex, thalamus and hippocampus- this being the most affected of these regions with an average of 105±46.1 positive cells in 1122 animals and 90±0.76 in G1122 animals.

Conversely, striatum and cortex still exhibit an increase in dying cells within G1122 brains compared to 1122 and controls (figure 3.10E). Though striatum did not reach significance (p= 0.15) there were 356±135 Tunel stained cells whereas 1122 had 133±61.8. This alteration was far more pronounced in cortex where G1122 had the highest number of dying cells (548±108) significantly more so than 1122 (p= 0.0004). Interestingly, this effect was bilateral, with contralateral cortex of G1122 also showing elevated numbers of dying cells (p= 0.003). Single ERK1 deletion proved additionally detrimental in the hypoxia-alone contralateral hemisphere, with a significant increase of Tunel immunoreactivity observed in striatum and external capsule compared to wildtype controls (figure 3.10G). All other contralateral regions remained at baseline expression.

Cell Specific Deletion of ERK 1 and 2- Discussion

Risk factors to neonatal brain injury are hard to identify due to the variability of response between patients. What remains clear is that beyond a critical threshold, cellular mechanisms fail ending in a two-phase energy failure response ultimately resulting in neuronal death, tissue lesion and poor neurological outcome.

Accumulating evidence suggests that members of the MAPK, including ERK1/2, JNK1-3, and ERK5 signalling cascade, provide a prevailing contribution to the cerebral response to hypoxia-ischemic (HI) insult. In adult models of focal cerebral ischemia, inhibitors of MEK1/2 gave rise to a range of neuroprotective effects dependent on the model used (Alessandrini et al., 1999; Ferrer et al., 2003; Namura et al., 2001). As the direct downstream target of MEK1/2, these selective inhibitors prevented ERK1/2 activation. Phosphorylated ERK (pERK) was observed to co-express with damage markers following neonatal HI in rodent models. As such, it is believed that the actions of MEK inhibition are through the prevention of ERK activity on downstream pro-apoptotic targets including Elk1, Bcl-2, and Bad. ERK promotes cell death through activation by growth factor receptors, Ca^{2+} channels or by binding to complexes with Src-tyrosine kinase.

Time course for phosphorylated ERK expression following HI

The Rice-Vannucci HI model is well characterised as a paradigm with which to study the molecular mechanisms underlying both white matter and grey matter pathology following insult to the late preterm/term newborn.

Postnatal day 7 (P7) mouse pups were subject to 30min exposure to 8% O_2 and analysed for injury induced somatic expression of pERK in the forebrain grey matter regions: cortex, striatum, hippocampus, thalamus, and pyriform cortex.

In most regions, ipsilateral expression of pERK was immediately nullified for the first 15min following insult when compared to sham hypoxia controls. This was followed by a rapid bilateral assent of expression that peaks at 1hr and is normalised by 4hr. This pattern of rapidly activated ERK is in line with the observations by other groups working both neonatal and adult models

(Alessandrini et al., 1999; van den Tweel et al., 2006; Wang et al., 2003b; Wang et al., 2004a) who established the pattern of pERK expression in both adult and neonatal rodent models of HI. Following Rice Vannucci model of unilateral carotid occlusion in P12 rat see bilateral expression changes of kinases and downstream hypoxia responder, HIF1a and HSP70 as well as cytokine response within first 6h following 90min HI.

In particular pAKT was down-regulated in both hemispheres whereas pERK and HIF1a were upregulated in both. Hypoxia alone controls were to a similar level as that observed in contralateral regions but in all three groups, expression greatly exceed sham surgery controls. MAP histological staining for neuronal damage confirmed damage to ipsilateral regions only as seen in our own model.

At 6 weeks post insult, there is still no histological damage to the contralateral hemisphere and pERK expression is higher in ipsilateral regions. This leads us to question changes in regulatory molecules that occur in both hemispheres after HI. As neither ischemia nor hypoxia alone were enough to induce damage, changes observed in both hemispheres are not neurotoxic or protective by themselves but need additional ischemia induced signals in the ipsilateral side to contribute to cell death (van den Tweel et al., 2006).

Where our results deviate is in the initial dampening of active ERK, between 0-15min, after insult. Giora Feuerstein and colleagues demonstrated that with 30min middle cerebral artery occlusion (MCAO) in adult C57/Bl6 mice, pERK expression was delayed until up to 10min following insult when a reperfusion stage of 3min was disallowed to occur. With reperfusion, ERK activation was immediately elevated, beyond that seen at 10min without reperfusion (Wang et al., 2003b). That pERK expression was only affected on the ipsilateral side to carotid artery occlusion (CROC) suggests that it is an affect from the combined hypoxic-ischemic insult and not hypoxia alone. The discrepancy of our studies to others may arise from the first 15min being the boundary time point for reperfusion in our animals.

Initial dampening of pERK was similarly observed in white matter expression. Due to the lack of neuronal bodies, the white matter regions of external and internal capsule, and the cortico-thalamic fibres were examined under the

electron microscope. The appearance of axonal pERK was only observed from 15min onwards, and normalising by 1hr. This was swiftly followed by white matter glial body expression of pERK from 2-4hr post insult. PERK appeared to be contained in clusters along the axon, adjacent to neighbouring pERK positive axons. That pERK positive axons bundle together following HI has not been reported before now. This effect coincides with others observations that cells showing cytoplasmic pERK activity are commonly adjacent to one another at the borders of ischemia-induced micro lesions (Wang et al., 2003b). Another study looked at regional distribution of ERK and pERK activity after HI in the P7 rat. After insult the subventricular zone, a region with high white matter content, saw earlier ERK phosphorylation at 30min followed by a second latent peak at 3-8hr. This was in contrast to grey matter regions were a single peak at 1hr was seen (Wang et al., 2004a).

Nucleation of pERK from the axon to neuronal soma occurs via vesicular transport, regulated by the Vementin/Importin-β1 complex (Gumy et al., 2010; Perlson et al., 2006). Phosphorylated ERK binds to Vementin at thr183 and tyr185 effectively allowing Vementin to occlude ERKs phosphor-acceptor sites, rendering it constitutively active (Perlson et al., 2006). Importin is a nuclear transporter, allowing the entry of pERK into the nucleus where it can act on downstream nuclear targets such as Elk1 (Gumy et al., 2010). One can theorise that this vesicle bound pERK is responsible for the clustering of pERK within the axonal tracts.

Within most forebrain regions, small neurons and glial cell bodies showed an extensive overlap in bilateral regulation of pERK activity. In pyriform cortex, ipsilateral neurons showed a pronounced and extended inhibition of pERK up to two hours post insult. From here, an increase until 4hr occurred followed by prolonged plateau of response until 24hr after which expression gradually declined. At the same time, the ipsilateral glia gave rise to a rapid and intense increase in immunoreactivity, peaking at 1hr and normalising by 2hr.

The pyriform cortex is a highly developed region of the rodent forebrain. Its three-tiered construction is an extension of the olfactory cortex, with strong links to the amygdala and hippocampus (Giessel and Datta, 2014; Gutiérrez-Castellanos et al., 2014). Cells of the pyriform have strong morphological

identity with large soma pyramidal neurons and small soma stellate astrocytes (He et al., 2014; Nacher et al., 2002). Using co-immunofluorescence, we were able to determine that at 15min post insult the majority of pERK positive cells were NeuN (a marker for neurons) negative and GFAP (astrocyte marker) positive (figure 3.2).

Whilst it is clear that the majority of pERK positive cells are astrocytes, pyriform does contain a subpopulation of small soma migratory interneurons-neurogliaform that are negative for NeuN (He et al., 2014; Nacher et al., 2002). These may account for pERK expressing cells that were both NeuN and GFAP negative within the region. Additionally this means we cannot exclude the idea that neuronal expression of pERK is earlier than 2hr, as the initial glial counts for pERK were based on morphology and so may have included neurogliaform cells amongst their numbers. Due to the equipment available, we were unable to add to this experiment as NeuN could not be lo-labelled with another marker, in this case pERK, within the experimental samples. For the same reason it was not possible to provide an illustrative figure to exemplify the counts.

Within the literature, there is no mention of regions showing pERK expression in glia to precede that of neurons after HI injury. However as only these experiments and those by Wang and colleagues (Wang et al., 2004a) have looked at regional regulation of pERK over whole hemisphere response, there is the possibility that cell specific expression is regulated on a region by region basis. Why ipsilateral glia response occurs prior to bilateral neuronal activity in pyriform awaits further research.

Damage markers for determining the extent of injury following HI in the neonatal brain

Within this thesis the following damage markers have been used collectively in order to understand to what extends the neonatal brain is injured by HI. Only by comparing changes in these staining's we are able to determine that the mutated/inhibited genes of interest are either a hindrance or help to neuroprotection. Markers include: microglia and astrocyte activation via increased expression of integrin αM and GFAP respectively, histological brain injury- a combination of microglia activation score and tissue loss score, the

latter gained by scoring the presence of nissl body formation and physical tissue damage. As extended microglia activation can lead to a confirmed phenotypic shift to phagocytic, the number of cells positive for αX integrin, expressed by microglia only at this latent phagocyte time point, were counted. In addition, the number of Tunel (terminal deoxynucleotidyl transferase dUTP nick end) positive cells was calculated per region as a measure of dying cells. Lastly a measure of infarct, lesions at the sites of cell death and tissue loss, was determined by measuring the volume of healthy tissue on the ipsilateral, HI hemisphere region as a percentage to its contralateral, hypoxia alone counterpart. Activation of microglia after HI is a hallmark feature of regional sensitivity to insult, often appearing just prior to neuronal damage or cell death markers. Without profiling for microglia cytokine release we cannot know whether those expressing increased αM are type 1, or pro-inflammatory, or type 2- anti-inflammatory. However, the consistent upregulation of αM does delineate a clear response to HI injury. It is only in combination with other markers such as nissl histology and αX expression that we can form a picture of whether microglial response is protective or detrimental. Close proximity to nissl body formation and structural damage to ipsilateral regions is suggestive of a detrimental phenotype in addition to phagocytic cell counts via αX expression. These markers combined give a robust score for brain injury. This is in addition to dying cell numbers in the same areas. Each marker is tested on sequential slides meaning that cells through each region are looked at in close proximity to one another. GFAP was studied to observe astrocyte activation. GFAP is perpetually expressed at low levels by astrocytes. However in multiple injury models it has been shown not only to be upregulated but localised to injured cells. Lastly a measurement of infarct following insult is a robust and well used analysis to show the extent and severity of damage.

Neuronal deletion of ERK2 promotes cell survival in neonatal cerebral response to HI

Pharmacological MEK1/2 inhibitors prove highly effective in reducing infarct volume and neuronal cell death following adult focal cerebral and global ischemic insult (Alessandrini et al., 1999; Jones and Bergeron, 2004; Li et al., 2008; Namura et al., 2001; Wang et al., 2003b; Wang et al., 2004b). Hans and

Holtzman attempted to utilise the highly selective inhibitor U0126 in the neonatal rat model, but with little success (Han and Holtzman, 2000). Since then, many other studies of ischemic insult, have been non-conciliatory as to whether ERK is acting in a pro-survival or pro-death manner (Almeida et al., 2005; Armstead et al., 2008; Bodart, 2010; Bogoyevitch and Court, 2004; Canals et al., 2003; Castro-Obregón et al., 2004; Chen et al., 2009; D'Cruz et al., 2005; de Bernardo et al., 2004; Feng et al., 2008; Guo et al., 2012; Ho et al., 2008; Jin et al., 2002; Luo and DeFranco, 2006; Narasimhan et al., 2009; Stanciu, 2000; Szydlowska et al., 2010; Wakade et al., 2008; Wang et al., 2004b; Zhang et al., 2007) .

Neuronal ERK activation, with the exception of pyriform cortex, precedes that of astrocytic activation. To test how cell specific activation of ERK contributes to injury, and to examine if these cellular responses are complimentary or opposing, we created selective ERK mutants where excision of the gene occurs via synapsin or glial driven cre recombinase respectively. Single neuronal ERK2 deletion mice were analysed next to wildtype ERK expressing controls. Mice with double mutation for neuronal ERK 2 and global ERK1 were compared to single ERK1 mutants and controls. Successful pERK inhibition was confirmed by immunohistochemistry, where double mutants showed 90% reduction following HI (figure 3.4).

Mortality rate for this experiment were high with 11 of 35 experimental animals dying before end point of 48hr. As noted there was no genetic cause for an increase in death rate amongst the pups. When analysing possible caused it became apparent that the information given is inaccurate. A total of 64 animals underwent surgery, however due to the animals being bred heterozygously; many were excluded from the experiment due to unrequired genotypes. All affected animals were from the first two litters of the same breeding pair and that of the 11, only 2 died in hypoxia. Typical period of death was between 24-48hr post deaths. Although it cannot be denied that human error may have led to their death, for example poor recovery practise post-surgery, it is not uncommon for dams, especially inexperienced ones to commit infanticide. Mann et al. (1983) showed that 25-40% of young C57/Bl6 dams, the strain on which our own animals are bred, will kill their pups. However those aged 45days

and older seldom do. Additionally levels of infanticide were reduced to 5% in age matched DBA dams indicating that this effect is strain mediated (Mann et al., 1983). More recently, studies have shown that both strain and parity will influence litter loss by comparing C57/Bl6 ad Bulb/C mice. The former had a mortality rate of 32% of litters whereas the latter had 20% with a significant increase in death of first litters. Parity, or previous parental experience of litter loss, did not affect later litter loss (Weber et al., 2013).

Microglia activation is a strong pre-emptive marker for cerebral cell damage. They typically exhibit a bi-functional response to injury. After initial insult, microglia are observed to surround, isolate off, injured tissue with their arborized dendrites. Later, microglia morphologically change into phagocytic phenotypes in order to remove cell debris. Alternatively, they can exacerbate existing damage by the release of proinflammatory and cytotoxic cytokines, neurotransmitters, glutamate, and nitric oxide synthase (Raivich, 2005). Previous work in this laboratory confirmed 48hr post-insult to be the considered time point in which to study the dynamics of microglia activation in the Rice-Vannucci mouse model of HI (Kendall et al., 2011a).

Neuronal deletion of ERK2 showed a clear reduction in active microglia within grey matter regions of the forebrain. Decreased activation ranged between 12-100% when compared to wild type controls, with significance reached in pyriform. Brain injury score which combined microglia activation and histological assessment of tissue loss reflected this loss of injury damage with a mild reduction in all grey matter regions. 30min exposure to 8% O_2 is enough to incite microglia activation and white matter injury, with axonal and oligodendrocyte (ODC) damage (Kendall et al., 2006; Skoff et al., 2001) but it proves here to be rate limiting as indicated by neuronal sparing with Tunel positive dying cells, observed in hippocampus only, and a lack of phagocytic microglia outside of the external capsule. For both markers, no change was distinguishable between mutants and controls.

With a more severe insult of 60min HI, cell dying throughout the cerebral forebrain, in addition to the formation of tissue lesions, particularly in the hippocampus, has been recorded (Lehnardt et al., 2003). With this level of HI, infarct has been linked to almost complete loss of hippocampus neurons as well

as significant damage to the cortex, thalamus, basal ganglia and white matter. In our mutants of ERK2 deletion in neurons, exposure to 60min of 8% O_2 exhibited a reduction in microglial activation by an average of 26%, up to 74% in cortex. This pattern of response was validated in brain injury score and in Tunel positive cell death with cortex, pyriform cortex, and striatum being regions of particular sensitivity. The difference between cohorts was almost significant with 2-way ANOVA P values between 0.06-0.09. Despite a clear effect on glial response to insult, HI lesion size remained unaffected.

ERK activation is strongly linked to cell death, despite its initial function in cell proliferation. The pro-apoptotic nature of ERK was first established in ODC cell cultures subject to H_2O_2. Here cell survival increased on application of the MEK selective inhibitor PD98059 (Bhat and Zhang, 1999). In neuronal cells, glutathione depletion led to ROS activation of ERK 1/2. U0126, a more specific MEK inhibitor, prevented neuronal cell death (Canals et al., 2003; de Bernardo et al., 2004). In vivo, hippocampus damage, following traumatic brain injury was reduced with post insult administration of PD98059 (Kwok-Tung Lu, 2011). Additionally ERK regulation of Tau, resulting in its sustained production (Kim and Choi, 2010), implicated ERK to be neurodegenerative in Alzheimer's disease. In a study of camptothecin-induced apoptosis in cortical neurons, pERK was sequestered to the nucleus within 4hr of camptothecin exposure. This resulted in the upregulation of pro-apoptotic transcription factors including Elk-1, Sap, and SP1 (Lesuisse and Martin, 2002). Lastly, in models of calpain toxicity, an influx of Ca^{2+} results in ROS production and subsequent Ras-mediated activation of C-Raf and ERK. ROS is able to sustain ERK activation via the inhibition of the scaffold proteins DUSP1 and 6 (Cagnol and Chambard, 2010; Martin and Pognonec, 2010). ROS activation of ERK resulted in dysfunction of the mitochondrial outer membrane inciting cytochrome C (CTC) release and cleavage of caspases 3 and 8 (Martin and Pognonec, 2010; Nowak et al., 2006; Nowak, 2002). ERK can further promote CTC release via the upregulation of Bax, PUMA, and Bad (Cagnol and Chambard, 2010).

Whilst our studies were insignificant, the neuroprotection of ERK deletion correlates well with the actions of MEK inhibitors in adult MCAO work. Alessandrini's group showed that in the adult gerbil model of focal cerebral

ischemia, infarct was reduced by 55%, suggesting that like our model, ERK must be acting alongside other complimentary or parallel pro-apoptotic pathways in order to induce cell death after HI (Namura et al., 2001). In fact, Luo et al. postulate that co-operation is essential due to ERKs polar roles in protection and degradation in conjunction to the observation that sustained ERK activation without neuro-trauma is unable to induce cell death (Luo and DeFranco, 2006).

Global ERK 1 deletion enhances neurodegenerative response to neonatal HI

Within this study, we have shown that neuron specific ERK2 deletion rescues neuronal cell death from HI injury. By deleting ERK1 globally, we observed a contrasting effect: ERK1 mutation results in an increase in extent of 30min HI induced damage compared to littermate controls. Microglial activation was increased by an average of 68%, brain injury- by 73% and Tunel positive cell death- by 67%. Additionally there was a 42% increase in the number of phagocytic microglia. In adult mouse forebrain, expression of ERK1 is significantly lower than that of ERK2, up to 6fold less in the frontal cortex (Ortiz et al., 1995). The complimentary and ubiquitous co-expression of ERK1 and 2 has led to the current paradigm that ERK1 is a fine tuner of ERK2 actions on cell growth and survival (Lefloch et al., 2008; Pouysségur and Lenormand, 2003). This is due to ERK2 activation of downstream nuclear targets, whereas ERK1 deletion showed no effect on either cell proliferation or maturation by nuclear target acquisition. Mice mutant for ERK 1 deletion are embryonically viable with no phenotypic differences to wild type littermates. However, developmental complications have associated ERK1 to thrombocyte dysfunction (Lefloch et al., 2008; Nekrasova et al., 2005), but conversely to long term potentiation within the hippocampus resulting in improved outcome after seizure (Rosenblum et al., 2002; Selcher et al., 2003) . Behavioural studies have linked the MAP3K gene on chromosome 16, encoding ERK1, to altered synaptic plasticity and associated behavioural abnormalities that include autism (Campbell et al., 2008; Engel et al., 2008; Fernandez et al., 2010; Pucilowska et al., 2012).

Despite these studies, there is little information as to how suppression of ERK1 can exacerbate injury in the neonatal HI mouse and further work is required to

elucidate the role of ERK1 in injury response. There are a couple of studies that that support ERK1 to regulate neuronal homeostasis, although the mechanisms in which it does so are still unclear. In the rat model of sciatic nerve ligation, an increase in ERK1 but not ERK2 activity was observed at the ligation site within the first hour of injury (Reynolds et al., 2001). The adverse effects of ERK1 could be due to its regulation of ERK2 activity. Under certain circumstances ERK1 can attenuate ERK2 signal and indeed, ERK2 upregulation is seen in ERK1$^{-/-}$ mice (Lefloch et al., 2008; Samuels et al., 2008; Selcher et al., 2003) which, as we have shown herein, promotes neuronal death following HI.

By examining the mutant mice for global ERK1 combined with neuronal ERK2 deletion, we see that damage is less severe than seen in the single ERK1 mutants. In double mutants, there is a modest recovery of ERK1 mutation induced neurodegeneration. Although not significant (P>0.09) microglia activation was reduced by 48% over the whole hemisphere with 73% in striatum. DNA fragmentation, as an indicator of cell death (Tunel) had a mean decrease of 32% of positive cells, with striatum reaching 74% and cortex- 81%. This suggests that ERK1 and ERK2 are interacting with one another, albeit disparagingly, to produce the response to HI observed.

We were unable to study the effects of double ERK -1 and -2 suppression under severe HI insult due to increased mortality rates of this genotype between 30-45min exposures to hypoxia. In sham surgery animals, there is no phenotypic difference between single ERK1 mutants and double mutants at P7. By P14, however the double mutants were significantly smaller and severely encephalitic with hydrocephalus resulting in death shortly after (figure 3.11).

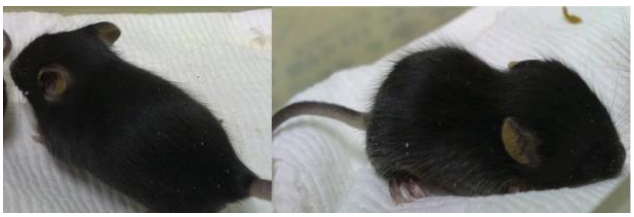

Figure 3.11 littermate 1122 (left) d14 pups compared to its S1122 littermate (right) before sacrifice. The S1122 pup is much smaller than its counterpart, with an enlarged cranium. On sacrifice, it was clear that this swelling was due to an increase in fluid between the skull and brain (not shown)

These observations were validated by Gary Landreth's group where they observed that double mutation of ERK, using pan-CNS ERK 2 deletions under

the EMX1 promoter, displayed cortical reduction by P10 with a lack of milk in their stomachs, suggesting they did not feed sufficiently. This led to the majority of double mutants dying within the first week of life. Of those that survived until P21, double mutants exhibited a 38% increase in neurological deficit (Nekrasova et al., 2005; Samuels et al., 2008).

Together this indicates that whilst deletion of ERK2 alone may be beneficial, but sustained deletion of both ERK1 and ERK2, especially during the developmental period, could give rise to poor neurological outcome and death.

ERK2 nullification in astrocytes further increases the adverse neuropathology due to ERK1 global deletion

There is an evident switch from neuronal to glial activity of ERK after HI. In addition, we observed that following neuronal ERK deletion, there was a greater incidence of pERK co-immunoreactivity with GFAP indicating a regulatory interaction between these two cells. As such, we focused on the analysis of ERK deletion in astrocytes. Single and global ERK1 mutant mice were compared to both double mutants for ERK1 and astrocytic ERK2, and to wild type controls.

Following exposure to 8% O_2 for 30min, the neuro-detrimental effects of ERK1 global deletion, seen in the previous experiment, were faithfully replicated. Surprisingly, double mutants exhibited an even greater deleterious effect with significantly higher expression of each damage marker. Cortex was the region most sensitive to injury with a 76% increase in microglial activation and brain injury score over that observed with single ERK1 deletion. DNA fragmentation, by Tunel immunoreactivity, was increased by 90% in cortex. Interestingly the detrimental effect of double mutation extended into the contralateral, hypoxia-alone, cortex although no other region was affected.

Han and Holtzman first indicated early ERK activation in astrocytes, following neonatal HI, in the P7 rat model. Here they observed high numbers of pERK expressing astrocytes, however the data remains unpublished (Han and Holtzman, 2000). In vitro studies on primary cortical astrocyte cultures from newborn mice, show that with exposure to either 4hr or 6hr ischemia activated ERK was pro-survival via its actions on anti-apoptotic Bcl-2 (Jiang et al., 2002).

Other in vitro studies had indicated astrocytes to protect ODC precursors, the cells most sensitive to oxidative stress in the neonate and as such held partially responsible for subsequent white matter injury, against H_2O_2 insult via the upregulation of pERK. Here, application of U0126 cancels the protective nature of astrocytes (Arai and Lo, 2010).

Contralateral cell death in cortex may be indicative of developmental dysregulation of astrocyte function that occurs from ERK2 deletion. Gary Landreth's laboratory also looked at ERK2 excision under the GFAP promoter in the developing mouse. They observed that whilst ODC precursor cells develop normally, there is a significant delay in maturation and reduced myelin production. Immature ODC are particularly sensitive to free radicals, cytokines and glutamate by their lack of antioxidant agents such as glutathione as well as glutamate uptake receptors and co-transporters. This is illustrated in figure 3.12. (Dewar et al., 2003). Glutathione sees a near immediate depletion following hypoxia ischemia, with no recovery for at least 24hr following insult (Wallin et al., 2000). Glial regulation of both neuronal and ODC survival is believed to derive from uptake of glutamate from the extracellular space in addition to reducing the actions of ROS on mitochondrial function (Bambrick et al., 2004). Astroglial uptake of glutamate at NMDA receptors is enhanced by ERK regulation rendering them active for longer (Szydlowska et al., 2010).

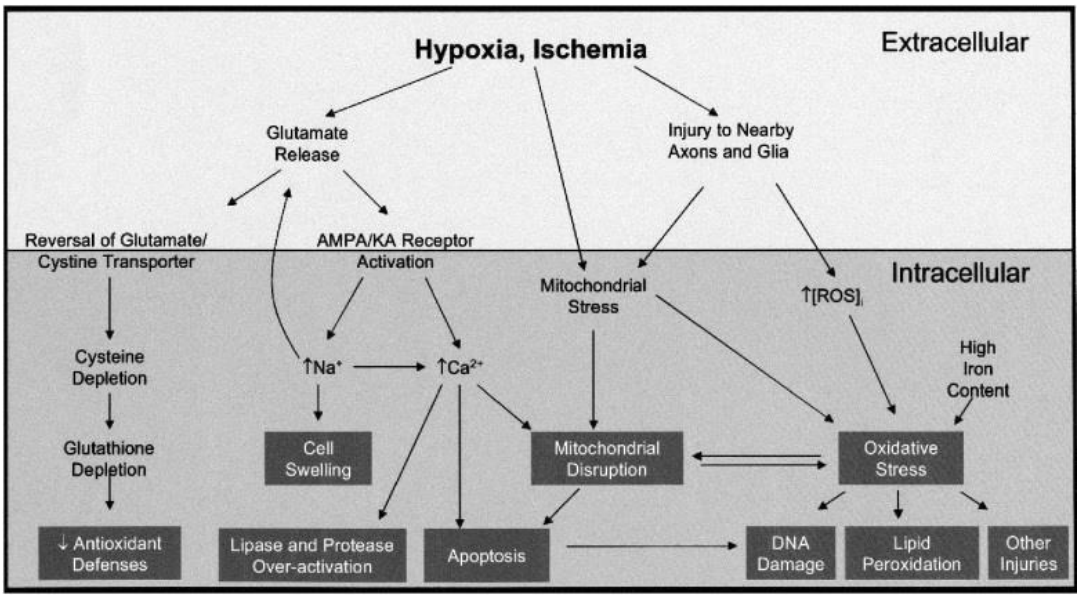

Figure 3.12 Potential mechanisms of cellular pathways in oligodendrocyte injury after hypoxia or ischemia. Reproduced with permission (Dewar et al. 2003).

The last implication of neuroprotective astrocytic ERK lies in studies with erythropoietin (EPO). Endogenous EPO is a glycoprotein hormone, essential for red blood cell production and as an antioxidant against ROS. Recombinant EPO was taken into clinical trials for neonatal HIE where it proved effective against mild insult (Perrone et al., 2013). EPO is shown to reduce NMDA mediated insult by increasing glutamate uptake in addition to up-regulation of Bcl-2 and down regulation of BCL2, Bax and IL-1β (Shen et al., 2009). Endogenous brain EPO is solely produced by astrocytes, whereas its receptors are located on neurons only (Lee et al., 2004; Shen et al., 2009). During hypoxia, activated ERK incites HIF1 in astrocytes, which in turn induces EPO synthesis. EPO can then promote astrocyte differentiation and oligodendrogenesis, replacing those lost in initial energy failure following insult (Lee et al., 2004).

Taken together these results suggest that ERK phosphorylation is a vital mechanism through which neurons and astrocytes respond to hypoxic-ischemic insult to the neonatal forebrain. They highlight the duality in pERK response is dependent on cell specific expression. Neuronal ERK deletion has a moderately protective effect following both mild and severe HI that only partially recovers the extent of HI induced damage. Astrocytic ERK deletion is both vastly and significantly detrimental, increasing cell death induced by mild HI.

Future work would focus on cell specific ERK1 suppression in order to differentiate abnormal developmental contributions to HI sensitivity. In addition, single ERK2 single deletion in astrocytes will indicate whether the extent of damage observed is cumulative to ERK1 global deletion or solely due to a lack of ERK2.

ERK Deletion in Endotoxin-Mediated HI- Results

Inflammation and infection are common factors in premature birth and increased risk of brain damage by cytokine activity on neurons and the blood brain barrier (Aziz et al., 2008; Hagberg et al., 2002a; Sadeghi et al., 2007). These cytokines include interleukins -1, -6, -8, -13, and TNFα (Bandow et al., 2012; Chock and Giffard, 2005; Kendall et al., 2011a). Their presence in the neonatal blood and cerebral spinal fluid closely associates to cerebral palsy. Excitotoxic hypoxia-ischemia (HI) induces an inflammatory response, contributing to secondary energy failure. Here, microglia release factors including TNFα, IL-1β, and IL-18 (Chock and Giffard, 2005; Dommergues et al., 2003; Hagberg et al., 2012; Kendall et al., 2011a; Polazzi and Monti, 2010) into the extracellular space where they can act on susceptible neurons and ODC precursors.

Bacterial endotoxins activate microglia and induce their release of pro-inflammatory cytokines via binding to pattern recognition receptors at the cell surface. These are most commonly toll-like receptors (TLR) and/or scavenger receptors (Coste et al., 2010; Gorina et al., 2011; Kim et al., 2010; Wang et al., 2009). The most experimentally exploited of endotoxins is lipopolysaccharide (LPS), found on the outer membrane of gram negative bacteria, due to its constant ability to incite inflammation.

In neonatal brain injury studies, systemic injection of LPS leads to an upregulation of pro-inflammatory cytokines and consequently increased neuronal and astroglial cell death (Jã et al., 2013). A defect in myelin formation and increased microglia activation is also observed (Chock and Giffard, 2005). The synergistic nature of LPS to HI shows the same underlying white matter and grey matter lesion formation as those seen in human babies subject to infection as well as HIE (Kendall et al., 2011a; Wang et al., 2009). The causes of these lesions include inflammation modulators, such as the TNF cluster of genes, acting through TLR 4 and myd88 present on blood vessel endothelia and microglia (Bandow et al., 2012; Coste et al., 2010; Kim et al., 2010).

Few studies exist that implicate ERK in LPS induced inflammation, and these are near exclusively in vitro (An et al., 2002; Gorina et al., 2011). Dendritic cell cultures from ERK 1 null mice show an increased expression of IL-12p70 and a decrease of anti-inflammatory IL-10 secretion in response to TLR stimulation. Hippocampal cultures exposed to combined LPS and interferon γ (IFNγ), a pro-death cytokine, were susceptible to damage due to nitric oxide (NO) production by co-cultured microglia. Using the MEK inhibitor PD98059, IFNγ induced NO production was reduced by 40%. In human monocytes, PD98059 recued LPS induction of TNFα gene expression in a dose-dependent manner. Indeed, inhibition of ERK decreased the release of several pro-inflammatory cytokines including IL-1 and IL-18. Tpl2, a unique MAP3K selective to ERK, is shown to activate ERK 1 and 2 in response to LPS. $Tpl2^{-/-}$ mice were partially resistant to LPS induced endotoxin shock due to a defect in the induction of TNFα (Bandow et al., 2012).

To date there is no study existing that examines ERKs capacity to modulate the inflammatory response flowing endotoxin sensitised ischemia. The previous chapter showed that neuronal deletion of ERK 2 is neuroprotective against both mild and severe HI, whereas ERK 2 deletion in astrocytes is detrimental. The following experiment looks at whether this duality of response is enhanced when HI insult to the neonatal mouse brain is combined with LPS driven inflammation.

Previous work in this lab, performed by Giles Kendall, showed that pre-treatment with 0.3μg/gBW LPS 12hr before 30min HI strongly increases overall brain damage compared with 30min HI alone (figure 4.1). A later titration study by Mariya Hristova, on a new catalogue batch of LPS, gave an improved dosage of 0.6μg/gBW (Chapter 2, figure 2.1).

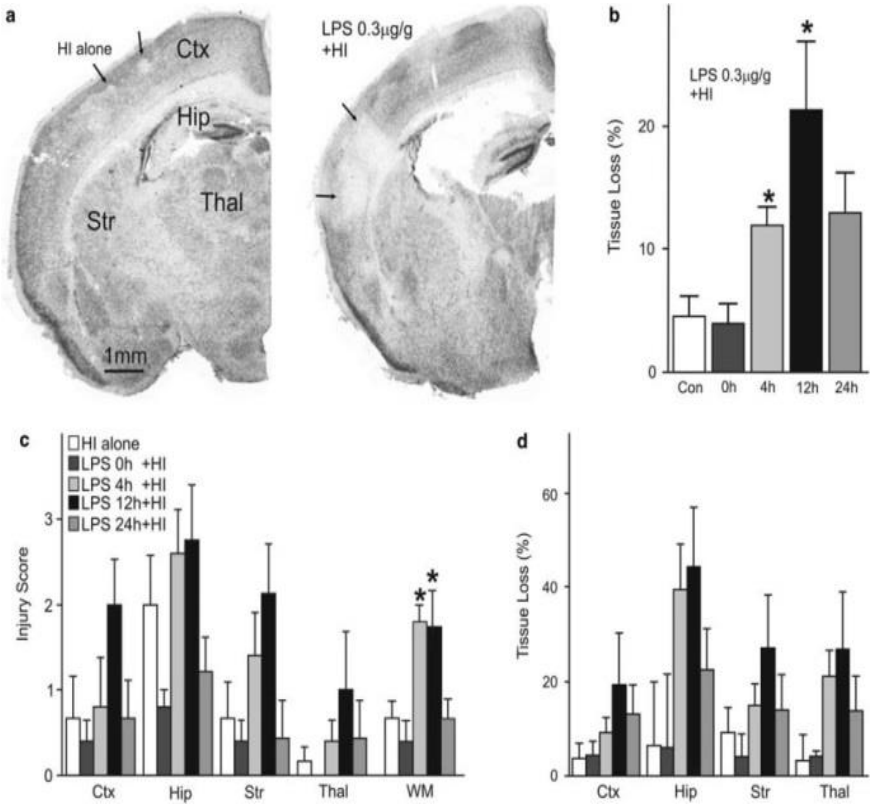

Figure 4.1 Effects of LPS, and LPS timing, on neonatal HI brain. (a) Pre-treatment with 0.3 mg/g LPS 12 h before HI insult (right) strongly increases overall brain damage, compared with 30-min HI alone (left), in Nissl-stained coronal forebrain sections. Note the small foci of cortical cell loss (arrows) on the left and much greater areas of necrotic tissue loss on the right. (b) Effect of time interval between LPS and HI insult on forebrain tissue loss, as percent of contralateral hemisphere. Effects of combined LPS/HI insult on regional tissue injury score (c) and regional tissue loss, as percent of contralateral brain region (d). (Figure 2, Kendall et al. 2010).

Sheldon and colleagues demonstrated that the Rice-Vannucci mouse model responds to HI in a strain-dependent manner (Sheldon et al., 1998). Eridan Rocha Ferreira, in our group, has replicated Sheldon's studies with LPS sensitised HI. Figure 4.2 shows her analysis of C57/Bl6 wild type mice, the background of the experimental ERK mice, and their clear response to LPS plus HI to an elevated degree than HI alone. Saline controls had an injury score en par to HI alone, indicating this increase to be due to the addition of endotoxin.

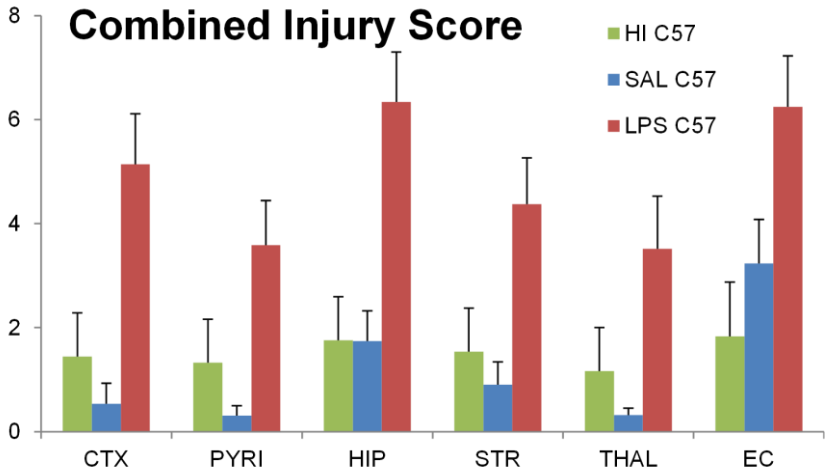

Figure 4.2 combined injury score- addition of microglia activation and neuronal loss scores, for C57/Bl6 wild type mice. P6 pups were subject to saline alone, o.6μg/gBW LPS or no injection 12 hours before 30min HI. Animals were assessed for αM and Nissl immunoreactivity. Saline and HI alone groups show a score on par with previous studies with mild HI. Combined LPS and HI (red) gave a 3fold increase in damage within all forebrain regions. (E. Rocha Ferreira, unpublished).

Neuronal ERK2 but not ERK1 activation is a significant contributor to the developing brains response to the developing brains response to inflammatory sensitisation of hypoxia-ischemia

Using the same breeding sets as seen in the previous chapter, P6 mice were injected intraperitoneal with 0.6μg/gBW of LPS/saline before being returned to dams. Twelve hours after the pups underwent left CROC, 2hr recovery and 30min hypoxia (8% O_2 balanced with N_2). The mice were then returned to the dams for 48hr at which point they were euthanized and their brains perfused and processed. 90 animals were required in total, of which 12 died between hypoxia and 48hr, in order to obtain cohorts of 10x 22 controls, 8x S22, 10x 1122, and 9x S1122 experimental pups. Genotypes were verified by PCR. Of those that died prior to sacrifice, no genotypic cause was found. Each of the experimental groups were analysed for microglial and astrocyte activation and recruitment to damaged areas, nissl body shrinkage, TUNEL positive cell death, and infarct volume.

Both microglial and astrocyte recruitment are strongly reduced in S22 animals compared to 22 controls and 1122 mutants (figure 4.3). Decreased microglial activation is observed in all forebrain regions with significance in thalamus where ANOVA analysis gave P values of 0.01 and 0.04 to controls and ERK1 mutants respectively. Comparison of S22 to S1122 thalamus was

only just insignificant (P=0.08). Cortex, pyriform cortex, striatum and external capsule saw a decrease in αM immunostaining by a third, however significance was not reached (P> 0.1) (figure 4.3Q). In contrast to 30min HI alone, the 1122 group no longer gives an elevation of microglia activation compared to littermate controls (figure 3Q). S1122 animals showed no difference in αM scores than that of either 22 controls or the 1122 pups.

Astrocyte activation and gliosis of HI damaged regions is perceivable higher in 22 controls and 1122 cohorts than in S22 and S1122. Single mutation of ERK2 in neurons saw a reduction in GFAP expression compared to controls and to double mutants for ERK1 and neuronal ERK2. Significance was observed in cortex (P<0.003), pyriform cortex (P<0.004), striatum (P<0.02), and external capsule (P<0.01). Both pyriform cortex and external capsule illustrate that, as with 30min HI alone, global deletion of ERK1 exacerbates damage seen in 22 animals, where P=0.04 and 0.07 respectively (figure 4.3S). This was partially recovered by combination with neuronal ERK2 deletion (P=0.01, and 0.03).

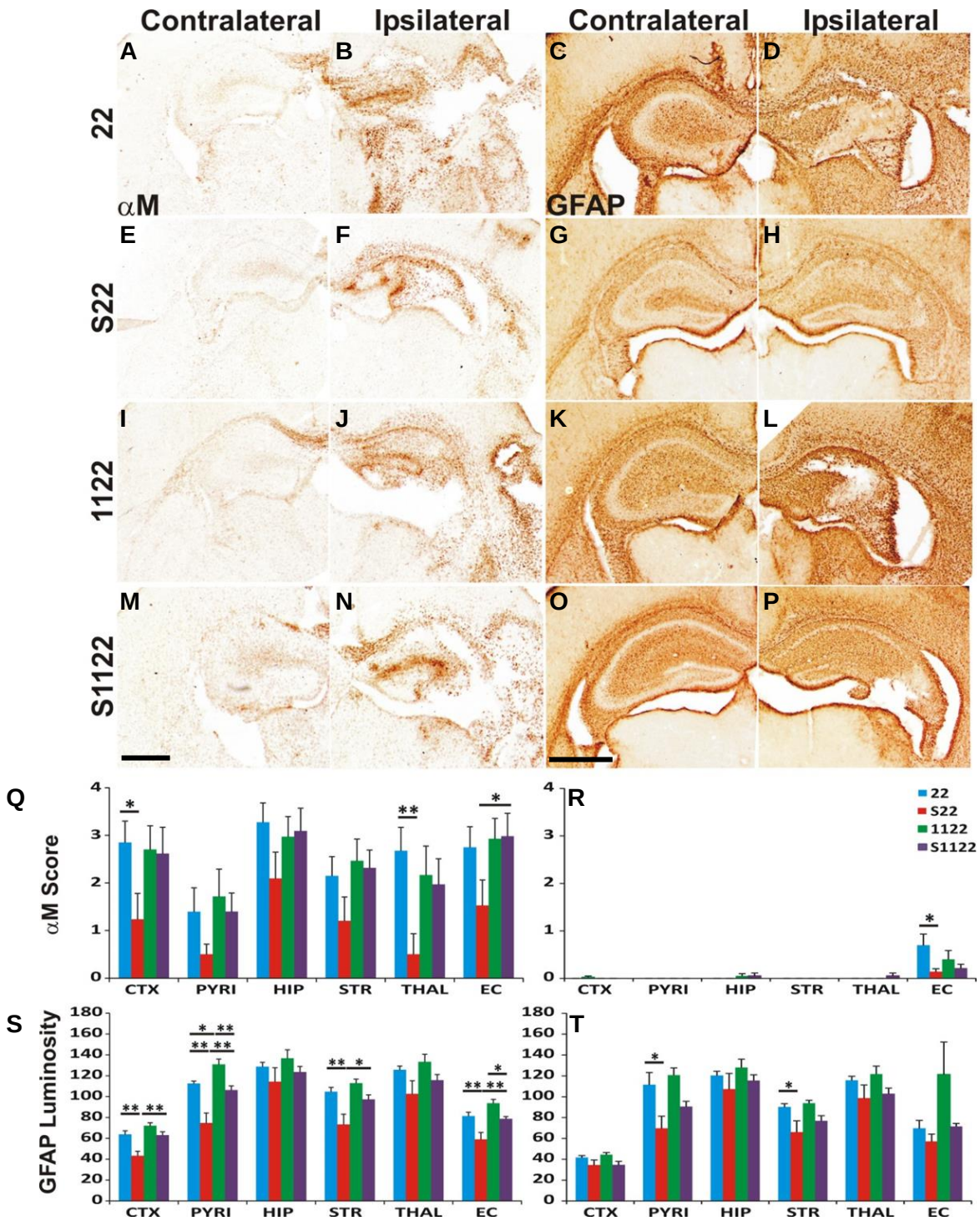

Figure 4.3 Neuronal ERK2 is required for non-neuronal cell activation and recruitment after combined LPS and 30min HI insult. Microglial (A-B, E-F, I-J, M-N, Q) and astrocyte (C-D, G-H, K-L, O-P, S-T) activation 2 days after insult. In 22 (A-D, Q, T) controls, and the S22 (E-H, Q, T), 1122 (I-L, R, U), and S1122 (M-P, R, U) mutant mice on the contralateral side (1st and 3rd column, S, V) and on the ipsilateral side (2nd and 4th column) to carotid artery occlusion. After insult, 22 mice showed a prominent increase in microglia and astrocyte activity. In S22, mutants this response is significantly decreased (Q, T) whereas S1122 mutants showed a modest decrease in astrocyte activation (U) only. 1122 response were unchanged from 22 controls (R, U). Scale bars indicate 0.5mm. *P<0.05, **P<0.01 by two way Anova posthoc TUKEY.

Nissl, as a histological marker for neuronal loss, was scored from 0 to 4 where zero saw no damage and a four is condensed nissl bodies and physical disruption of the surrounding area. TUNEL will label dying cells by tagging the terminal ends of nucleic acids. In this experiment, the number of TUNEL positive cells was counted over three 20x magnification fields for each region between animals of each experimental group. Nissl and TUNEL were strongly decreased in in all forebrain regions compared to controls. Both 1122 and S1122 animals maintained a high level of immunoreactivity on par with that of 22 littermates (figure 4.4).

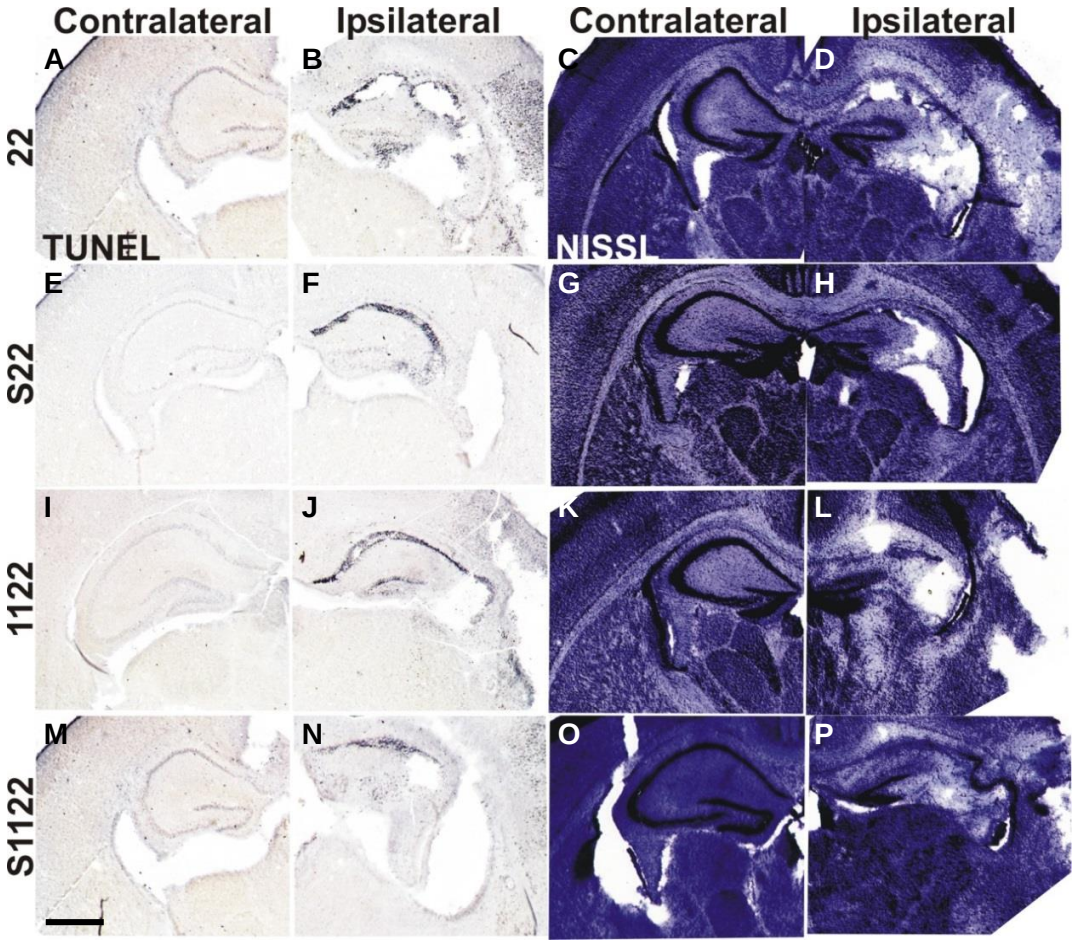

Figure 4.4 Neuronal ERK 2 deletion without ERK1 global deletion significantly decreases the number of dying cells following combined LPS and 30min HI. Tunel (A-B, E-F, I-J, M-N) and neuronal loss (C-D, G-H, K-L, O-P) were analysed 2 days after insult in 22 (A-D) controls, and the S22 (E-H), 1122 (I-L), and S1122 (M-P) mutant mice on the contralateral side (1st and 3rd column, S, V) and on the ipsilateral side (2nd and 4th column) to carotid artery occlusion. Following insult, 22 mice showed a large increase in the number of Tunel+ dying cells as well as neuronal loss (scored by tissue damage seen with cresyl violet histology). In S22 mutants this response is significantly decreased (E, H) whereas 1122 and S1122 mutants were unchanged (J, L, N, P) from 22 controls. Scale bar indicates 0.5mm.

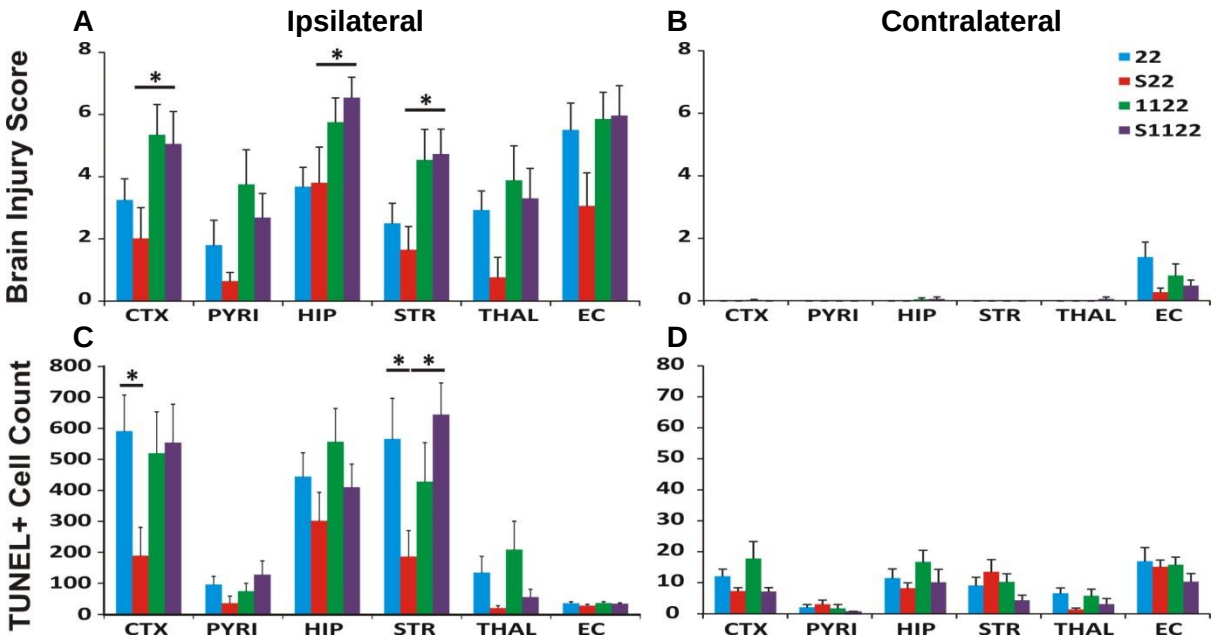

Figure 4.5 Quantification of Tunel+ dying cells and cresyl violet histology, indicating the extent of neuronal loss, in S22, S1122, 1122, and S1122 transgenic mutant mice. S22 (A) showed a great reduction in neuronal loss. Neuronal loss, measured as an injury score (where 0 is no damage and 4 is extensive tissue loss) using cresyl violet histology of nissl body formation. In addition, they exhibited a decrease in the number of dying cells (D), counted over 3 fields at 20x magnification. The hemisphere contralateral to carotid occlusion showed no increase in damage above baseline developmental cell death (C, F). *P<0.05, **P< 0.01 by two way Anova plus posthoc TUKEY.

Of the two, nissl was the more dramatically affected. When combined with microglial activation (αM immunoreactivity), a mean brain injury score was obtained (figure 4.5A). Neuronal ERK2 deletion resulted in strong reduction of active microglia in grey matter injury with 81% in thalamus, 79% in pyriform, 62% in striatum, 66% in cortex, and 43% in hippocampus when compared to controls. White matter showed a more modest decrease of 44%. Neuroprotective effect of neuronal ERK2 mutation was abrogated by combination with global ERK1 deletion. This was true for all forebrain regions, but significantly in hippocampus (P=0.03), striatum (P=0.02), and Cortex (P= 0.03) (figure 4.5A). Tunel proved similarly affected in neuron-specific ERK2 mutants if insignificantly so. Cortex and striatum exhibited the greatest reduction of cell death by 67%. Double mutants resulted in a significant loss of protection by neuronal ERK2 deletion alone with P=0.04 and 0.03 in striatum and cortex respectively (figure 4.5C).

Infarct volume is taken as a percentage of regional loss of ipsilateral areas from their contralateral counterparts. Here, the pattern of tissue loss in each

group verifies the patterns seen with nissl scoring and Tunel positive cell counts. Whilst 1122 saw very little change to that of 22 controls, neuronal ERK2 deletion alone proved highly neuroprotective with up to a 5fold decrease (in striatum) in lesion size. When all regions were combined, the total percentage of volume loss of S22 animals was 14.10±4.67 whilst in 22 controls it was 44.21±5.66 (figure 4.6). This was highly significant, with P= 0.009. Significance also occurred in cortex (P= 0.004). As seen with brain injury and cell death, combination of ERK2 and ERK1 mutations resulted in a complete reversal of neuroprotection offered by single ERK2 mutation in both cortex (P<0.05) and over the total hemisphere (P=0.057).

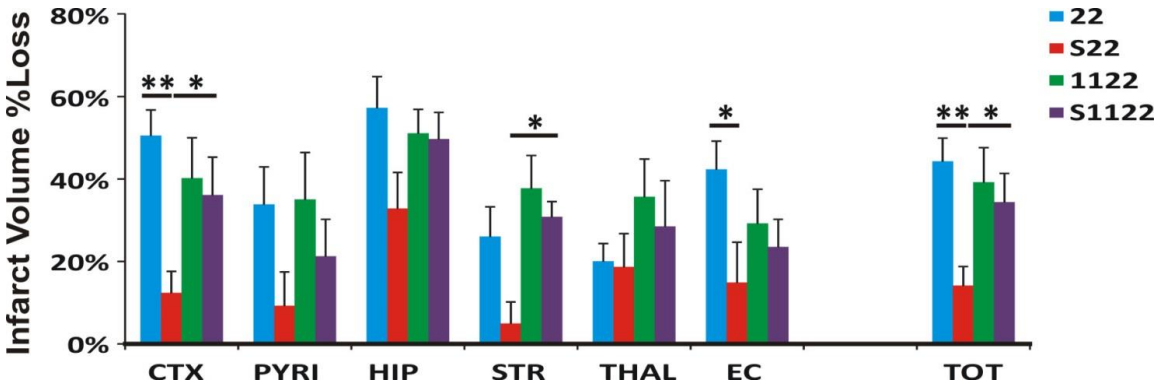

Figure 4.6 Infarct volume loss of each forebrain region. Loss was assessed measuring the areas of intact cresyl violet staining, bilaterally for each forebrain region, and calculating the ipsilateral regions as percentages of the contralateral (uninjured) hemisphere. The Percentage of tissue loss reflects the cell death seen above with nissl score and Tunel+ counts. S22 animals saw a dramatic decrease in lesion size compared to 22 controls. There was no difference between S1122 and 1122 cohorts. *P<0.05, **P<0.005.

Astrocyte ERK expression is not required for neuroprotection following endotoxin-sensitised hypoxia/ischemic injury

Kendall et al. showed that LPS plus 30min HI gives rise to a greater number of GFAP positive astrocytes in the affected forebrain regions than that seen with HI alone (Kendall et al., 2011a). The previous chapter indicates that astrocytic expression of ERK is required for cell survival following HI injury. As such, along with neuronal ERK deletion, it was important to establish whether astroglial ERK contributes to the injury response with endotoxin-sensitised HI in the neonatal mouse brain. In purified rodent brain astrocyte cultures, LPS was shown to trigger TLR4 present on the astrocyte cell surface. In addition ERK exhibited control of Egr-1 expression and influenced MyD88-dependent MMP-9 expression (Gorina et al., 2011).

Microglia activation, astrocyte recruitment, brain injury, cell death, and infarct volume were all analysed and assessed in 1122 animals (n=6) and G1122 animals (n=4). At P6, the mouse pups were injected intraperitoneal with 0.6μg/gBW of LPS/saline before being returned to dams. Twelve hours after the pups underwent left CROC, 2hr recovery and 30min hypoxia. The pups were sacrificed at 48hr following insult. Five sections per brain were retrieved for each marker immunostaining.

In contrast to HI-alone, neither global deletion of ERK 1 nor astrocyte specific deletion of ERK 2 had any impact on LPS sensitised HI injury. Indeed whilst previously knocking out ERK 2 in astrocytes, alongside global ERK 1 deletion, proved highly detrimental, here a very modest decrease of our damage markers were observed in G1122 animals compared to 1122 littermates (figure 4.7). Tunel was the most sensitive marker with a 2-6fold reduction observed in cortex, hippocampus, and thalamus (figure 7T). No significance was achieved, P> 0.1.

From this data, we can see that whilst neuronal ERK 2 plays a modest role in the brain response to hypoxia/ischemia alone, in the presence of endotoxin induced inflammation it is a major contributor to the resulting damage. Interestingly, whilst with mild HI alone ERK 1 activation may be neuroprotective, its effects are overwhelmed by the significantly severer insult when HI is combined with LPS.

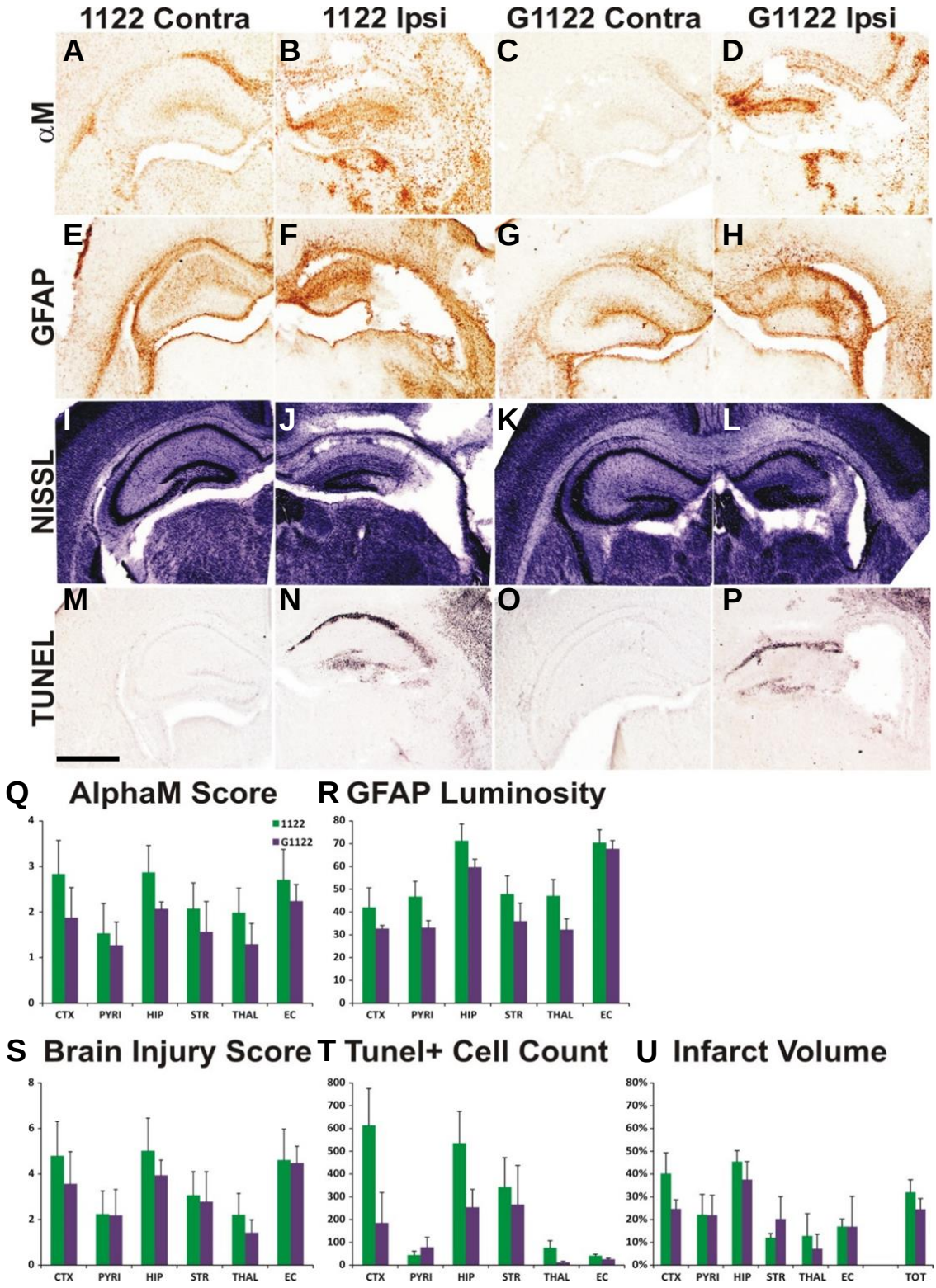

Figure 4.7 ***Effect of 0.6μg/gbw LPS 12hr prior to 30min hypoxia exposure to P6 mutant mice with astrocyte deletion of ERK 2, on a global ERK 1 KO background compared to ERK 1 global KO littermates. At 48hr post insult, the animals were assessed for microglia (AlphaM, A-D, Q) and astrocyte (GFAP, E-H, R) activation neuronal loss (Nissl score, I-L, S), dying cells (TUNEL, M-P, T), and infarct volume (Nissl histology, U). A mild decrease in each marker was observed in G1122 animals but not to a significant extent. Scale bar indicates 0.5mm. Significance was assessed by 2-tailed student t-test where p≤ 0.5.***

ERK deletion in endotoxin-mediated HI- Discussion

This laboratory, in addition to others, has emphasised maternal and/or fetal infection to sensitise the brain to perinatal hypoxic ischemic insult, contributing up to 5% of all cerebral palsy cases (Chock and Giffard, 2005; Kendall et al., 2011a; Wang et al., 2009). Here we have used lipopolysaccharide (LPS) which provides a synergistic effect in combination to HI (Hagberg et al., 2012; Kendall et al., 2011a), to examine how neuronal or astrocyte ERK activation may regulate the neonatal mouse response to endotoxin induced HI injury. LPS can upregulate pro-apoptotic and –inflammatory cytokines including IL-1β, IL-6, IL-8, and TNFα, and chemokines including iNOS and COX-2 (Bandow et al., 2012; Chock and Giffard, 2005; Kendall et al., 2011a). LPS is regulated by pattern recognition receptors, specifically toll-like receptors 3 and 4, to incite microglia activation and successive cytokine release (Bandow et al., 2012; Gorina et al., 2011; Kim et al., 2010). Kendall et al. also showed that with LPS combined with 30min 8% O_2 exposure, adhesion molecules such as ICAM1 and CXCL1 are upregulated, resulting in disruption and instability of the blood brain barrier (Kendall et al., 2011a).

Neuronal ERK2 is required for recruitment of non-neuronal cells in response to LPS sensitised HI

Both single neuronal ERK2 mutation and double ERK1 and neuronal ERK2 mutation resulted in a very strong reduction in damage 2days following LPS mediated HI insult. Single mutants exhibited a 2.6fold decrease in microglia and 1.4fold decrease in astrocyte activation when compared to controls with significant difference in cortex and thalamus. Global ERK1$^{-/-}$ exhibited a damage response on par to wild type littermate controls. This is in contrast to the effects of ERK1 deletion in hypoxia alone where injury seen exceeded that of controls (figure 3.7). This advocates the protective effect of ERK1 to be restricted by the extent of multifactorial insult. Both wild type and ERK1 mutant mice gave rise to an extensive damage response following LPS and HI. Combined mutation of ERK1 and neuronal ERK 2 partially recovered insult, indicated by decreased (1.2fold) astrocyte activation.

The conundrum of activated glia as harmful or beneficial in neuronal injury response is an ongoing debate (Polazzi and Monti, 2010; Streit, 1993). De-ramification and increased amoeboid morphology of microglia associates to the presence of cell debris indicating that the greater the more extensive activation of microglia the greater number of dying and dead cells present. Additionally, glial TNFα is released at a higher rate after LPS stimulation, further contributing to neuronal damage (Chock and Giffard, 2005). As such, a reduction in glial activation and recruitment to an area of ischemia-induced infarction is a strong indicator of decreased cellular injury response by prevention of both endogenous and LPS incited inflammatory response and gliosis giving rise to enhanced neuronal survival.

Single deletion of ERK2 in neurons protects against cell loss and extent of infarct

Diminished glial response in neuronal ERK2 mutants strongly correlated to a reduction in brain injury (62%) and Tunel positive cell death (57%). Preservation of regional cell loss was validated by measurements of infarct with a mean reduction in lesion volume of 68%, up to 81% in striatum. No reduction of cell death or tissue loss was observed with double mutation of ERK1 and neuronal ERK2, which highlights the need to further examine cell specific deletion of ERK1 as an endogenous protective agent in the neonate under these experimental conditions.

LPS enhances insult by acting at TLR4 via the recruitment of the adapter protein MYD88. In neonatal mice, TLR4/MYD88 complex is responsible for the release of IL-1α, IL-5, IL-6, IL-7 and TNFα following combined LPS and 10% O_2 exposure (Wang et al., 2009). On mutation of global MYD88, the pro-inflammatory response of microglial cytokine release was suppressed. In vitro studies in dendritic cells and in renal cells have indicated that LPS/TLR4/MYD88 induction of genes encoding proinflammatory cytokines is mediated by the phosphorylation and nuclear relocation of ERK1/2 (An et al., 2002; Watts et al., 2011). MYD88 can form a functional complex directly with ERK1/2 via the recruitment of a scaffold protein MKP3 (tpl2) which prevents ERK dephosphorylation, rendering it constitutively active (Bandow et al., 2012).

MKP3 had similarly been implicated in the dysregulation of TLR2/MYD88 activation of ERK, resulting in transcription of its nuclear target Elk-1 and subsequent upregulation of IL-1β and IL-10 (Chen et al., 2014; Coste et al., 2010).

Lastly, pERK promotes DAPK cleavage of caspase 8 via its activation by pro-inflammatory TNFα. In LPS mediated inflammation, TNFα is able to bind to its selective death receptor TNFR1 which in turns activates ERK through the Ras/C-Raf/MEK kinase cascade (Alexander and Acott, 2003). PERK translocates to the nucleus where it further phosphorylates RSK, ATF2, Elk-1, Ets-1, and C-Jun promoting apoptosis and increased inflammatory response. Previous work in our laboratory has already established that deletion of the TNF cluster of genes which includes TNFα, Lymphotoxinα, and Lymphotoxinβ, suppresses neuronal loss following LPS sensitised HI in the neonatal mouse (Kendall et al., 2011a). As such, we can supposition that neurodegenerative actions of neuronal ERK2 is via early MYD88 binding in response to LPS/TLR interactions and initiation of cytokine release, as well as downstream involvement in TNFα mediated cell death pathways.

When compared side by side we observe that the role of ERK 2 in neonatal brain damage differs between insult types. With hypoxia alone injury deletion of ERK 2 results in clear reduction in active microglia, and some decrease in dying cell populations in grey matter regions with known sensitivity to HI such as cortex, striatum and hippocampus. However this mild difference in response suggests ERK 2 to be part of a number of regulatory factors rather than pivotal to neuronal survival after insult. When HI is combined synergistically with LPS, seen herein this chapter, protection from cell loss, plus reduced glial activity becomes much greater in the ERK 2 mutants. One possibility is that ERK 2 activity is driven by inflammation. After HI alone there is an endogenous pro-inflammatory response via the release of cytokines and chemokines. This is following ATP exhaustion and mitochondrial disruption resulting in ROS and subsequent ERK activation. When endotoxin is introduced pro-inflammatory pathways now gain multiple activators, making ERKs involvement more prominent in driving this response, thus the strong neuroprotective phenotype in these mutants after LPS plus HI. As these studies are the first to describe

differentiating roles between ERK 1 and ERK 2 in neonatal HI it is difficult to conclude whether independent overexpression of ERK 1 or inhibition of ERK 2 is sufficient to result in neuroprotection. It does seem apparent however that ERK2 deletion either by itself or in combined therapy can protect against cerebral damage depending on the form of insult received.

Deletion of Astrocytic ERK expression does not contribute to LPS sensitised HI insult in the neonatal mouse

On exposure with 30min HI, mutants with combined deletion of global ERK1 and astrocyte-specific ERK2 exhibited a strong injurious response. Using the same breeding sets, P7 pups were subject to LPS sensitised HI that, surprisingly, resulted in little change when compared to ERK1 single mutant littermates. Mild decrease in damage marker immunoreactivity was observed, with Tunel positive cell death proving most affected by a mean reduction of 69% in double mutants. Reduced DNA fragmentation did not correlate to a reduction in infarct volume where no difference was discernable between groups.

The absence of response with ERK2 deletion in astrocytes, as exhibited after 30min HI alone, may well be due to combined LPS and HI injury resulting in a saturation of damage within these animals, meaning that that any change by double mutation of ERK is overwhelmed. Conclusions, however, are difficult to draw from these data due to the small population size of each cohort where N= 6 in ERK1 mutants and N= 4 in ERK1 and astrocyte ERK2 mutants. Increasing group size would provide a much stronger basis on which to examine ERK response in astrocytes and its involvement in LPS sensitised HI.

Tentatively, one could postulate that a conflict occurs between the neuronal and ODC protective effect of astrocytic pERK action at NMDA receptors (Szydlowska et al., 2010) and LPS stimulation of ERK-mediated release of pro-inflammatory cytokines and transduction of pro-apoptotic transcription factors (Alexander and Acott, 2003). In addition one recent paper indicates that following LPS stimulation NO release from astrocytes is mediated though ERK phosphorylation via the suppression of the scavenger receptor SR-A (Murgas et al., 2014). This corroborates with previous studies that observe LPS immuno-stimulation of astrocytes results in increased iNOS generation. This was

inhibited with the administration of PD98059 (Yoo et al., 2005). Together this suggests that inhibiting astrocytic ERK activity has the potential to be protective following LPS stimulation. In our model of combined insult, this beneficial effect is overwhelmed by the deleterious effect of ERK2 deletion in astrocytes in response to ischemia.

Pharmacological Inhibition of ERK- Results

In this study, we have looked at the role of ERK in neonatal brain injury with transgenic mutant mice. Other studies exist which investigate the role of ERK in both adult and neonatal brain ischemia via the use of pharmacological inhibitors of ERK activation (Alessandrini et al., 1999; D'Cruz et al., 2005; Gu et al., 2001; Han and Holtzman, 2000; Namura et al., 2001; Uemura et al., 1991; Wang et al., 2005; Wang et al., 2003b). Such inhibitors are selective to MEK 1/2 due to a lack of any that directly target ERK itself. One major issue that has arisen from such work is the non-ideal requirement for these compounds to be delivered intracranially to have an effect in the neonate. This chapter will explore the use of the MEK selective inhibitor SL327, injected intraperitoneal, both 20min prior and 1hr following hypoxia-ischemic insult to P7 wildtype mice.

Controversy has arisen over the role of ERK 1/2 in cell death. After inhibition, ERK has shown to both increase neuronal apoptosis whilst significantly reducing cell death in other instances. Two compounds, PD98059, and U0126 have shown that they can suppress activation of MAPK cascade by binding to MEK 1 and 2, therefore preventing its activation by RAF (Roberts and Der, 2007; Santarpia et al., 2012; Trujillo, 2011). Consequently, either ERK1 or 2 are phosphorylated. In immature neuronal cell cultures, both PD98059 and U0126 reduced nitric oxide induced cell death following glutathione depletion (Canals et al., 2003; de Bernardo et al., 2004). Additionally, Alessandrini et al (1999) used an adult mouse model of middle cerebral artery occlusion to look at the effects of ERK inhibition in this model of insult using PD98059. PD98059 was administered intracerebroventricularly 30min prior to insult. A 36-55% reduction in infarct volume was observed. The same group used an adult gerbil model of ischemia to test the more selective U0126 (Namura et al., 2001). Here the inhibitor was administered intravenously prior to insult. They saw that hippocampus was protected from damage and that overall a 42% reduction in infarct occurred. Introduction of U0126 1hr post insult was still neuroprotective, though not to a significant degree.

Our laboratory group previously investigated the use of U0126 as a pharmacological agent with which to study ERK activation in the neonatal

mouse model of HI injury. They observed very mixed results with little or no change in both phosphorylation of ERK and damage response following intraperitoneal injection (not shown). Dr Mariya Hristova was able to clarify that this was due to U0126 being too large a molecule to cross the blood brain barrier (BBB). Hristova found however that SL327, an analogue of U0126, does cross the BBB (see figure 5.1 for a comparison). Though one study has shown a neuroprotective role of SL327 in adult mice following ischemia (Wang et al., 2003b) it remains to be seen whether this effect can be conserved in the neonatal Rice-Vannucci mouse model of perinatal brain injury.

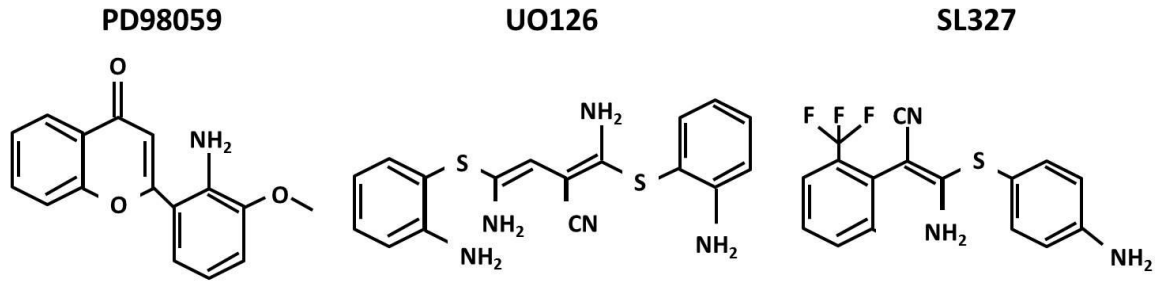

Name	MW	Selectivity of Inhibition	IC50	Notes
PD98059	267.28	Potent against active MEK 1 Weakly against active MEK 2	4μM 50μM	Partial inhibition of active MEK Mutates Ser 218 & 222 to Glu
UO126	426.56	Highly specific against MEK 1 and MEK 2	0.07μM 0.06μM	100-fold higher affinity for MEK than PD98059
SL327	335.35	Specific against MEK 1 and MEK 2	0.18μM 0.22μM	Homologue of UO126 Crosses the blood brain barrier

Figure 5.1 Chemical structure and properties of the MEK 1 and 2 inhibitors- PD98059, UO126, and SL327. Though UO126 has a greater affinity to block the activation of MEK 1/2 than PD98059, its large molecular weight means it does not easily cross the blood brain barrier (BBB). Its structural analogue SL327, however, does cross the BBB whilst still retaining specificity to MEK 1 and 2 inhibitions.

SL327 is a cell permeable vinylogous cyanamide, first used in mice to test the role of MAPK in hippocampus dependent learning (Atkins et al., 1998). Its actions selectively inhibit MEK 1/2 dependent phosphorylation of ERK. Hristova performed a dose response between 0-133μg/gBw, dissolved in 100% EtOH, for optimising the concentration required and reducing toxicity in P7 mice. The mice were injected with SL327 20min prior to mild (30min) HI and allowed to survive for 15min. Although 30μg/gBw gave over 80% inhibition of pERK, 133μg/gBw resulted in 100% attrition of pERK immunoreactivity in all forebrain grey matter regions with no toxic side effects. As such, this is the dose used in all further experiments (figure 5.2).

Inhibition of ERK phosphorylation is neuroprotective with SL327 injection prior to mild HI insult

To study the effects of SL327-inhibition of ERK has on tissue damage markers; twenty-two P7 C57/Bl6 pups were injected 20min prior to 30min exposure to 8% oxygen. Ten had 133µg/gBw SL327 dissolved in 1µl/g ethanol and twelve with 1µl/g EtOH alone. Pups were allowed to recover until 48hr when sacrificed. Five sections of forebrain were taken per pup and assessed for neuronal loss, TUNEL positive cell death, microglia activation and astroglia recruitment. Regions of interest include the periventricular white matter- external capsule, and surrounding grey matter regions: striatum, pyriform cortex, cortex, hippocampus, and thalamus.

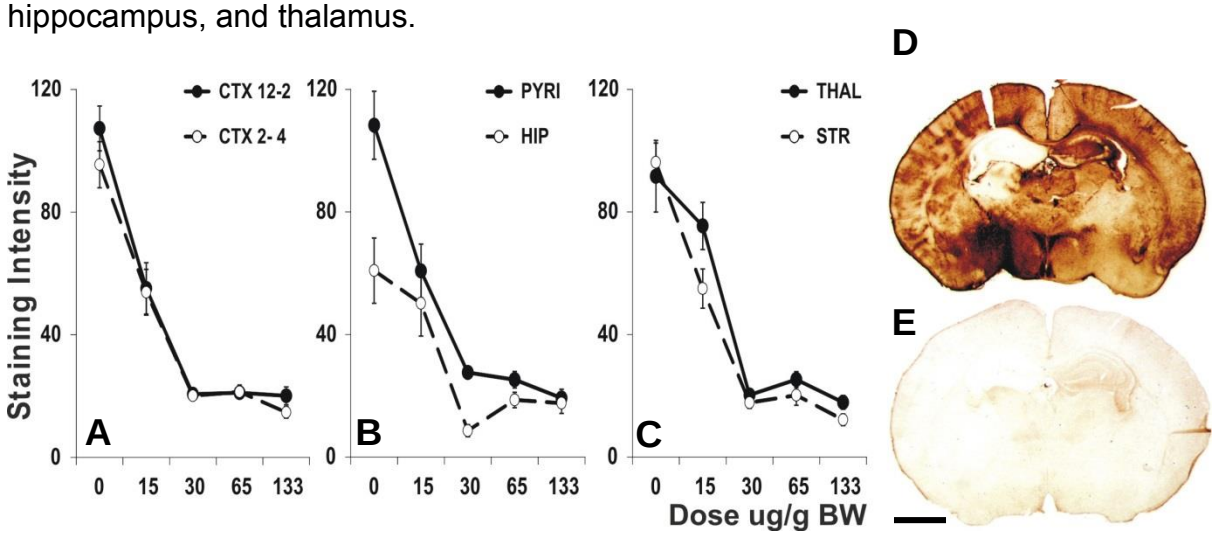

Figure 5.2 Dose responses for SL327 Inhibition of pERK immunoreactivity (staining intensity) with MEK/ERK inhibitor SL327, applied 20 minutes prior to 30 minutes HI insult (µg/g body weight/BW). Note the similar inhibition curves across different forebrain regions. A: CTX 12-2 right dorsal cerebral cortex (12 to 2 O'clock segment), CTX 2-4 right middle cerebral cortex (2-4 O'clock segment). B: PYRI-pyriform cortex, Hip-hippocampus C: THAL-thalamus, STR-striatum. Increasing the dose from 15 to 30 µg/g was associated with an 80% reduction in immunoreactivity. D-E: Effects of EtOH alone (D) or of 133µg/gBW SL327 (E) on pERK immunoreactivity following 30min HI insult and 15min recovery. Scale bar indicates 1mm

The microglia marker-αM shows that in all regions, including external capsule, there is strong activation in EtOH treated animals with an average score of 1.01± 0.23 over all forebrain regions. SL327, when applied 20min prior to HI results in large decrease in αM expression (figure 5.3I). T-test statistical analysis revels this decrease to be significant in external capsule (p=0.002), striatum (p=0.04), cortex (p=0.05), and hippocampus (p=0.004). Thalamus saw no change between the two groups.

Nissl staining was carried out in order to calculate the loss of neuronal cell bodies. Histological mean brain injury was calculated by combining neuronal loss to microglial activation scores. Cortex, hippocampus, and thalamus are all highly susceptible to damage as seen in the EtOH treated pups, whereas, like αM, thalamus remained unaffected. Addition of SL327 significantly reduces tissue loss (figure 5.3J), with a 2fold decrease within the cortex (p=0.0001), hippocampus (P=0.01) and external capsule (P= 0.01) and a trend to decrease in striatum.

DNA fragmentation is a classical marker for dying cells, indicating the severity of damage. Addition of SL327 gives rise to a decrease in the number of dying cells in striatum (p=0.03) and hippocampus (p=0.04) compared to EtOH controls (figure 5.3K). Hippocampus saw the greatest number of dying cells with 27.7±7.11 positive counts in the EtOH treated group. This was reduced to 10.8± 2.29 in SL327 treated animals. Thalamus, cortex and external capsule remain unaffected by the application of SL327. It was also observed that these latter regions do not experience as high number of TUNEL positive dying cells as seen in striatum and hippocampus.

Lastly, sections were labelled for GFAP to determine the migration of astroglia to HI damaged regions. Number and density of astroglia remains wholly unaffected by HI in both treatment cohorts. There is a similar level of expression between regions implicating astroglia to be unsusceptible to systemic ERK inhibition.

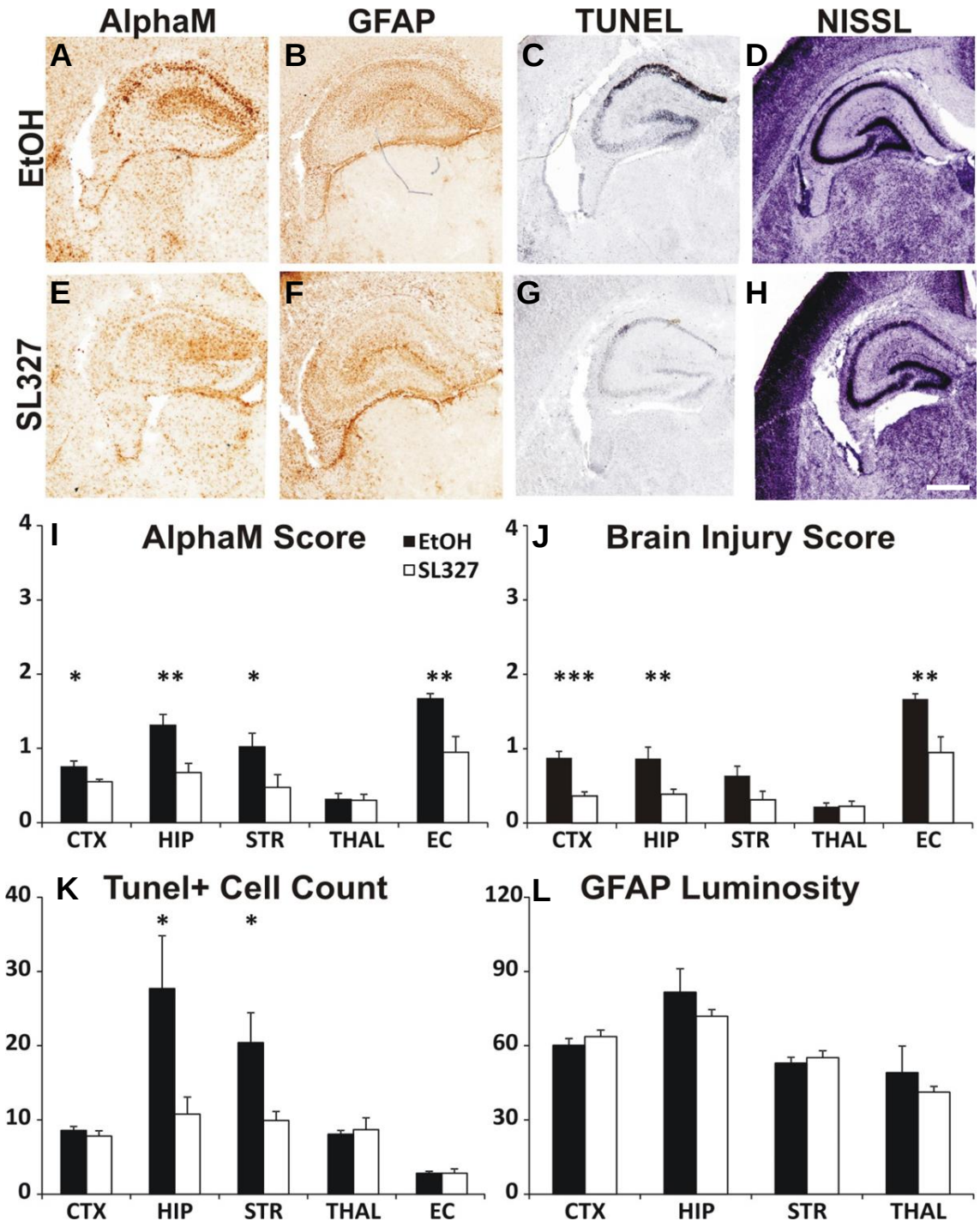

Figure 5.3 Effect of SL327 on neuronal loss, cell death, microglial activation and astroglia activation when applied 20min before 30min HI. Regions studied were striatum (STR), hippocampus (HIP), thalamus (THAL), cortex (CTX), and external capsule (EC). Assessment was at 20x magnification eye field (mean plus SEM over 3 fields). A, E, I: Levels of alphaM+ microglia are significantly decreased in the SL327 group in white matter (EC) as well as in most grey matter regions (STR, CTX, HIP). B, F, L: The levels of GFAP+ astroglia do not seem affected by the application of SL327 C, G, K: The number of TUNEL+ cells in the SL327 group is lower when compared to control animals, significantly so in STR and HIP. D, H, and J: Neuronal loss and subsequent brain injury score is significantly decreased in the SL327 treated group. Scale bar indicates 0.25mm. Analysis over T-test gave significance when p<0.05 (*), p<0.01 (**), and p<0.005 (***).

Pharmaceutical inhibition of ERK one hour following mild HI insult reduces microglial activation but not cell damage

Injection of SL327 prior to HI gave an essential basis from which to proceed with investigating the therapeutic benefits of SL327 in the neonatal hypoxic/ischemic brain. However, injection of SL327 before injury has actually occurred is not a viable window of use. The experiment was thusly expanded to establish whether neuroprotection is still seen when SL327 is injected 1hr after mild insult.

Twelve postnatal day 7 C57/Bl6 mice were subject to 30min HI before being allowed to recover with their dams. At 1hr post HI, six pups were injected with 133µg/gBw SL327 dissolved in 1µl/g ethanol and six with 1µl/g EtOH alone. Pups were allowed to survive until 48hr before sacrifice. Five forebrain sections per animal were stained for neuronal loss, TUNEL positive cell death, microglia activation and astroglia migration as described in the previous experiment (figure 5.4).

Microglial activation is upregulated and localized to regions of cellular injury during hypoxia ischemia, thus tissue damage was assessed via detection of the cell surface marker αM by immunocytochemistry. Immediately a marked difference could be seen between the contralateral (control) and ipsilateral (experimental) hemispheres of control animals, with the experimental side suffering greater tissue damage seen predominantly in the external capsule, cortex and hippocampus. This difference was distinctly reduced in the SL327 treated group. External capsule, cortex, and hippocampal regions showed marked reduction in αM stain in the SL327 treated animals, suggestive of a neuroprotective effect (figure 5.4l). T-test analysis revealed a statistically significant reduction in microglial activation after administration of SL327, with more than a two-fold decrease in both the hippocampus and cortex ($p=0.02$; $p=0.05$ respectively). External capsule also showed a significantly large reduction in microglia activation ($p=0.05$). This indicated SL327 to have a neuroprotective influence.

A nissl stain was carried out to visualise damage to the neuronal cell bodies. Assessment of brain injury revealed little apparent damage on analysis of four

grey matter regions: the cortex, striatum, hippocampus, thalamus, and white matter: external capsule. The striatum (EtOH= 1.00±0.29, SL327= 0.60±0.19), hippocampus (EtOH= 2.13±0.24, SL327= 0.95±0.18) and external capsule (EtOH= 2.75±0.63, SL327= 1.20±0.37) proved most susceptible to cell damage with significant reduction after SL327 treatment seen in hippocampus (P=0.01) (figure 5.4J). It was observed that the highest tissue injury score across all regions only reached 2.75 in the external capsule, corresponding to minimal evidence of damage without infarct. In addition, the striatum of the EtOH treated group exhibited clusters of shrunken cells not seen in the SL327 treated group (not shown).

This pattern is faithfully replicated with Tunel immunoreactivity. There is very little apparent staining in thalamus, cortex, or external capsule. In addition, there is no change in immunoreactivity in these regions between the two treated groups. Striatum and hippocampus evidenced elevated numbers of TUNEL+ dying cells within the EtOH group (striatum= 16.69±12.08, hippocampus= 43±33.14). This rise was considerably reduced in the SL327 treated group, despite never reaching significance (p=0.49 and p=0.52 respectively). Lack of significance could be due to high variance within the ethanol treated group, the hippocampal region produced a high degree of variability with a SEM of 33.1 or low n values.

Sections labelled for GFAP saw no significant difference in any of the five brain regions assessed between mice injected with ethanol or SL327 was evident. The pattern and degree of activation was similar between both control and SL327 groups Findings were consistent amongst ipsilateral and contralateral sides suggesting no protective effect of ERK1/2 inhibition on astroglial induction. T-test analysis revealed no significant reduction in response to SL327 injection across any of the five brain regions (figure 5.4L).

This points out to a time window of protective effect of SL327 up to 1h following insult. Moreover, it also underscores the importance of ERK activation in mediating neonatal HI brain injury.

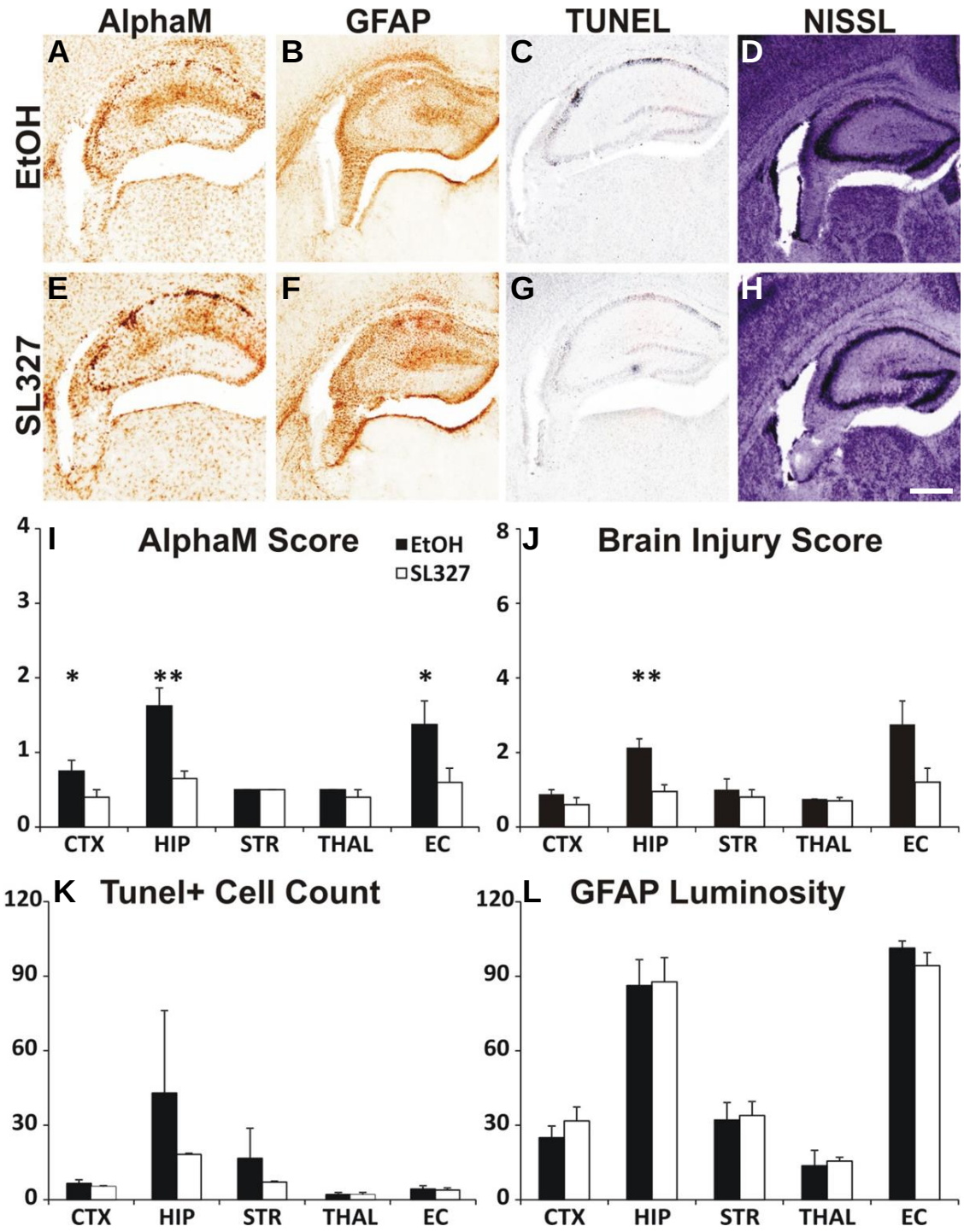

Figure 5.4 Effect of SL327 on neuronal loss, cell death, microglial activation and astroglia activation when applied 60min after 30min HI. When SL327 was applied at 1h following the HI insult the levels of microglial activation in EC, CTX and HIP were decreased, but cell death, neuronal loss and GFAP+ astroglia appeared unaffected. A, E, I: the levels of alphaM+ microglia are significantly decreased in the SL327 group in EC, Ctx, and Hip. GFAP+ astroglia (B, F, L), number of Tunel positive cells (C, G, K) and neuronal loss (D, H, J) are all unaffected by the application of SL327. Scale bar indicates 0.25mm. Analysis over T-test gave significance when *p<0.05.

ERK inhibition one hour following severe HI insult- gives no change in peak expression of damage markers at 16hr survival

In our mouse model of hypoxia/ischemia, there are two levels of severity considered: mild, 30min, and severe, 60min. Both are relevant for the mapping of cellular mechanisms underlying conditions such as cerebral palsy. As such, it is vital that any therapeutic interventions can be neuroprotective with both forms of injury.

It was essential to test the effects of SL327 following 60min HI in p7 C57/Bl6 pups. SL327 was injected 1hr post insult and the pups allowed recovering for 16hr, peak expression for some damage markers as verified by a time course of most damage markers with 60min hypoxia (chapter 2 figure 2.2), or 48hr, as is consistent with SL327 injected after 30min HI. The experimental litters were observed over the two survival times for any mortality.

Twenty-three pups were subject to either 133μg/gBW SL327 dissolved in 1μl/g ethanol (n=11) or 1μl/gBw EtOH (n=12) alone at 60min after 60min HI before recovery. The pups were then allowed a survival time of 16hr. The animals were perfused and the brains fixed as before. Damage was assessed by levels of microglia activation, neuronal loss and Tunel positive cell death. Five sections per brain were retrieved for each immuno-stain (figure 5.5).

Both treatment groups exhibited high percentage of survivability, above 80%, with no difference between groups as verified by chi squared statistical analysis (P= 0.5) (figure 5.5I).

After HI, there is a high level of αM immunoreactivity in the EtOH treated group in all forebrain regions including thalamus. When we look at the regions independently, we see that there is a very modest elevation of activated microglia in the external capsule, pyriform cortex and cortex of SL327 treated animals compared to EtOH controls though not significantly so (p> 0.3). Striatum remains unchanged between the groups, with a score of 1.15±0.28 in EtOH and 1.14±0.15 in SL327 treated animals (figure 5.5K). Conversely, hippocampus and thalamus both saw a 35% decrease with SL327 treatment compared to EtOH. This was not significant p= 0.16 and p= 0.13 respectively.

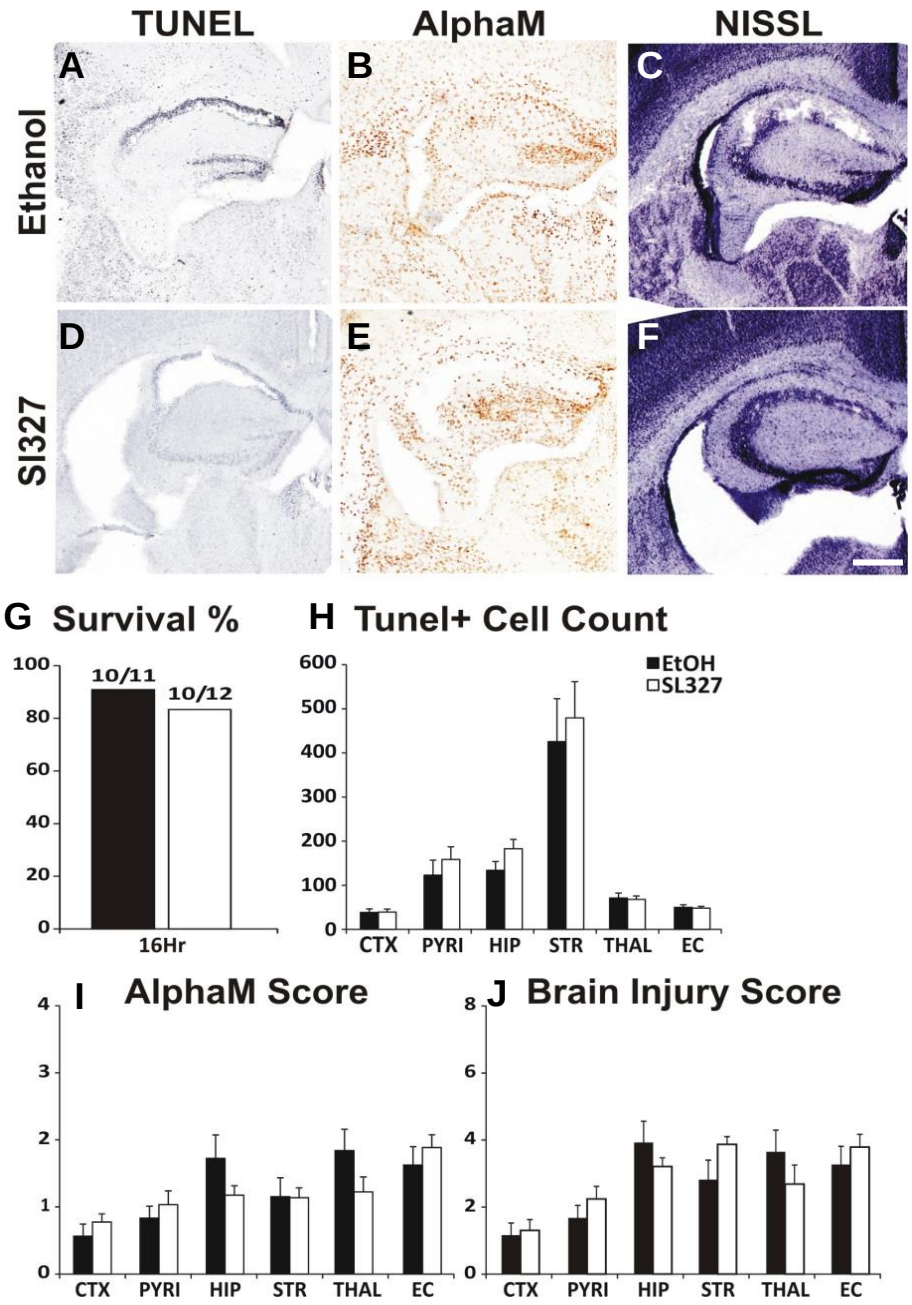

Figure 5.5 SL327 injected 60min after 60min HI with 16hr survival , effect of SL327 on survivability, microglia activation and TUNEL+ cell death when injected 1hr after 60min hypoxic/ischemic insult. Assessment was at 20x magnification eye field (mean plus SEM over 3 fields). I: at 16hr after 60min HI, there is no strong mortality rate in pups treated with SL327 or with EtOH. AlphaM (A, E, J) and Tunel+ cell death (B, F, K) immunoreactivity with 16hr survival is unchanged between the SL327 and EtOH treated groups. Tunel expression is 3fold higher at 16hr compared to 48hr. Neuronal loss (C, G, L) was unaffected in all forebrain regions bar HIP were a significant reduction in SL327 treated group was observed. Scale bar indicates 0.25mm. Analysis of survival percentage by chi squared test, analysis of damage markers by T-test gave significance when *p<0.05.

This pattern of response was similar in brain injury. Striatum and external capsule showed a mild increase from 2.8± 0.58, 3.25±0.54 respectively in EtOH treated group to 3.84±0.23, 3.77±0.38 in SL327 treated group, whist cortex, and pyriform cortex remained unchanged. Hippocampus and thalamus had a

modest reduction in neuronal loss with SL327 treatment compared to EtOH alone (figure 5.5L). Significance was not reached (P>0.1).

Tunel positive cell death proved a more variable in its immunostaining with no difference between the two groups in any of the forebrain regions.

ERK inhibition one hour following severe HI insult- strongly increases survival at 48hr following injury

The experiment was repeated with a survival time of 48hr. Here there is a dramatic influence of SL327 on pup survival. EtOH only treated pups exhibited a high occurrence of death between 16-48hr, with only 9 of 23 animals (39%) surviving compared to the SL327 treated group where 15 of 18 animals (83%) survived (figure 5.6I). Chi squared statistical analysis showed this difference between groups to be highly significant with p=0.002. The groups were assessed for αM, nissl, and Tunel damage markers.

AlphaM immunoreactivity saw a modest decrease in expression in all forebrain regions of the SL327 treated group. No significance was reached with p>0.53.

Nissl and TUNEL staining showed a pattern of expression comparable to that seen with 16hr survival time point. As with microglial activation, a reduction in neuronal loss or dying cells with SL327 treatment occurred. By combining the scores of these two markers, a modest reduction in mean brain injury could be observed in SL327 treated pups compared to EtOH treated controls. There was a reduction in neuronal loss and subsequent 1.5-2fold decrease in injury was observed in cortex, pyriform cortex, and thalamus, whilst hippocampus, striatum and external capsule remained relatively unaffected between the two groups. This reduction in damage was greatest in cortex (51%), and thalamus (44%) respectively (figure 5.6L).

Tunel proved variable between the individual regions. External capsule, pyriform cortex and thalamus had very few Tunel positive dying cells, an average count of 22.85±1.75 (figure 5.6J). Striatum and hippocampus, the two areas in this experiment most responsive to 60min HI, saw an increase in dying cells within the SL327 treated group compared to EtOH alone with the highest count occurring in striatum (230.83±62.31), though not significant occurred (p> 0.2). In

contrast, cortex had a 3fold decrease in the number of dying cells in SL327 treated animals compared to EtOH. No significance occurred (P=0.4).

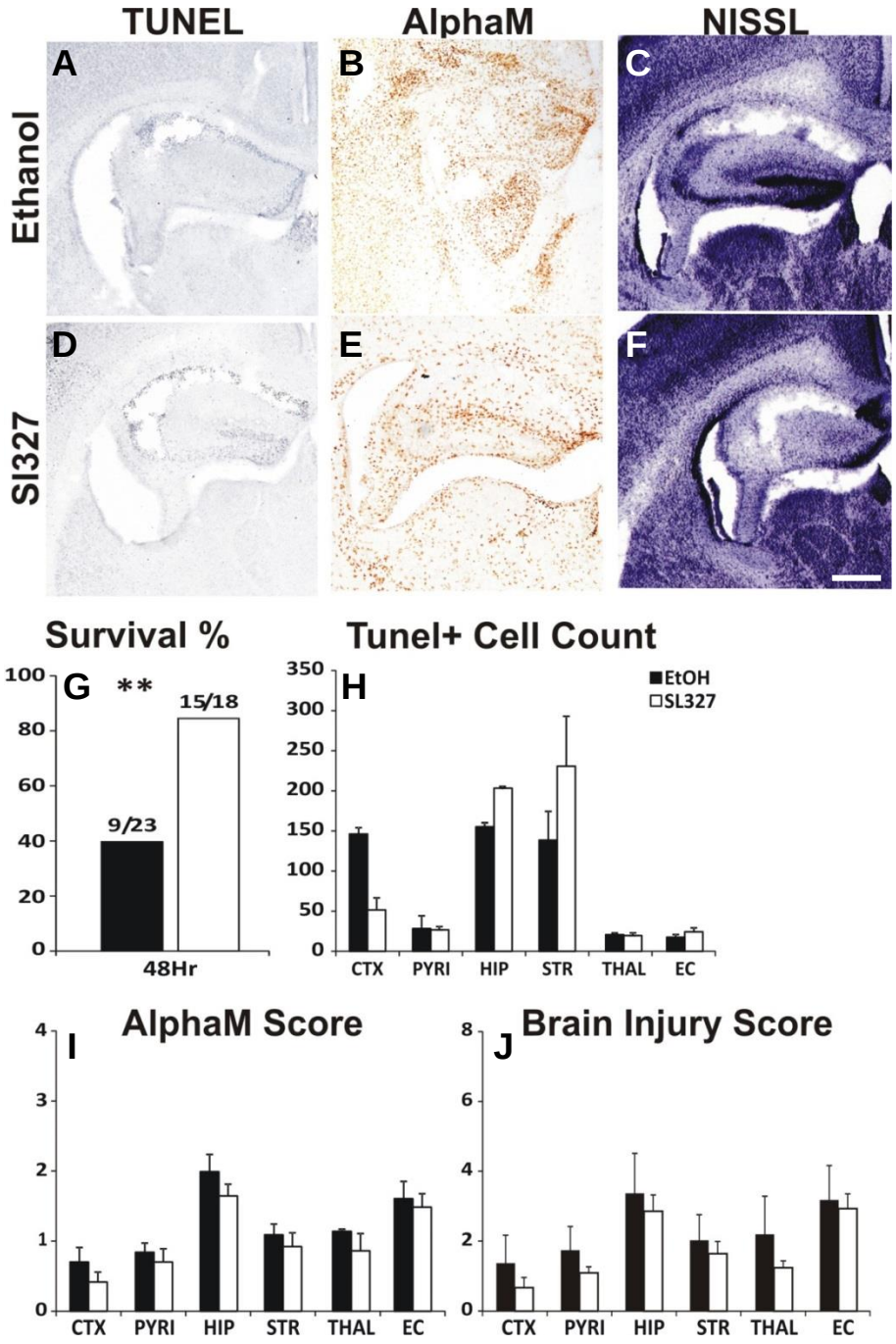

Figure 5.6 Effect of SL327 on survivability, microglia activation and TUNEL+ cell death when injected 1hr after 60min hypoxic/ischemic injury with 48hr survival time points. Assessment was at 20x magnification eye field (mean plus SEM over 3 fields). I: At 48hr post insult, pup survival when treated with EtOH alone was reduced to 39% compared to those treated with SL327 who had a survival percentage of 83%. Difference was significant at p=0.004. A, D, H: Tunel+ dying cells are unaffected by the presence of SL327. AlphaM (B, E, I) there is a trend to decrease in the SL327 group compared to EtOH alone at 48hr post insult. C, F, and J: Nissl showed an increase in neuronal loss within striatum, cortex, hippocampus and thalamus of the SL327 group compared to EtOH controls. However, this may be a direct effect from survivors of EtOH treatment being non-responders to HI insult. Scale bar indicates 0.25 mm. Analysis of survival percentage by chi squared test, analysis of damage markers by T-test gave significance when *p<0.05 **p<0.01.

From this data, it is evident that SL327 does partially reduce damage caused by 30min hypoxia-ischemia in the neonatal brain. Whilst its application increases the survivability of pups following more severe insult, it its therapeutic use against neuronal cell death remains inconclusive. This may be due to the non-responsive nature of the surviving members of the EtOH control group.

Pharmacological Inhibition of ERK- Discussion

Until the recent introduction of ATP competitive ERK selective inhibitors, observations of suppressed ERK activation in HI injury response has utilised selective MEK1/2 inhibitors. The most commonly used are PD98059 and U0126. Alessandrini et al. were the first to study the effects of PD98059 inhibition of MEK/ERK by its administration 30min prior to transient MCAO in adult mice (Alessandrini et al., 1999). 24hr after insult saw a 55% reduction in infarct. Neuroprotection was still visible at 72hr with a 36% decrease in infarct when compared to sham treated controls. Application of P38 MAPK inhibitor SB203580 had no effect on outcome. Additionally, C-Fos upregulation was observed following MEK inhibition, an event associated to neuronal survival (Uemura et al., 1991). U0126 showed a much greater affinity for both MEK1 and 2 leading to higher specificity against ERK1/2 activity. The same group showed that pre-treatment of U0126 to bilateral CROC in adult gerbil, reduced the loss of hippocampal neurons in addition to an overall reduction of 42% infarct, which associated to improved neurological outcome. Here they showed that U0126 is able to prevent phosphorylation of MEK, and as such ERK, but is unable to inactivate already phosphorylated pERK levels or gene expression. This suggests that while U0126 is effective at preventing downstream effects of MEK it does not inhibit upstream components of the signalling cascade.

U0126 has been effectually introduced into neonatal models of ERK activity. In rat pups, U0126 was injected intracerebroventricularly in two doses prior to CROC and 2.5hr 8% O_2 exposure where it blocks BDNF activation of ERK1, by 100% and ERK2 by 75%. However there was no change to levels of injury induced cleaved caspase 3 or infarct volume (Han and Holtzman, 2000).

Previous work by our laboratory, unpublished, attempted to introduce systemic U0126 administration into the neonatal mouse Rice-Vannucci model of HI brain injury. Pre-treatment 20min prior to 30min HI did not reduce pERK expression following insult, nor had an effect on HI induced damage suggesting that the increased molecular weight of U0126 proved too large for crossing the tightly regulated blood brain barrier. As such, we repeated these studies with the U0126 analogue SL327 whose size is a third less that U0126 without losing

specificity for either MEK1 or 2. SL327 was first used in 1998 in studies of long-term potentiation within the rat hippocampus. Intraperitoneal administration of SL327 resulted in reduced associative learning factors, a consequence of impaired LTP (Atkins et al., 1998). In adult mice, SL327 administered systemically 15min prior to MCAO, significantly reduced infarct by up to 64% and associative neurological abnormalities (Wang et al., 2003b).

To examine whether SL327 was effective in our own mouse model of neonatal HI injury, a dose response was performed with IP treatment of SL327 at 20min prior to 30min HI. SL327 was dissolved in 100% EtOH, which was well tolerated by the P7 pup, as the recommended media of DMSO proved highly toxic and resulted in death. A titration of SL327 at doses between 8 to 133μg/gBw showed complete inhibition of pERK immunoreactivity at the highest concentration. 30μg/gBw was able to reduce ERK activity by 80% however, as 133μg/gBw proved non-toxic, this was the concentration chosen. That even low dose was able to affect forebrain pERK expression re-enforced SL327 ability to cross the blood brain barrier.

Selective inhibition of ERK prior to mild HI is neuroprotective

SL327 was introduced i.p 20min before 30min exposure to HI in P7 C57/Bl6 mice. Damage markers were assessed 2day after insult, in line with the studies using ERK mutants. Pre-treatment with SL327 resulted in decreased levels of microglia activation, histological brain injury, and Tunel positive cell death in both white matter (external capsule) and grey matter regions of the neonatal forebrain compared to EtOH control treated littermates. The extent of GFAP positive astrocyte recruitment remained unaffected.

In vitro studies have shown that in mixed cultures of neurons and glia, U0126 added 30min prior to glutathione depletion, prevented subsequent cell death. Additionally pre-treatment prevents the activation of ERK through ROS. In contrast to our own studies, activation of astrocytes was completely abolished (de Bernardo et al., 2004). In H_2O_2 treated glial cell cultures, 60% of cells die, but with administration of PD98059 at the same time as insult completely nullifies cell death (Bhat and Zhang, 1999). As these studies were conducted in vitro, like for like comparisons are difficult to make. The cultures in both studies

include either total or half quantities of glia which would have gained a greater exposure to the inhibitors once they were added then these cells would otherwise have in vivo by diffuse intraperitoneal injection. In addition, it's been extensively recorded that the longer cells are left in culture the more likely that their gene expression profile. As such, although these studies show a change in GFAP response it does not make a conclusive argument that this is what would be observed in vivo. Indeed the data herein is the first to examine changes in GFAP expression following ERK inhibition in a model of neonatal HI.

In white matter of SL327 treated pups, scores for both αM immunoreactivity and histological brain injury were significantly reduced by 43%. Striatum and hippocampus were grey matter regions most affected by treatment, exhibiting up to 55% reduction. Tunel positive cell death was similarly diminished, although not in external capsule where relatively few cell bodies reside. Striatum and hippocampus were again the strongest responding regions to treatment with a respective 50% and 60% reduction in cell death.

Protective outcome from SL327 was retained when administered 1hr after mild HI. 1hr was chosen as a secondary time point for treatment in order to prevent the peak of ERK expression between 1-2hr, as indicated by the pERK time course in figures 3.1 and 2. In addition, when looking at pyriform cortex, 1hr is the switch point from glial to neuronal expression (figure 3.2). Investigation into the effects of cell specific deletion of ERK demonstrated that glial ERK expression is neuroprotective under HI conditions whereas neuronal is detrimental. As such an injection time that could block the latter whilst minimalizing the effect on the former was desired. Examination of white matter injury saw a 56% reduction in microglia activation and histological injury score. Hippocampus was equally affected with a 60% reduction in both markers. DNA fragmentation, whilst not significant, still had a 57% decrease in dying cells within striatum and hippocampus of treated animals. As with pre-treatment, GFAP immunoreactivity remained unaffected between groups. In a clinical setting, pre-treatment to insult in the infant is not viable.

In vivo studies explore the suppression of cytokine release following HI by application of U0126 both 20min prior and immediately following MCAO in the adult mouse. Here pre-treatment significantly reduced infarct volume, levels of

phosphorylated Elk-1 and IL-1β mRNA levels. In contrast to our own observations, post-treatment saw no change in outcome compared to sham-treated controls. Alessandrini's group also looked at pre versus post treatment in adult rodent models of focal cerebral ischemia. A greater reductive effect on infarct was observed with pre-treatment of PD98059, by 55%, while post treatment of U0126 was still protective, if slightly less so at 42% (Alessandrini et al., 1999; Namura et al., 2001).

Post-treatment of SL327 prevents morbidity but not cerebral injury following severe HI insult

Positive response of pERK inhibition after mild insult logically led to the hypothesis that inhibition could be protective after severe insult as well. Pre-treatment at 20min prior to 60min 8% O_2 exposure saw an 80-90% reduction in pERK expression within the neonatal forebrain at 15min post-insult (figure 5.1), illustrating SL327 to be effective in preventing increased ERK activity due to stronger insult. 133μg/gBw SL327 was systemically administered 1hr following HI. Damage markers were examined at two time points: 16hr, which corresponds to peak neuronal cell death after 60min HI and 48hr as optimised in our previous experiment.

At 16hr post insult there was no change in microglia activation, brain injury score or the prevalence of DNA fragmentation following SL327 treatment when compared to EtOH alone. This suggests that the effect of post-treatment with SL327 does not diminish peak activation of neuronal cell death pathways, or the recruitment of non-neuronal factors as a result of severe insult. As SL327 is an analogue of U0126, we can assume that its actions are via the prevention of MEK phosphorylation in opposed to dephosphorylation of already active MEK. If MEK/ERK pro-apoptotic signalling pathways were instigated during prolonged HI exposure, application of SL327 would be unable to prevent their downstream affects, only the sustained response by preventing further MEK/ERK activity.

Previous studies have implicated that in models of severe ischemic insult, MEK inhibition is insufficient to reduce neuropathological outcome. In the adult rat model of four artery occlusion, pre-treatment of PD98059 at 20min before insult, saw ablation of pERK expression however there was no difference in

hippocampal CA1 pyramidal cell survival (Gu et al., 2001). The same was seen with an intracerebroventricular injection of U0126, in combination with hypothermia treatment, for cardiac arrest in adult rats. Administration of U0126 at 30min after resuscitation was insufficient to reduce infarct in the hippocampus (D'Cruz et al., 2005).

A survival time point of 48hr provided a more promising outcome with significant increase in survival observed between the treated and untreated groups (figure 5.6). For most forebrain regions, markers for damage remained unaffected with the exception of cortex, which saw a 40% reduction in active microglia, and 50% reduction in histological brain injury score following SL327 treatment. Moreover, the morbidity of this cohort dramatically improved compared to EtOH treated controls. Interestingly, damage marker expression in both groups was similar to those of SL327 post insult treated pups subject to 30min HI. Normally, with increased insult one would expect the control group at least to exhibit much higher levels of marker immunoreactivity.

The Rice-Vannucci mouse model of HI does exhibit biological variability in the response of individual pups to HI. Previous studies have indicated that mice exposed to the same hypoxic-ischemic insult may demonstrate either minor ipsilateral cellular and tissue reaction to insult with intact contralateral side, or severe cerebral deterioration with formation of a large ischemic lesions of the ipsilateral cortex, and contralateral ventriculomegaly and thinning of the cortex (Ten et al., 2004). In addition it is known that C57/Bl6 mice have differing formation of circle of Willis (figure 5.7) resulting in multiform compensation for carotid artery occlusion (McColl et al., 2004). This becomes problematic due to varying degrees of severity due to either increased vascularisation resulting in little ischemic damage via unilateral carotid occlusion, or the more desirable partial ischemia by an incomplete circle of Willis. Therefore we can supposition that the surviving mice of EtOH-treated control group may have the potential to give little or no response to hypoxia-ischemic insult. In the adult rodent model of stroke, it has been suggested that by switching to a distal, in opposed to proximal, hypoxic model this variability can be overcome. The researchers occluded the distal middle cerebral artery prior to hypoxia, and in doing so were still able to achieve ipsilateral lesion, clearly bordered and delineated from the

unaffected contralateral hemisphere with “exceptionally low variability” (Doyle et al., 2012). Although not tested in the neonatal rodent, this may lead the way to a more robust response in the Rice-Vannucci model of HI. In the more immediate future, the addition of numbers to the untreated cohort should decrease variability and the influence of outliers. Alternatively by performing a bilateral carotid occlusion, it will remove an intracranial control, but also prevent vascular compensation, making the survivors of both treated and non-treated groups be subject to similar ischemic conditions. In turn this could confirm SL327 as therapeutic following severe HI injury.

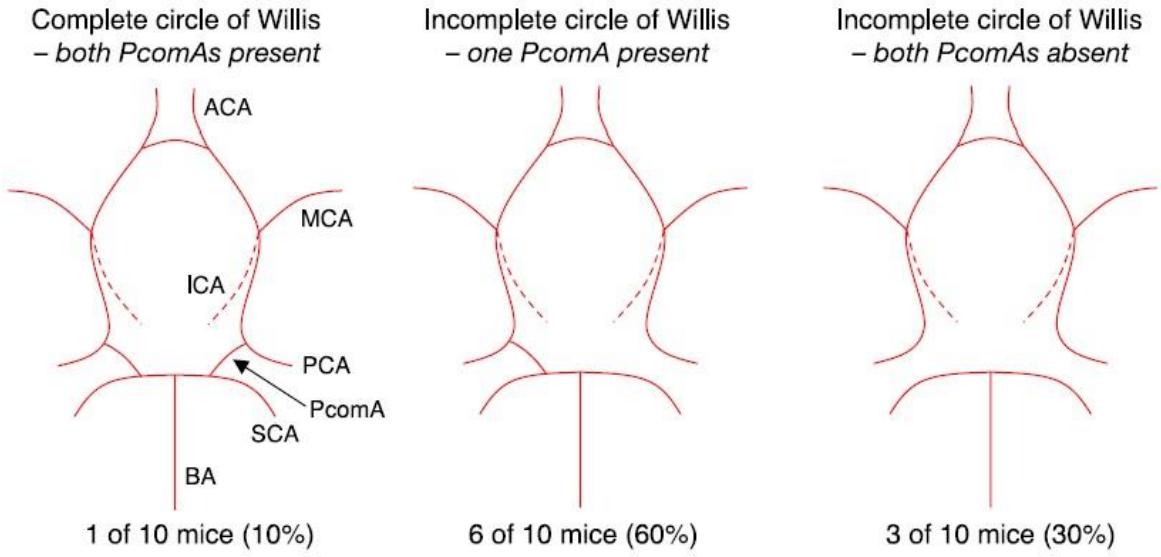

Figure 5.7 Integrity and differing artery organisation of the circle of Willis in C57Bl/6J mice. Anterior cerebral artery (ACA); middle cerebral artery (MCA); posterior cerebral artery (PCA); posterior communicating artery (PcomA); superior cerebellar artery (SCA); basilar artery (BCA); internal carotid artery (ICA). Reproduced with permission, McCoy et al. 2004.

Our studies herein indicate that early neuronal pERK expression is pro-apoptotic; this is rescued by neuron specific excision of ERK. Latent astrocytic ERK proved pro-survival. Introduction of SL327 at 1hr following prolonged HI may inhibit glial pERK expression, reducing the efficacy of endogenous neuroprotective mechanisms. Despite this, increased survivability in addition to reduced sustained injury at 2 days post insult does suggest SL327 to be a potential therapeutic agent against neonatal HI.

There remains a possibility that the limited protective nature of SL327 is an indirect consequence of ERK5 inhibition. U0126 is shown to successfully prevent ERK5 phosphorylation in addition to its actions on ERK1 and 2. In vitro

studies in PC12 and Hela, both PD98059 and U0126 exhibited strong inhibition of ERK5 in response to EGF (Kamakura et al., 1999; Mody et al., 2001). These inhibitors bind ERK5 at its phosphor-acceptor TEY sequence, homologous to that of ERK1/2, (Kamakura et al., 1999) in a dose-dependent manner.

Distribution of ERK5 in the rodent forebrain is localised to the olfactory bulb and cortex, hippocampus, amygdala and, to a lesser degree, cerebral cortex (Di Benedetto et al., 2007). Following global ischemia in the adult rat, pERK5 is rapidly upregulated within the first hour post insult, peaking at 30min. suppression of Ca^{2+} channel activity saw a significant reduction of pERK5 expressing hippocampal CA3 cells which associated to increased neuronal loss (Wang et al., 2005). The same group also showed that the ERK5/MEF2C pathway contributed to the anti-apoptotic effect of pre-conditioning to global ischemic insult. ERK5 activation occurs via the action of Ca^{2+} influx in NMDA receptors. Its suppression via antisense oligonucleotides results in increased CA1 hippocampal cell death (Wang et al., 2009).

Similar to ERK2, ERK5 null mice are embryonically lethal at E10.5 (Di Benedetto et al., 2007; Newbern et al., 2011; Nishimoto and Nishida, 2006). A new study of pan CNS deletion of ERK5, using nestin-driven cre recombinase, show that while these animals are viable, the number of GABAergic interneurons of the olfactory bulb was reduced in conjunction to an increase of developmental cell death within the subventricular zone (Zou et al., 2012).

Together these studies imply that use of high dose SL327 is only partially successful in reducing HI induced damage by possible actions at ERK5. Recent developments have given rise to two ERK selective, ATP competitive, inhibitors: SCH772984 and FR180204 (Anastassiadis et al., 2013; Morris et al., 2013) whose greater selectivity should prevent suppression of pERK5 seen with U0126.

In summary, the experiments herein suggest that pharmacological inhibition of ERK1/2 activation is highly effective as a therapeutic agent against mild HI insult. Whether preventing ERK phosphorylation is neuroprotective in severe HI models remains unclear. By introducing selective inhibitors of ERK1/2 in

opposed to MEK1/2 we can establish if SL327 shows reduced efficacy by its prevention of ERK5-mediated pro-survival pathways.

Neuroepithelial Deletion of C-Jun- Results

C-Jun N-terminal Kinase (JNK), a member of the MAPK superfamily that also included ERK, directly activates C-Jun, a major component of the AP-1 transcription family complexes. AP-1 proteins have the capacity to dimerise in order to form functional sequence-specific transcription factors that then bind to their DNA target sites. The regulatory properties of AP-1 depend on the subunit composition leading to differentially modulated gene transcription (Plotnikov et al., 2011; Runchel et al., 2011). A number of extracellular signals activate JNKs. JNK phosphorylation leads them to further phosphorylate C-Jun at serine 63 and 73, and threonine 91 and 93 of the N-terminal (Bermudez et al., 2010; Bogoyevitch et al., 2010; Centeno et al., 2007; Davies and Tournier, 2012; Meng and Xia, 2011; Wagner and Nebreda, 2009).

Following cerebral ischemia, C-Jun is selectively induced, and implicated as a master regulator of gene expression in the post ischemic neuron, particularly when excitotoxicity occurs (Akaji et al., 2003; Centeno et al., 2007; Guan et al., 2006; Mrsić-Pelcić et al., 2008; Pirianov et al., 2007; Sommer et al., 1995). Molecular studies in cerebral ischemia show a rapid increase in AP-1 binding and activity of pJNK2 and 3, coinciding with C-Jun phosphorylation (Akaji et al., 2003; Centeno et al., 2007; Sommer et al., 1995). Indeed, C-Jun mRNA expression in both hippocampus and the corpus callosum is observed within 1hr of insult. In vivo HI studies have further investigated the contribution of the JNK/C-Jun/AP1 pathway. Here global deletion of JNK3 is neuroprotective in neonatal mouse cerebral ischemia (Pirianov et al., 2007). In the neonatal rat, an upregulation of C-Jun and C-Fos is detectable in striatum, cortex and hippocampus after exposure to 3hr 8% O_2. Strong C-Jun immunoreactivity was associated to apoptotic, but not necrotic, cells in both HI and focal ischemia in P9 rats (Nijboer et al., 2010).

Targeting C-Jun in the neonatal model of HI has so far required the use of selective JNK inhibitors (Nijboer et al., 2013; Nijboer et al., 2010; Repici et al., 2007; Zhao et al., 2012). As such it remains to be seen what effect cell specific deletion of C-Jun will have on the perinatal brain response to insult. Since C-Jun global knockouts are embryonically lethal, a conditional CNS C-Jun mutant was created. This utilised cre-recombinase under the control of the nestin

promoter. Nestin is an intermediate filament protein that contains a CNS specific enhancer region in the second intron. It is expressed in multipotent stem cells that give rise to neurons, glia and oligodendrocytes. Microglia are thought to derive from mesenchymal origins and as such do not express nestin.

Generation of transgenic mutant mice lacking C-Jun in neuroepithelial lineage cells

CNS specific C-Jun mutant animals were generated by crossing mice with the C72 Jun allele flanked by LoxP sites (C-Jun$^{Fl/Fl}$) with mice expressing cre recombinase under the control of the nestin promoter (Nestin-Cre). The resultant F1 generation were subsequently crossed, producing mutants with homozygous deletion of C-Jun in nestin positive cells. Littermates lacking the cre transgene remained functionally unchanged in terms of C-Jun expression and thus served as controls.

Both C-Jun$^{Fl/Fl}$ and Nestin-Cre were confirmed via PCR and immunohistochemistry. Mice heterozygous for floxed C-Jun gave rise to a 350bp band for the presence of the floxed gene, and 300bp for the wild type gene. Cre-recombinase positive animals show a band at 750bp.

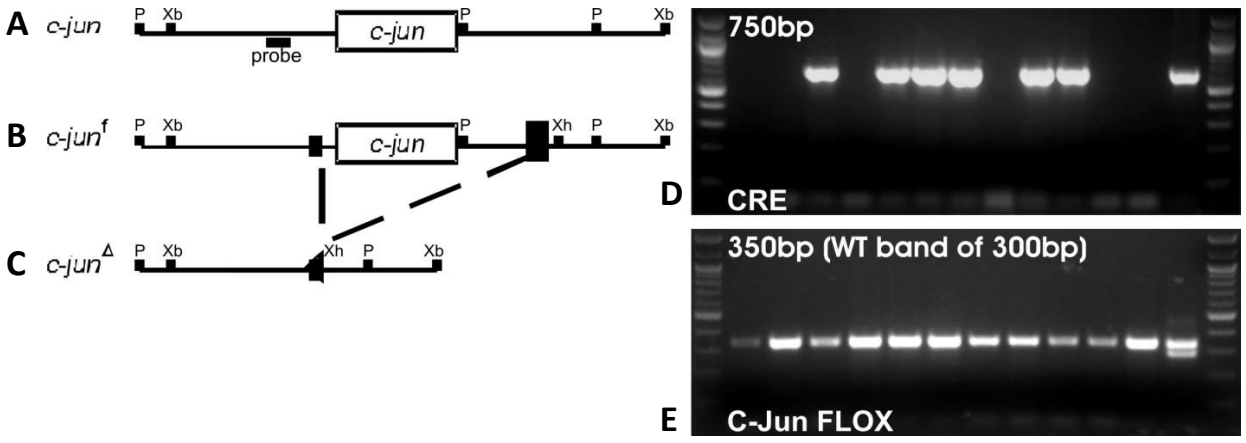

Figure 6.1 Schematic representation of wild type C-Jun (A), floxed C-Jun (B), and deleted C-Jun (C). ☐ Codes for open reading frame, ʙ are untranslated regions of C-Jun, and ○ is LoxP sites. Adapted from Behrens et al. 2002. CNS-specific deletion of C-Jun was achieved using Nestin-Cre excision of floxed C-Jun. Agarose gel electrophoresis of PCR products were visualised to detect C-Jun floxed/wild type at 350bp and 300bp respectively (E), and Nestin-Cre allele at 750bp (D). Whilst all animals with homozygous C-Jun floxed will show the appropriate bands, only those positive for Cre are mutants for nestin C-Jun deletion.

Tissue specific loss of neuronal C-Jun was confirmed by immunohistochemistry for C-Jun in both control C-Jun$^{Fl/Fl}$ (JJ) controls, where n=2, and mutant Nestin-

Cre: C-Jun $^{Fl/Fl}$ (NJJ) mice, where n=2. Postnatal day 7 (P7) pups were subject to 30min hypoxia following left carotid artery occlusion (CROC). They were allowed to recover with dams for 2hr before sacrifice. The mice were perfused with 4% PFA for 2.5min after which the forebrains were extracted, post fixed in 4% PFA for 1hr and cryoprotected in a 30% saturated sucrose solution. 24-48hr later, these were frozen on dry ice, cryosectioned into 40μm slices and stored at -80°C until required. Five equal distant sections were used per brain and stained with an anti-C-Jun antibody. A complete absence of C-Jun was observed in NJJ forebrains (figure 6.2B) whilst the control animals (figure 6.2A) presented a normal degree and distribution of C-Jun.

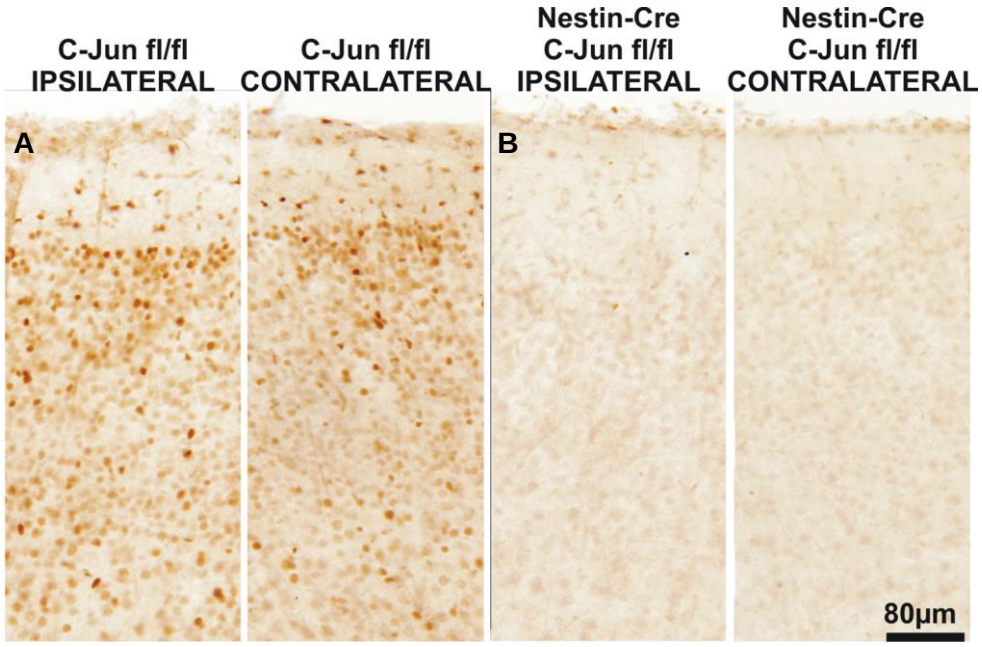

Figure 6.2 C-Jun upregulation following 30min HI. Immunohistochemistry analysis of C-Jun expression revealed the complete loss of neuronal C-Jun in Nestin-Cre: C-JunFl/Fl (NJJ) animals (B) in comparison to a normal degree and pattern of expression in C-JunFl/Fl (JJ) mice (A). C-Jun was analysed by light microscopy at 10x magnification.

Although immunohistochemistry confirmed neuronal loss of C-Jun expression it remained to be confirmed in which non-neuronal cells expression may occur. Immunofluorescence co-labelling of C-Jun with markers of microglia (alphaM integrin), oligodendrocytes (NG2), and astrocytes (GFAP) was performed in order to confirm non-neuronal expression of C-Jun in NJJ mice following HI. As illustrated in figure 6.3, C-Jun (red) strongly localised to GFAP (green) positive cells in the JJ controls (figure 6.3A). By looking under a higher magnification (64x) it was revealed that C-Jun localises to the nucleus (white arrows, figure 6.3E) the abolition of which is seen in transgenic mutants (figure 6.3B and F). Further, NG2 labelled oligodendrocytes displayed prominent C-Jun (red) rich

nuclei in JJ group which again is absent in NJJ (figure 6.G-H). In contrast, the number of C-Jun positive microglia remained unchanged between groups (figure 6.3I-K) confirming expression to be nullified in nestin expressing cells only.

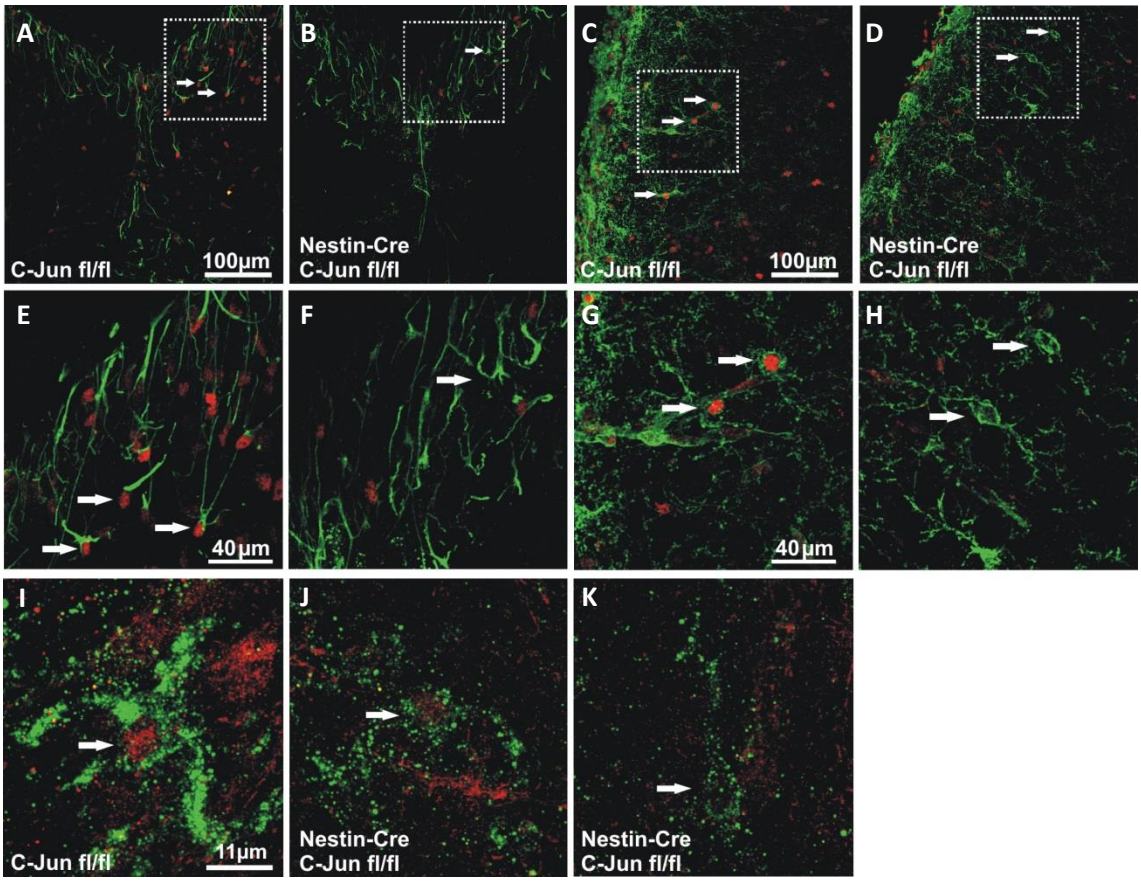

Figure 6.3 confocal imaging of JJ and NJJ mice at 2hr following 30min HI. C-Jun expression was deleted in astrocytes and oligodendrocytes but not microglia in NJJ animals. Images were captured at 25x magnification or 64 magnifications (I-K). A-B, E-F: co-labelling of C-Jun (red) and astrocytes in JJ (A, E) and NJJ (B, F) animals. C-D, G-H: co-labelling of C-Jun (red) and oligodendrocytes (green). Microglia are intensely stained with C-Jun in JJ (I) and NJJ (J-K) animals in equal amounts.

Neuroepithelial deletion of C-Jun exacerbates cell damage in then neonatal forebrain following hypoxia/ischemic insult

Neuronal cell deaths, in addition to the recruitment of non-neuronal cells, are commonly observed at injury sites caused by HI in the neonatal forebrain. Activation of cell death occurs within the first 48hr of insult. To examine C-Jun's role in mediating cellular response to HI, we analysed the expression of damage markers following exposure of transgenic mice for nestin-cre driven C-Jun deletion to 30min 8% O_2. Markers included microglia activation and phagocytic phenotype via use of anti-αM and -αX integrin antibodies, Tunel positive cell death and cresyl violet histology staining (figure 6.4). The latter

gives a morphological indication of neuronal loss by chromatolysis. Regions of interest included external capsule (WM) and grey matter areas: striatum; pyriform cortex; cerebral cortex; hippocampus; and thalamus.

Thirty one P7 mouse pups underwent left carotid artery occlusion (CROC) followed by 30min HI in accordance to the Rice-Vannucci model of rodent neonatal hypoxia/ischemic insult. This model allows an intracranial control of the hemisphere contralateral to CROC as hypoxia alone is insufficient to induce damage. After hypoxia, pups were returned to dams for 2days when they were sacrificed. Between hypoxia and 48hr six animals died, regardless of genotype. Of the surviving mice, brains were perfused and processed as previously described. Genotypes were confirmed by PCR resulting in 14x JJ controls and 11x NJJ mutants. For each damage marker, 5 sections were retrieved per brain.

The activation and recruitment of microglia to regions sensitive to HI is a preceding event to damage. Following mild insult, a trend towards increased activation is observed in NJJ animals compared to littermate JJ controls. Hippocampus proved most sensitive to insult with an average score of 1.29±0.12 (NJJ) and 1.06±0.25 (JJ). External capsule, striatum and thalamus also exhibited a 0.5-3fold elevation in αM scores for mutant mice. This was insignificantly so with $P>0.1$. In contrast, cortex saw a reduction in αM immunoreactivity with NJJ mice in both ipsilateral and contralateral hemispheres. By student t-test, $p=0.05$ in NJJ contralateral cortex compared to JJ (figure 6.5A). All contralateral forebrain regions, aside from cortex, saw low baseline microglia activation with no change between groups (figure 6.5B).

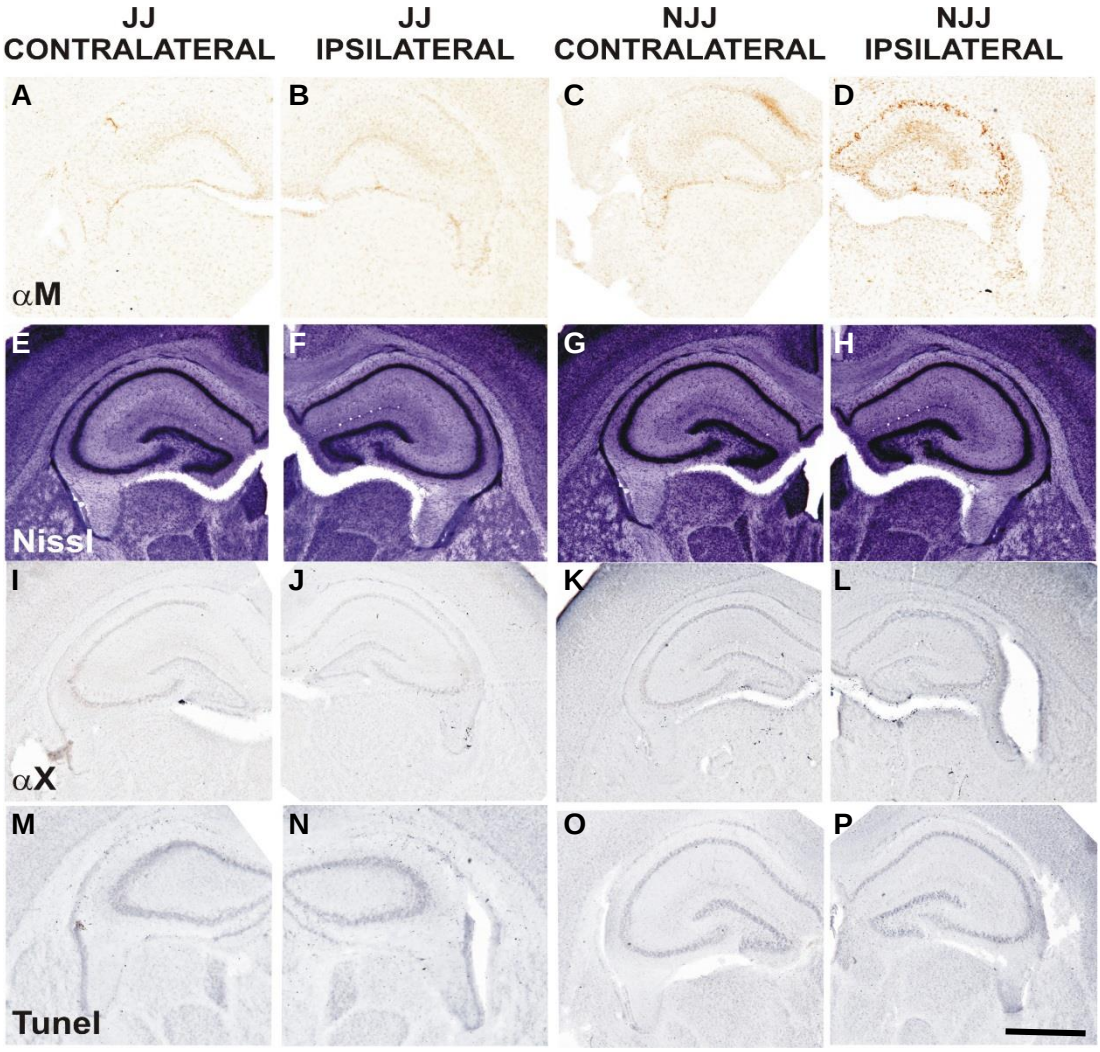

Figure 6.4 Illustrative response of both contralateral (1st and 3rd column) and ipsilateral (2nd and 4th column) hemisphere of P7 mice subject to 30min HI. Transgenic mutant mice with neuroepithelial specific homozygous deletion of C-Jun, using Nestin-driven cre recombinase, were compared to C-Jun competent (JJ) littermate controls. Forebrain sections were analysed for microglia activation (A-D) and phagocytic phenotype (I-L), neuronal loss (E-H), Tunel+ cell death (M-P). Scale bar indicates 0.5mm. Analysis was performed at 20x eye field (mean plus SEM over 3 fields).

AlphaX is employed to determine the number of phagocytic microglia present as a consequence of dead cells and cellular debris. Whilst activated microglia are clearly seen at 48hr post insult, this time point is potentially too early to observe those with a phagocytic phenotype. By looking at each forebrain region following mild HI, the number of αX positive cells did not change between the ipsilateral and contralateral hemispheres (figure 6.4I-L). In addition, there was no difference between NJJ and JJ animals with respective average ipsilateral counts of 2.8±0.7 and 3.4±0.8 respectively (figure 6.5E-F).

The numbers of Tunel positive dying cells combined with cresyl violet histology of tissue damage allow us to gauge the extent of cell loss due to HI insult. Increased expression occurred in both groups in the ipsilateral regions

compared to the contralateral counterparts. In the NJJ brain, both markers were highly expressed compared to JJ animals.

Neuronal loss, from the cresyl violet histology and the formation of nissl bodies, is measured using a semi-quantitative scoring system where 0 is a lack of damage and 4 is extensive tissue loss. Due to the lack of soma present in the white matter region: external capsule, it cannot be scored. The remaining grey matter regions: striatum; pyriform cortex; cortex; hippocampus; and thalamus all saw a strong increase in nissl score of NJJ versus JJ groups. The cresyl violet histological score was combined with αM immunoreactivity for microglia activation to give a mean brain injury score (figure 6.5C-D). As observed with microglia activation, hippocampus (JJ= 1.66±0.53, NJJ= 2.68±0.87), striatum (JJ= 0.67±0.34, NJJ= 1.86±0.73), and external capsule (JJ= 1.17±0.43, NJJ= 1.64±0.66) were the most sensitive to insult although insignificantly so ($P>0.09$). Cortex (JJ= 0.57±0.37, NJJ= 1.20±0.56), pyriform cortex (JJ= 024±0.10, NJJ= 0.32±0.12), and thalamus (JJ= 0.17± 0.08, NJJ= 0.81±0.45) were more modestly affected.

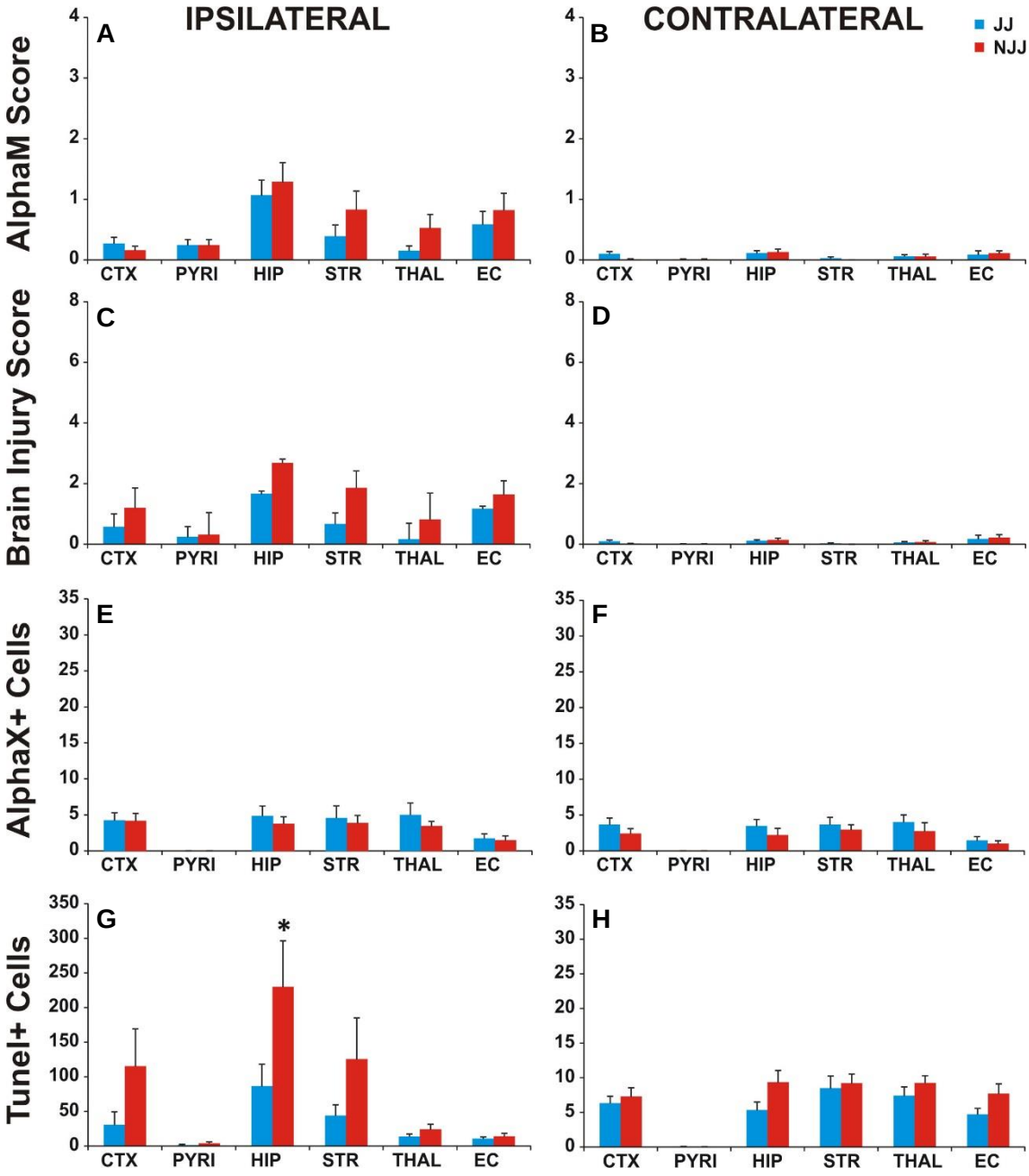

Figure 6.5 Transgenic mutant mice were created to compare pan-CNS selective deletion of C-Jun to wild type expression in mild hypoxic-ischemic injury to the neonatal mouse brain Forebrain sections were analysed for microglia activation (A-B), brain injury (C-D), presence of phagocytic microglia (E-F) Tunel+ cell death (G-H). A-L: analysis of forebrain regions for damage markers. Regions include external capsule (EC), striatum (STR), pyriform cortex (PYR), cortex (CTX), hippocampus (HIP), and thalamus (THAL). A: microglia activation is increased in the presence of neural C-Jun deletion (NJJ). Trend to increase damage in mutants was observed by brain injury score (combined assessment for activated microglia and neuronal loss by nissl body formation) and in the number of Tunel+ dying cells (C-D, G-H) E-F: Recruitment of phagocytic microglia remains unchanged between groups. B, D, F, H: Contralateral hemisphere to carotid occlusion (hypoxia alone intracranial control), baseline levels of active and phagocytic microglia are seen in the white matter (B and F). Developmental cell death occurs in all regions bar pyriform with no difference between groups (H). * indicates a student t-test P value ≤ 0.05.

Tunel indicates dying cells by binding to the nick ends of fragmented DNA. The number of Tunel positive dying cells saw a trend to increase in NJJ mutants similar to that of brain injury scores. Contralateral regions exhibit a baseline level of developmental cell death equal in both cohorts. This degree of change

is far exceeded in ipsilateral regions (figure 6.5H). Hippocampus had a significant 63% increase in dying cell numbers within NJJ animals compared to JJ (JJ= 86.49±31.77, NJJ= 229.82±66.30), p=0.04 (figure 6.5G). Striatum and cortex were also strongly effected with 65-74% increase in NJJ animals (Striatum: JJ= 44.07±15.53; NJJ= 125.48±59.94, cortex: JJ= 30.56±18.89; NJJ= 115.22± 53.93) however significance was not reached, P>0.1. External capsule and thalamus saw a milder 0.5-2fold increase in dying cell numbers of NJJ animals than JJ, whilst pyriform cortex did not exceed contralateral baseline immunoreactivity in either group.

Severe HI insult exacerbates the detrimental nature of nestin driven C-Jun deletion

To verify the adverse effects seen with 30min HI on nestin controlled C-Jun deletion, the above experiment was repeated with the change of increased severity of hypoxia. 60min hypoxia results in greater grey matter damage and the development of infarct lesions not seen with 30min hypoxia. Eleven NJJ animals and eighteen JJ littermate controls were subject to 60mon 8% O_2 with a survival time of 48hr. Forebrains were assessed for microglia activation (αM), phagocytic microglia (αX), neuronal loss (cresyl violet), dying cells (Tunel), and the extent of infarction (figure 6.6). Infarct volume is measured by calculating the loss of area for each ipsilateral region as a percentage of its contralateral counterpart. As with mild hypoxic insult, a strong increase in ipsilateral damage was observed in NJJ animals when compared to JJ controls.

By scoring αM immunoreactivity, a 2-3fold increase in microglia activation was revealed in ipsilateral NJJ forebrains. Analysis of the individual regions, this increase was significant within external capsule (p= 0.05), striatum (p= 0.05), cortex (p= 0.04), and hippocampus (p=0.02) (figure 6.7A). Pyriform cortex (JJ= 0.34±0.11, NJJ= 0.74±0.21) and thalamus (JJ= 0.32±0.13, NJJ= 0.81±0.32) saw an increase in microglia activation in NJJ mutants compared to JJ, although insignificantly so, p>0.1. Contralateral external capsule did exhibit levels of αM immunoreactivity that exceeded baseline within both cohorts. NJJ external capsule had a significantly greater score than JJ, p=0.02 (figure 6.7B). All other contralateral regions remained at baseline levels.

30min HI was insufficient to activate phagocytic microglia at 48hr after injury. With severe 60min HI a modest increase in αX positive cells becomes evident. This indicates that greater score for activated microglia seen with 60min HI coincides with a change to phagocytic phenotype. External capsule and striatum saw the largest increase in αX positive cell numbers with a 25% and 50% increase respectively in NJJ animals (figure 6.7E).

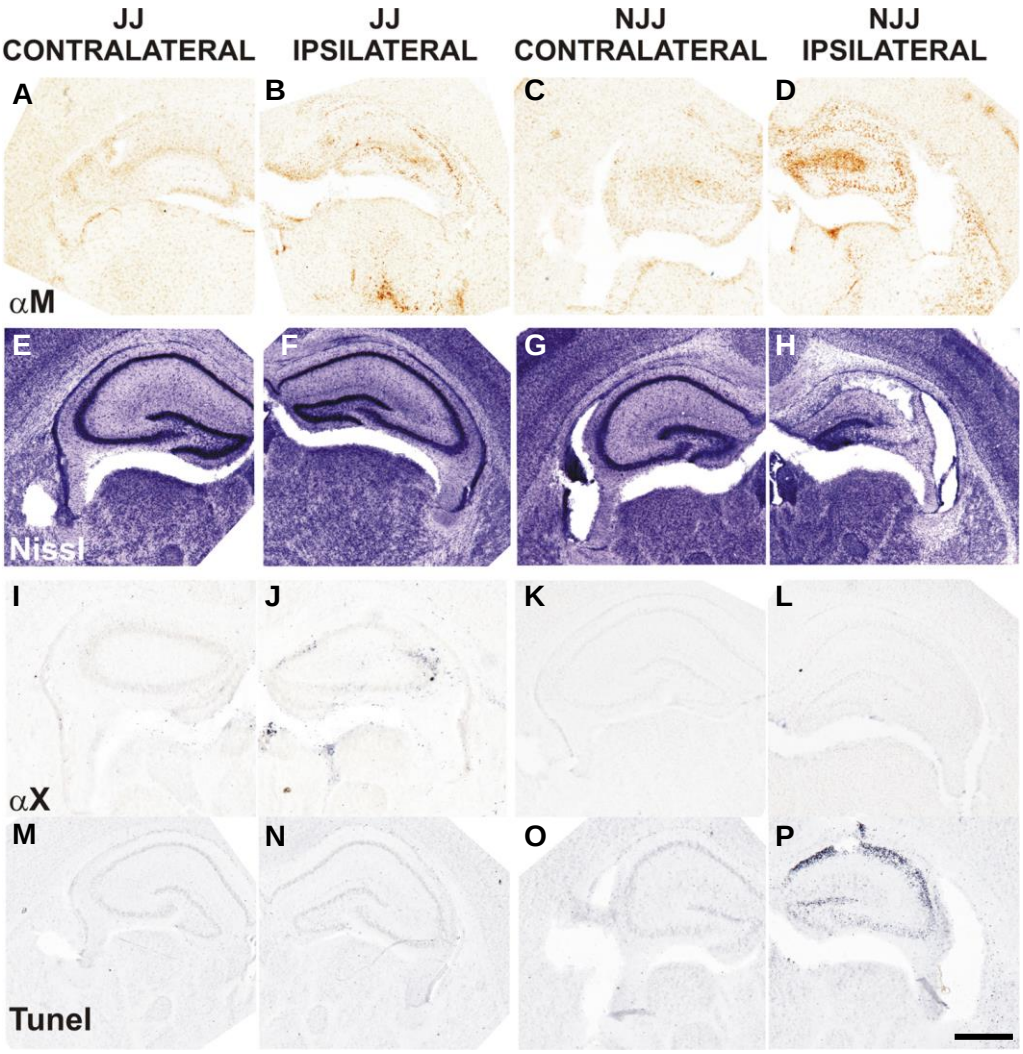

Figure 6.6 Illustrative response of both contralateral (1st and 3rd column) and ipsilateral (2nd and 4th column) hemisphere of P7 mice subject to 60min HI. Transgenic mutant mice with neuroepithelial specific homozygous deletion of C-Jun, using Nestin-driven cre recombinase (NJJ), were compared to C-Jun competent (JJ) littermate controls. Forebrain sections were analysed for microglia activation (A-D) and phagocytic phenotype (I-L), neuronal loss (E-H), Tunel+ cell death (M-P). Scale bar indicates 0.5mm.

Mean brain injury follows suit with striatum, external capsule and hippocampus obtaining a significant increase in mean brain injury score of 3.34±0.69, 3.09±0.64 and 3.61±0.74 for NJJ mutants and 1.45±0.50, 1.49±0.41 and 1.59±0.53 for JJ controls (figure 6.7C). By student t-test, P value was 0.03, 0.04, and 0.03 respectively. In cortex, pyriform, cortex, and thalamus brain

injury was higher in NJJ than JJ with an average score between them of 1.18±0.39. Lastly, the contralateral NJJ white matter also had an increase in neuronal loss and injury above baseline, due to cross over at the corpus callosum, which was highly significant with P=0.002 (figure 6.7D).

Increased tunel positive dying cells in NJJ mutants seen following mild hypoxia is augmented following 60min hypoxia. A significant increase in tunel immunoreactivity is observed in striatum (P=0.02), cortex (P= 0.02), and hippocampus (P=0.04) (figure 6.7G). Striatum saw the greatest number of dying cells with an average of 371.05±87.53 for NJJ and 153.20±46.10 for controls.

Despite this evident loss of neurons and the increased presence of dying cells in NJJ forebrain regions, formation of lesions proved less differentiated between the two groups. External capsule (23.46±4.45%) and hippocampus (28.46±7.55%) were the two regions whose extend of tissue volume loss exceeded that of control animals (external capsule: 9.50±3.56%, Hippocampus: 18.69±4.97%). This increase was to a significant degree in external capsule, p= 0.01(figure 6.7I).

Together these results indicate that C-Jun is required for neuroprotection against hypoxic/ischemic injury on a cellular level, but is not a major factor to overall tissue damage at 2days post insult.

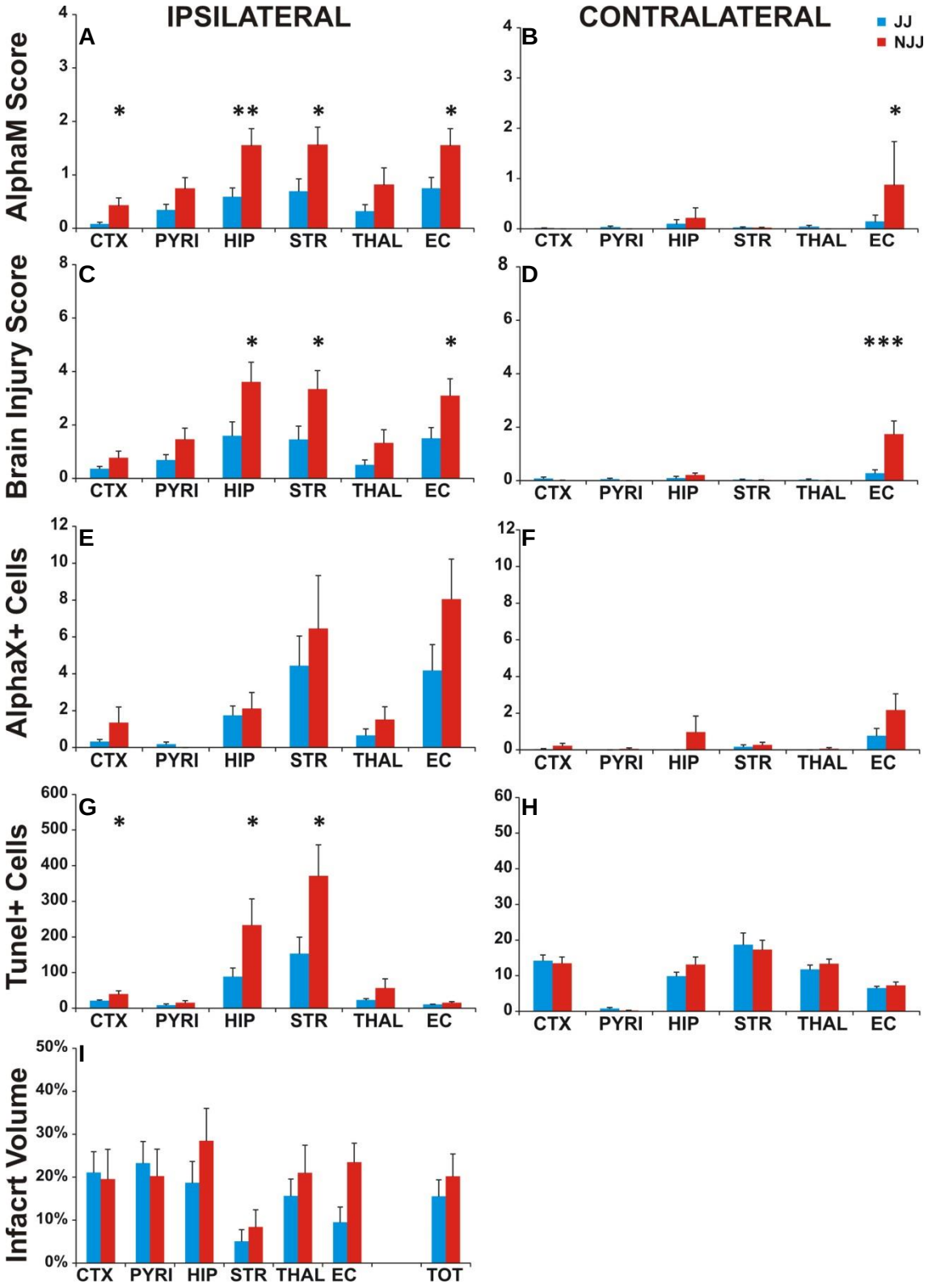

Figure 6.7 Transgenic mutant mice were created to compare pan-CNS selective deletion of C-Jun to wild type expression with 60min hypoxic-ischemic injury to the neonatal mouse brain Forebrain sections were analysed for microglia activation (A- B), brain injury (C-D), presence of phagocytic microglia (E-F) and Tunel+ cell death (G-H) and the extent of infarction (I). A: microglia activation is increased in the presence of neural C-Jun deletion (NJJ) to a higher degree to that seen with 30min HI. A difference between the two groups is now more pronounced in brain injury score as we;; as in the number of Tunel positive dying cells (C-D, G-H) E-F: Recruitment of phagocytic microglia indicates a modest rise from baseline expression, with more αX immunoreactivity in NJJ animals compared to JJ.. B, D, F, H: Contralateral hemisphere to carotid occlusion (hypoxia alone intracranial control). * indicates a student t-test P value ≤ 0.05. **P<0.01.

Neuroepithelial C-Jun has a passive role in cellular response to endotoxin-sensitised HI in a manner imitating that with HI alone

Cerebral ischemia leads to the selective induction of nuclear transcription factors including AP1 family members C-Jun, JunB and JunD as well as their counterparts C-Fos, FosB, Fra1 and Fra2. In addition JNK upregulation is observed in oligodendrocytes and their precursors following apoptotic stimuli by TNF and other pro-inflammatory cytokines.

Previous work by this laboratory, as well as data herein this thesis, show maternal-fetal infection to act in synergy with HI, exacerbating the degree of brain injury caused by either endotoxin or HI alone. These studies have utilised lipopolysaccharide (LPS), the endotoxin found on the outer membrane of gram negative bacteria. In vitro studies show JNK signalling precedes cell death by inflammation induced apoptosis. As such it is considered a predominant pathway for cytokine production from LPS and/or hypoxia exposed microglia. Primary microglia cultures from the neonatal rat demonstrate the presence of all three JNK isoforms. After LPS stimulation, an increase in total nuclear JNK in addition to phosphorylated C-Jun is observed. Additionally AP1 induces upregulation of pro-inflammatory target genes: COX2, TNFα and IL-6. In vivo, P2 rat pups saw selective white matter damage after exposure to LPS sensitised HI (90min 8% O_2) (Wang et al., 2012b). White matter injury associates with increase in activated microglia, TNFα production and oligodendrocyte precursor apoptosis. Selective inhibition of JNK resulted in a reduction of activated microglia, TNF immunoreactivity, and cleaved caspase 3 expression in endothelial of the blood brain barrier and in oligodendrocyte precursor cells.

So far this chapter has demonstrated that pan-CNS neuroepithelial lineage cells are more sensitive to injury when lacking C-Jun. The following experiment aims to explore whether C-Jun activation is a required component for the developing pathology from combined LPS and HI insult. P6 mouse pups with nestin driven C-Jun deletion were subject to 0.6μg/gbw LPS 12hr prior to 30min HI, and allowed to recover for 48hr before sacrifice. C-Jun$^{fl/fl}$ littermate controls were run along aside. Brains were perfused and processed as previously described. PCR verified genotypes, resulting in 10xJJ controls and 10xNJJ mutant animals.

Forebrain regions were assessed for microglia and astrocyte activation (αM and GFAP immunoreactivity), brain injury, combining neuronal loss (cresyl violet histology) and αM, Tunel positive cell death and the extent of infarction.

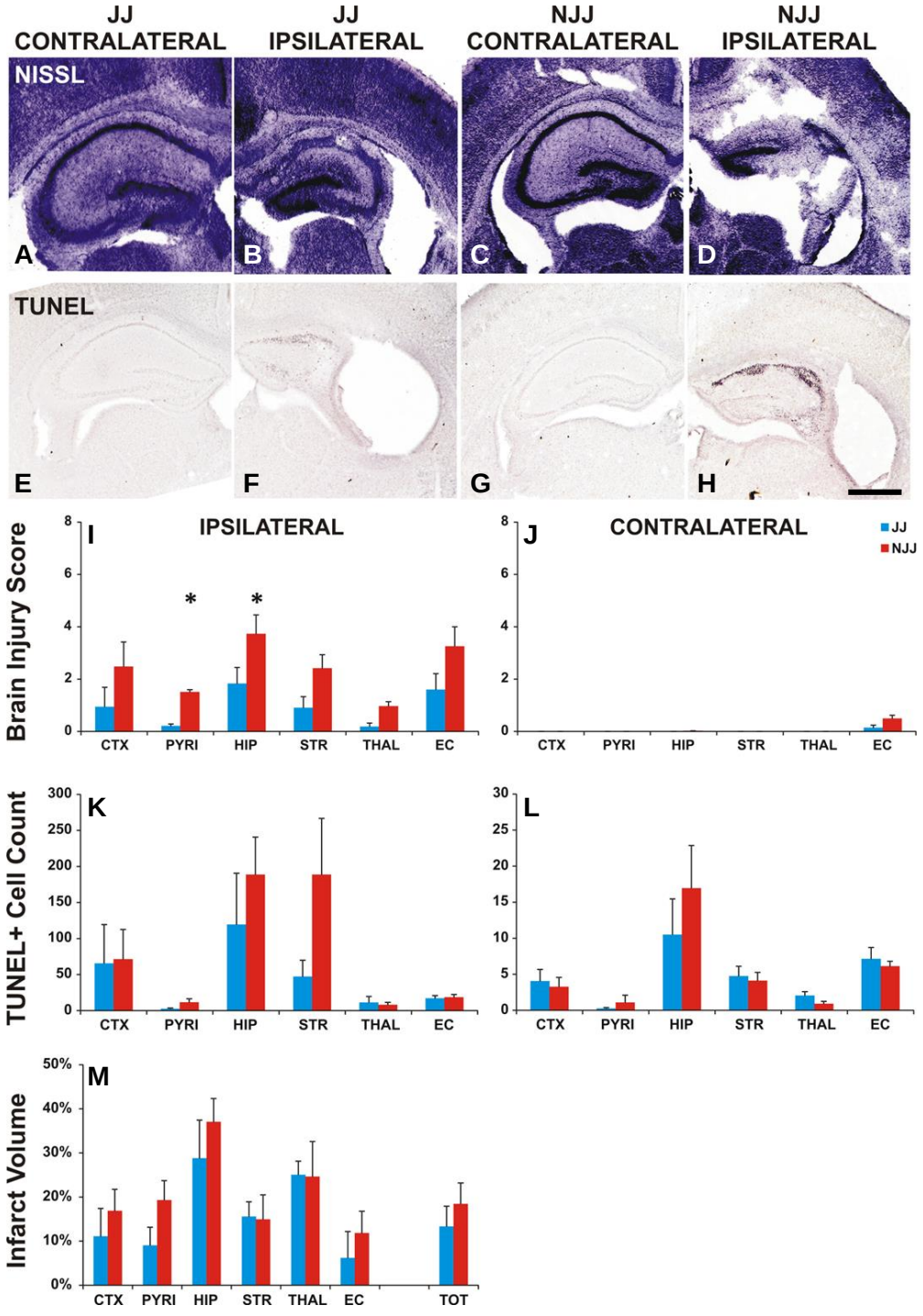

Figure 6.8 Quantification of Tunel+ dying cells and a combined score for microglia activation and cresyl violet histology, indicating the extent of neuronal loss (brain injury score), in JJ and NJJ transgenic mutant mice. NJJ (A-D, I-J) showed a significant rise in brain injury. In addition they exhibited an increase in the number of dying cells (G-H, K-L), counted over 3 fields at 20x magnification. The hemisphere contralateral to carotid occlusion showed no increase in damage above baseline developmental cell death (J, L). M: Infarct volume loss of each forebrain region. Loss was assessed measuring the areas of intact cresyl violet staining, bilaterally for each forebrain region, and calculating the ipsilateral regions as percentages of the contralateral (uninjured) hemisphere. No change in volume size was observed between groups. Scale bar indicates 0.5mm. *P<0.05 by student T-test.

Two days after insult, the extent of cellular damage was far greater in NJJ transgenic mutants than that in littermate controls. When forebrain regions were individually assessed, an elevation in microglia activation and neuronal loss were observed in external capsule, striatum, pyriform cortex, cortex, and hippocampus with no one region being more sensitive to damage than the other. Mean brain injury was the most predominantly affected marker with the greatest discrepancy between NJJ and JJ groups (figure 6.8A-D and I). Significance was reached in striatum, $p=0.03$ (JJ=0.34±0.22, NJJ= 1.41±0.40), pyriform cortex, $p= 0.04$ (JJ= 0.11±0.05, NJJ= 0.54±0.32), and hippocampus, $p=0.01$ (JJ= 0.73±0.32, NJJ=1.94±0.31). External capsule, cortex, and thalamus had a 3-7fold increase of tissue loss in NJJ animals to JJ, this was not statistically significant, $p>0.1$.

Tunel positive cell death was highest in striatum (JJ= 47.09±22.85, NJJ= 188.70±77.99) and hippocampus (JJ= 119.27±71.34, NJJ= 188.52±52.06) with a 75% and 37% increase in NJJ animals compared to JJ (figure 6.8E-H and K). This was statistically insignificant with $p>0.11$. Other forebrain regions proved less well defined with both low numbers and no difference between the mutants and controls observed in external capsule, pyriform cortex, and thalamus (average number of dying cells =18.55±3.84). The ipsilateral cortex saw an increase in dying cells (JJ= 66.53±53.84, NJJ= 71.40±41.23) after insult, giving a modest 8% increase in NJJ animals.

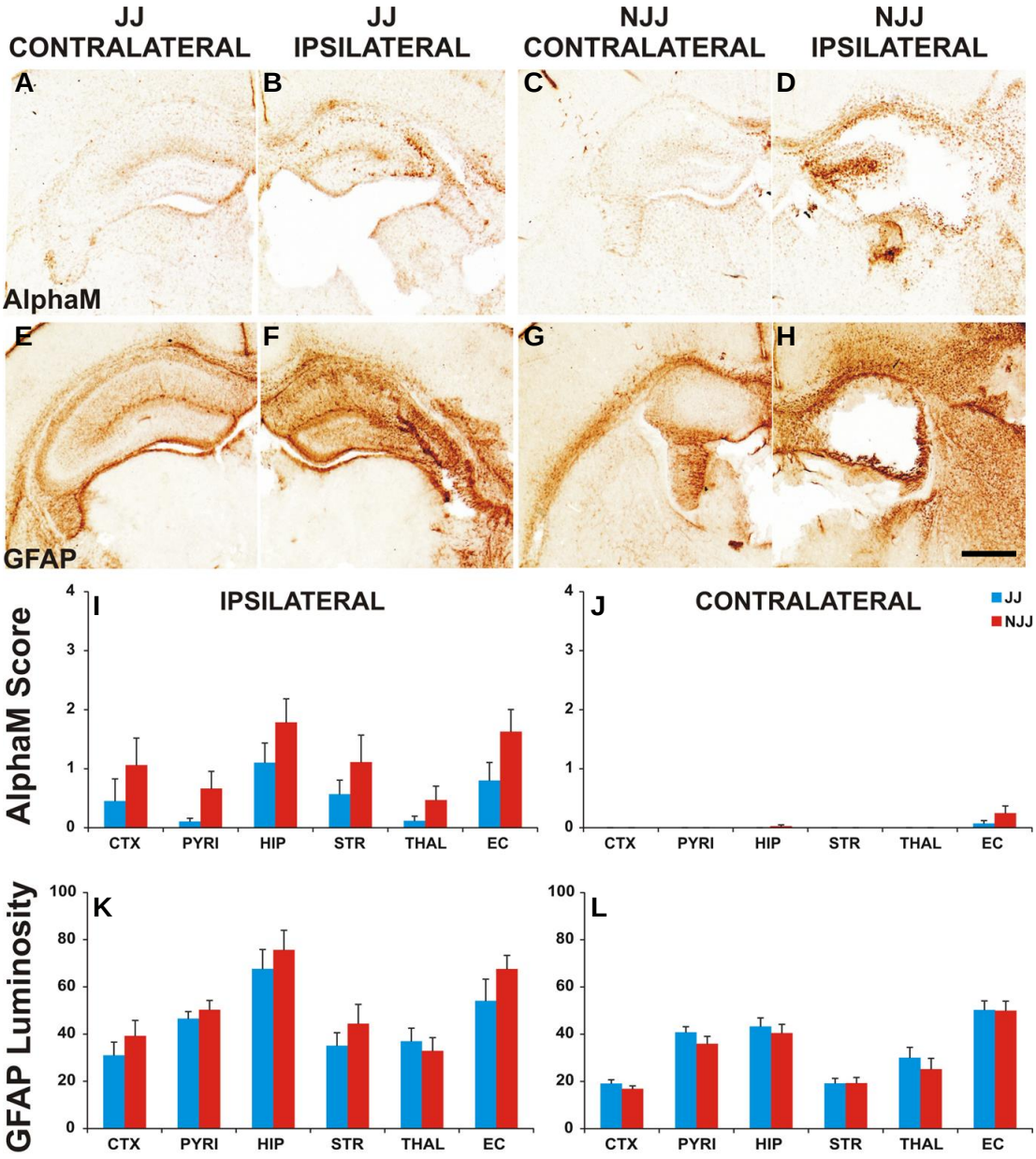

Figure 6.9 Neural C-Jun is responsible for some non-neuronal cell activation and recruitment after combined LPS and 30min HI insult. Microglial (A-D, I-J) and astrocyte (E-H,K-L) activation 2 days after insult in wild type (A-B, E-F) controls, and the NJJ (C-D, G-H) mutant mice on the contralateral side (1st and 3rd column, J,L) and on the ipsilateral side (2nd and 4th column, I, K) to carotid artery occlusion. After insult JJ mice showed a prominent increase in microglia and astrocyte activity. In NJJ mutants, this response is strongly increased in terms of active microglia (I), whilst astrocyte recruitment saw a much more modest rise (K). Scale bar indicates 0.5mm. Changes in damage markers were insignificant by T-test, with P>0.05.

Microglial activation occurred to a greater extent in all NJJ forebrain regions than seen in JJ littermates. Striatum (0.57±0.24, NJJ= 1.11±0.46), hippocampus (JJ= 1.1±0.33, NJJ= 1.78±0.40) and external capsule (JJ= 0.8±0.31, NJJ= 1.63±0.38) had the highest scores with a 35-51% increase. Pyriform cortex, whilst exhibiting a more modest level of αM immunoreactivity, gave the greatest difference between the groups with 84% higher score for NJJ than JJ animals (figure 6.9A-D and I). This nearly reached significance with P=0.07.

Compared to the contralateral intracranial control hemisphere, the number of GFAP positive cells, an indicator of active astrocytes and gliosis, recruited to the individual ipsilateral forebrain regions were higher by 27-50% (figure 6.8E-H). Between experiment groups, an increase although not significant, is seen within the external capsule (JJ= 54.08±9.19, NJJ= 67.54±5.80), striatum (JJ= 35.01±5.53, NJJ= 44.36±8.27), cortex (JJ= 30.99±5.58, NJJ= 39.16±6.61), and hippocampus (JJ= 67.61±8.17, NJJ= 75.64±8.30) (figure 6.8K).

Whilst intracellular damage is highly evident in transgenic mutants after LPS sensitised HI, little change was seen in infarct volume between cohorts. Total hemisphere volume loss was comparable between groups with a percentage of 13.71±4.60% in JJ mice and 18.41±4.79% in NJJ (figure 6.8M).

Nestin positive cells include neurons, glia and oligodendrocytes derived from neuroepithelia. C-Jun deletion within this collective group greatly aggravates sensitivity of the neonatal brain to hypoxic ischemic alone and in synergy to endotoxin. This suggests C-Jun to be a positive regulator of cellular response to HI injury.

Neuroepithelial Deletion of C-Jun- Discussion

JNK/MAPK, typically activate following stress stimuli including ischemia, is a major contributor to HI injury. In adult mouse models of focal cerebral ischemia, pJNK, and pERK but not P38, is rapidly upregulated (Herdegen et al., 1998) via the ASK1/MKK4 pathway (Zhang et al., 2003). Following oxidative stress, JNK phosphorylation of C-Jun induces cell death through upregulation of pro-apoptotic FasL, Bim and dp5 (Besirli and Johnson, 2003). Increased Bim expression further induces Bax-mediated CTC release from mitochondria, which in turn initiates the pro-apoptotic caspase cascade (Hambleton et al., 1996; Kuan et al., 2003). Additionally C-Jun/AP1 transcription activities will release pro-inflammatory cytokines via the actions of FADD and TRAF2 at TNF receptors (Deng et al., 2003b; Hidding et al., 2002; Huang et al., 2009).

Both adult and neonatal studies elucidate JNK inhibition to improve cellular damage, infarct volume, and neurological outcome. Whilst some studies attribute this to the suppression of JNK phosphorylation of C-Jun and subsequent AP1 activity (Dong et al., 2009; Guan et al., 2006; Herdegen et al., 1998; Kuan et al., 2003; Michiels et al., 2001; Mrsić-Pelcić et al., 2008; Nijboer et al., 2009; Pirianov et al., 2007), others have evidenced that JNK may be acting independent of downstream C-Jun phosphorylation (Guan et al., 2006; Nijboer et al., 2013; Zhao and Herdegen, 2009; Zhao et al., 2012) suggesting that the evidence tying upregulation of C-Jun to HI damage response is indirect. In order to establish C-Jun's contribution to neonatal HI, we utilised a mouse mutant of C-Jun excision in neuroepithelial lineage cells by nestin promoter driven cre recombinase.

Neuroepithelia derived cells in the CNS, targeted by nestin expression, include populations of neurons, astrocytes, oligodendrocytes (ODC), and Schwann cells (Kohno et al., 2006; Raivich et al., 2004; Vukojevic et al., 2010). Immunohistochemistry for phosphorylated C-Jun in C57/Bl6 wildtype mice saw bilateral neuronal expression with peak activity at 2hr following CROC and 30min exposure to 8% O_2. In nestin driven C-Jun mutant mice, pC-Jun immunoreactivity is fully ablated. Bilateral expression following insult corroborates with previous studies of neonatal HI (Dragunow et al., 1994; Dragunow et al., 1993; Ginet et al., 2009; Munell et al., 1994).

Double labelling of C-Jun with NG2, a marker of ODCs, and GFAP for astrocytes exhibited inhibition of pC-Jun within these cells in additional to neuronal response. Microglial expression remained unaffected as expected due to their mesodermal origin.

Nestin driven C-Jun deletion increases pro-death response to neonatal HI

Following mild HI injury to the P7 mouse pup, microglia activation was higher in both white matter and the majority of grey matter regions of ipsilateral C-Jun mutant forebrain when compared to wildtype littermates. On average, this increase was 34%. This response was validated by enhanced brain injury- 53%. The number of phagocytic microglia did not exceed those in the contralateral, hypoxia alone, regions. Tunel positive dying cells were only present in cortex, hippocampus, and striatum, the archetypical grey matter regions damaged in neonatal HI. Increased dying cell numbers were observed in all three regions within the mutant pups, with a significant difference of 63%, compared to control animals, in hippocampus.

Increasing severity of insult to 60min resulted in exacerbation of the deleterious effect of NJJ following mild HI. AlphaM immunoreactivity, histological brain injury and DNA fragmentation all exhibited significantly higher levels of expression in both white matter and all grey matter regions in C-Jun mutants. Microglial activation was increased, on average by 3fold, up to 5fold in cortex, with both brain injury score and Tunel positive cell death was 2fold higher in mutants. Phagocytic microglia still remained at low numbers, although with 60min HI; each region saw counts above baseline, with a 2fold increase in mutants than controls.

Detrimental cellular biochemical response to HI is evident with C-Jun deletion. On a tissue level neurodegeneration proved less clearly defined with only white matter and hippocampus seeing a change to infarct volume, an increase of 1.5-2.5fold, in the nestin: C-Jun cohort. All other regions were unchanged in lesion size.

Previous work by our group studied the effect of nestin driven C-Jun deletion in an adult mouse facial axotomy model. Here suppression of C-Jun resulted in several regenerative defects. Although cell survival increased following

axotomy, surviving motoneurons were atrophic. In addition, we observed reduced target muscle innervation and enhanced perineuronal sprouting, lymphocyte recruitment and microglial activation (Raivich et al., 2004). Together this suggests C-Jun to positively regulate neuronal response to injury.

Adult models of ischemic insult saw resistance to apoptotic cell death in mice null for JNK3 (Kuan et al., 2003). Equally, use of small peptide JNK inhibitors D-JNKi and L-JNKi reduced pC-Jun expression after neonatal HI. Suppression of the C-Jun/AP1 pathway was associated to reduction in pro-death proteases, calpain, caspase 3 and autophagosome formation (Benakis et al., 2012; Ginet et al., 2009; Guan et al., 2006; Nijboer et al., 2013; Repici et al., 2007; Zhao et al., 2012).

Contrary to this, our results indicate a strong neuroprotective effect of endogenous C-Jun expression within the collective of cells positive for nestin. Absence of strong infarct change suggests that C-Jun's involvement is part of a biochemical cascade culminating in delayed neuronal response to insult. In gerbil models of ischemic pre-condition to stroke, C-Jun was selectively phosphorylated in hippocampal CA1 neurons. Cells positive for C-Jun went on to survive both the initial ischemia and subsequent excitotoxic ischemic insult (Herdegen et al., 1997; Sommer et al., 1995).

Some in vitro studies have observed a neuroprotective function of C-Jun. Studies on transformed fibroblasts have shown C-Jun to inhibit TNFα induced apoptosis via P53/P21. P53 and its target gene, the CDK inhibitor P21 are upregulated in C-Jun$^{-/-}$ cells (Eferl et al., 2003). In a mouse model of liver cancer, C-Jun mediated cell survival occurs through a P53 independent manner. Here C-Fos induced apoptosis is suppressed via C-Jun activity at TRE 305 AP1 binding region of the C-Fos promoter. C-Fos induces SIRT6 transcription, which represses Survivin by reducing H3K9 acetylation and NF-κB activity (Min et al., 2012). Cleaved caspase 3 and Tunel positive cell death were both increased in the C-Jun deficient liver. Lastly, in vivo, fetal rat hippocampus tissue was transplanted into the excitotoxicity lesions induced in adult rat hippocampus and striatum. Fetal neurons exhibit upregulation of C-Jun up to 6months after grafting. Enhanced C-Jun activity associated to regeneration activity by grafted neurons (Aznar et al., 1995).

Equally, this effect may be developmental. By looking upstream to C-Jun, nestin driven deletion of MKK4, which together with MKK7 dual phosphorylated JNK, in mice gives rise to abnormal growth development and increased motor deficit. JNK phosphorylation was reduced by 80% in cortex, hippocampus and cerebellar of mutants, correlating to an equal reduction in pC-Jun expression, at P3 (Wang et al., 2007). Lastly, poor myelin production by ODCs was observed. Similarly, nestin MKK7$^{-/-}$ mice were undistinguishable from littermates during embryogenesis but died immediately after birth. Following dissection, defects in brain development were observed including ventriculomegaly, reduced striatal volume and disrupted axonal tracts (Yamasaki et al., 2011). Nestin C-Jun mutants do not exhibit any of these neuropathology or morbidity driven traits. Nonetheless increased neurodegenerative outcome following both peripheral and central neuronal insult suggests that in at least one of the nestin positive cell groups, if not a collective effect, requires the endogenous MKK4/MKK7/JNK/C-Jun pathway to be intact during development. This supposition is validated by the protective nature of D-JNKi inhibition of JNK activity. D-JNKi acts by preventing the JNK phosphorylation of its C-Jun N-terminal kinase binding domain (JBD) dependent targets. MKK4 and MKK7 are both JBD containing allowing JNK to autoregulate its own activity (Repici et al., 2009). Systemic administration of D-JNKi shows reduction of both MKK4/7 and C-Jun activity in adult rat cortical neurons with no ill effect. This suggests that aberrant brain morphology is due to an absence of C-Jun at development and not postnatal.

Together with the currently literature, our findings suggest that due to the detrimental nature of early developmental C-Jun deletion, the neuroprotective traits of JNK inhibition in postnatal HI are independent of C-Jun activity. Furthermore, that developmental C-Jun activity is required for optimal regulation of neuro- and glial-genesis, allowing for unencumbered cellular response to insult.

Pan CNS C-Jun deletion reduces neuronal survival following synergistic endotoxin-mediated HI

Nestin C-Jun mutants were subject to combined insult of LPS and 30min HI. Increase in damage response was observed to be comparable to that following

60min HI alone. Significant enhancement of suppressed C-Jun mediated neurodegeneration occurred in brain injury score of pyriform cortex and hippocampus. Pyriform cortex, hippocampus and striatum all showed elevated Tunel positive cell death in mutant mice, with a 1.5 to 4.5fold increase despite a lack of significance. Total ipsilateral hemisphere infarct volume was increased from 28%, up to 53% in pyriform.

Non-neuronal cell recruitment proved more modestly affected with an average increase of 60% of microglia activity across the mutant ipsilateral forebrain regions. Effect of suppressed C-Jun did not extend to GFAP positive astrocyte recruitment. Knockout of C-Jun in neuroepithelial lineage cells is still deleterious after neonatal mouse exposure to endotoxin sensitised HI. Where neuronal ERK deletion, in previous chapters, played a greater role in combined inflammation and HI insult response, C-Jun deletion saw greater significance with 60min exposure to HI alone.

While it is easy to assume that C-Jun does not regulate exogenous inflammatory response in the neonatal cerebral brain, this is a conclusion contradictory to current paradigms.

LPS dependant release of pro-inflammatory cytokine from microglia has been documented as mediated through C-Jun/AP1 upregulation of COX-2, TNFα and IL-6 expression (Arndt et al., 2004; Hambleton et al., 1996; Hidding et al., 2002; Liu et al., 2007). P2 rat pups subject to LPS and 90min HI saw white matter damage to associate to TNFα immunoreactivity. Suppression of TNFα occurred following systemic administration of ATP competitive JNK inhibitor AS601245. JNK inhibition resulted in significantly reduced microglial activation, IgG extravasation, and cleaved caspase-3 in the endothelial cells and ODC progenitors, and subsequent increase in myelin production (Wang et al., 2012b). Speculatively we could say that in our neonatal mouse model of LPS mediated HI insult, significant change between controls and mutants is prohibited due to the ability of neuroepithelial deletion of C-Jun to prevent LPS/inflammatory response becoming overwhelmed by its developmental-mediated injurious response to ischemic stress.

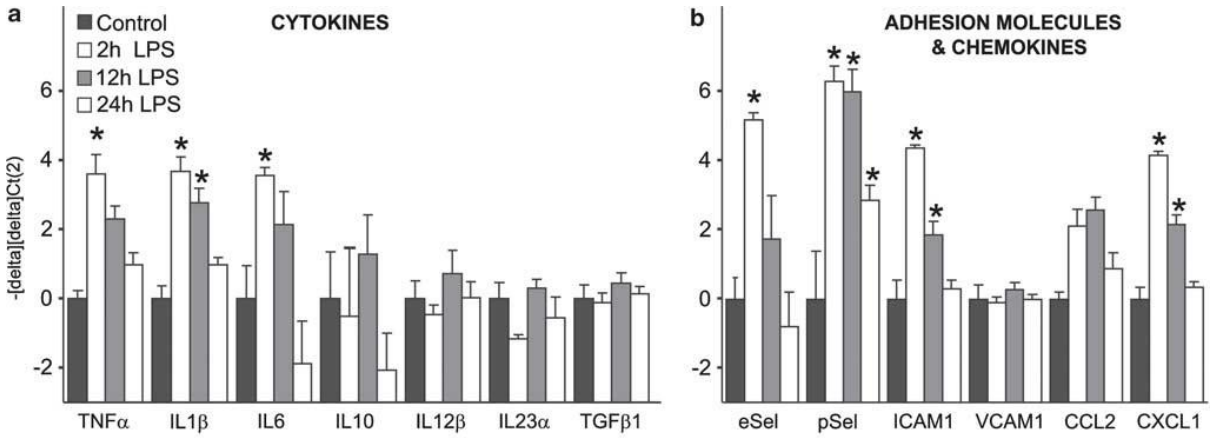

Figure 6.10 LPS-induced mRNA expression for cytokines, chemokines and adhesion molecules: regulation and cellular localization. (a, b) Taqman microarray detection of amplified forebrain cDNA for TNFα, interleukin 1β (IL1β), IL6, IL10, IL12β, IL23α and TGFβ1 (a), and E-Selectin (eSel), P-Selectin (pSel), ICAM1, VCAM1, CCL2 and CXCL1 (b), at different time intervals (2–24 h) following intraperitoneal injection of 0.3 mg/g LPS. Forebrain tissue from untreated mice was used as a control. (Kendall et al. 2012).

Previous work in our laboratory examined the time dependent increase in both cytokine and chemokine mRNA expression in response to LPS administration in the P7 mouse (Kendall et al., 2011a). In order to confirm whether C-Jun can influence LPS induced inflammation the same array could be repeated in the nestin: C-Jun mutant.

Specific deletion of C-Jun in neuroepithelial linage cells results in strong increase of cell death and microglial activation in grey matter regions following severe HI. AQ more discreet effect is observed in subcortical external capsule white matter. Trend to increase is similarly apparent with more moderate 30min insult, albeit to a lesser extent. This is suggestive that C-Jun positively regulates the cellular response to injury. In addition, embryonic expression of C-Jun is vital for optimal brain development. Abrogation of C-Jun at early stages, i.e. E7 for nestin driven cre excision of C-Jun, may account for greater sensitivity to postnatal insult. Despite current paradigms, neuroepithelial deletion of C-Jun does not significantly alter the detrimental effect of LPS sensitised HI.

Cell Specific Deletion of C-Jun- Results

We have shown that pan-CNS C-Jun plays a distinct role in HI injury response. What remains to be determined is the cell specific expression that contributes to the detrimental effects seen by nestin driven deletion. The principle experiments preceding this chapter show a pronounced effect of C-Jun deletion on both white and grey matter forebrain regions. In addition, we have confirmed that C-Jun is rapidly phosphorylated in both neurons and glia following 30min HI. Non-neuronal C-Jun activation was particularly marked in GFAP positive astrocytes and oligodendrocytes. This implies that both neuronal and glial C-Jun expression may contribute to the detrimental effect seen with nestin driven deletion. What remains unclear is whether it is the combined effect of cell specific expression or predominately one over the other that is responsible.

In order to validate the role of individual cell specific C-Jun expression on cell death and inflammation, transgenic mice carrying the neuron specific promoter synapsin coupled with cre recombinase (Syn-Cre) were bred with C-Jun$^{fl/fl}$ mice to produce, in the F2 generation, mice lacking C-Jun selectively in neurons- Syn-Cre: C-Jun$^{fl/fl}$ (SJJ) and C-Jun competent littermate controls- C-Jun$^{fl/fl}$ (JJ). GFAP driven cre (GFAP-Cre) recombinase as similarly used in order to elucidate the involvement of astrocytic C-Jun function.

Neuronal C-Jun contributes to neuronal damage following endotoxin-mediated hypoxia/ischemia

Twenty-two P6 transgenic mice for synapsin driven removal of C-Jun (SJJ, n=6) and their controls (JJ, n=16) were injected with 0.6µg/gBW LPS 12hr before 30min HI. The mice were returned to dams for recovery until 48hr post insult when they were sacrificed. Brains were perfused and processed as previously described.

Non-neuronal cell recruitment to the foci of injured neurons is an integral part of the immune response to infection and HI. Microglia and astrocytes activation in SJJ and JJ forebrain regions were evaluated by integrin αM and GFAP immunoreactivity (figure 7.1A-H). The previous chapter shows that Nestin driven C-Jun deletion resulted in a strong increase in glial activation. In contrast, mice with neuronal C-Jun deletion show a trend to decrease in both activated

microglia and astrocytes when compared to JJ animals. This was just not significant with student t-test P value >0.07.

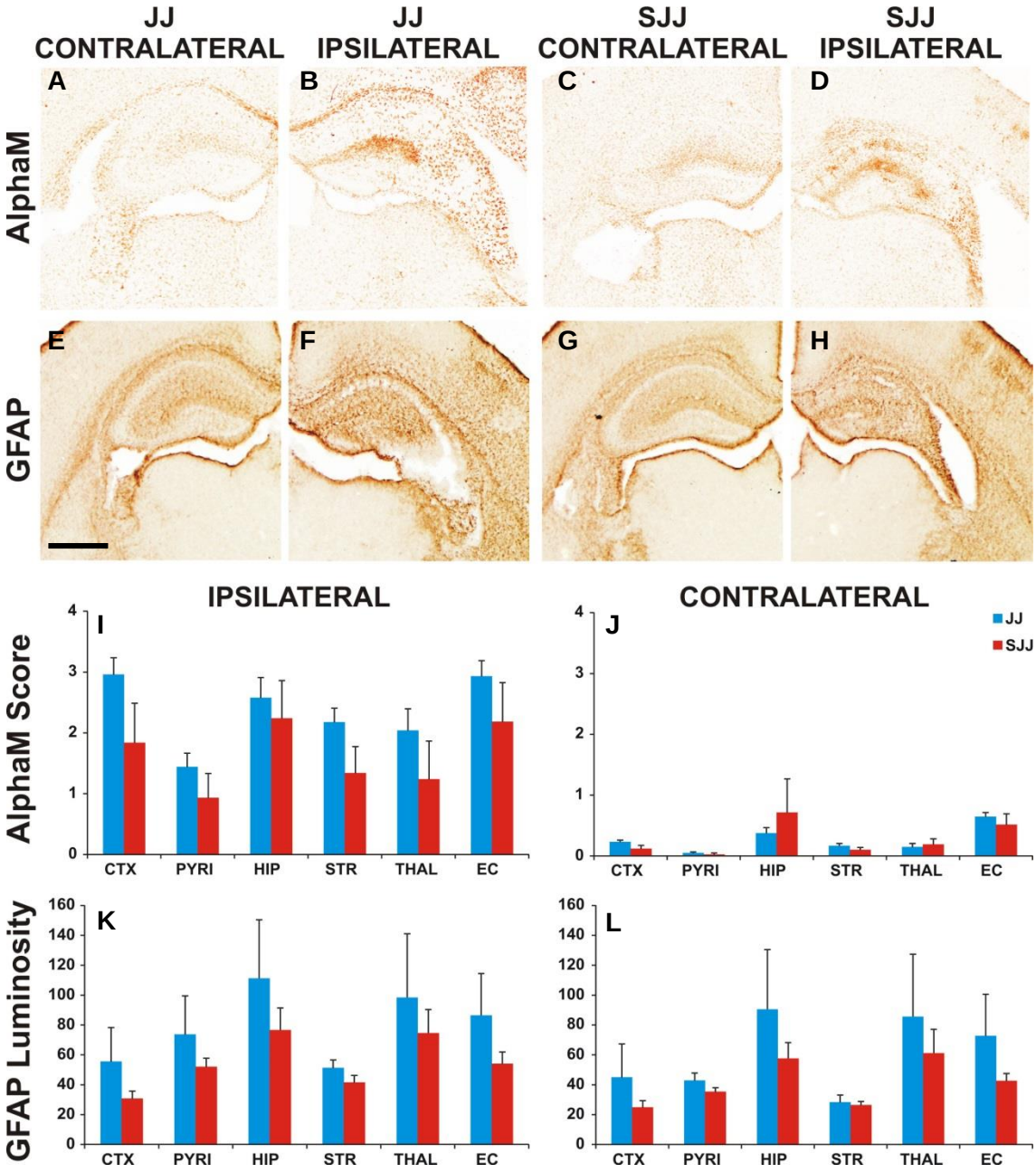

Figure 7.1 Neuronal C-Jun is required for non-neuronal cell activation and recruitment after combined LPS and 30min HI insult. Microglial (A-D, I-J) and astrocyte (E-H, K-L) activation 2 days after insult in JJ (A-B, E-F)) controls, and the SJJ (C-D, G-H) mutant mice on the contralateral side (1st and 3rd column, J, L) and on the ipsilateral side (2nd and 4th column, I. K) to carotid artery occlusion. After insult JJ mice showed a prominent increase in microglia and astrocyte activity. In SJJ mutants this response is decreased (I, K). Significance however was not reached. Analysis of forebrain regions for damage markers was performed at 20x magnification. Scale bar indicates 0.5mm. Regions include external capsule (EC), striatum (STR), pyriform cortex (PYR), cortex (CTX), hippocampus (HIP), and thalamus (THAL).

Striatum and cortex exhibit the greatest number of active microglia with a 40% reduction in SJJ compared to JJ (striatum: JJ= 2.18±0.23, SJJ= 1.34±0.44, cortex: JJ= 2.96±0.28, SJJ= 1.84±0.65) (figure 7.1I). Astrocytes were most

present in hippocampus (JJ= 111±39.25, SJJ= 76.54±14.82) whilst external capsule and cortex saw the greatest difference between cohorts with a 40-48% reduction in SJJ animals (figure 7.1K). Due to high variability within the JJ group this difference was insignificant ($p>0.1$).

Neuronal loss is quantified by a scoring system from 0 to 4, where zero is no damage and four is extensive tissue loss and nissl body formation. This is combined with αM immunoreactivity score to give a mean brain injury score. The ipsilateral forebrain exhibits a moderate reduction in endotoxin-sensitised HI damage in the SJJ hippocampus (49%) with significance of $p=0.03$, cortex (36%), and thalamus (51%), whilst striatum, external capsule saw a more modest reduction at 32% and 24% respectively (figure 7.2I). Pyriform remained unchanged between mutants and controls. Interestingly, the difference in contralateral hippocampus of mutant pups was highly significant with $p=0.002$ (figure 7.2J).

Cell loss is illustrated by the number of Tunel positive dying cells per region. In suit to microglial activation, striatum and cortex were most affected by injury with the greatest number of Tunel positive cells (striatum: JJ= 831.35±208.29, SJJ= 342.57±214.45, cortex: JJ= 536.72±178.56, SJJ= 119.53±73.79). SJJ cohort saw a diminution in dying cell numbers in all forebrain regions with significance reached within external capsule ($p=0.01$), cortex ($p=0.04$), and thalamus ($p=0.02$) (figure 7.2K). Interestingly this was more pronounced in the contralateral hemisphere with all regions bar pyriform cortex showing a significant reduction of Tunel positive cells within the SJJ group ($p=0.01$-0.05) (figure 7.2L). This suggests neuronal C-Jun aids in the regulation of developmental neuronal loss, a process integral in maintaining optimal cell interactions within the growing CNS.

What remains the same between nestin and synapsin driven deletion of C-Jun is the restriction of damage response to a cellular level and not to tissue. As with the NJJ transgenic mutants, no change was seen in the extent of infarct, either regionally or over the entire ipsilateral hemisphere, between SJJ and JJ controls.

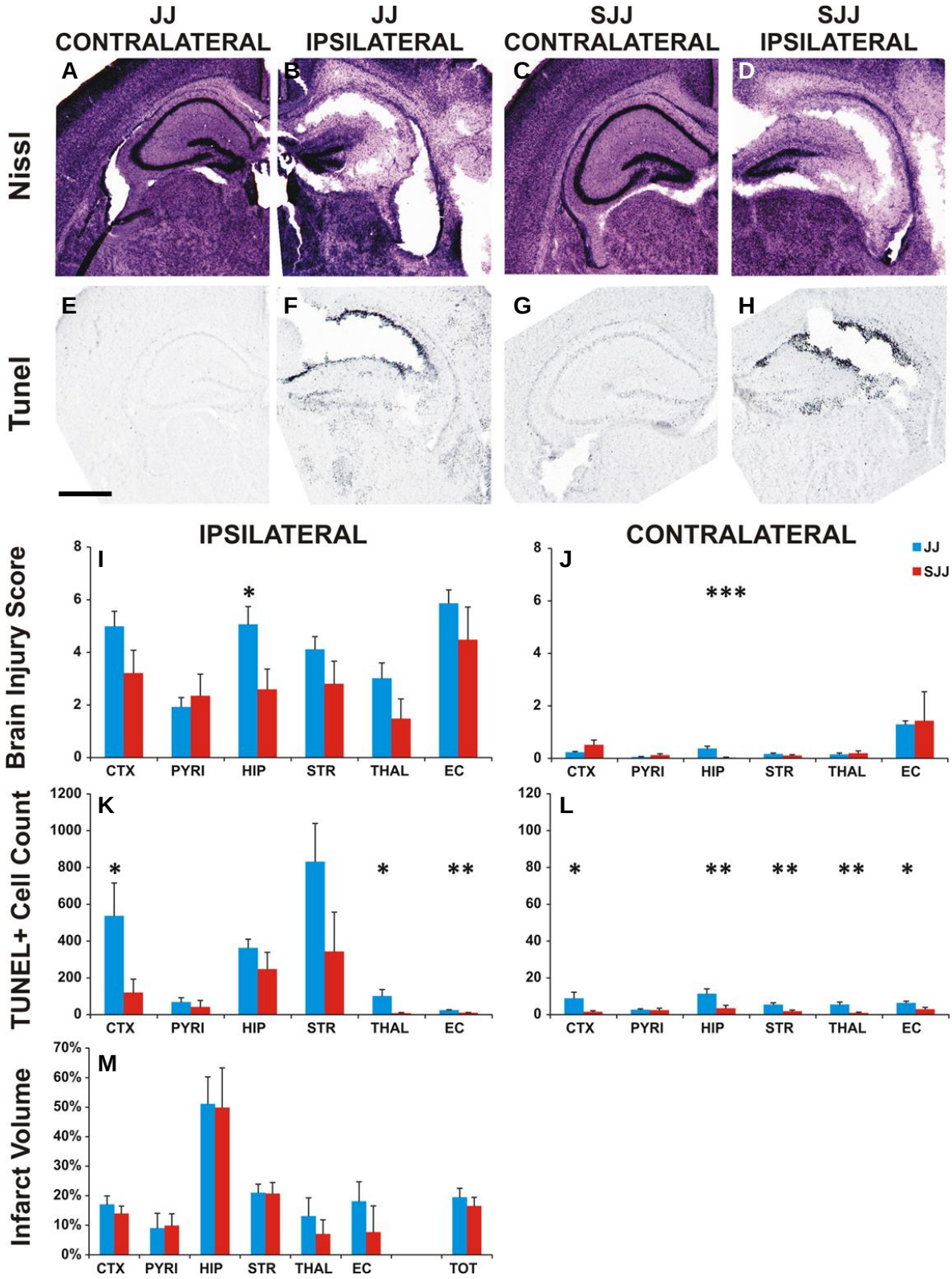

Figure 7.2 Quantification of Tunel+ dying cells, regional tissue loss and a combined score for microglia activation and cresyl violet histology, brain injury score, in JJ and SJJ transgenic mutant mice. SJJ (C-D, I) showed a significant decrease in brain injury. In addition they exhibited a strong reduction in the number of dying cells (G-H, K), counted over 3 fields at 20x magnification. The hemisphere contralateral to carotid occlusion a decrease in baseline cell death in the SJJ cohort (J, L). M: Infarct volume loss of each forebrain region. Loss was assessed measuring the areas of intact cresyl violet staining, bilaterally for each forebrain region, and calculating the ipsilateral regions as percentages of the contralateral (uninjured) hemisphere. No change in volume size was observed between groups. Scale bar indicates 0.5mm. *P<0.05, **P<0.01 by student T-test.

Astrocytic expression of C-Jun has no contribution to neonatal brain response to damage from combined inflammation and HI nor HI alone

Astrocyte specific activation of C-Jun has been associated to neuroprotection via the upregulation of 14-3-3-γ under ischemic conditions in vitro. 14-3-3-γ, a member of the 14-3-3 acidic proteins, binds to p-122 Bad, preventing pro-apoptotic bad from entering mitochondria (Dong et al., 2009). Conversely, Ca^{2+} influx induces glial fibrillary acidic protein (GFAP) upregulation, and subsequent gliosis, in a JNK/C-Jun/AP1 dependent manner (Gao et al., 2013). Together with our own data that indicates rapid C-Jun upregulation in astrocytes following HI, these studies beg the question whether C-Jun expression in astrocytes is required for neonatal brain protection against insult.

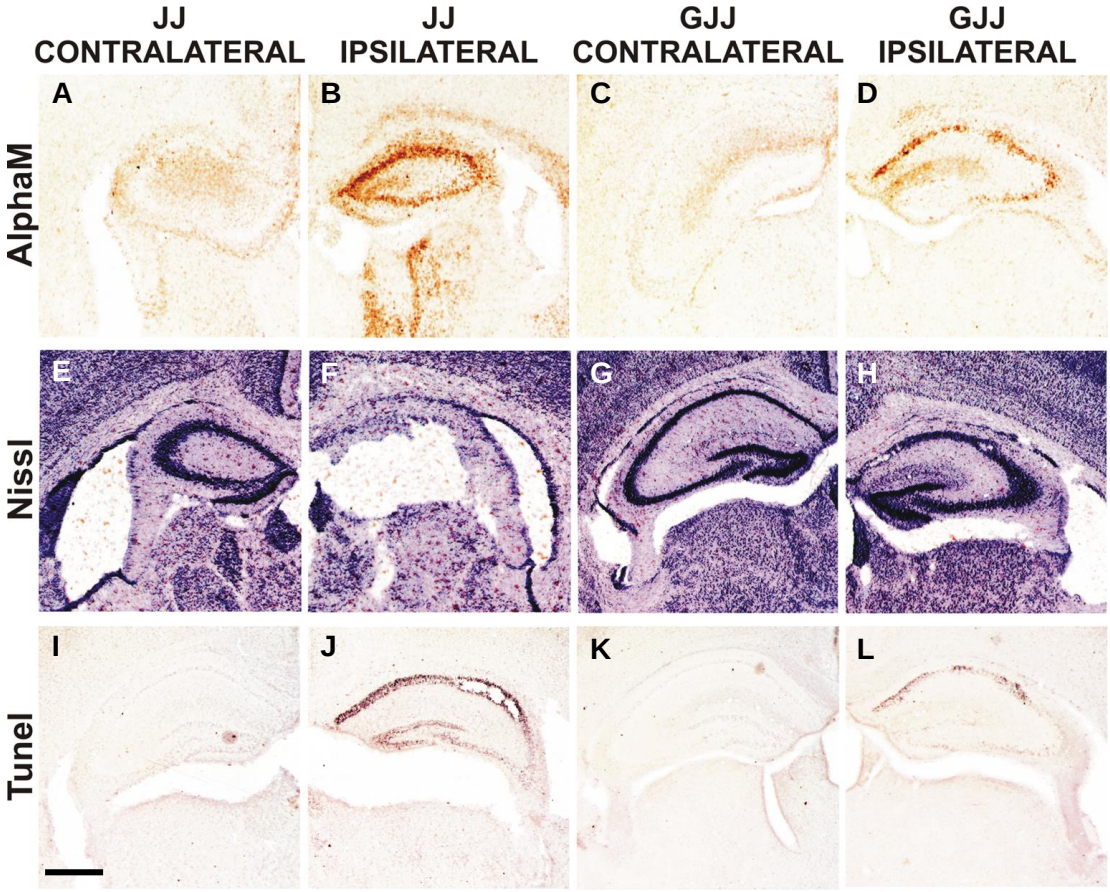

Figure 7.3 Illustrative response of both contralateral (1st and 3rd column) and ipsilateral (2nd and 4th column) hemisphere of P7 mice subject to 60min HI. Transgenic mutant mice with astrocyte specific homozygous deletion of C-Jun (GJJ), using GFAP-driven cre recombinase, were compared to C-Jun competent (JJ) littermate controls. Forebrain sections were analysed for microglia activation (A-D), neuronal loss (E-H), and Tunel+ cell death (M-P). Regions of interest included external capsule (EC), striatum (STR), pyriform cortex (PYR), cortex (CTX), hippocampus (HIP), and thalamus (THAL).Analysis was performed at 20x eye field. Scale bar indicates 0.5mm.

Cre recombinase under the GFAP promoter allowed excision of C-Junfl/fl specifically in astrocytes (GJJ), whilst allowing all other CNS cell types to

express wild type C-Jun. Homozygous astrocyte C-Jun deletion was assessed after both severe HI exposure and LPS sensitised HI.

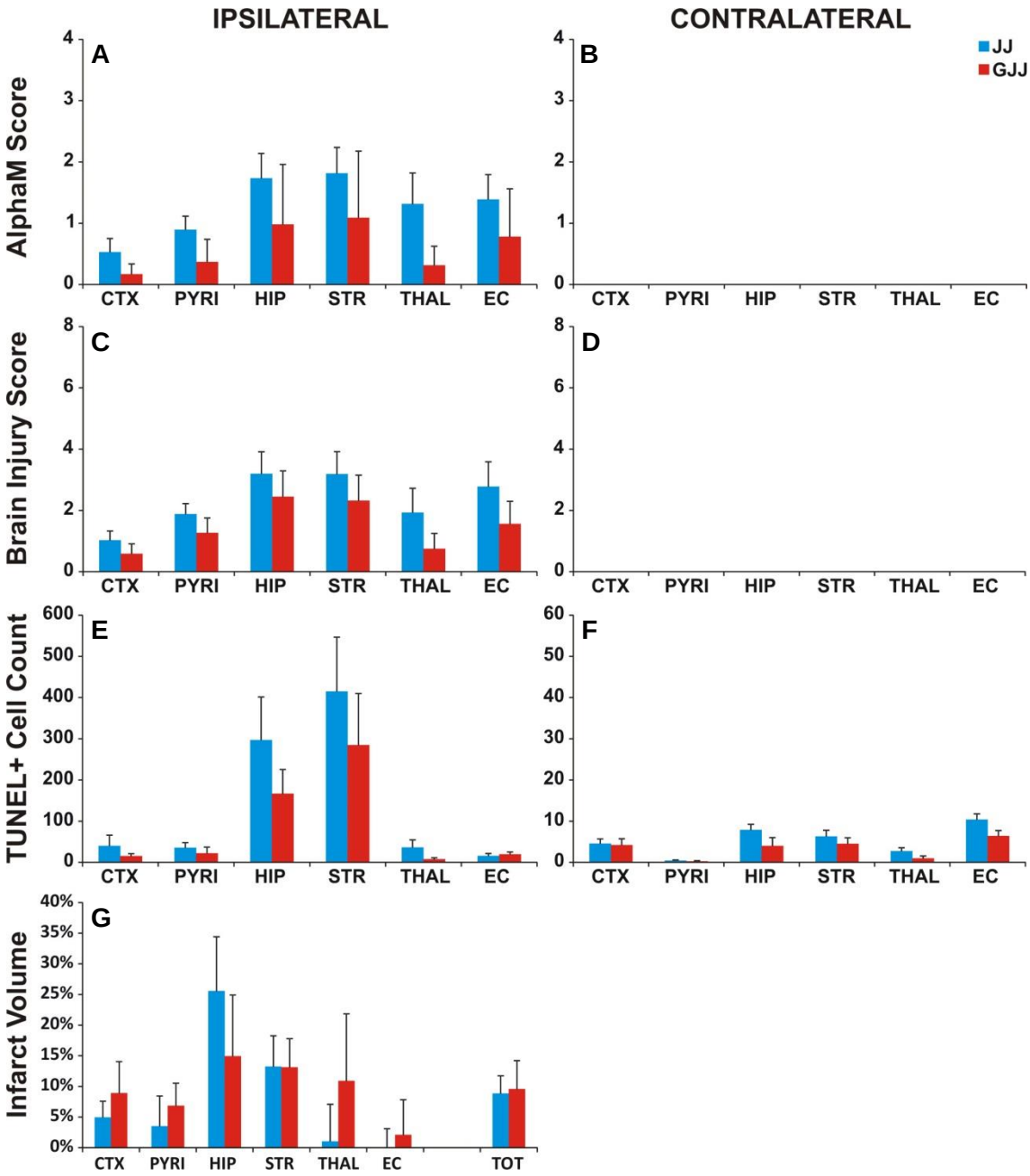

Figure 7.4 Transgenic mutant mice were created to astrocyte selective deletion of C-Jun to wild type expression in severe hypoxic-ischemic injury to the neonatal mouse brain Forebrain sections were analysed for microglia activation (A-B), brain injury (C-D), Tunel+ cell death (E-F) and the extend of infarction (G). A: microglia activation is modestly decreased in the presence of glial C-Jun deletion (GJJ). Trend to reduced damage in mutants was observed by brain injury score and in the number of Tunel positive dying cells (C-D, E-F), but no change was observed between groups in terms of volume of tissue lost by infarct. Analysis by mean±SEM, *P<0.05, **P<0.01 by student T-test.

Mutant mice were compared to non-cre expressing C-Junfl/fl (JJ) littermate controls. Nine JJ controls and eight GJJ transgenic mutant P7 mice underwent left carotid artery occlusion followed by 60min hypoxia. Animals were returned

to dams for 48hr when sacrificed. The brains were perfused, processed, and analysed as previously described.

Microglial, indicated by αM immunoreactivity (figure 7.3A-D), were more active following HI than witnessed with hypoxia alone (hemisphere contralateral to carotid occlusion). When the individual forebrain regions were assessed, a mild trend towards decreased microglia activation was observed in GJJ animals than seen in JJ controls. Striatum was most sensitive to insult (JJ=1.82±0.42, GJJ=1.09±0.41) whereas it is the thalamus that sees the greatest reduction, by 77%, between the groups (JJ= 1.32±0.51, GJJ= 0.31±0.25) (figure 7.4A). However significance by student t-test was not achieved, P>0.09.

Analysis of brain injury, by the presence of activated microglia, nissl bodies and structural tissue damage; Tunel positive cell death; and infarct volume soon elucidated no change in damage response between JJ and GJJ cohorts (figure 7.3E-L). Both JJ and GJJ mice expressed low scores of brain injury with an average score of 2.33±0.61 in controls and 1.49±0.62 in mutants (figure 7.4C).

Dying cells were predominately seen within the ipsilateral striatum and hippocampus, with a decrease in numbers observed in GJJ animals, 30% and 45% respectively, than in JJ littermates (figure 7.4E). However, this was insignificantly so, P>0.3. Furthermore, the extent of infarction remained both unchanged and low percentage between groups, with total loss, over the ipsilateral hemisphere; being 8.83±2.89% for JJ animals and 9.55±4.64% for GJJ (figure 7.4G).

In endotoxin-sensitised HI, astrocyte recruitment has a potential role in immune response to CNS infection via the release of pro-inflammatory IL-1 and the JNK dependent degradation of connexion 43, a vital component of gap junctions that maintain the integrity of the blood brain barrier. Using the same breeding sets as the preceding experiment, fifteen P6 mouse pups were subject to an IP injection of 0.6μg/gBW LP, followed 12hr later by left carotid occlusion and 30min hypoxia. Sacrifice was at 48hr post hypoxia.

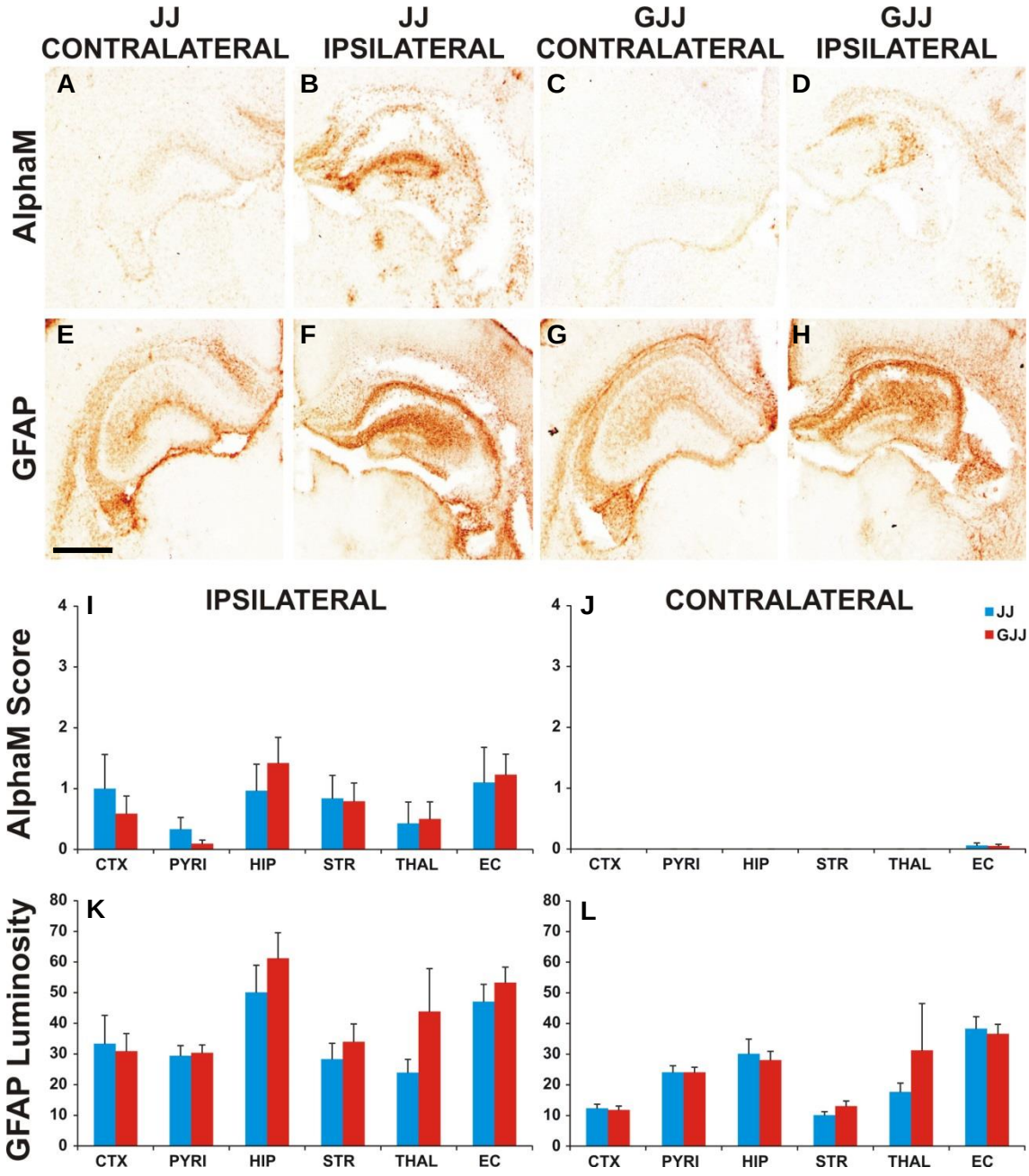

Figure 7.5 Effect of 0.6μg/gbw LPS 12hr prior to 30min hypoxia exposure to P6 mutant mice with astrocyte deletion of C-Jun compared to wild type C-Jun expressing littermates. At 48hr post insult, the animals were assessed for microglia (AlphaM, A-D, and I-J) and astrocyte (GFAP, E-H, and K-L) activation. Both non-neuronal cells were observed more active in the ipsilateral hemisphere (I, K) compared to contralateral with no difference in immunoreactivity between groups. Scale bar indicates 0.5mm.

PCR revealed the genotypes to be 7x JJ controls and 8x GJJ mutants. The forebrain regions: external capsule; striatum; pyriform cortex; cortex; hippocampus and thalamus were assessed for damage markers.

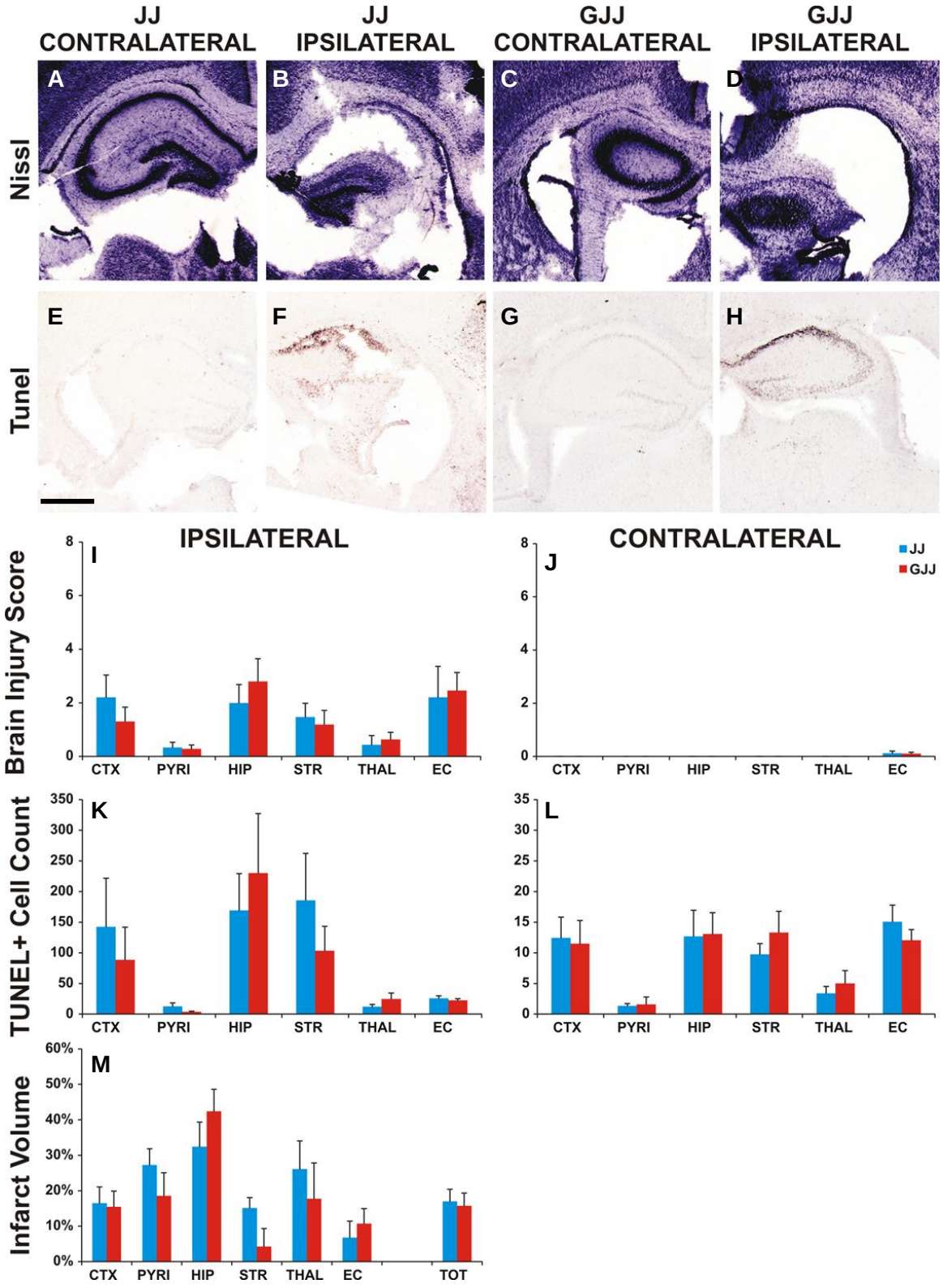

Figure 7.6 Quantification of Tunel+ dying cells, regional tissue loss and a combined score for microglia activation and cresyl violet histology, indicating the extent of neuronal loss (brain injury score), in JJ and GJJ transgenic mutant mice following LPS-sensitised HI. GJJ showed no change in all damage markers for cell loss when compared to littermate controls. Scale bar indicates 0.5mm.

Astrocytic deletion of C-Jun gives no clear difference, when compared to controls, in the cellular response to LPS and HI combined. Unlike 60min HI,

where a modest decline in microglia activation was observed in GJJ animals, there was no change in αM immunoreactivity after LPS plus 30min HI with an overall average score of 0.78±0.42 for the controls and 0.77±0.28 (figure 7.5A-D, I) in the transgenic mutants. Equally, astrocyte activation in the ipsilateral hemisphere had no difference between JJ and GJJ littermates (figure 7.5E-H, K). The overall average value for GFAP luminosity in JJ was 35.33±6.13, and 42.26±6.94 in GJJ.

Neuronal loss and Tunel positive cell death were strongly elevated in the ipsilateral hemispheres of both groups than the intracranial contralateral control hemisphere (figure 7.6A-D and E-H). From this, it was evident that striatum, cortex and hippocampus were the most effected regions. However, like with microglia activation, there was no significantly discernable difference between groups ($p>0.39$) (figure 7.6I and K). Infarct volume was equally unaffected by deletion of C-Jun in astrocytes (figure 7.6M).

Nestin positive cells include neurons, astroglia and oligodendrocytes, derived from mesenchymal neuroepithelial. Deletion of C-Jun within this group of cells has led to a strongly increased sensitivity to hypoxia/ischemic insult and endotoxin synergistic HI. This chapter aimed to separate the individual cell specific expression of C-Jun in order to understand which of the nestin positive cell types contribute to the increased damage seen. Interestingly neither synapsin positive neurons nor GFAP positive astrocytes contribute to the deleterious effects seen with nestin. Indeed neuronal specific C-Jun deletion proved modestly neuroprotective whilst astrocytic deletion played no role in injury response. It remains to be seen whether C-Jun deletion in oligodendrocytes would shed light on whether detriment is due to their selective C-Jun dependent response alone or whether it is the combination of all three cell types that is required.

Cell Specific Deletion of C-Jun- Discussion

Nestin driven C-Jun deletion resulted in an exacerbation of HI and LPS sensitised HI induced neuronal damage in the neonatal mouse cerebral brain. In order to delineate the specific cells responsible for this neurodegenerative activity, we introduced C-Jun excision in neurons, using synapsin driven cre recombinase, or astrocytes, GFAP driven cre recombinase. In preliminary experiments we observed that with mild HI both neurons and astrocytes saw high levels of co-expression following insult.

Neuronal C-Jun mutants and their wildtype littermate controls were subject to combined insult of LPS and 30min 8% O_2 exposure. The effects of HI alone could not be examined due to a non-genotypic high morbidity rate, 66%, when exposed to between 30-60min HI. Unlike reduced survivability observed with neuronal ERK2 deletion, these pups died during hypoxia and not due to infanticide by the dams. As these experiments were conducted in parallel to others involving multiple genotypes, and similarly bred on the C57/Bl6 background, the cause of these deaths are less likely to neither be due to errors in surgery or hypoxia calibration nor strain dependant, although these cannot be fully excluded.

Neuronal C-Jun deletion can partially recover neuronal death following endotoxin sensitised HI

Synapsin driven excision of C-Jun results in a bilateral decrease in tissue loss following histological assessment. Ipsilateral hippocampus and thalamus saw a 50% reduction in brain injury with a mean decrease of 28% across all forebrain regions. Contralateral hippocampus was similarly affected with 10% less tissue loss in mutant mice than controls. Pattern of response was similarly reflected, to a higher degree, in Tunel immunoreactivity. On average ipsilateral forebrain regions contained 4fold less dying cells in mutants. Contralaterally, the difference between groups was similar with an average of 3.6fold reduction. Reduction in histological tissue loss and cell death did not give strong suppression of lesion formation. Measurements of infarct volume saw a modest 10-20% reduction in most regions bar hippocampus where a strong 50% decrease was observed.

Recruitment of non-neuronal cells, including microglia and astrocytes is a key factor in cerebral brain reaction to ischemic insult. Often activation of these cells pre-empt lesion formation by localising to regions of injured neurons. 48hr post-injury, C-Jun mutants saw a 30% reduction in the number of active microglia and astrocytes in regions ipsilateral to carotid occlusion. Difference in cohort αM immunoreactivity was just insignificant, $p>0.07$. Although microglial activity was unchanged in contralateral regions, GFAP positive astrocytes were similarly reduced, at 29%, to that seen ipsilateral.

Neuronal C-Jun deletion presents a strong, if not clearly significant, reduction in injury response to combined infection/HI insult, to a similar degree to that seen in other studies that utilise JNK inhibitors or mutations.

All 3 isoforms of JNK are present in the developing mouse brain, JNK3 near exclusively so, where they are able to phosphorylate C-Jun. Transgenic deletion of JNK3 gave rise to a 2fold decrease in the number of mice without infarct lesions following cerebral ischemia (Kuan et al., 2003) whereas assessment of JNK2 mutants saw no change compared to controls. HI insult in neonatal $JNK3^{-/-}$ mice resulted in attenuation of pC-Jun and ATF2 activity that correlated to reduced cleaved caspase3, Bim/PUMA expression, and a 42% mean decrease in tissue loss (Pirianov et al., 2007). A different adult study saw an opposing effect where JNK1 deletion resulted in a 50% increase in cortical cell death, JNK2 deletion was mildly neuroprotective and JNK3 deletion had no effect. In addition combined JNK2 and 3 deletion enhanced the neuroprotective role of suppressed JNK2, however this was insignificantly so (Brecht et al., 2005). That JNK can exhibit differing reactions to ischemia suggests that activation of each specific form is a key factor in directing C-Jun to a pro-survival or pro-apoptotic state.

Small peptide inhibitors including D-JNKi target all three isoforms by competitively preventing JNK binding the scaffold protein JIP1 (JNK-interacting protein), a complex required for JNK interactions with both upstream and downstream JBD (C-Jun N-terminus kinase binding domain) via the linking the 20aa terminal JBD of JIP1/IB1 to a 10aa HIV–TAT transporter sequence (Nijboer et al., 2013; Vivès et al., 1997; Wang et al., 2003a). D-JNKi has been effective in showing strong neuroprotection against FCI in adult mice and

adolescence rats (Borsello et al., 2003; Guan et al., 2006; Repici et al., 2007). In the neonatal P7 rat however, it has had been demonstrated to have limited effect in a manner replicated in our results. Repeated IP injection following 2hr exposure to 8% O_2 saw a reduction in cleaved caspase3, calpain and neuronal autophagy but no change to infarct. This indicates that JNK, in this model, is also acting on a biochemical but not tissue level.

Administration of D-JNKi, and its counterpart L-JNKi, clearly exhibited a suppression of nuclear translocation of pC-Jun and downstream AP-1 activation. Despite this, there exist a growing number of studies indicating inhibition of JNK produces a strong neuroprotective effect independent of C-Jun. Systemic L-JNKI treatment immediately following 120min HI, in P7 rats, resulted in suppression of nuclear AP1 cleavage of caspase3 and a 30% reduction of infarct. Conversely upstream mediators of apoptosis, caspase 8 and 9, Bid and mitochondrial CTC release, in addition to cytokine production remained unaffected (Nijboer et al., 2010).

Using the more stable retro-inverse form- D-JNKi, the same group saw that treatment inhibited phosphorylation of nuclear C-Jun and AP1 activity in conjunction with reduced production of TNFα, IL-1β, CINC-1 and MIP2 cytokines/chemokines by 24 h post insult. While it was expected that this was the pathway responsible for neuroprotection of D-JNKi, using a specific mitochondrial scaffold protein (SAB) based JNK inhibitor- SAB_{KIM1} equally protected cerebral brain from HI injury by prevention of JNK induced BIM/PUMA mediated pro-apoptotic events whilst suppressing Bcl-2 anti-apoptotic events at the outer membrane (Nijboer et al., 2013; Zhao et al., 2012).

That HI in the neonate can instigate both C-Jun dependent and independent apoptotic pathways of JNK activity, explains why neuronal deletion of C-Jun is only partially protective in our studies.

C-Jun null mice are embryonically lethal at E10.5 due to malformation of heart septum and incomplete separation of aorta and pulmonary artery in addition to severe liver abnormalities (Eferl et al., 1999). In addition, early developmental deletions of MKK4 and 7 resulted in postnatal growth and brain abnormalities and early morbidity (Wang et al., 2007; Yamasaki et al., 2011). Where nestin

expression occurs early in embryogenesis, E7.5, synapsin is not apparent until E12. As such, C-Jun deletion under the synapsin promoter is less affected by developmental contributions to sensitivity to HI seen in nestin C-Jun mutants.

Glial deletion of C-Jun provides mild protection against HI induced cell damage

With exposure to 60mn HI alone, astrocytic C-Jun mutants, where C-Jun is excised by GFAP driven cre recombinase, saw minor reduction in damage response compared to wildtype littermate controls.

Microglial activation, illustrated by αM immunoreactivity, initially exhibits an overall mean decrease of 55%. Significance was not reached due to high variability within each group. When taken into account, diminished αM expression in hippocampus differs from controls by only 5%. Brain injury and Tunel positive cell death showed a more stable reduction of 38% less tissue loss and dying cells in mutants. Similar to neuronal C-Jun mutants, Infarct volume remained unchanged between groups.

Any neuroprotection by inhibiting astrocyte C-Jun activity did not extend to a response to combined LPS and HI insult. Neither levels of non-neuronal cell recruitment, nor cell death markers were changed between cohorts.

How C-Jun expression in astrocytes could mediate neurodegeneration following HI injury remains poorly understood amongst current literary studies. Tentatively, we can say that prevention of endogenous inflammatory response to ischemia, shown to exacerbate secondary energy failure and induce death receptor mediated apoptosis, is the root of neuronal survival observed in astrocyte C-Jun mutants after HI injury. Active microglia and astrocytes, following cerebral injury, are the main source for CNS derived cytokine/chemokines that include TNFα, IL-1β, IL-6, IL-8, and COX-2 (Bohatschek et al., 2004; Chock and Giffard, 2005; Gorina et al., 2011; Hidding et al., 2002). Cytokine release from astrocytes is mediated through Fas as part of the intrinsic cell death pathway. Binding of Fas at death receptor will result in caspase 8 cleaving of pro-apoptotic caspases, and Bid activation that stimulates CTC release from mitochondria. Mutations in Fas and FasL correlated to reduced pJNK activity and subsequent cytokine release (Niu et al., 2012). In HEK293 cells, FasL is able to act directly on AP-1 promoting IL-8 upregulation.

Using a dominant negative form of C-Jun, IL-8 and caspase 8 activity was ablated in a similar fashion to NF-κB inhibition (Matsumoto et al., 2007). Cyclooxygenase 2 (COX-2), whose peroxidase activity results in the formation of free radicals, mRNA expression in astrocytes is nullified on inhibition of JNK (Gorina et al., 2011).

Lastly, in adult male mice undergoing transient MCAO, the chemokine KC/CXCL1 (keratinocyte derived chemokine) is strongly upregulated in areas of infarct at 4-7hr following ischemia. KC/CXCL1 is a mouse ortholog of IL-8 found principally in astrocytes. Its production is dependent on TNFα activation of C-Jun/AP1 but not JNK (Benakis et al., 2012). In contrast, in vitro studies of newborn mouse astrocytes indicate that, after ischemia, C-Jun/AP1 activity results in upregulation of 14-3-3-γ. 14-3-3-γ was protective against astrocyte cell death by forming complexes with P112-Bad, averting Bads entry into mitochondria and ensuing CTC release (Dong et al., 2009).

It is clear that future work is required to disassemble the cell-cell interactions between astrocytes and neurons following neonatal hypoxic-ischemic insult. While C-Jun deletion may reduce endogenous inflammatory response to injury, it had no effect on LPS mediated inflammation, synergistic to HI. As such we cannot discount the possibility that neuroprotection from astrocyte C-Jun deletion is via indirect pathways.

Alternative mechanisms: Role of oligodendrocyte C-Jun expression in neonatal HI

Improved outcome following HI in both neuronal and astrocytic mutants for C-Jun imply that neither cell type is responsible for the degenerative response observed in nestin C-Jun deletion. Oligodendrocytes (ODC) are the third and final group of cells derived from neuroepithelia. At this current point in time, we are unable to examine how ODC specific C-Jun may contribute to HI-induced cerebral damage in the neonate.

Within scientific literature, there is evidence that ODC C-Jun inactivation would be detrimental to neuronal survival following insult, similar to that seen in our original nestin driven C-Jun deletion studies. ODC are the myelin producing cells of the CNS, with Schwann cells being their functional counterpart in the

PNS (Fan et al., 2010; Kaur and Ling, 2009; Pirianov et al., 2006b; van Velthoven et al., 2010). They are shown have increased sensitivity to ischemic insult. (Alderliesten et al., 2011; Almeida et al., 2005; Arai and Lo, 2010; Bartha et al., 2006; Canals et al., 2003; Chu et al., 2004; Derrick et al., 2004; Hagberg et al., 2002a; Heinz and Provenzale, 2009; Lesuisse and Martin, 2002; Northington, 2006; Zatorre et al., 2012). Reduction in myelin production increases neuronal sensitivity to damage by increased exposure to extracellular cytotoxins in addition to abnormal action potential potentiation.

In collaboration with Axel Behrens laboratory, our group have shown that specific C-Jun deletion in Schwann cells resulted in increased motoneuron cell death, poor functional recovery, and re-innervation of muscle targets after facial nerve axotomy (Fontana et al., 2012). More recently, ERK1/2 and JNK activity have been associated to ODC precursor proliferation, maturation and regulation of myelin formation. In ODC cells isolated from sprague-dawley rats JNK activity rapidly increase immediate-early gene (IEG) mediated proliferation via upregulation of C-Jun, C-Fos, and C-Myc. Application of the JNK inhibitor SP600125 nullified IEG production, delaying proliferation and maturation of ODC (Zhang et al., 2014).

Conversely, in a model of LPS sensitised HI in the pre-term brain, P2 rat pups exhibited reduced ODC apoptosis and increased myelin basic protein immunoreactivity following JNK inhibition (Wang et al., 2012b). As such, simply by eliminating neuronal and astrocyte involvement, we cannot confirm that ODC are the source of neurodegenerative actions by nestin C-Jun mutation. Future work is required to look at selective excision form ODC under the NG2 promoter driven cre recombinase.

Functional mutation of C-Jun phosphorylation - Results

The previous experiments have clearly delineated a duality in neuroprotection following HI due to cell selectivity of C-Jun expression. Pan-brain C-Jun deletion gave high susceptibility to HI across the forebrain regions, whereas neuron-specific deletion was significantly protective. However neither give indication to the molecular mechanism underlying C-Jun activation to produce these results.

C-Jun interactions occur at three specific sites. Firstly by JNK1-3 phosphorylation at N-terminal ser63 and 73 and thr91 and 93. Secondly, dephosphorylation of thr239, resulting in C-Jun ubiquitination by FBW7 ubiquitin ligase and subsequent deactivation. Lastly, C-terminal lysine acetylation near aa257-276 by P300- leading to deactivation, or by ERK-resulting in activation (Raivich, 2008; Vries et al., 2001; Wang et al., 2006).

Multiple studies show JNK to phosphorylate C-Jun, and consequentially upregulated AP1-induced gene transcription, immediately following hypoxia/ischemia in neonatal animal models. Others, using JIP-1 derived JNK inhibitory peptide D-JNKi, have revealed that following exposure to 10% O_2, MKK4 and 7 (upstream activators of JNK) and C-Jun activity are equally unaffected in both treated and untreated mice (Ginet et al., 2009). This suggests that C-Jun activation can still occur in this model via a JNK independent pathway.

Global C-Jun null mice are embryonically lethal at E10.5-15.5. However, JNK dependent C-Jun activation following neuronal injury is still demonstrable by functional knock out of some or all of its N-terminal phosphorylation sites. JunAA mutant mice have a removal of serine 63 and 73 phosphorylation by conversion of serine to alanine. JunAA mice are viable with no developmental deficits albeit slightly diminutive compared to wild types (Ruff et al., 2012). In kainite-induced excitotoxicity, JunAA mice had a greater neuronal survival of dopaminergic cells than wild types. This level of protection was on par to that seen in $JNK3^{-/-}$ mice. In addition, trophic factor deprivation and DNA damage incited neuronal death were significantly delayed (Brecht et al., 2005; Hidding et al., 2002).

This laboratory has established that prevention of C-Jun phosphorylation, by mouse mutants with global JNK 1, 2, or 3 deletions, or JunAA had a mild effect on peripheral nerve regeneration following facial nerve axotomy (Ruff et al., 2012). Based on this one may postulate that removal of all four activating N-terminal phosphorylation sites will enhance neuroprotection in the neonatal HI model of brain injury. Jun4A mice (Behrens, UK) contain substitution mutations of serine 63 and 73, and also threonine 91 and 93, into alanine. These exchanges to alanine prevent JNK/C-Jun interactions and thus prevent activation of C-Jun via phosphorylation.

N-terminal phosphorylation of C-Jun is ineffective in neuroprotection following HI

The following study utilises heterozygous breeding of Jun4A mice in order to produce homozygous Jun4A mutants and wild type littermate controls. Genotype was verified by PCR where Jun4A gave positive band at 248bp and the wild type allele at 198bp.

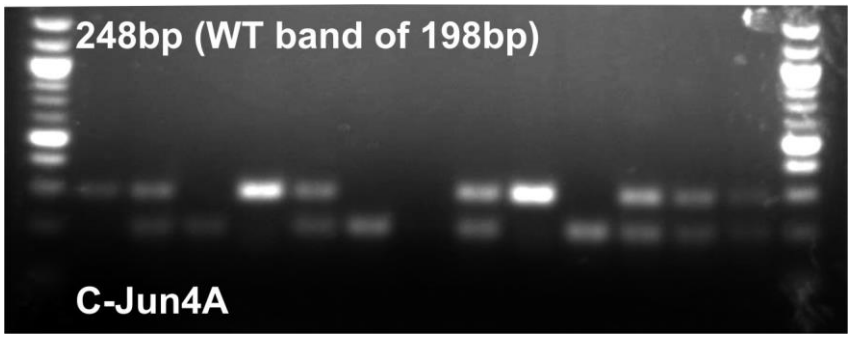

Figure 8.1 Agarose gel electrophoresis of PCR products were visualised to detect Jun4A or wild type C-Jun expression with positive bands at 298bp and 198bp respectively.

Neonatal pups were subject to either 60min HI at P7 or to 0.6µg/gBW LPS at P6 followed by left carotid artery occlusion and 30min HI 12hr later. All animals were sacrificed 48hr after hypoxia. After perfusion and processing, the forebrains were assessed for damage markers including microglia and astrocyte activation (αM and GFAP immunoreactivity), neuronal loss (cresyl violet histology), cell death (Tunel), and extent of infarct volume (figure 8.2).

By using the Rice-Vannucci model of HI in the neonatal mouse, we are able to compare hypoxic ischemic damage in the hemisphere ipsilateral to carotid artery occlusion, and compare it to the undamaged non-ischemic contralateral hemisphere. Following 60min exposure to 8% O_2, both wild type (Jun, n=10)

and Jun4A (n=9) pups exhibited an increase level of microglia activation and neuronal loss within the ipsilateral forebrain. Both white matter and grey matter regions showed comparative levels of αM expression and the presence of nissl bodies, with no difference between Jun and Jun4A cohorts.

Highest score for microglia activity was achieved in the external capsule (white matter) with an average of 2.96±0.45 in the wild type animals and 2.10±0.56 in Jun4A. Grey matter regions had a uniform level of activation between them

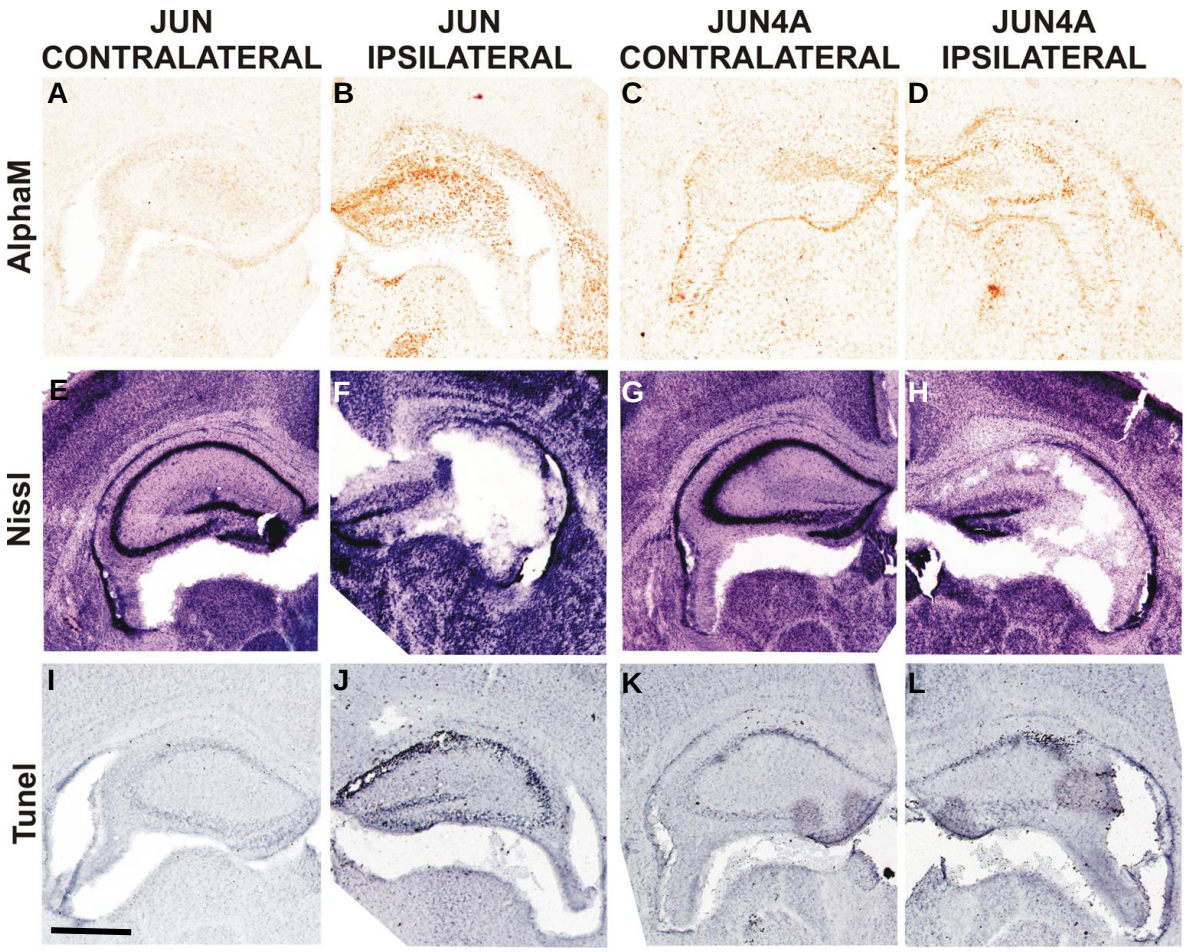

Figure 8.2 Illustrative response of the ipsilateral hemisphere in P7 mice to 60min HI. Transgenic mutant mice had their N-terminal serine 63 and 73, and threonine 91 and 93 replaced with alanine (JUN4A), rendering C-Jun unable to be phosphorylated by JNK. Mutants homozygous for JUN4A were compared to wild type (JUN) littermates. Forebrain sections were analysed for microglia activation (A-D), neuronal loss and infarct volume (E-H), and Tunel+ cell death (I-L). Scale bar indicates 0.5mm.

(Average for Jun= 1.76±0.27, Jun4A= 1.67±0.11). Striatum and hippocampus saw the greatest neuronal loss (striatum: Jun= 1.30±0.38, Jun4A= 1.56±0.53; hippocampus: Jun= 1.68±0.42, Jun4A= 1.36±0.50) (figure 8.3A). This pattern of increased damage response within both groups is validated by analysis of lesion infarction. Here total area loss was 12.33±3.43% in Jun mice and 17.17±3.67% in Jun4A (figure 8.3G).

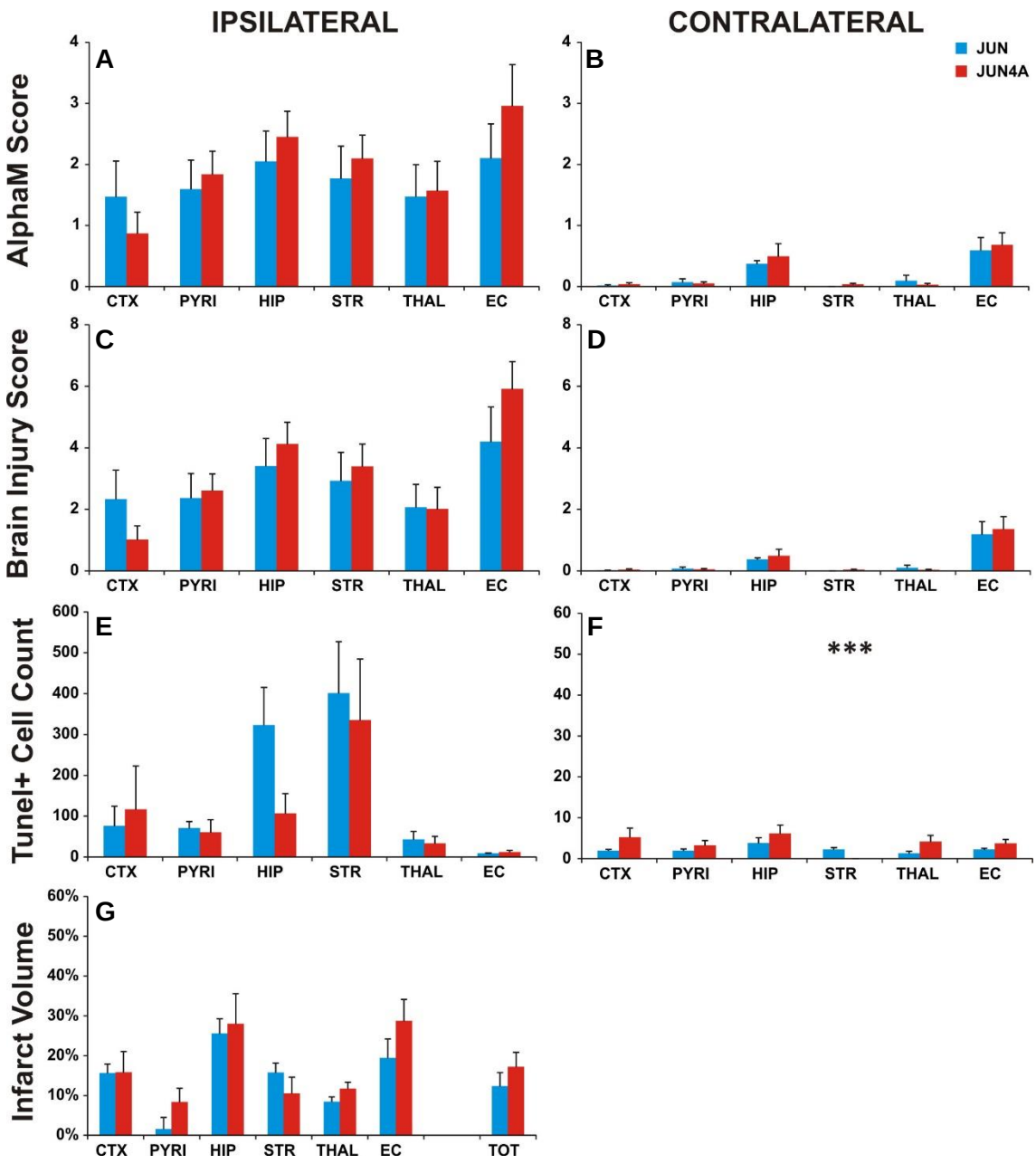

Figure 8.3 Transgenic mutant mice were created to create functional knock outs of C-Jun by the exchange of N-terminal serine 63 and 73, and threonine 91 and 93 into alanine. Two mutant variations were compared: wild type (JUN), and homozygous knock outs (JUN4A). Forebrain sections were analysed for microglia activation (A-B), Brain injury score (C-D), Tunel+ cell death (E-F), and infarct volume (G). Analysis at 20x eye field (mean plus SEM over 3 fields) and student t-test used where significance is p<0.05. A-F: analysis of forebrain regions for damage markers. Regions include external capsule (EC), striatum (STR), pyriform cortex (PYR), cortex (CTX), hippocampus (HIP), and thalamus (THAL). A: microglia activation is mildly increased in the absence of C-Jun phosphorylation. C: This rise in damage was reflected in brain injury score (combination of alphaM score and tissue damage score, as assessed by cresyl violet histology). E-G: Tunel+ dying cells and the extent of infarction were unchanged between groups. B, D, and F: Contralateral hemisphere to carotid occlusion (hypoxia alone intracranial control). *** indicates a student t-test P value ≤ 0.001.

Histological combined injury assessment was performed using microglial activation (αM immunoreactivity) and neuronal cell loss (nissl) scoring system where 0 is the lack of active amoeboid microglia and of nissl bodies and 4 is widespread active microglia recruitment and mechanical tissue loss. Both

groups showed elevated injury in the ischemic ipsilateral hemisphere, however there was little difference between the wild type JUN controls and their Jun4A littermates. External capsule was the region most sensitive to insult (JUN= 4.20±1.13, JUN4A= 5.91±0.89), with a mild 29% rise in injury score in JUN4A pups (figure 8.3C). Thalamus was the least effected (JUN= 2.06±0.75, JUN4A= 2.01±0.71) with an equal score for the two groups.

Tunel positive cell death showed a more modest increase in the number of dying cells present within the ipsilateral external capsule, pyriform cortex, cortex and thalamus, while the striatum (Jun= 400.96±126.19, Jun4A= 335.28±149.52) and hippocampus (Jun= 322.85±92.20, Jun4A= 106.56±48.62) were more strongly affected. Interestingly hippocampus of the Jun4A animals had a decrease in Tunel immunoreactivity compared to Jun, with significance almost reached by student t-test, p=0.06 (figure 8.3E). In all other regions, there was no change between groups.

C-Jun N-terminal phosphorylation plays a modest role in cellular response after endotoxin sensitised HI injury

After LPS stimulation, primary microglia cultures from the neonatal rat demonstrate an increase in total nuclear JNK in addition to phosphorylated C-Jun. Here JNK/C-Jun/Ap-1 pathway was indicated as a strong mediator of LPS induction of pro-inflammatory cytokine release from glia in regions of ischemic damage. Its activation precedes cell death by inflammation induced apoptosis (Waetzig et al., 2005). The previous experiment has shown that Jun4A does not change the neonatal brains response to hypoxia alone. However the role of JNK/C-Jun/AP1 in cytokine upregulation suggests that Jun4A may result in neuroprotection after HI when combined with inflammation.

Ten Jun4A and ten Jun P6 mouse pups were injected i.p with 0.6µg/gBW LPS 12hr prior to 30min HI. The animals were sacrificed on P9. The brains were perfused and processed as previously described and analysed for damage markers.

Microglial activation was moderately higher in Jun4a forebrain regions, ipsilateral to carotid occlusion, compared to wild type littermates. When the regions were examined individually: external capsule- 35%, striatum- 49%,

cortex- 46%, hippocampus- 27%, and thalamus had 60% increase (figure 8.4A-D, I). Pyriform cortex remained relatively unaffected between the two groups (8% increase in Jun4A compared to Jun). This increase in αM expression was insignificant, with P>0.15.

Recruitment of active astrocytes was less delineated between cohorts. Hippocampus showed the highest sensitivity to HI (Jun= 74.26±8.44, Jun4A= 69.49±6.99) whilst striatum saw the greatest difference, with a 34% increase in activated astrocytes in Jun4A animals (figure 8.4E-H, K). External capsule, pyriform cortex, cortex, and thalamus did not exhibit any difference in GFAP luminosity between Jun4A and Jun littermates.

Using a semi-quantitative scoring system, neuronal loss was assessed by the presence of nissl bodies as well as structural damage to regional tissue. This was combined with scores for activated microglia to give a mean brain injury score. Striatum, cortex and hippocampus exhibited higher scores, and thus greater degree of loss, in Jun4A animals compared to Jun controls. Striatum saw a 45% increase, cortex- 42%, hippocampus- 33%, and external capsule- 35%, although this was insignificant by student t-test (P>0.29) (figure 8.5I). Pyriform cortex and thalamus proved less sensitive to insult with low scores which were unchanged between the groups (pyriform: Jun= 0.92±0.79, Jun4A= 1.08±0.38; thalamus: Jun= 0.75±0.70, Jun4A= 1.06±0.37).

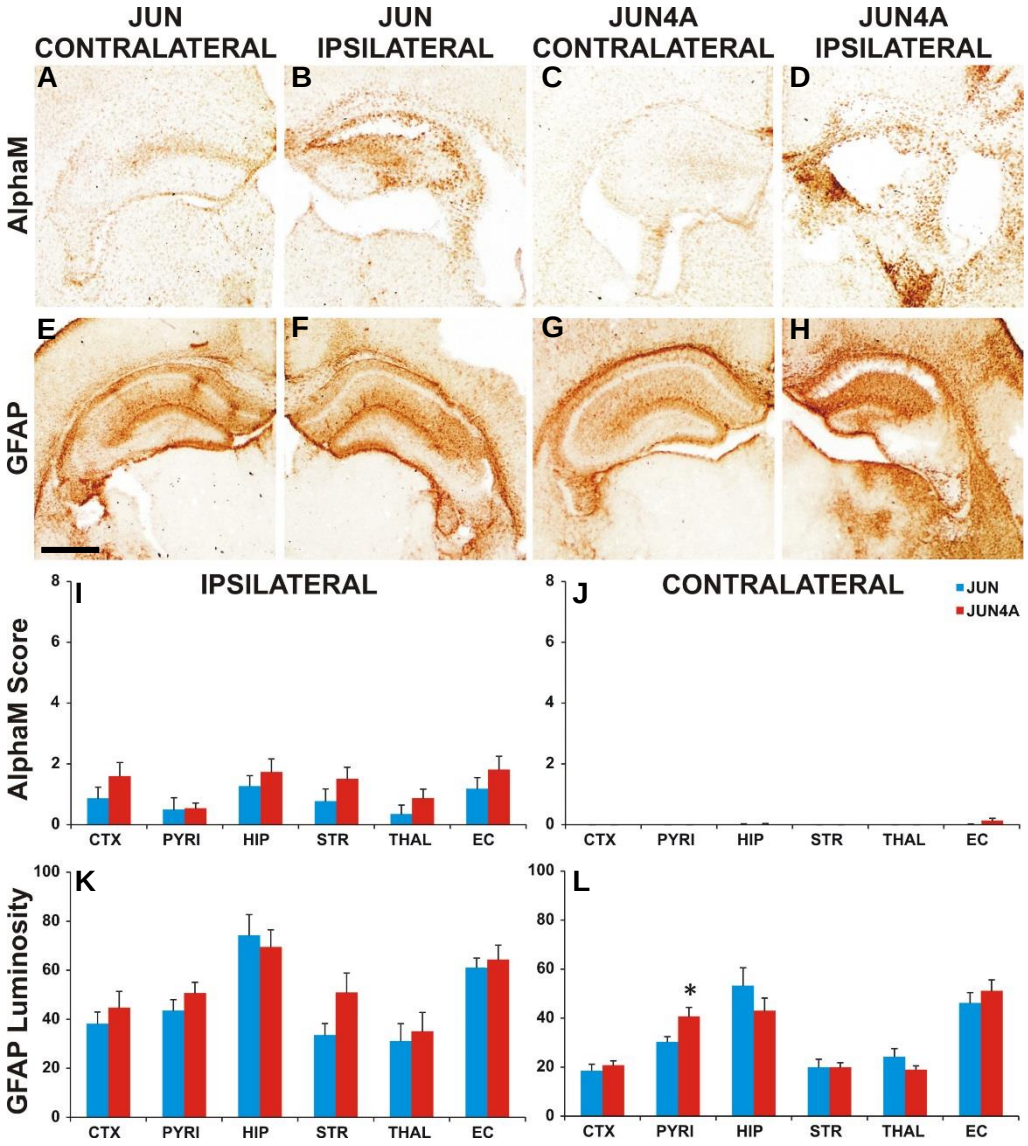

Figure 8.4 C-Jun phosphorylation plays a minor role in non-neuronal cell activation and recruitment after combined LPS and 30min HI insult. Microglial (A-D, I-J) and astrocyte (E-H, K-L) activation, 2 days after insult, in Jun wild type (A-B, E-F, I-L) controls, and the JUN4A (C-D, G-H, I-L) mutant mice. Both were assessed on the contralateral side (1st and 3rd column) and on the ipsilateral side (2nd and 4th column) to carotid artery occlusion. After insult, JUN mice showed a modest increase in microglia and astrocyte activity. In JUN4A mutants, this response is increased further. Scale bar indicates 0.5mm. *P<0.05 by student t-test.

This pattern of response was reflected in Tunel immunoreactivity (figure 8.5A-D, K). External capsule, pyriform cortex and thalamus evidenced very few dying cells, averaging between 7.25-9.70 in Jun animals and 6.88-15.3 in Jun4A, numbers that barely exceed those of the contralateral counterparts. Striatum (Jun= 38.4±24.4, Jun4A= 154±60.1), cortex (Jun= 68.3±65.8, Jun4A= 230±81.4), and hippocampus (Jun= 80.5±34.6, Jun4A= 172.0±50.5) were more dramatically effected with an increase in dying cells in the Jun ipsilateral forebrain which was then exceeded in Jun4A littermates. Due to the variability in response between animals, this difference was not significant, P>0.12.

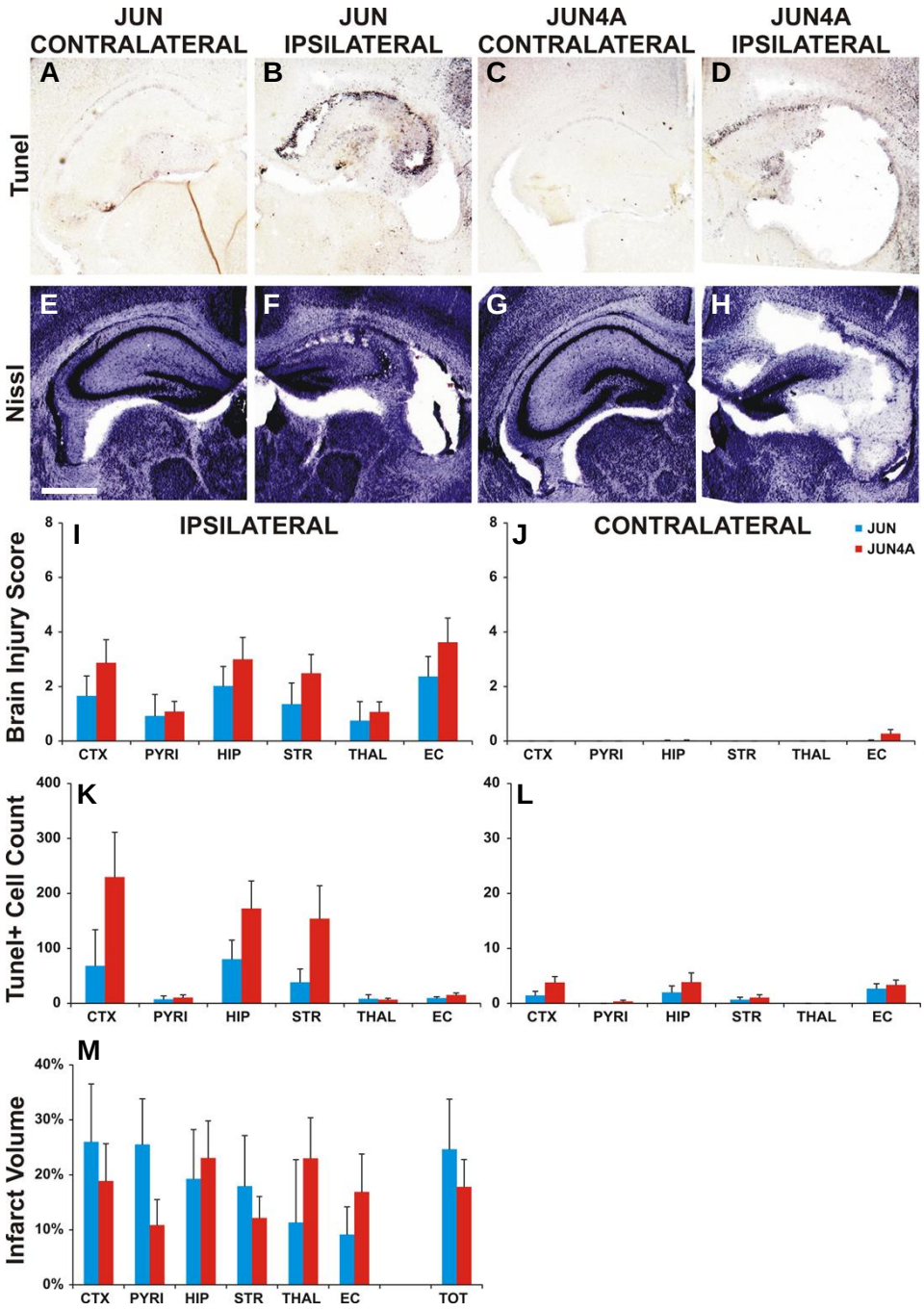

Figure 8.5 C-Jun phosphorylation prevents cell loss after combined LPS and 30min HI insult. At 48hr post insult, Tunel positive dying cell numbers (A-D, K-L) are higher in JUN4A mutants than in JUN wild type littermates. This increase was also apparent by brain injury score (I-J). Despite this difference between groups, significance was not reached, nor was the extent of infarct (E-H, M) affected by higher cell loss. **Scale bar indicates 0.5mm.**

Replacement of N-terminal ser63 and 73, and thr91 and 93 renders C-Jun unable to be phosphorylated by JNK. Our current data shows that this functional knock out of C-Jun activity exacerbates damage caused by endotoxin mediated HI insult. However, this effect is to a milder degree than that seen with neuroepithelial C-Jun deletion implying that JNK phosphorylation of C-Jun is not the only pathway of activation involved. The lack of statistical significance corresponds to the negative results produced in the adult neuronal axotomy model employed by this laboratory (Ruff et al. 2010).

Functional mutation of C-Jun phosphorylation- Discussion

Controversy still remains as to whether protection seen with JNK inhibition in neonatal HI is acting through C-Jun/AP1 pathways or via independent activity at the neuronal mitochondria (Ginet et al., 2009; Nijboer et al., 2010; Pirianov et al., 2007; Zhao and Herdegen, 2009; Zhao et al., 2012). Herein this thesis we had shown a conflict in response by early developmental pan CNS deletion of C-Jun, an area effect similar to pharmacological JNK intervention, resulting in exacerbation of HI damage. This contrasted to late-development neuron specific C-Jun deletion where neuroprotection occurs to a similar degree to that in JNK3$^{-/-}$ mice.

To understand the involvement of JNK phosphorylation of C-Jun in the P7 Rice-Vannucci mouse model of HI we have utilised the Jun4a mutant. These mice have had the phosphor-acceptor sites of the C-Jun N-terminal, ser63/73 and thr91/93, converted to alanine, fully nullifying JNKs ability to activate C-Jun (Aguilera et al., 2011).

C-Jun N-terminal phosphorylation is a minor player in neonatal cerebral brain response to HI

Little change was observed between Jun4a mice and wild type counterparts following 60min HI. In endotoxin-mediated HI insult, Jun4a mutation gave rise to a modest increase in brain injury score with mean difference of 33% and DNA fragmentation- 41% in ipsilateral forebrain regions. Active microglia was similarly affected with a 50% increase in striatum and mean difference of 37% across the regions. There was no effect on GFAP immunoreactivity or infarct volume size. Whilst insignificant this response is reminiscent to that observed with nestin C-Jun mutants.

Collectively this data herein points to a conclusion that enhanced protection against cerebral ischemia by JNK inhibition is, for the most part, independent of C-Jun phosphorylation. Potentially, by direct interference of JNK at the mitochondria outer membrane suppressing the actions of pro-apoptotic Bim. On the other hand, C-Jun evidences a JNK independent role in nestin expressing cells to regulate neuronal survival following HI.

A similar response of Jun4a to nestin C-Jun mutants was previously shown by this group, albeit to a milder effect, in the adult facial nerve axotomy model of peripheral nerve injury. Here nestin deletion of C-Jun resulted in increased atrophy of surviving motoneurons within the facial motor nucleus, delayed axonal regenerations, and poor re-innervation of the target muscles (Raivich et al., 2004). When repeated with JunAA mice, which had ser63/73 of the C-Jun N-terminal converted to alanine, mild increase in atrophic neurons were observed in addition to higher GFAP immunoreactivity and a modest decline in post-axotomy CD44 levels (Ruff et al., 2012).

One explanation for these observations is that developmental C-Jun inhibition can result in increased postnatal and adult susceptibility to injury. C-Jun null mice die between E10.5 and E13.5 due to heart deformities (Eferl et al., 1999; Pirianov et al., 2006a; Repici et al., 2007). Nestin expression is seen as early as E7 (Vukojevic et al., 2010), excision of MKK4 and 7, upstream from JNK/C-Jun, in nestin positive cells while embryonically viable resulted in strong phenotypic liver and brain abnormalities culminating in death soon after birth (Wang et al., 2007; Yamasaki et al., 2011). Observations on JunAA mice saw no evident neuronal abnormalities; however, primary JunAA fibroblasts from E12.5 embryos have delayed proliferation and hypersensitivity to ultraviolet-induced death, accompanied by reduced AP-1 activity. Additionally these mice were distinctively diminutive in size by P20 compared to wild type littermates (Behrens et al., 1999; Ruff et al., 2012). Together this provides compelling evidence that early inhibition of C-Jun function can result in both neurological and cardiac deficits that continue through the mouse lifespan, increasing sensitivity to insult and overwhelming endogenous coping mechanism present.

MAPK pathway crosstalk in neonatal HI

The deleterious nature of Jun4a suggests that neuroprotection by synapsin driven C-Jun excision is independent of JNK phosphorylation. This may be due to the relative late embryonic expression of synapsin, E12, or due to C-Jun as a downstream target of other signalling pathways stress response pathways.

Multiple studies exist showing parallel MAPK cascades crosstalk in order to enhance cellular response to stimuli (Kayahara et al., 2005; Leppä et al., 1998;

Meng and Xia, 2011; Shaul and Seger, 2007). ERK1/2 is able to activate C-Jun directly through inhibition of GSK3 bonding at thr239 on C-Jun C-terminal. Phosphorylation by GSK3 renders C-Jun unable to bind DNA and upregulate AP1 (Aronov et al., 2009; Meng and Xia, 2011; Shaul and Seger, 2007). ERK1/2 can also indirectly activate C-Jun by its phosphorylation of P300 which in turn acetylates lysine 268, 271, and 273 of C-Jun forming a DNA binding complex able to further enhance C-Jun transductional function (Liu et al., 2007; Raivich, 2008; Vries et al., 2001; Wang et al., 2006).

In this thesis we have examined the therapeutic effect of ERK inhibition, using the selective MEK inhibitor SL327, where pre-treatment before mild insult resulted in a significant reduction in both neuronal and non-neuronal response to HI. In addition to fully ablating pERK expression, we likewise observed a complete inhibition of C-Jun immunoreactivity suggesting that ERK mediated C-Jun activation is involved in the neonatal mouse response to cerebral ischemia (figure 8.6).

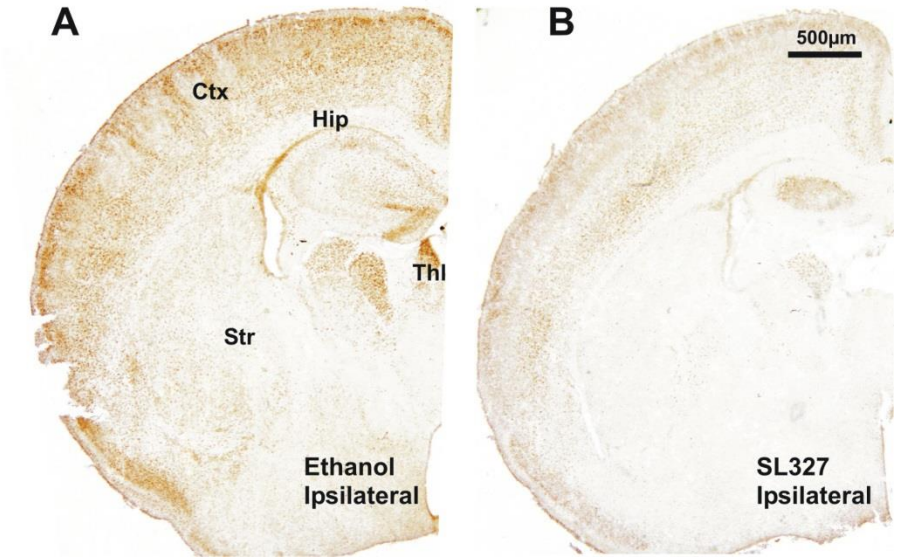

Figure 8.6 Injection of 133ug/gBw SL327 20min prior to 30min exposure to 8% O_2 markedly reduced C-Jun expression. Light microscopy at 1x magnification. Immunohistochemistry revealed a distinct reduction of C-Jun induction within the cerebral cortex (Ctx), thalamus (Thl), striatum (Str), and hippocampus (Hip). In SL327 treated P7 C57/Bl6 mice (B) when compared to EtOH control treated littermates (A).

How ERK and C-Jun mediate cell survival in ischemic injury warrants a closer investigation of these cross activation pathways through selective amino acid replacement, similar to the exchange of N-terminal serine and threonine to alanine in Jun4a mutants. Given the striking differences between cell specific ERK and C-Jun mutations in damage response, unravelling the molecular

pathways involved is fundament to enhancing their capacity as targets in improved neurological outcome following neonatal HI.

Chapter 9- Summary of Results

During neonatal HI insult, once a critical threshold is reached, cellular mechanisms begin to fail due to an insufficiency in ATP supply leading to a two-phase neurotoxic cascade. Principally primary energy failure-resulting in immediate and necrotic cell death, followed by a latent period of up to 6hr in which reperfusion occurs. The length of this respite is dictated by the severity of the primary energy failure. Afterwards, secondary neuronal cell death occurs due to multiple molecular imbalances instigated by excitotoxic oxidative stress and mitochondria failure. This secondary phase can last up to a day after insult, and is considered the most responsible for neuronal loss and abnormal neurological outcome.

The neonatal mouse model of hypoxia-ischemia

In the following thesis, we have utilised the P7 mouse Rice-Vannucci model of either HI injury, HI alone in moderate (30 min exposure to 8% O2) or severe (60 min exposure) form, or moderate HI with sensitisation by LPS at 12hr prior to insult.

Whilst no single model is ideal, each provides a preferential advantage depending on the research question and materials used. Rodents also have a good baseline of data to back them and have the advantage of large litter sizes. They are utilised for histological findings after injury as well as long term behavioural outcome. However due to their small size, multiple organ monitoring as well as some *in vivo* imaging techniques are limited.

Rice and Vannucci modified an adult rat model of stroke, described by Levine in 1960 (Rice et al., 1981). Experimental animals were compared to CROC alone and naïve littermates. In 92% of experimental animals, injury included neuronal changes and damage to the ipsilateral cerebral cortex, corpus striatum, hippocampus, and thalamus. Fifty-six percent of these also had tissue infarct in regions surrounding the middle cerebral artery. Unlike Levine's model, necrosis of the subcortical WM was greater in the ipsilateral hemisphere and spreading from myelinated foci.

The Rice Vannucci model was tailored to mice with modifications to the length of hypoxia being the most changeable factor. Mice have the advantage of there being a high number of commercially available genetically modified strains including global or conditional knockouts (KO) of target genes. It is for this reason that we have employed this model in our laboratory.

In context to other studies using the Rice-Vannucci model, this work illustrates a change in both white matter and grey matter of the brain following HI. Tunel positive immunoreactivity and measurement of infarct allow a clear insight into loss of tissue matter following HI. Despite this, neither is sufficient to further delineate whether white matter damage is predominantly axonopathy or a result of ODC damage. Whilst we are able to demonstrate a number of cellular processes, such as neurotoxic cascade, activation of MAPK and glial recruitment to loci of damage occur within hours to days of insult, much work still remains to identify how these processed are interrelated and therefore how pharmacological interventions may modify the neurological outcome. Neither this nor previous studies have shown significant histological injury to the contralateral hemisphere to carotid occlusion, it is impossible to rule out that both hemispheres are affected by insult. This tends towards an underestimation of injury when comparing occluded to non-occluded regions giving a trend towards non-significant results.

A point of contention in these studies is the role of microglia. Be it protective or detrimental to injury response. All three models of insult used result in both morphological changes of microglia from ramified resting to amoeboid active states. Similarly we observe changes in integrin expression. Within this thesis brain injury score is used which includes the assessment of both αMβ2 integrin immunoreactivity and neuronal morphology and nissl body formation. Combined and alone these correlate to quantitative measurements such as infarct volume implicating microglial activation to be integral in injury response. However this does not directly demonstrate their role in neonatal HI. Microglia have specific function within the CNS, including immune surveillance, cytokine production and phagocytosis. Once activated to an ‘alert’ phenotype, competing theorise exist for the downstream mechanisms including loss of normal microglial-neuronal support, hence reduced neuroprotection (Neumann et al., 2006) or increased

brain injury resulting from the production of further proinflammatory mediators (Hagberg and Mallard, 2005). Indeed both mechanisms may be involved.

To summarise, by utilising the Rice-Vannucci model of neonatal mouse HI we are able to study both grey and white matter injury as well as draw comparisons in those regions affected by moderate, severe or endotoxin sensitised HI. The damage markers utilised give a clear picture in terms of immune cell recruitment and the formation of infarction and cell death in all three models. However there is a limitation to the histological use of integrin's as an indicator of microglial activation as this does not communicate whether increased immunoreactivity is positive or negative in injury response. In addition it remains to be qualified whether some αMβ2 expressing cells, particularly under more severe HI, are in fact peripheral macrophages.

MAPK cascade in neonatal HI

The mitogen activated protein kinases (MAPK) are a complex group of serine-threonine kinases, serving as secondary messenger systems required to transfer extracellular signals from the cell surface throughout the cell to the nucleus. All four subfamilies of MAPK cascades have been linked to cerebral upregulation under hypoxic ischemic conditions. Following HI, multiple stimuli of MAPK are released including growth factors, cytokines, glutamate and FR. Indirect activation and phosphorylation can occur due to ischemic loss of cell integrity and dysfunction. Whether the activation of these pathways is due to cell loss or whether they actually regulate the mechanism underlying HI insult remains to be seen.

ERK has shown a dichotomy of response to HI. It is upregulated in the ischemic core of HI induced lesions and co-expresses with markers of apoptosis. Inhibition of ERK has both resulted in a reduction of neuronal loss and also a prevention of BDNF induced neuronal survival. JNK inhibition after HI results in reduced neuronal death in by the prevention of AP-1 assembly. However variable differences in infarct volume were seen in neonatal models of HIE.

Owing to their extensive control over normal cell function, the MAPK kinases have a potential role in the induction of cell death resulting from hypoxic conditions. This study focuses on two of the major MAPK pathways: ERK 1 and

2, and JNK. Whether they are neuroprotective remains unclear, as does their cell specific actions. This study aims to elucidate the answer to these questions.

ERK can be both protective and detrimental to neonatal HI injury dependent on specific cell type expression

In most regions, ipsilateral expression of pERK was immediately nullified for the first 15min following insult when compared to sham hypoxia controls. This was followed by a rapid bilateral assent of expression that peaks at 1hr and is normalised by 4hr. This pattern of activated ERK is in line with the observations by other groups working both neonatal and adult models (Alessandrini et al., 1999; van den Tweel et al., 2006; Wang et al., 2003b; Wang et al., 2004a) who established the pattern of pERK expression in both adult and neonatal rodent models of HI.

Cells of the pyriform have strong morphological identity with large soma pyramidal neurons and small soma stellate astrocytes (He et al., 2014; Nacher et al., 2002). Using co-immunofluorescence, we were able to determine that the majority of pERK positive cells were NeuN (a marker for neurons) negative and GFAP (astrocyte marker) positive. It is possible that cell specific expression is regulated on a region-by-region basis. Why ipsilateral glia response occurs prior to bilateral neuronal activity in pyriform awaits further research.

Initial dampening of pERK was equally observed in white matter. The appearance of axonal pERK occurred from 15min onwards, normalising by 1hr. This was swiftly followed by white matter glial body expression of pERK from 2-4hr post insult. PERK appeared to be contained in clusters along the axon, adjacent to neighbouring pERK positive axons. That pERK positive axons bundle together following HI has not been reported before now. This effect coincides with others observations of cells showing cytoplasmic pERK activity is commonly adjacent to one another at the borders of ischemia-induced micro lesions (Wang et al., 2003b).

Neuronal deletion of ERK2 showed a clear and significant reduction in active microglia. This pattern of response was validated in brain injury score and in Tunel positive cell death with cortex, pyriform cortex, and striatum being regions of particular sensitivity.

LPS mediated HI insult, both single neuronal ERK2 mutation and double ERK1 and neuronal ERK2 mutation resulted in a very strong reduction in damage at 2 days. Single mutants exhibited a 2.6fold decrease in microglia and 1.4fold decrease in astrocyte activation that strongly correlated to a reduction in brain injury and Tunel positive cell death. Preservation of regional cell loss was validated by measurements of infarct. No reduction of cell death or tissue loss was observed with double mutation of ERK1 and neuronal ERK2.

Following oxidative stress, ROS activation of ERK results in dysfunction of the mitochondrial outer membrane inciting cytochrome C (CTC) release and cleavage of caspase 3 and 8 (Martin and Pognonec, 2010; Nowak et al., 2006; Nowak, 2002). ERK can further promote CTC release via the upregulation of Bax, PUMA, and Bad (Cagnol and Chambard, 2010). The neuroprotection of ERK deletion correlates well with the actions of MEK inhibitors in adult MCAO work. Alessandrini's group showed that in the adult gerbil model of focal cerebral ischemia, infarct was reduced by 55%, suggesting that like our model, ERK must be acting alongside other complimentary or parallel pro-apoptotic pathways in order to induce cell death after HI (Namura et al., 2001).

LPS/TLR4/MYD88 induction of genes encoding proinflammatory cytokines is mediated by the phosphorylation and nuclear relocation of ERK1/2 (An et al., 2002; Watts et al., 2011). How LPS/TLR/MYD88 interacts with members of the MAPK cascade can be seen summarised in figure 9.1. MYD88 can form a functional complex directly with ERK1/2 via the recruitment of a scaffold protein MKP3 (tpl2) which prevents ERK dephosphorylation, rendering it constitutively active (Bandow et al., 2012). MKP3 had been previously implicated in the dysregulation of TLR2/MYD88 activation of ERK, resulting in transcription of its nuclear target Elk-1. Coste et al. tested the ability of the MyD88-E52A mutant construct to activate the NF-κB or the RAS/ERK/ELK pathways. They showed MyD88-E52A were unable to activate NF-κB, however retained the ability to activate the RAS/ERK/ELK pathway. Additionally, MKP3, the major ERK-specific phosphatase involved in functional ERK down regulation, binds to ERK via the same conserved D domain present in MyD88. The same group showed MyD88 is capable of preventing MKP3-mediated ERK dephosphorylation and that MKP3 down regulation by RNA interference in *MyD88*$^{-/-}$ MEFs led to the

restoration of full ERK phosphorylation (Coste et al., 2010). In addition, MD-2, a protein associated to the extracellular domain of TLR4, when expressed in HEK cells gives rise to an increase in ERK/ELK1 activity after LPS stimulation (Yang et al., 2000).

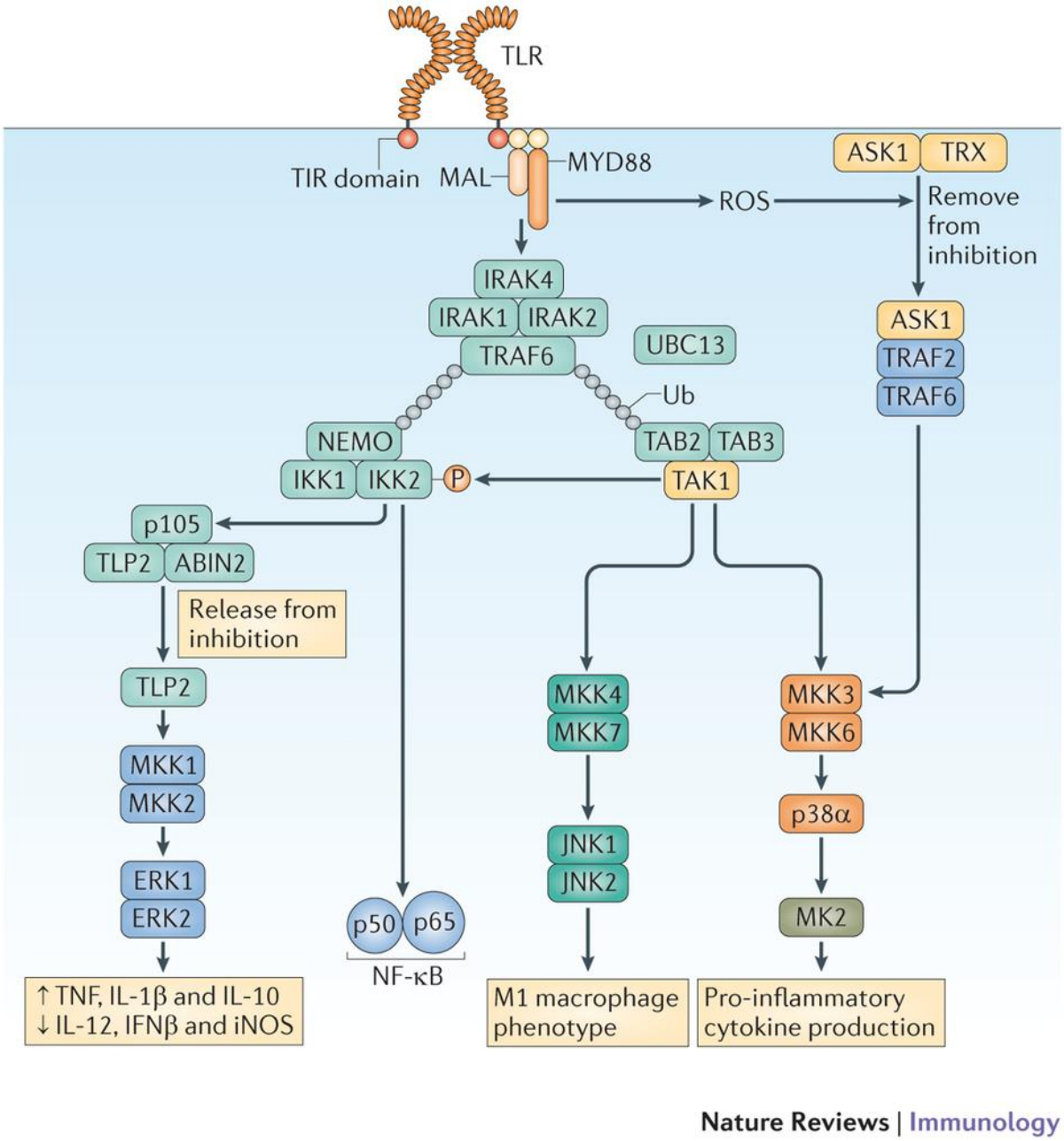

Figure 9.3 Following ligand binding to TLRs, IL-1 receptor-associated kinase 4 (IRAK4) is recruited to MYD88. IRAK4 then forms a complex with the related kinases IRAK1 and IRAK2 which leads to the activation of the MAPK and NF-κB pathways. Reproduced with permission (Arthur and Ley, 2013).

By deleting ERK1 globally, we observed a contrasting effect to ERK2 mutants, where ERK1 mutation resulted in an increase in extent of 30min HI induced damage compared to littermate controls. Global ERK1 deletion is embryonically

viable with no phenotypic differences to wild type littermates. However, developmental complications have associated ERK1 to thrombocyte dysfunction (Lefloch et al., 2008; Nekrasova et al., 2005), and sustained long term potentiation within the hippocampus resulting in improved outcome after seizure (Rosenblum et al., 2002; Selcher et al., 2003) . Behavioural studies have linked the MAP3K gene on chromosome 16, encoding ERK1, to altered synaptic plasticity and associated behavioural abnormalities that include autism (Campbell et al., 2008; Engel et al., 2008; Fernandez et al., 2010; Pucilowska et al., 2012).

Under certain circumstances ERK 1 can attenuate ERK 2 signal (Lefloch et al., 2008) and indeed, ERK 2 upregulation is seen in ERK $1^{-/-}$ mice (Lefloch et al., 2008; Samuels et al., 2008; Selcher et al., 2003) which, as we have shown herein, promotes neuronal death following HI. We were unable to study the effects of double ERK 1 and neuronal ERK 2 deletions with severe HI insult due to increased mortality rates of this genotype.

Mutants for global ERK 1 and astrocyte specific ERK 2 deletion exhibited a greater deleterious effect than global ERK1 deletion alone, with significantly higher expression of each damage marker. Cortex was the region most sensitive to injury with a 76% increase in microglial activation and brain injury. DNA fragmentation, by Tunel immunoreactivity, was increased by 90%.

In vitro studies indicate astrocytes to protect ODC precursor cells, the cells most sensitive to oxidative stress in the neonate and as such held partially responsible for subsequent white matter injury, against H_2O_2 insult via the upregulation of pERK. Here, application of U0126 cancels the protective nature of astrocytes (Arai and Lo, 2010). In vivo, other studies looked at ERK2 excision under the GFAP promoter in the developing mouse. They observed that whilst ODC precursor cells develop normally, they evidence a significant delay in maturation and reduced myelin production (Fyffe-Maricich et al., 2011). This suggests a developmental requirement of astrocytic ERK2 expression for normal ODC genesis.

Our future work would focus on cell specific ERK1 suppression in order to differentiate abnormal developmental contributions to HI sensitivity. This gains

the benefit of being able to assess long-term behavioural outcomes due to HI and LPS sensitised HI. In addition, single ERK2 deletion in astrocytes will indicate whether the extent of damage observed is cumulative to ERK1 global deletion or solely due to a lack of ERK2.

Pre-treatment with SL327, a selective inhibitor of MEK and analogue of U0126, resulted in decreased levels of microglia activation, histological brain injury, and Tunel positive cell death 48hr after mild HI insult. Protective outcome from SL327 was retained when administered 1hr after HI. These observations are on par with current paradigms where pre-treatment of U0126 to bilateral CROC in the adult gerbil, reduced the loss of hippocampal neurons in addition to an overall decrease of infarct which associated to improved neurological outcome (Namura et al., 2001). Other In vivo studies explored the suppression of cytokine release following HI by application of U0126 both 20min prior and immediately following MCAO in the adult mouse.

Post-treatment of SL327 after 60min 8% O2 exposure had diminished efficacy in protecting the neonatal mouse brain from ischemic damage. At 16hr post insult there was no change in microglia activation, brain injury score or the prevalence of DNA fragmentation following SL327 treatment when compared to EtOH alone. A survival time point of 48hr provided a more promising outcome. While markers for damage remained unaffected, the survival of this cohort was dramatically improved from 30% in EtOH treated controls to 83%.

Studies using PD98059 and U0126 saw that in addition to ERK1/2 inhibition, ERK5 phosphorylation was prevented in a dose-dependent manner. As ERK5 has shown to be neuroprotective after ischemic insult in adult rodents, it is plausible that use of high dose SL327 is only partially successful in reducing HI damage by its actions at ERK5. Recent developments have given rise to two ERK selective, ATP competitive, inhibitors: SCH772984 and FR180204 (Anastassiadis et al., 2013; Morris et al., 2013) whose greater selectivity should prevent suppression of pERK5 seen with U0126. In addition, by increasing the numbers of control animals we could elucidate a stronger difference between treated and untreated animals. Long-term behavioural studies would confirm the protective effects of ERK inhibition on neurological outcome. Lastly, the

opportunity to combine therapy with, for example, hypothermia could augment the partial protection observed with both.

C-Jun deletion is neuroprotective via JNK independent pathways in neonatal HI

Neuroepithelia derived cells in the CNS, targeted by nestin expression, include populations of neurons, astrocytes, oligodendrocytes (ODC), and Schwann cells (PNS) (Kohno et al., 2006; Raivich et al., 2004; Vukojevic et al., 2010). Immunohistochemistry for phosphorylated C-Jun in C57/Bl6 wild type mice saw bilateral neuronal expression with peak activity at 2hr following CROC and 30min exposure to 8% O_2. In nestin driven C-Jun mutant mice, pC-Jun immunoreactivity is fully ablated. Double labelling of C-Jun with NG2, a marker of ODCs, and GFAP for astrocytes exhibited inhibition of pC-Jun within these cells in additional to neuronal response. Microglial expression remained unaffected as expected due to their mesodermal origin.

Sixty-minute exposure to hypoxia-ischemia resulted in exacerbation of the deleterious affect seen following mild HI. AlphaM immunoreactivity, histological tissue loss and DNA fragmentation all exhibited significantly higher levels of expression in both white matter and all grey matter regions in the C-Jun mutant pups. Microglial activation was increased, on average by 3fold, up to 5fold in cortex, both brain injury score and Tunel positive cell death were 2fold higher in mutants. When subject to combined insult of LPS and 30min HI, nestin C-Jun mutants exhibited increased damage response that was comparable to 60min HI alone. Significant enhancement of suppressed C-Jun mediated neurodegeneration occurred

Previous work by our group studied the effect of nestin driven C-Jun deletion in an adult mouse facial axotomy model. Here suppression of C-Jun resulted in several regenerative defects. Although cell survival increased following axotomy, surviving motoneurons were atrophic in addition to reduced target muscle innervation and enhanced perineuronal sprouting, lymphocyte recruitment and microglial activation (Raivich et al., 2004). Together this suggests C-Jun to positively regulate neuronal response to injury.

Synapsin driven excision of C-Jun results in a bilateral decrease in tissue loss following histological assessment with a mean decrease of brain injury by 28%

across all forebrain regions. Contralateral hippocampus was similarly affected with 10% less in mutant mice than controls. Pattern of response was similar in Tunel immunoreactivity, where ipsilateral forebrain regions contained 4fold less dying cells in mutants. Lastly, C-Jun mutants saw a 30% reduction in the number of active microglia and astrocytes. Astrocytic C-Jun mutants saw a more modest reduction in damage response compared to wild type littermate controls.

In the P7 rat, systemic L-JNKI treatment immediately following 120min HI resulted in suppression of nuclear AP1 cleavage of caspase3 and a reduction of infarct. Conversely, upstream mediators of apoptosis, caspase 8 and 9, Bid and mitochondrial CTC release, in addition to cytokine production, remained unaffected (Nijboer et al., 2010). That HI in the neonate can instigate both C-Jun dependent and independent apoptotic pathways of JNK activity, could well explain why neuronal deletion of C-Jun is only partially protective in our studies.

C-Jun null mice are embryonically lethal at E10.5 due to malformation of heart septum and incomplete separation of aorta and pulmonary artery in addition to severe liver abnormalities (Eferl et al., 1999). Early developmental deletions of MKK4 and 7 resulted in postnatal growth and brain abnormalities and early morbidity (Wang et al., 2007; Yamasaki et al., 2011). Where nestin expression occurs early in embryogenesis, E7.5, synapsin and GFAP is not apparent until E12-15. As such, C-Jun deletions under cell specific promoters are less affected by developmental contributions to sensitivity to HI seen in nestin C-Jun mutants.

Within current literature, there is evidence that ODC C-Jun inactivation would be detrimental to neuronal survival following insult, similar to that seen in our original nestin driven C-Jun deletion studies. ODC are the myelin producing cells of the CNS, with Schwann cells being their functional counterpart in the PNS. In collaboration with Axel Behrens laboratory, our group have shown that specific C-Jun deletion in Schwann cells resulted in increased motoneuron cell death, poor functional recovery, and re-innervation of muscle targets after facial nerve axotomy (Fontana et al., 2012). It remains possible that ODC are the source of neurodegenerative actions by nestin C-Jun mutation.

To better understand involvement by JNK phosphorylation of C-Jun in the P7 Rice-Vannucci mouse model of HI we have utilised the Jun4a mutant. These mice have had the phosphor-acceptor sites of the C-Jun N-terminal, ser63/73 and thr91/93, converted to alanine, fully nullifying JNKs ability to activate C-Jun (Aguilera et al., 2011).

Functional deletion of C-Jun activation by JNK resulted in little change between Jun4a mice and wild type counterparts following 60min HI. In endotoxin-mediated HI insult, Jun4a mutation gave rise to a modest increase in brain injury score, DNA fragmentation and active microglia. There was no effect on GFAP immunoreactivity or infarct volume size. Whilst insignificant this response is reminiscent to that observed with nestin C-Jun mutants.

A similar response of Jun4a to nestin C-Jun mutants was previously shown by this group, albeit to a milder effect, in the adult facial nerve axotomy model of peripheral nerve injury. As shown, nestin deletion of C-Jun resulted in increased atrophy of surviving motoneurons within the facial motor nucleus, delayed axonal regenerations, and poor re-innervation of the target muscles (Raivich et al., 2004). When repeated with JunAA mice, which had ser63/73 of the C-Jun, N-terminal converted to alanine, mild increases in atrophic neurons were observed.

Together this provides compelling evidence that early inhibition of C-Jun function can result in both neurological and cardiac deficits that continue through the mouse lifespan, increasing sensitivity to insult and overwhelming endogenous coping mechanism present.

Future work is required to look at selective excision form ODC under the NG2 promoter driven cre recombinase as well as combined cell selective deletion of C-Jun to understand the polar effects of nestin to single synapsin or astrocyte C-Jun deletion. In addition, previous work in our laboratory examined the time dependent increase in both cytokine and chemokine mRNA expression in response to LPS administration to the P7 mouse (Kendall et al., 2011). In order to confirm whether C-Jun can influence LPS induced inflammation the same array could be repeated in the nestin: C-Jun mutant. Lastly, D-JNKi, a highly selective JNK inhibitor, could be utilised to observe whether suppression of JNK

phosphorylation is neuroprotective in our neonatal mouse model of ischemic injury. If administered to synapsin: C-Jun mutants we could better understand whether neuroprotection is dependent on the inhibition of the JNK/C-Jun/AP-1 or whether C-Jun and JNK are acting in complimentary or parallel pathways to each other.

There remains a question of how ERK and C-Jun could be acting together to increase both cellular and biochemical response to HI in the neonatal brain. Multiple studies exist showing parallel MAPK cascades crosstalk in order to enhance cellular response to stimuli (Kayahara et al., 2005; Leppä et al., 1998; Meng and Xia, 2011; Shaul and Seger, 2007). ERK1/2 is able to activate C-Jun directly through inhibition of GSK3. ERK also indirectly activate C-Jun by its phosphorylation of P300

In chapter 5, we showed that the selective MEK inhibitor SL327, when administered before mild insult, resulted in a significant reduction in both neuronal and non-neuronal response to HI. In addition to ablated ERK phosphorylation, we observed a complete inhibition of C-Jun immunoreactivity suggestive of ERK mediated C-Jun activation. How ERK and C-Jun mediate cell survival in ischemic injury warrants a closer investigation of these cross activation pathways through selective amino acid replacement, similar to the exchange of N-terminal serine and threonine to alanine in Jun4a mutant.

To conclude, this and previous studies have demonstrated that, in the first hours following hypoxia-ischemia, there is a rapid increase in both ERK and C-Jun phosphorylation. Cell specific mutations reveal that both ERK2 and C-Jun inhibition in neurons give rise to strong protection against cell death, tissue loss and microglial recruitment. In contrast, astrocytic deletion proved more contentious. Where C-Jun mutants gave a modest reduction in damage, ERK deletion in these cells was highly detrimental. Despite this, pharmaceutical inhibition with SL327 proved effective in both pre and post treatment of mild HI and increased survival when administered after severe insult. Global deletion of ERK1, pan CNS deletion of C-Jun and prevention of C-Jun phosphorylation by JNK resulted in development-associated increased sensitivity to postnatal hypoxic-ischemia.

Together this confirms the therapeutic potential of ERK1/2 and/or JNK inhibition after mild HI with the possibility of combined therapy to contest neurodegeneration by severe insult. Similar patterns of expression suggest that the therapeutic window where inhibition could be beneficial is restricted to 1hr and that pre-emptive inhibition during the developmental stage of infancy could diminish endogenous biochemical survival mechanisms, significantly worsening the outcome. Future work will focus on delineating how these two pathways interact in response to neonatal brain injury. In addition, we will examine the use of higher specificity ATP competitive inhibitors in order to reduce secondary suppression of other MAPK signalling mechanisms.

Reference List

Acarin, L., B. Gonz´lez, B. Castellano, and A.J. Castro. 1996. Microglial response to N-methyl-D-aspartate-mediated excitotoxicity in the immature rat brain. *The Journal of Comparative Neurology*. 367:361-374.

Adiseshaiah, P., D.V. Kalvakolanu, and S.P. Reddy. 2006. A JNK-independent signaling pathway regulates TNF alpha-stimulated, c-Jun-driven FRA-1 protooncogene transcription in pulmonary epithelial cells. *Journal of immunology (Baltimore, Md. : 1950)*. 177:7193-7202.

Aguilera, C., K. Nakagawa, R. Sancho, A. Chakraborty, B. Hendrich, and A. Behrens. 2011. c-Jun N-terminal phosphorylation antagonises recruitment of the Mbd3/NuRD repressor complex. *Nature*. 469:231-235.

Ahola, T., R. Lapatto, K.O. Raivio, B. Selander, L. Stigson, B. Jonsson, F. Jonsbo, G. Esberg, S. Stövring, S. Kjartansson, T. Stiris, K. Lossius, K. Virkola, and V. Fellman. 2003. N-acetylcysteine does not prevent bronchopulmonary dysplasia in immature infants: a randomized controlled trial. *The Journal of pediatrics*. 143:713-719.

Akaji, K., S. Suga, T. Fujino, K. Mayanagi, J. Inamasu, T. Horiguchi, S. Sato, and T. Kawase. 2003. Effect of intra-ischemic hypothermia on the expression of c-Fos and c-Jun, and DNA binding activity of AP-1 after focal cerebral ischemia in rat brain. *Brain Research*. 975:149-157.

Alderliesten, T., L.S.D. Vries, M.J.N.L. Benders, C. Koopman, and F. Groenendaal. 2011. MR Imaging and Outcome of Term Neonates with Perinatal Asphyxia : Value of Diffusion. 261.

Alessandrini, a., S. Namura, M.a. Moskowitz, and J.V. Bonventre. 1999. MEK1 protein kinase inhibition protects against damage resulting from focal cerebral ischemia. *Proceedings of the National Academy of Sciences of the United States of America*. 96:12866-12869.

Alexander, J.P., and T.S. Acott. 2003. Involvement of the Erk-MAP Kinase Pathway in TNFα Regulation of Trabecular Matrix Metalloproteinases and TIMPs. *Investigative Ophthalmology & Visual Science*. 44:164-169.

Almeida, R.D., B.J. Manadas, C.V. Melo, J.R. Gomes, C.S. Mendes, M.M. Grãos, R.F. Carvalho, a.P. Carvalho, and C.B. Duarte. 2005. Neuroprotection by BDNF against glutamate-induced apoptotic cell death is mediated by ERK and PI3-kinase pathways. *Cell death and differentiation*. 12:1329-1343.

An, H., Y. Yu, M. Zhang, H. Xu, R. Qi, X. Yan, S. Liu, W. Wang, Z. Guo, J. Guo, Z. Qin, and X. Cao. 2002. Involvement of ERK, p38 and NF-κB signal transduction in regulation of TLR2, TLR4 and TLR9 gene expression induced by lipopolysaccharide in mouse dendritic cells. *Immunology*. 106:38-45.

Anastassiadis, T., K.C. Duong-Ly, S.W. Deacon, A. Lafontant, H. Ma, K. Devarajan, R.L. Dunbrack, J. Wu, and J.R. Peterson. 2013. A Highly Selective Dual Insulin Receptor (IR)/Insulin-like Growth Factor 1 Receptor (IGF-1R) Inhibitor Derived from an Extracellular Signal-regulated Kinase (ERK) Inhibitor. *Journal of Biological Chemistry*. 288:28068-28077.

Arai, K., and E.H. Lo. 2010. Astrocytes protect oligodendrocyte precursor cells via MEK/ERK and PI3K/Akt signaling. *Journal of Neuroscience Research*. 88:758-763.

Armstead, W.M., D.B. Cines, K. Bdeir, I. Kulikovskaya, S.C. Stein, and A.A.-R. Higazi. 2008. uPA impairs cerebrovasodilation after hypoxia/ischemia through LRP and ERK MAPK. *Brain research*. 1231:121-131.

Arndt, P.G., N. Suzuki, N.J. Avdi, K.C. Malcolm, and G.S. Worthen. 2004. Lipopolysaccharide-induced c-Jun NH2-terminal kinase activation in human neutrophils: role of

phosphatidylinositol 3-Kinase and Syk-mediated pathways. *The Journal of biological chemistry*. 279:10883-10891.

Aronov, A.M., Q. Tang, G. Martinez-Botella, G.W. Bemis, J. Cao, G. Chen, N.P. Ewing, P.J. Ford, U.A. Germann, J. Green, M.R. Hale, M. Jacobs, J.W. Janetka, F. Maltais, W. Markland, M.N. Namchuk, S. Nanthakumar, S. Poondru, J. Straub, E. ter Haar, and X. Xie. 2009. Structure-Guided Design of Potent and Selective Pyrimidylpyrrole Inhibitors of Extracellular Signal-Regulated Kinase (ERK) Using Conformational Control. *Journal of Medicinal Chemistry*. 52:6362-6368.

Arthur, J.S.C., and S.C. Ley. 2013. Mitogen-activated protein kinases in innate immunity. *Nat Rev Immunol*. 13:679-692.

Atkins, C.M., J.C. Selcher, J.J. Petraitis, J.M. Trazaskos, and J.D. Sweatt. 1998. The MAPK cascade is required for mammalian associative learning. *Naure Neuroscience*. 1:602-609.

Aziz, K., M. Chadwick, M. Baker, and W. Andrews. 2008. Ante- and intra-partum factors that predict increased need for neonatal resuscitation. *Resuscitation*. 79:444-452.

Aznar, S., N. Tønder, S. Bele, M. Kiessling, J. Zimmer, and P. Gass. 1995. c-JUN, KROX-24, and c-FOS Expression in Hippocampal Grafts Placed in Excitotoxic Hippocampal Lesions of the Rat. *Experimental Neurology*. 136:205-211.

Back, S.A., B.H. Han, N.L. Luo, C.A. Chricton, S. Xanthoudakis, J. Tam, K.L. Arvin, and D.M. Holtzman. 2002. Selective Vulnerability of Late Oligodendrocyte Progenitors to Hypoxia–Ischemia. *The Journal of Neuroscience*. 22:455-463.

Bailey, S.L., P.A. Carpentier, E.J. McMahon, W.S. Begolka, and S.D. Miller. 2006. Innate and Adaptive Immune Responses of the Central Nervous System. 26:149-188.

Bambrick, L., T. Kristian, and G. Fiskum. 2004. Astrocyte Mitochondrial Mechanisms of Ischemic Brain Injury and Neuroprotection. *Neurochem Res*. 29:601-608.

Bandow, K., J. Kusuyama, M. Shamoto, K. Kakimoto, T. Ohnishi, and T. Matsuguchi. 2012. LPS-induced chemokine expression in both MyD88-dependent and -independent manners is regulated by Cot/Tpl2-ERK axis in macrophages. *FEBS Letters*. 586:1540-1546.

Bartha, A., N. Newton, S.E.G. Hamrick, O.A. Glenn, D. Xu, J.C. Partridge, and D.M. Ferriero. 2006. Tensor Imaging of Sequential Studies in Neonates with Encephalopathy.533-547.

Bax, M., and K.B. Nelson. 1993. Birth Asphyxia: a Statement. *Developmental Medicine & Child Neurology*. 35:1022-1024.

Baxter, P., C. Morris, P. Rosenbaum, N. Paneth, A. Leviton, M. Goldstein, M. Bax, A. Colver, D. Damiano, H.K. Graham, G.O. Brien, and T.M.O. Shea. 2004. The Definition and Classification of Cerebral Palsy Contents Foreword Historical Perspective Definition and Classification Document.1-44.

Behrens, a., M. Sibilia, and E.F. Wagner. 1999. Amino-terminal phosphorylation of c-Jun regulates stress-induced apoptosis and cellular proliferation. *Nature genetics*. 21:326-329.

Benakis, C., A. Vaslin, C. Pasquali, and L. Hirt. 2012. Neuroprotection by inhibiting the c-Jun N-terminal kinase pathway after cerebral ischemia occurs independently of interleukin-6 and keratinocyte-derived chemokine (KC/CXCL1) secretion. *Journal of Neuroinflammation*. 9:76.

Benders, M.J.N.L., A.F. Bos, C.M.A. Rademaker, M. Rijken, H.L. Torrance, F. Groenendaal, and F. van Bel. 2006. Early postnatal allopurinol does not improve short term outcome after severe birth asphyxia. *Archives of Disease in Childhood - Fetal and Neonatal Edition*. 91:F163-F165.

Bermudez, O., G. Pagès, and C. Gimond. 2010. The dual-specificity MAP kinase phosphatases: critical roles in development and cancer. *American journal of physiology. Cell physiology*. 299:C189-C202.

Besirli, C.G., and E.M. Johnson. 2003. JNK-independent activation of c-Jun during neuronal apoptosis induced by multiple DNA-damaging agents. *The Journal of biological chemistry*. 278:22357-22366.

Bhat, N.R., and P. Zhang. 1999. Hydrogen peroxide activation of multiple mitogen-activated protein kinases in an oligodendrocyte cell line: role of extracellular signal-regulated kinase in hydrogen peroxide-induced cell death. *Journal of neurochemistry*. 72:112-119.

Blair, E., and F. Stanley. 1993. Aetiological pathways to spastic cerebral palsy. *Paediatric and Perinatal Epidemiology*. 7:302-317.

Blumberg, R.M., E.B. Cady, J.S. Wigglesworth, J.E. McKenzie, and A.D. Edwards. 1997. Relation between delayed impairment of cerebral energy metabolism and infarction following transient focal hypoxia-ischaemia in the developing brain. *Exp Brain Res*. 113:130-137.

Bodart, J.-F.L. 2010. Extracellular-regulated kinase-mitogen-activated protein kinase cascade: unsolved issues. *Journal of cellular biochemistry*. 109:850-857.

Bogoyevitch, M.a., and N.W. Court. 2004. Counting on mitogen-activated protein kinases--ERKs 3, 4, 5, 6, 7 and 8. *Cellular signalling*. 16:1345-1354.

Bogoyevitch, M.a., K.R.W. Ngoei, T.T. Zhao, Y.Y.C. Yeap, and D.C.H. Ng. 2010. c-Jun N-terminal kinase (JNK) signaling: recent advances and challenges. *Biochimica et biophysica acta*. 1804:463-475.

Bohatschek, M., C.U.a. Kloss, K. Pfeffer, H. Bluethmann, and G. Raivich. 2004. B7.2 on activated and phagocytic microglia in the facial axotomy model: regulation by interleukin-1 receptor type 1, tumor necrosis factor receptors 1 and 2 and endotoxin. *Journal of neuroimmunology*. 156:132-145.

Bohatschek, M., A. Werner, and G. Raivich. 2001. Systemic LPS Injection Leads to Granulocyte Influx into Normal and Injured Brain: Effects of ICAM-1 Deficiency. *Experimental Neurology*. 172:137-152.

Borsello, T., P.G.H. Clarke, L. Hirt, A. Vercelli, M. Repici, D.F. Schorderet, J. Bogousslavsky, and C. Bonny. 2003. A peptide inhibitor of c-Jun N-terminal kinase protects against excitotoxicity and cerebral ischemia. *Nat Med*. 9:1180-1186.

Boulton, T.G., S.H. Nye, D.J. Robbins, N.Y. Ip, E. Radziejewska, S.D. Morgenbesser, R.a. DePinho, N. Panayotatos, M.H. Cobb, and G.D. Yancopoulos. 1991. ERKs: a family of protein-serine/threonine kinases that are activated and tyrosine phosphorylated in response to insulin and NGF. *Cell*. 65:663-675.

Brecht, S., R. Kirchhof, A. Chromik, M. Willesen, T. Nicolaus, G. Raivich, J. Wessig, V. Waetzig, M. Goetz, M. Claussen, D. Pearse, C.-Y. Kuan, E. Vaudano, A. Behrens, E. Wagner, R.A. Flavell, R.J. Davis, and T. Herdegen. 2005. Specific pathophysiological functions of JNK isoforms in the brain. *European Journal of Neuroscience*. 21:363-377.

Bromberg-White, J.L., N.J. Andersen, and N.S. Duesbery. 2012. MEK genomics in development and disease. *Briefings in functional genomics*. 11:300-310.

Brücken, A., A. Cizen, C. Fera, A. Meinhardt, J. Weis, K. Nolte, R. Rossaint, T. Pufe, G. Marx, and M. Fries. 2013. Argon reduces neurohistopathological damage and preserves functional recovery after cardiac arrest in rats. *British Journal of Anaesthesia*. 110:i106-i112.

Budd, S.L. 1998. Mechanisms of Neuronal Damage in Brain Hypoxia/Ischemia: Focus on the Role of Mitochondrial Calcium Accumulation. *Pharmacology & Therapeutics*. 80:203-229.

Cagnol, S., and J.-C. Chambard. 2010. ERK and cell death: mechanisms of ERK-induced cell death--apoptosis, autophagy and senescence. *The FEBS journal*. 277:2-21.

Cai, Z., Z.-L. Pan, Y. Pang, O.B. Evans, and P.G. Rhodes. 2000. Cytokine Induction in Fetal Rat Brains and Brain Injury in Neonatal Rats after Maternal Lipopolysaccharide Administration. *Pediatr Res*. 47:64-64.

Cakir, O., K. Erdem, A. Oruc, N. Kılınc, and N. Eren. 2003. Neuroprotective effect of N-acetylcysteine and hypothermia on the spinal cord ischemia–reperfusion injury. *Cardiovascular Surgery*. 11:375-379.

Campbell, D.B., C. Li, J.S. Sutcliffe, A.M. Persico, and P. Levitt. 2008. Genetic evidence implicating multiple genes in the MET receptor tyrosine kinase pathway in autism spectrum disorder. *Autism Research*. 1:159-168.

Canals, S., M.J. Casarejos, S.D. Bernardo, R.M. Solano, and M.A. Mena. 2003. Selective and persistent activation of extracellular signal-regulated protein kinase by nitric oxide in glial cells induces neuronal degeneration in glutathione-depleted midbrain cultures. *Molecular and Cellular Neuroscience*. 24:1012-1026.

Carmichael, S.T., I. Archibeque, L. Luke, T. Nolan, J. Momiy, and S. Li. 2005. Growth-associated gene expression after stroke: evidence for a growth-promoting region in peri-infarct cortex. *Experimental Neurology*. 193:291-311.

Castro-Obregón, S., R.V. Rao, G. del Rio, S.F. Chen, K.S. Poksay, S. Rabizadeh, S. Vesce, X.-K. Zhang, R.a. Swanson, and D.E. Bredesen. 2004. Alternative, nonapoptotic programmed cell death: mediation by arrestin 2, ERK2, and Nur77. *The Journal of biological chemistry*. 279:17543-17553.

Centeno, C., M. Repici, J.-Y. Chatton, B.M. Riederer, C. Bonny, P. Nicod, M. Price, P.G.H. Clarke, S. Papa, G. Franzoso, and T. Borsello. 2007. Role of the JNK pathway in NMDA-mediated excitotoxicity of cortical neurons. *Cell death and differentiation*. 14:240-253.

Cetinkaya, M., T. Alkan, F. Ozyener, a.I.M. Kaf, t.M.A. Kur, and N. Koksal. 2011. Possible Neuroprotective Effects of Magnesium Sulfate and Melatonin as Both Pre- and Post-Treatment in a Neonatal Hypoxic-Ischemic Rat Model. *Neonatology*. 99:302-310.

Chau, V., K.J. Poskitt, and S.P. Miller. 2009. Advanced neuroimaging techniques for the term newborn with encephalopathy. *Pediatric neurology*. 40:181-188.

Chavez-Valdez, R., L.J. Martin, and F.J. Northington. 2012. Programmed Necrosis: A Prominent Mechanism of Cell Death following Neonatal Brain Injury. *Neurology research international*. 2012:257563.

Chen, H., J. Sohn, L. Zhang, J. Tian, S. Chen, and L.F. Bjeldanes. 2014. Anti-inflammatory effects of chicanine on murine macrophage by down-regulating LPS-induced inflammatory cytokines in IκBα/MAPK/ERK signaling pathways. *European Journal of Pharmacology*. 724:168-174.

Chen, J., M. Rusnak, P.J. Lombroso, and A. Sidhu. 2009. Dopamine promotes striatal neuronal apoptotic death via ERK signaling cascades. *The European journal of neuroscience*. 29:287-306.

Chock, V.Y., and R.G. Giffard. 2005. Development of neonatal murine microglia in vitro: changes in response to lipopolysaccharide and ischemia-like injury. *Pediatric research*. 57:475-480.

Chu, C.T., D.J. Levinthal, S.M. Kulich, E.M. Chalovich, and D.B. DeFranco. 2004. Oxidative neuronal injury. The dark side of ERK1/2. *European journal of biochemistry / FEBS*. 271:2060-2066.

Chung, Y.H., K.M. Joo, H.C. Lim, M.H. Cho, D. Kim, W.B. Lee, and C.I. Cha. 2005. Immunohistochemical study on the distribution of phosphorylated extracellular

signal-regulated kinase (ERK) in the central nervous system of SOD1G93A transgenic mice. *Brain research*. 1050:203-209.

Colver, A.F., M. Gibson, E.N. Hey, S.N. Jarvis, P.C. Mackie, and S. Richmond. 2000. Increasing rates of cerebral palsy across the severity spectrum in north-east England 1964–1993. *Archives of Disease in Childhood - Fetal and Neonatal Edition*. 83:F7-F12.

Coste, I., K. Le Corf, A. Kfoury, I. Hmitou, S. Druillennec, P. Hainaut, A. Eychene, S. Lebecque, and T. Renno. 2010. Dual function of MyD88 in RAS signaling and inflammation, leading to mouse and human cell transformation. *The Journal of Clinical Investigation*. 120:3663-3667.

Costeloe, K., E. Hennessy, A.T. Gibson, N. Marlow, A.R. Wilkinson, and E.S.G. for the. 2000. The EPICure Study: Outcomes to Discharge From Hospital for Infants Born at the Threshold of Viability. *Pediatrics*. 106:659-671.

Coumans, A.B.C., J. Middelanis, Y. Garnier, H.-M. Vaihinger, S.L. Leib, M.U. Von Duering, T.H.M. Hasaart, A. Jensen, and R. Berger. 2003. Intracisternal Application of Endotoxin Enhances the Susceptibility to Subsequent Hypoxic-Ischemic Brain Damage in Neonatal Rats. *Pediatr Res*. 53:770-775.

Cowan, F., M. Rutherford, F. Groenendaal, P. Eken, E. Mercuri, G.M. Bydder, L.C. Meiners, L.M.S. Dubowitz, and L.S. de Vries. 2003. Origin and timing of brain lesions in term infants with neonatal encephalopathy. *Lancet*. 361:736-742.

D'Cruz, B.J., E.S. Logue, E. Falke, D.B. DeFranco, and C.W. Callaway. 2005. Hypothermia and ERK activation after cardiac arrest. *Brain research*. 1064:108-118.

Davies, C., and C. Tournier. 2012. Exploring the function of the JNK (c-Jun N-terminal kinase) signalling pathway in physiological and pathological processes to design novel therapeutic strategies. *Biochemical Society Transactions*. 40:85-89.

de Bernardo, S., S. Canals, M.J. Casarejos, R.M. Solano, J. Menendez, and M.a. Mena. 2004. Role of extracellular signal-regulated protein kinase in neuronal cell death induced by glutathione depletion in neuron/glia mesencephalic cultures. *Journal of neurochemistry*. 91:667-682.

de Vries, L.S., and M.J. Jongmans. 2010. Long-term outcome after neonatal hypoxic-ischaemic encephalopathy. *Archives of Disease in Childhood - Fetal and Neonatal Edition*. 95:F220-F224.

Deng, W. 2010. Neurobiology of injury to the developing brain. *Nat Rev Neurol*. 6:328-336.

Deng, W., P.A. Rosenberg, J.J. Volpe, and F.E. Jensen. 2003a. Calcium-permeable AMPA/kainate receptors mediate toxicity and preconditioning by oxygen-glucose deprivation in oligodendrocyte precursors. *Proceedings of the National Academy of Sciences*. 100:6801-6806.

Deng, Y., X. Ren, L. Yang, Y. Lin, and X. Wu. 2003b. A JNK-dependent pathway is required for TNFalpha-induced apoptosis. *Cell*. 115:61-70.

Dérijard, B., M. Hibi, I.H. Wu, T. Barrett, B. Su, T. Deng, M. Karin, and R.J. Davis. 1994. JNK1: a protein kinase stimulated by UV light and Ha-Ras that binds and phosphorylates the c-Jun activation domain. *Cell*. 76:1025-1037.

Derrick, M., N.L. Luo, J.C. Bregman, T. Jilling, X. Ji, K. Fisher, C.L. Gladson, D.J. Beardsley, G. Murdoch, S.a. Back, and S. Tan. 2004. Preterm fetal hypoxia-ischemia causes hypertonia and motor deficits in the neonatal rabbit: a model for human cerebral palsy? *The Journal of neuroscience : the official journal of the Society for Neuroscience*. 24:24-34.

Dewar, D., S.M. Underhill, and M.P. Goldberg. 2003. Oligodendrocytes and Ischemic Brain Injury. *J Cereb Blood Flow Metab*. 23:263-274.

Di Benedetto, B., C. Hitz, S.M. Hölter, R. Kühn, D.M. Vogt Weisenhorn, and W. Wurst. 2007. Differential mRNA distribution of components of the ERK/MAPK signalling cascade in the adult mouse brain. *The Journal of Comparative Neurology*. 500:542-556.

Dickey, E.J., S.N. Long, and R.W. Hunt. 2011. Hypoxic ischemic encephalopathy--what can we learn from humans? *Journal of veterinary internal medicine / American College of Veterinary Internal Medicine*. 25:1231-1240.

Dixon, G., N. Badawi, J.J. Kurinczuk, J.M. Keogh, S.R. Silburn, S.R. Zubrick, and F.J. Stanley. 2002. Early Developmental Outcomes After Newborn Encephalopathy. *Pediatrics*. 109:26-33.

Dobbing, J., and J. Sands. 1978. Head circumference, biparietal diameter and brain growth in fetal and postnatal life. *Early Human Development*. 2:81-87.

Dommergues, M.-a., F. Plaisant, C. Verney, and P. Gressens. 2003. Early microglial activation following neonatal excitotoxic brain damage in mice: a potential target for neuroprotection. *Neuroscience*. 121:619-628.

Dong, Y., H.D. Liu, R. Zhao, C.Z. Yang, X.Q. Chen, X.H. Wang, L.T. Lau, J. Chen, and A.C.H. Yu. 2009. Ischemia activates JNK/c-Jun/AP-1 pathway to up-regulate 14-3-3γ in astrocyte. *Journal of Neurochemistry*. 109:182-188.

Doyle, K.P., N. Fathali, M.R. Siddiqui, and M.S. Buckwalter. 2012. Distal hypoxic stroke: A new mouse model of stroke with high throughput, low variability and a quantifiable functional deficit. *Journal of Neuroscience Methods*. 207:31-40.

Dragunow, M., E. Beilharz, E. Sirimanne, P. Lawlor, C. Williams, R. Bravo, and P. Gluckman. 1994. Immediate-early gene protein expression in neurons undergoing delayed death, but not necrosis, following hypoxic-ischaemic injury to the young rat brain. *Molecular Brain Research*. 25:19-33.

Dragunow, M., D. Young, P. Hughes, G. MacGibbon, P. Lawlor, K. Singleton, E. Sirimanne, E. Beilharz, and P. Gluckman. 1993. Is c-Jun involved in nerve cell death following status epilepticus and hypoxic-ischaemic brain injury? *Molecular Brain Research*. 18:347-352.

Druilhe, A., L. S, and P. M. 2003. Glucocorticoid-induced apoptosis in human eosinophils : Mechanisms of action.481-495.

Dugan, L.L., and D.W. Choi. 1994. Excitotoxicity, free radicals, and cell membrane changes. *Annals of Neurology*. 35:S17-S21.

Duggan, P.J., E.F. Maalouf, T.L. Watts, M.H.F. Sullivan, S.J. Counsell, J. Allsop, L. Al-Nakib, M.A. Rutherford, M. Battin, I. Roberts, and A.D. Edwards. 2001. Intrauterine T-cell activation and increased proinflammatory cytokine concentrations in preterm infants with cerebral lesions. *The Lancet*. 358:1699-1700.

Eferl, R., R. Ricci, L. Kenner, R. Zenz, J.-P. David, M. Rath, and E.F. Wagner. 2003. Liver Tumor Development: c-Jun Antagonizes the Proapoptotic Activity of p53. *Cell*. 112:181-192.

Eferl, R., M. Sibilia, F. Hilberg, A. Fuchsbichler, I. Kufferath, B. Guertl, R. Zenz, E.F. Wagner, and K. Zatloukal. 1999. Functions of c-Jun in Liver and Heart Development. *The Journal of Cell Biology*. 145:1049-1061.

Eklind, S., C. Mallard, A.-L. Leverin, E. Gilland, K. Blomgren, I. Mattsby-Baltzer, and H. Hagberg. 2001. Bacterial endotoxin sensitizes the immature brain to hypoxic–ischaemic injury. *European Journal of Neuroscience*. 13:1101-1106.

Elmahdy, H., A.-R. El-Mashad, H. El-Bahrawy, T. El-Gohary, A. El-Barbary, and H. Aly. 2010. Human recombinant erythropoietin in asphyxia neonatorum: pilot trial. *Pediatrics*. 125:e1135-1142.

Emsley, J.G., P. Arlotta, and J.D. Macklis. 2004. Star-cross'd neurons: astroglial effects on neural repair in the adult mammalian CNS. *Trends in neurosciences*. 27:238-240.

Engel, S.R., T.K. Creson, Y. Hao, Y. Shen, S. Maeng, T. Nekrasova, G.E. Landreth, H.K. Manji, and G. Chen. 2008. The extracellular signal-regulated kinase pathway contributes to the control of behavioral excitement. *Mol Psychiatry*. 14:448-461.

Fan, X., C.J. Heijnen, M.A. van der Kooij, F. Groenendaal, and F. van Bel. 2011. Beneficial Effect of Erythropoietin on Sensorimotor Function and White Matter After Hypoxia-Ischemia in Neonatal Mice. *Pediatr Res*. 69:56-61.

Fan, X., A. Kavelaars, C.J. Heijnen, F. Groenendaal, and F. van Bel. 2010. Pharmacological neuroprotection after perinatal hypoxic-ischemic brain injury. *Current neuropharmacology*. 8:324-334.

Faulkner, S., A. Bainbridge, T. Kato, M. Chandrasekaran, A.B. Kapetanakis, M. Hristova, M. Liu, S. Evans, E. De Vita, D. Kelen, R.D. Sanders, a.D. Edwards, M. Maze, E.B. Cady, G. Raivich, and N.J. Robertson. 2011. Xenon augmented hypothermia reduces early lactate/N-acetylaspartate and cell death in perinatal asphyxia. *Annals of neurology*. 70:133-150.

Feng, Y., P.G. Rhodes, and A.J. Bhatt. 2008. Neuroprotective effects of vascular endothelial growth factor following hypoxic ischemic brain injury in neonatal rats. *Pediatric research*. 64:370-374.

Fernandez, B.A., W. Roberts, B. Chung, R. Weksberg, S. Meyn, P. Szatmari, A.M. Joseph-George, S. MacKay, K. Whitten, B. Noble, C. Vardy, V. Crosbie, S. Luscombe, E. Tucker, L. Turner, C.R. Marshall, and S.W. Scherer. 2010. Phenotypic spectrum associated with de novo and inherited deletions and duplications at 16p11.2 in individuals ascertained for diagnosis of autism spectrum disorder. *Journal of Medical Genetics*. 47:195-203.

Ferrer, I., B. Friguls, E. Dalfó, and A.M. Planas. 2003. Early modifications in the expression of mitogen-activated protein kinase (MAPK/ERK), stress-activated kinases SAPK/JNK and p38, and their phosphorylated substrates following focal cerebral ischemia. *Acta Neuropathol*. 105:425-437.

Ferriero, D.M., D.M. Holtzman, S.M. Black, and R.A. Sheldon. 1996. Neonatal Mice Lacking Neuronal Nitric Oxide Synthase Are Less Vulnerable to Hypoxic–Ischemic Injury. *Neurobiology of Disease*. 3:64-71.

Fontana, X., M. Hristova, C. Da Costa, S. Patodia, L. Thei, M. Makwana, B. Spencer-Dene, M. Latouche, R. Mirsky, K.R. Jessen, R. Klein, G. Raivich, and A. Behrens. 2012. c-Jun in Schwann cells promotes axonal regeneration and motoneuron survival via paracrine signaling. *The Journal of cell biology*. 198:127-141.

Francisco, S., and L. Linda. 2005. Patterns of brain injury in term neonatal encephalopathy.

Fyffe-Maricich, S.L., J.C. Karlo, G.E. Landreth, and R.H. Miller. 2011. The ERK2 Mitogen-Activated Protein Kinase Regulates the Timing of Oligodendrocyte Differentiation. *The Journal of Neuroscience*. 31:843-850.

Gaffney, G., S. Sellers, V. Flavell, M. Squier, and A. Johnson. 1994. Case-control study of intrapartum care, cerebral palsy, and perinatal death. *BMJ*. 308.

Gao, K., C.R. Wang, F. Jiang, A.Y.K. Wong, N. Su, J.H. Jiang, R.C. Chai, G. Vatcher, J. Teng, J. Chen, Y.-W. Jiang, and A.C.H. Yu. 2013. Traumatic scratch injury in astrocytes triggers calcium influx to activate the JNK/c-Jun/AP-1 pathway and switch on GFAP expression. *Glia*. 61:2063-2077.

Gehrmann, J., R.B. Banati, C. Wiessnert, K.A. Hossmann, and G.W. Kreutzberg. 1995. Reactive microglia in cerebral ischaemia: an early mediator of tissue damage? *Neuropathology and Applied Neurobiology*. 21:277-289.

Giessel, A.J., and S.R. Datta. 2014. Olfactory maps, circuits and computations. *Current Opinion in Neurobiology*. 24:120-132.

Gilland, E., E. Bona, and H. Hagberg. 1998. Temporal changes of regional glucose use, blood flow, and microtubule-associated protein 2 immunostaining after hypoxia-ischemia

in the immature rat brain. *Journal of cerebral blood flow and metabolism : official journal of the International Society of Cerebral Blood Flow and Metabolism*. 18:222-228.

Ginet, V., J. Puyal, G. Magnin, P.G.H. Clarke, and A.C. Truttmann. 2009. Limited role of the c-Jun N-terminal kinase pathway in a neonatal rat model of cerebral hypoxia–ischemia. *Journal of Neurochemistry*. 108:552-562.

Ginhoux, F., M. Greter, M. Leboeuf, S. Nandi, P. See, S. Gokhan, M.F. Mehler, S.J. Conway, L.G. Ng, E.R. Stanley, I.M. Samokhvalov, and M. Merad. 2010. Fate Mapping Analysis Reveals That Adult Microglia Derive from Primitive Macrophages. *Science*. 330:841-845.

Ginhoux, F., S. Lim, G. Hoeffel, D. Low, and T. Huber. 2013. Origin and differentiation of microglia. *Frontiers in Cellular Neuroscience*. 7.

Girard, S., H. Kadhim, N. Beaudet, P. Sarret, and G. Sébire. 2009. Developmental motor deficits induced by combined fetal exposure to lipopolysaccharide and early neonatal hypoxia/ischemia: A novel animal model for cerebral palsy in very premature infants. *Neuroscience*. 158:673-682.

Gluckman, P.D., J.S. Wyatt, D. Azzopardi, R. Ballard, A.D. Edwards, D.M. Ferriero, R.A. Polin, C.M. Robertson, M. Thoresen, A. Whitelaw, and A.J. Gunn. 2005. Selective head cooling with mild systemic hypothermia after neonatal encephalopathy: multicentre randomised trial. *The Lancet*. 365:663-670.

Goldenberg, R.L., J.C. Hauth, and W.W. Andrews. 2000. Intrauterine Infection and Preterm Delivery. *New England Journal of Medicine*. 342:1500-1507.

Gorina, R., M. Font-Nieves, L. Márquez-Kisinousky, T. Santalucia, and A.M. Planas. 2011. Astrocyte TLR4 activation induces a proinflammatory environment through the interplay between MyD88-dependent NFκB signaling, MAPK, and Jak1/Stat1 pathways. *Glia*. 59:242-255.

Greenwood, C., P. Yudkin, S. Sellers, L. Impey, and P. Doyle. 2005. Why is there a modifying effect of gestational age on risk factors for cerebral palsy? *Archives of Disease in Childhood - Fetal and Neonatal Edition*. 90:F141-F146.

Greisen, G. 2005. Autoregulation of cerebral blood flow in newborn babies. *Early human development*. 81:423-428.

Gu, Z., Q. Jiang, and G. Zhang. 2001. Extracellular signal-regulated kinase 1/2 activation in hippocampus after cerebral ischemia may not interfere with postischemic cell death. *Brain Research*. 901:79-84.

Guan, Q.H., D.S. Pei, Y.Y. Zong, T.L. Xu, and G.Y. Zhang. 2006. Neuroprotection against ischemic brain injury by a small peptide inhibitor of c-Jun N-terminal kinase (JNK) via nuclear and non-nuclear pathways. *Neuroscience*. 139:609-627.

Guillemin, G.J., and B.J. Brew. 2004. Microglia, macrophages, perivascular macrophages, and pericytes: a review of function and identification. *Journal of Leukocyte Biology*. 75:388-397.

Gumy, L.F., C.L. Tan, and J.W. Fawcett. 2010. The role of local protein synthesis and degradation in axon regeneration. *Experimental Neurology*. 223:28-37.

Gunn, A.J., and L. Bennet. 2009. Fetal Hypoxia Insults and Patterns of Brain Injury: Insights from Animal Models. *Clinics in Perinatology*. 36:579-593.

Gunn, A.J., J.T. Parer, E.C. Mallard, C.E. Williams, and P.D. Gluckman. 1992. Cerebral Histologic and Electrocorticographic Changes after Asphyxia in Fetal Sheep. *Pediatr Res*. 31:486-491.

Guo, R.-B., G.-F. Wang, A.-P. Zhao, J. Gu, X.-L. Sun, and G. Hu. 2012. Paeoniflorin Protects against Ischemia-Induced Brain Damages in Rats via Inhibiting MAPKs/NF-κB-Mediated Inflammatory Responses. *PLoS ONE*. 7:e49701.

Gutiérrez-Castellanos, N., C. Pardo-Bellver, F. Martínez-García, and E. Lanuza. 2014. The vomeronasal cortex – afferent and efferent projections of the posteromedial cortical nucleus of the amygdala in mice. *European Journal of Neuroscience*. 39:141-158.

Hagberg, H., P. Gressens, and C. Mallard. 2012. Inflammation during fetal and neonatal life: implications for neurologic and neuropsychiatric disease in children and adults. *Annals of neurology*. 71:444-457.

Hagberg, H., R. Ichord, C. Palmer, J.Y. Yager, and S.J. Vannucci. 2002a. Animal Models of Developmental Brain Injury: Relevance to Human Disease. *Developmental Neuroscience*. 24:364-366.

Hagberg, H., and C. Mallard. 2005. Effect of inflammation on central nervous system development and vulnerability. *Current Opinion in Neurology*. 18:117-123.

Hagberg, H., C. Mallard, C. Rouseet, and X. Wang. 2009. Apoptotic mechanisms in the immature brain: involvement of mitochondria. *Journal of child …*. 24:1141-1146.

Hagberg, H., D. Peebles, and C. Mallard. 2002b. Models of white matter injury: Comparison of infectious, hypoxic-ischemic, and excitotoxic insults. *Mental Retardation and Developmental Disabilities Research Reviews*. 8:30-38.

Hambleton, J., S.L. Weinstein, L. Lem, and A.L. DeFranco. 1996. Activation of c-Jun N-terminal kinase in bacterial lipopolysaccharide-stimulated macrophages. *Proceedings of the National Academy of Sciences*. 93:2774-2778.

Han, B.H., and D.M. Holtzman. 2000. BDNF protects the neonatal brain from hypoxic-ischemic injury in vivo via the ERK pathway. *The Journal of neuroscience : the official journal of the Society for Neuroscience*. 20:5775-5781.

He, X., X.M. Zhang, J. Wu, J. Fu, L. Mou, D.H. Lu, Y. Cai, X.G. Luo, A. Pan, and X.X. Yan. 2014. Olfactory experience modulates immature neuron development in postnatal and adult guinea pig piriform cortex. *Neuroscience*. 259:101-112.

Hedtjärn, M., A.-L. Leverin, K. Eriksson, K. Blomgren, C. Mallard, and H. Hagberg. 2002. Interleukin-18 Involvement in Hypoxic–Ischemic Brain Injury. *The Journal of Neuroscience*. 22:5910-5919.

Hedtjärn, M., C. Mallard, Y. Iwakura, and H. Hagberg. 2005. Combined Deficiency of IL-1β18, but Not IL-1αβ, Reduces Susceptibility to Hypoxia-Ischemia in the Immature Brain. *Developmental Neuroscience*. 27:143-148.

Heinz, E.R., and J.M. Provenzale. 2009. Imaging findings in neonatal hypoxia: a practical review. *AJR. American journal of roentgenology*. 192:41-47.

Herdegen, T., F.-X. Claret, T. Kallunki, A. Martin-Villalba, C. Winter, T. Hunter, and M. Karin. 1998. Lasting N-Terminal Phosphorylation of c-Jun and Activation of c-Jun N-Terminal Kinases after Neuronal Injury. *The Journal of Neuroscience*. 18:5124-5135.

Herdegen, T., P. Skene, and M. Bähr. 1997. The c-Jun transcription factor – bipotential mediator of neuronal death, survival and regeneration. *Trends in Neurosciences*. 20:227-231.

Hickey, W.F., K. Vass, and H. Lassmann. 1992. Bone Marrow-derived Elements in the Central Nervous System: An Immunohistochemical and Ultrastructural Survey of Rat Chimeras. *Journal of Neuropathology & Experimental Neurology*. 51.

Hidding, U., K. Mielke, V. Waetzig, S. Brecht, U. Hanisch, A. Behrens, E. Wagner, and T. Herdegen. 2002. The c-Jun N-terminal kinases in cerebral microglia: immunological functions in the brain. *Biochemical pharmacology*. 64:781-788.

Higgins, R.D., and S. Shankaran. 2009. Hypothermia for hypoxic ischemic encephalopathy in infants ≥36weeks. *Early human development*. 85:S49-S52.

Himpens, E., C. Van den Broeck, a. Oostra, P. Calders, and P. Vanhaesebrouck. 2008. Prevalence, type, distribution, and severity of cerebral palsy in relation to

gestational age: a meta-analytic review. *Developmental medicine and child neurology*. 50:334-340.

Ho, Y., R. Samarasinghe, M.E. Knoch, M. Lewis, E. Aizenman, and D.B. Defranco. 2008. Selective Inhibition of Mitogen-Activated Protein Kinase Phosphatases by Zinc Accounts for Extracellular Neuronal Cell Death. 74:1141-1151.

Hong, S.J., T.M. Dawson, and V.L. Dawson. 2004. Nuclear and mitochondrial conversations in cell death: PARP-1 and AIF signaling. *Trends in pharmacological sciences*. 25:259-264.

Hristova, M., D. Cuthill, V. Zbarsky, A. Acosta-Saltos, A. Wallace, K. Blight, S.M.K. Buckley, D. Peebles, H. Heuer, S.N. Waddington, and G. Raivich. 2010. Activation and deactivation of periventricular white matter phagocytes during postnatal mouse development. *Glia*. 58:11-28.

Huang, B.Y., and M. Castillo. 2008. Hypoxic-Ischemic Brain Injury: Imaging Findings from Birth to Adulthood. *RadioGraphics*. 28:417-439.

Huang, G., L. Shi, and H. Chi. 2009. Regulation of JNK and p38 MAPK in the immune system: signal integration, propagation and termination. *Cytokine*. 48:161-169.

Impey, L., C. Greenwood, K. MacQuillan, M. Reynolds, and O. Sheil. 2001. Fever in labour and neonatal encephalopathy: a prospective cohort study. *BJOG: An International Journal of Obstetrics & Gynaecology*. 108:594-597.

Infante, S.K., A.F. Oberhauser, and J.R. Perez-Polo. 2013. Bax phosphorylation association with nucleus and oligomerization after neonatal hypoxia-ischemia. *Journal of neuroscience research*. 91:1152-1164.

Irving, E.a., and M. Bamford. 2002. Role of mitogen- and stress-activated kinases in ischemic injury. *Journal of cerebral blood flow and metabolism : official journal of the International Society of Cerebral Blood Flow and Metabolism*. 22:631-647.

Iwata, O., J.S. Thornton, M.W. Sellwood, S. Iwata, Y. Sakata, M.A. Noone, F.E. O'Brien, A. Bainbridge, E. De Vita, G. Raivich, D. Peebles, F. Scaravilli, E.B. Cady, R. Ordidge, J.S. Wyatt, and N.J. Robertson. 2005. Depth of delayed cooling alters neuroprotection pattern after hypoxia-ischemia. *Annals of Neurology*. 58:75-87.

Jã, K., a.S. Naylor, J. Dean, H. Hagberg, C. Mallard, and K. Järlestedt. 2013. Decreased survival of newborn neurons in the dorsal hippocampus after neonatal LPS exposure in mice. *Neuroscience*. 253:21-28.

Jacobs, S.E. 2005. Selective head cooling with mild systemic hypothermia after neonatal encephalopathy: multicentre randomised trial. *The Journal of pediatrics*. 147:122-123.

Järlestedt, K., A.S. Naylor, J. Dean, H. Hagberg, and C. Mallard. 2013. Decreased survival of newborn neurons in the dorsal hippocampus after neonatal LPS exposure in mice. *Neuroscience*. 253:21-28.

Jatana, M., I. Singh, A.K. Singh, and D. Jenkins. 2006. Combination of systemic hypothermia and N-acetylcysteine attenuates hypoxic-ischemic brain injury in neonatal rats. *Pediatric research*. 59:684-689.

Jeffrey, K.L., T. Brummer, M.S. Rolph, S.M. Liu, N.a. Callejas, R.J. Grumont, C. Gillieron, F. Mackay, S. Grey, M. Camps, C. Rommel, S.D. Gerondakis, and C.R. Mackay. 2006. Positive regulation of immune cell function and inflammatory responses by phosphatase PAC-1. *Nature immunology*. 7:274-283.

Jiang-Qin Liu, Tze-Fun Lee, Chao Chen, David L. Bagim, and Po-Yin Cheung. 2010. N-Acetylcysteine Improves Hemodynamics and Reduces Oxidative Stress in the Brains of Newborn Piglets with Hypoxia-Reoxygenation Injury. *Journal of Neurotrauma*. 27:1865-1873.

Jiang, Z., Y. Zhang, X. Chen, P.Y. Lam, H. Yang, Q. Xu, and A.C.H. Yu. 2002. Activation of Erk1/2 and Akt in astrocytes under ischemia. *Biochemical and Biophysical Research Communications*. 294:726-733.

Jin, K., X.O. Mao, Y. Zhu, and D.a. Greenberg. 2002. MEK and ERK protect hypoxic cortical neurons via phosphorylation of Bad. *Journal of neurochemistry*. 80:119-125.

Johnston, M.V., W. Nakajima, and H. Hagberg. 2002. Mechanisms of Hypoxic Neurodegeneration in the Developing Brain. *The Neuroscientist*. 8:212-220.

Johnston, M.V., W.H. Trescher, A. Ishida, W. Nakajima, and A. Zipursky. 2001. The Developing Nervous System: A Series of Review Articles: Neurobiology of Hypoxic-Ischemic Injury in the Developing Brain. *Pediatr Res*. 49:735-741.

Jones, M.W., E. Morgan, J.E. Shelton, and C. Thorogood. 2007. Cerebral Palsy: Introduction and Diagnosis (Part I). *Journal of pediatric health care : official publication of National Association of Pediatric Nurse Associates & Practitioners*. 21:146-152.

Jones, N.M., and M. Bergeron. 2004. Hypoxia-induced ischemic tolerance in neonatal rat brain involves enhanced ERK1/2 signaling. *Journal of neurochemistry*. 89:157-167.

Junttila, M.R., S.-P. Li, and J. Westermarck. 2008. Phosphatase-mediated crosstalk between MAPK signaling pathways in the regulation of cell survival. *The FASEB journal : official publication of the Federation of American Societies for Experimental Biology*. 22:954-965.

Kamakura, S., T. Moriguchi, and E. Nishida. 1999. Activation of the Protein Kinase ERK5/BMK1 by Receptor Tyrosine Kinases: IDENTIFICATION AND CHARACTERIZATION OF A SIGNALING PATHWAY TO THE NUCLEUS. *Journal of Biological Chemistry*. 274:26563-26571.

Kaminska, B., A. Gozdz, M. Zawadzka, A. Ellert-Miklaszewska, and M. Lipko. 2009. MAPK signal transduction underlying brain inflammation and gliosis as therapeutic target. *Anatomical record (Hoboken, N.J. : 2007)*. 292:1902-1913.

Kaur, C., and E.a. Ling. 2009. Periventricular white matter damage in the hypoxic neonatal brain: role of microglial cells. *Progress in neurobiology*. 87:264-280.

Kavčič, A., and D.B. Vodušek. 2005. A historical perspective on cerebral palsy as a concept and a diagnosis. *European Journal of Neurology*. 12:582-587.

Kayahara, M., X. Wang, and C. Tournier. 2005. Selective Regulation of c-jun Gene Expression by Mitogen-Activated Protein Kinases via the 12-O-Tetradecanoylphorbol-13-Acetate- Responsive Element and Myocyte Enhancer Factor 2 Binding Sites. *Molecular and Cellular Biology*. 25:3784-3792.

Kendall, G.S., M. Hristova, M. Hirstova, S. Horn, D. Dafou, A. Acosta-Saltos, B. Almolda, V. Zbarsky, P. Rumajogee, H. Heuer, B. Castellano, K. Pfeffer, S.a. Nedospasov, D.M. Peebles, and G. Raivich. 2011a. TNF gene cluster deletion abolishes lipopolysaccharide-mediated sensitization of the neonatal brain to hypoxic ischemic insult. *Laboratory investigation; a journal of technical methods and pathology*. 91:328-341.

Kendall, G.S., M. Hristova, V. Zbarsky, A. Clements, D.M. Peebles, N.J. Robertson, and G. Raivich. 2011b. Distribution of pH changes in mouse neonatal hypoxic-ischaemic insult. *Developmental neuroscience*. 33:505-518.

Kendall, G.S., N.J. Robertson, O. Iwata, D. Peebles, and G. Raivich. 2006. N-Methyl-isobutyl-amiloride Ameliorates Brain Injury When Commenced Before Hypoxia Ischemia in Neonatal Mice. *Pediatr Res*. 59:227-231.

Kim, E.K., and E.-J. Choi. 2010. Pathological roles of MAPK signaling pathways in human diseases. *Biochimica et biophysica acta*. 1802:396-405.

Kim, G., J.M. Han, and S. Kim. 2010. Toll-like receptor 4-mediated c-Jun N-terminal kinase activation induces gp96 cell surface expression via AIMP1 phosphorylation. *Biochemical and Biophysical Research Communications*. 397:100-105.

Kim, R., M. Emi, K. Tanabe, S. Murakami, Y. Uchida, and K. Arihiro. 2006. Regulation and interplay of apoptotic and non-apoptotic cell death. *The Journal of Pathology*. 208:319-326.

Kinouchi, R., M. Takeda, L. Yang, U. Wilhelmsson, A. Lundkvist, M. Pekny, and D.F. Chen. 2003. Robust neural integration from retinal transplants in mice deficient in GFAP and vimentin. *Nat Neurosci*. 6:863-868.

Kitagawa, K. 2012. Ischemic tolerance in the brain: endogenous adaptive machinery against ischemic stress. *Journal of neuroscience research*. 90:1043-1054.

Kohno, H., T. Sakai, and K. Kitahara. 2006. Induction of nestin, Ki-67, and cyclin D1 expression in Müller cells after laser injury in adult rat retina. *Graefe's Arch Clin Exp Ophthalmo*. 244:90-95.

Kondoh, T., H. Uneyama, H. Nishino, and K. Torii. 2002. Melatonin reduces cerebral edema formation caused by transient forebrain ischemia in rats. *Life Sciences*. 72:583-590.

Krägeloh-Mann, I., A. Helber, I. Mader, M. Staudt, M. Wolff, F. Groenendaal, and L. DeVries. 2002. Bilateral lesions of thalamus and basal ganglia: origin and outcome. *Developmental medicine and child neurology*. 44:477-484.

Kreutzberg, G.W. 1996. Microglia: a sensor for pathological events in the CNS. *Trends in Neurosciences*. 19:312-318.

Kuan, C.-Y., A.J. Whitmarsh, D.D. Yang, G. Liao, A.J. Schloemer, C. Dong, J. Bao, K.J. Banasiak, G.G. Haddad, R.A. Flavell, R.J. Davis, and P. Rakic. 2003. A critical role of neural-specific JNK3 for ischemic apoptosis. *Proceedings of the National Academy of Sciences*. 100:15184-15189.

Kwok-Tung Lu, C.-L.S., Peter Y.Y. Wo, Hao-Han Yen, Tsao-Hao Tang, Ming-Chong Ng, Min-Lang Huang, Yi-Ling Yang. 2011. Hippocampal Neurogenesis after Traumatic Brain Injury Is Mediated by Vascular Endothelial Growth Factor Receptor-2 and the Raf/MEK/ERK Cascade. *Journal of Neurotrauma*. 28:441-450.

Lee, S.M., T.H.N. Nguyen, M.H. Park, K.S. Kim, K.J. Cho, D.C. Moon, H.Y. Kim, D.Y. Yoon, and J.T. Hong. 2004. EPO receptor-mediated ERK kinase and NF-kappaB activation in erythropoietin-promoted differentiation of astrocytes. *Biochemical and biophysical research communications*. 320:1087-1095.

Lee, W., P. Mitchell, and R. Tjian. 1987. Purified transcription factor AP-1 interacts with TPA-inducible enhancer elements. *Cell*. 49:741-752.

Lefloch, R., J. Pouysségur, and P. Lenormand. 2008. Single and combined silencing of ERK1 and ERK2 reveals their positive contribution to growth signaling depending on their expression levels. *Molecular and cellular biology*. 28:511-527.

Lehnardt, S., L. Massillon, P. Follett, F.E. Jensen, R. Ratan, P.a. Rosenberg, J.J. Volpe, and T. Vartanian. 2003. Activation of innate immunity in the CNS triggers neurodegeneration through a Toll-like receptor 4-dependent pathway. *Proceedings of the National Academy of Sciences of the United States of America*. 100:8514-8519.

Leppä, S., R. Saffrich, W. Ansorge, and D. Bohmann. 1998. Differential regulation of c-Jun by ERK and JNK during PC12 cell differentiation. *The EMBO Journal*. 17:4404-4413.

Lesuisse, C., and L.J. Martin. 2002. Immature and mature cortical neurons engage different apoptotic mechanisms involving caspase-3 and the mitogen-activated protein kinase pathway. *Journal of cerebral blood flow and metabolism : official journal of the International Society of Cerebral Blood Flow and Metabolism*. 22:935-950.

Levine, S. 1960. Anoxic-Ischemic Encephalopathy in Rats. *The American Journal of Pathology*. 36:1-17.

Li, L., A. Lundkvist, D. Andersson, U. Wilhelmsson, N. Nagai, A.C. Pardo, C. Nodin, A. Stahlberg, K. Aprico, K. Larsson, T. Yabe, L. Moons, A. Fotheringham, I. Davies, P. Carmeliet, J.P. Schwartz, M. Pekna, M. Kubista, F. Blomstrand, N. Maragakis, M.

Nilsson, and M. Pekny. 2007. Protective role of reactive astrocytes in brain ischemia. *J Cereb Blood Flow Metab*. 28:468-481.

Li, L., Y. Xiong, Y. Qu, M. Mao, W. Mu, H. Wang, and D. Mu. 2008. The requirement of extracellular signal-related protein kinase pathway in the activation of hypoxia inducible factor 1 alpha in the developing rat brain after hypoxia-ischemia. *Acta Neuropathol*. 115:297-303.

Lieberman, E., E. Eichenwald, G. Mathur, D. Richardson, L. Heffner, and A. Cohen. 2000. Intrapartum Fever and Unexplained Seizures in Term Infants. *Pediatrics*. 106:983-988.

Lindstrom, K., B. Hallberg, M. Blennow, K. Wolff, E. Fernell, and M. Westgren. 2008. Moderate neonatal encephalopathy: Pre- and perinatal risk factors and long-term outcome. *Acta Obstetricia et Gynecologica Scandinavica*. 87:503-509.

Lindström, K., P. Lagerroos, C. Gillberg, and E. Fernell. 2006. Teenage Outcome After Being Born at Term With Moderate Neonatal Encephalopathy. *Pediatric neurology*. 35:268-274.

Little, W.J. 1843. Course of Lectures on the Deformities of the Human Frame. *Clin Orthop Relat Res*. 470:1252-1256.

Liu, X.-H., D. Kwon, G.P. Schielke, G.-Y. Yang, F.S. Silverstein, and J.D.E. Barks. 1999. Mice Deficient in Interleukin-1 Converting Enzyme Are Resistant to Neonatal Hypoxic-Ischemic Brain Damage. *J Cereb Blood Flow Metab*. 19:1099-1108.

Liu, Y.-W., C.-C. Chen, J.-M. Wang, W.-C. Chang, Y.-C. Huang, S.-Y. Chung, B.-K. Chen, and J.-J. Hung. 2007. Role of transcriptional factors Sp1, c-Rel, and c-Jun in LPS-induced C/EBPdelta gene expression of mouse macrophages. *Cellular and molecular life sciences : CMLS*. 64:3282-3294.

Liu, Y., F.S. Silverstein, R. Skoff, and J.D.E. Barks. 2002. Hypoxic-ischemic oligodendroglial injury in neonatal rat brain. *Pediatric research*. 51:25-33.

Low, J.A., B.G. Lindsay, and E.J. Derrick. 1997. Threshold of metabolic acidosis associated with newborn complications. *American journal of obstetrics and gynecology*. 177:1391-1394.

Lu, Z., and S. Xu. 2006. ERK1/2 MAP kinases in cell survival and apoptosis. *IUBMB Life*. 58:621-631.

Luca, A.D., M.R. Maiello, A.D. Alessio, M. Pergameno, and N. Normanno. 2012. The RAS / RAF / MEK / ERK and the PI3K / AKT signalling pathways : role in cancer pathogenesis and implications for therapeutic approaches.17-27.

Luo, Y., and D.B. DeFranco. 2006. Opposing roles for ERK1/2 in neuronal oxidative toxicity: distinct mechanisms of ERK1/2 action at early versus late phases of oxidative stress. *The Journal of biological chemistry*. 281:16436-16442.

Ma, D., M. Hossain, A. Chow, M. Arshad, R.M. Battson, R.D. Sanders, H. Mehmet, A.D. Edwards, N.P. Franks, and M. Maze. 2005. Xenon and hypothermia combine to provide neuroprotection from neonatal asphyxia. *Annals of Neurology*. 58:182-193.

Ma, Y.-z., N. Ning, W.-b. He, J.-w. Li, J.-f. Hu, S.-f. Chu, and N.-h. Chen. 2013. Claulansine F promotes neuritogenesis in PC12 cells via the ERK signaling pathway. *Acta Pharmacol Sin*. 34:1499-1507.

Maki, Y., T.J. Bos, C. Davis, M. Starbuck, and P.K. Vogt. 1987. Avian sarcoma virus 17 carries the jun oncogene. *Proceedings of the National Academy of Sciences*. 84:2848-2852.

Mallard, C., A.-K. Welin, D. Peebles, H. Hagberg, and I. Kjellmer. 2003. White Matter Injury Following Systemic Endotoxemia or Asphyxia in the Fetal Sheep. *Neurochem Res*. 28:215-223.

Manabat, C., B.H. Han, M. Wendland, N. Derugin, C.K. Fox, J. Choi, D.M. Holtzman, D.M. Ferriero, and Z.S. Vexler. 2003. Reperfusion Differentially Induces Caspase-3

Activation in Ischemic Core and Penumbra After Stroke in Immature Brain. *Stroke*. 34:207-213.

Mann, M.A., C. Kinsley, J. Broida, and B. Svare. 1983. Infanticide exhibited by female mice: Genetic, developmental and hormonal influences. *Physiology & Behavior*. 30:697-702.

Marlow, N., A.S. Rose, C.E. Rands, and E.S. Draper. 2005. Neuropsychological and educational problems at school age associated with neonatal encephalopathy. *Archives of Disease in Childhood - Fetal and Neonatal Edition*. 90:F380-F387.

Martin, D.P., R.E. Schmidt, P.S. DiStefano, O.H. Lowry, J.G. Carter, and E.M. Johnson. 1988. Inhibitors of protein synthesis and RNA synthesis prevent neuronal death caused by nerve growth factor deprivation. *The Journal of Cell Biology*. 106:829-844.

Martin, P., and P. Pognonec. 2010. ERK and cell death: cadmium toxicity, sustained ERK activation and cell death. *FEBS Journal*. 277:39-46.

Matsumoto, N., R. Imamura, and T. Suda. 2007. Caspase-8- and JNK-dependent AP-1 activation is required for Fas ligand-induced IL-8 production. *FEBS Journal*. 274:2376-2384.

McColl, B.W., H.V. Carswell, J. McCulloch, and K. Horsburgh. 2004. Extension of cerebral hypoperfusion and ischaemic pathology beyond MCA territory after intraluminal filament occlusion in C57Bl/6J mice. *Brain research*. 997:15-23.

Mebratu, Y., and Y. Tesfaigzi. 2009. How ERK1/2 activation controls cell proliferation and cell death: Is subcellular localization the answer? *Cell cycle (Georgetown, Tex.)*. 8:1168-1175.

Meng, Q., and Y. Xia. 2011. c-Jun, at the crossroad of the signaling network. *Protein & Cell*. 2:889-898.

Michiels, C., E. Minet, G. Michel, D. Mottet, J.P. Piret, and M. Raes. 2001. HIF-1 and AP-1 cooperate to increase gene expression in hypoxia: role of MAP kinases. *IUBMB life*. 52:49-53.

Miller, S., E. Yan, M. Castillo-Meléndez, G. Jenkin, and D. Walker. 2005. Melatonin provides neuroprotection in the late-gestation fetal sheep brain in response to umbilical cord occlusion. *Developmental Neuroscience*. 27:200-210.

Min, L., Y. Ji, L. Bakiri, Z. Qiu, J. Cen, X. Chen, L. Chen, H. Scheuch, H. Zheng, L. Qin, K. Zatloukal, L. Hui, and E.F. Wagner. 2012. Liver cancer initiation is controlled by AP-1 through SIRT6-dependent inhibition of survivin. *Nat Cell Biol*. 14:1203-1211.

Mody, N.Y., J. Leitch, C. Armstrong, J. Dixon, and P. Cohen. 2001. Effects of MAP kinase cascade inhibitors on the MKK5 / ERK5 pathway. 502:21-24.

Mori, T., N. Tateishi, Y. Kagamiishi, T. Shimoda, S. Satoh, S. Ono, N. Katsube, and T. Asano. 2004. Attenuation of a delayed increase in the extracellular glutamate level in the peri-infarct area following focal cerebral ischemia by a novel agent ONO-2506. *Neurochemistry International*. 45:381-387.

Morris, E.J., S. Jha, C.R. Restaino, P. Dayananth, H. Zhu, A. Cooper, D. Carr, Y. Deng, W. Jin, S. Black, B. Long, J. Liu, E. DiNunzio, W. Windsor, R. Zhang, S. Zhao, M.H. Angagaw, E.M. Pinheiro, J. Desai, L. Xiao, G. Shipps, A. Hruza, J. Wang, J. Kelly, S. Paliwal, X. Gao, B.S. Babu, L. Zhu, P. Daublain, L. Zhang, B.A. Lutterbach, M.R. Pelletier, U. Philippar, P. Siliphaivanh, D. Witter, P. Kirschmeier, W.R. Bishop, D. Hicklin, D.G. Gilliland, L. Jayaraman, L. Zawel, S. Fawell, and A.A. Samatar. 2013. Discovery of a Novel ERK Inhibitor with Activity in Models of Acquired Resistance to BRAF and MEK Inhibitors. *Cancer Discovery*. 3:742-750.

Morton, S., R.J. Davis, A. McLaren, and P. Cohen. 2003. A reinvestigation of the multisite phosphorylation of the transcription factor c-Jun. *The EMBO Journal*. 22:3876-3886.

Mrsić-Pelcić, J., G. Pelcić, D. Vitezić, D. Ljubicić, G. Zupan, and A. Simonić. 2008. Activation of ERK and JNK MAP kinases in optic nerves of rats exposed to global cerebral ischemia. *Psychiatria Danubina*. 20:456-460.

Munell, F., R.E. Burke, A. Bandele, and R.M. Gubits. 1994. Localization of c-fos, c-jun, and hsp70 mRNA expression in brain after neonatal hypoxia-ischemia. *Developmental Brain Research*. 77:111-121.

Murgas, P., F.A. Cornejo, G. Merino, and R. Bernhardi. 2014. SR-A Regulates the Inflammatory Activation of Astrocytes. *Neurotox Res*. 25:68-80.

Nacher, J., G. Alonso-Llosa, D. Rosell, and B. McEwen. 2002. PSA-NCAM expression in the piriform cortex of the adult rat. Modulation by NMDA receptor antagonist administration. *Brain Research*. 927:111-121.

Nadjar, a., C. Combe, P. Busquet, R. Dantzer, and P. Parnet. 2005. Signaling pathways of interleukin-1 actions in the brain: anatomical distribution of phospho-ERK1/2 in the brain of rat treated systemically with interleukin-1beta. *Neuroscience*. 134:921-932.

Nair, S., H. Hagberg, R. Krishnamurthy, C. Thornton, and C. Mallard. 2013. Death associated protein kinases: molecular structure and brain injury. *International journal of molecular sciences*. 14:13858-13872.

Namura, S., K. Iihara, S. Takami, I. Nagata, H. Kikuchi, K. Matsushita, M.a. Moskowitz, J.V. Bonventre, and a. Alessandrini. 2001. Intravenous administration of MEK inhibitor U0126 affords brain protection against forebrain ischemia and focal cerebral ischemia. *Proceedings of the National Academy of Sciences of the United States of America*. 98:11569-11574.

Napoli, I., L.a. Noon, S. Ribeiro, A.P. Kerai, S. Parrinello, L.H. Rosenberg, M.J. Collins, M.C. Harrisingh, I.J. White, A. Woodhoo, and A.C. Lloyd. 2012. A central role for the ERK-signaling pathway in controlling Schwann cell plasticity and peripheral nerve regeneration in vivo. *Neuron*. 73:729-742.

Narasimhan, P., J. Liu, Y.S. Song, J.L. Massengale, and P.H. Chan. 2009. VEGF Stimulates the ERK 1/2 signaling pathway and apoptosis in cerebral endothelial cells after ischemic conditions. *Stroke; a journal of cerebral circulation*. 40:1467-1473.

Nekrasova, T., C. Shive, Y. Gao, K. Kawamura, R. Guardia, G. Landreth, and T.G. Forsthuber. 2005. ERK1-deficient mice show normal T cell effector function and are highly susceptible to experimental autoimmune encephalomyelitis. *Journal of immunology (Baltimore, Md. : 1950)*. 175:2374-2380.

Neumann, J., M. Gunzer, H.O. Gutzeit, O. Ullrich, K.G. Reymann, and K. Dinkel. 2006. Microglia provide neuroprotection after ischemia. *The FASEB Journal*.

Newbern, J.M., X. Li, S.E. Shoemaker, J. Zhou, J. Zhong, Y. Wu, D. Bonder, S. Hollenback, G. Coppola, D.H. Geschwind, G.E. Landreth, and W.D. Snider. 2011. Specific functions for ERK/MAPK signaling during PNS development. *Neuron*. 69:91-105.

Nieto-Sampedro, M. 1999. Neurite Outgrowth Inhibitors in Gliotic Tissue. *In* The Functional Roles of Glial Cells in Health and Disease. Vol. 468. R. Matsas and M. Tsacopoulos, editors. Springer US. 207-224.

Niijima, S., D.B. Shortland, M.I. Levene, and D.H. Evans. 1988. Transient hyperoxia and cerebral blood flow velocity in infants born prematurely and at full term. *Archives of Disease in Childhood*. 63:1126-1130.

Nijboer, C.H., H.J.C. Bonestroo, J. Zijlstra, A. Kavelaars, and C.J. Heijnen. 2013. Mitochondrial JNK phosphorylation as a novel therapeutic target to inhibit neuroinflammation and apoptosis after neonatal ischemic brain damage. *Neurobiology of disease*. 54:432-444.

Nijboer, C.H., C.J. Heijnen, F. Groenendaal, F. van Bel, and A. Kavelaars. 2009. Alternate pathways preserve tumor necrosis factor-alpha production after nuclear factor-

kappaB inhibition in neonatal cerebral hypoxia-ischemia. *Stroke; a journal of cerebral circulation*. 40:3362-3368.

Nijboer, C.H., M.a. van der Kooij, F. van Bel, F. Ohl, C.J. Heijnen, and A. Kavelaars. 2010. Inhibition of the JNK/AP-1 pathway reduces neuronal death and improves behavioral outcome after neonatal hypoxic-ischemic brain injury. *Brain, behavior, and immunity*. 24:812-821.

Nishimoto, S., and E. Nishida. 2006. MAPK signalling: ERK5 versus ERK1/2. *EMBO reports*. 7:782-786.

Niu, F.-n., X. Zhang, X.-m. Hu, J. Chen, L.-l. Chang, J.-w. Li, Z. Liu, W. Cao, and Y. Xu. 2012. Targeted mutation of Fas ligand gene attenuates brain inflammation in experimental stroke. *Brain, Behavior, and Immunity*. 26:61-71.

Northington, F.J. 2006. Brief update on animal models of hypoxic-ischemic encephalopathy and neonatal stroke. *ILAR journal / National Research Council, Institute of Laboratory Animal Resources*. 47:32-38.

Northington, F.J., R. Chavez-Valdez, and L.J. Martin. 2011. Neuronal cell death in neonatal hypoxia-ischemia. *Annals of neurology*. 69:743-758.

Noshita, N., T. Sugawara, T. Hayashi, A. Lewén, G. Omar, and P.H. Chan. 2002. Copper/zinc superoxide dismutase attenuates neuronal cell death by preventing extracellular signal-regulated kinase activation after transient focal cerebral ischemia in mice. *The Journal of neuroscience : the official journal of the Society for Neuroscience*. 22:7923-7930.

Nowak, G., G.L. Clifton, M.L. Godwin, and D. Bakajsova. 2006. Activation of ERK1/2 pathway mediates oxidant-induced decreases in mitochondrial function in renal cells. *American Journal of Physiology - Renal Physiology*. 291:F840-F855.

Nowak, G.y. 2002. Protein Kinase C-α and ERK1/2 Mediate Mitochondrial Dysfunction, Decreases in Active Na+ Transport, and Cisplatin-induced Apoptosis in Renal Cells. *Journal of Biological Chemistry*. 277:43377-43388.

Olson, E.E., and R.J. McKeon. 2004. Characterization of cellular and neurological damage following unilateral hypoxia/ischemia. *Journal of the neurological sciences*. 227:7-19.

Ortiz, J., H.W. Harris, X. Guitart, R.Z. Terwilliger, J.W. Haycock, and E.J. Nestler. 1995. Extracellular signal-regulated protein kinases (ERKs) and ERK kinase (MEK) in brain: regional distribution and regulation by chronic morphine. *The Journal of neuroscience : the official journal of the Society for Neuroscience*. 15:1285-1297.

Paco, C., J. Florido, M. Garrido, S. Prados, and L. Navarrete. 2011. Umbilical cord blood acid–base and gas analysis after early versus delayed cord clamping in neonates at term. *Arch Gynecol Obstet*. 283:1011-1014.

Pan, J., Q. Xiao, C.-Y. Sheng, Z. Hong, H.-Q. Yang, G. Wang, J.-Q. Ding, and S.-D. Chen. 2009. Blockade of the translocation and activation of c-Jun N-terminal kinase 3 (JNK3) attenuates dopaminergic neuronal damage in mouse model of Parkinson's disease. *Neurochemistry International*. 54:418-425.

Panerai, R.B., A.W.R. Kelsall, J.M. Rennie, and D.H. Evans. 1995. Cerebral Autoregulation Dynamics in Premature Newborns. *Stroke*. 26:74-80.

Paneth, N. 2008. Establishing the Diagnosis of Cerebral Palsy. *Clinical Obstetrics and Gynecology*. 51:742-748.

Panteliadis, C., P. Panteliadis, and F. Vassilyadi. 2013. Hallmarks in the history of cerebral palsy: From antiquity to mid-20th century. *Brain and Development*. 35:285-292.

Peebles, D., and M. Hanson. 2002. Antepartum hypoxia and the developing fetus. *In* Birth Asphyxia and the Brain. Futura Publishing Co., New York. 215-241.

Peebles, D.M., and J.S. Wyatt. 2002. Synergy between antenatal exposure to infection and intrapartum events in causation of perinatal brain injury at term. *BJOG: An International Journal of Obstetrics & Gynaecology*. 109:737-739.

Pei, J.-J., H. Braak, W.-L. An, B. Winblad, R.F. Cowburn, K. Iqbal, and I. Grundke-Iqbal. 2002. Up-regulation of mitogen-activated protein kinases ERK1/2 and MEK1/2 is associated with the progression of neurofibrillary degeneration in Alzheimer's disease. *Molecular Brain Research*. 109:45-55.

Perlson, E., I. Michaelevski, N. Kowalsman, K. Ben-Yaakov, M. Shaked, R. Seger, M. Eisenstein, and M. Fainzilber. 2006. Vimentin Binding to Phosphorylated Erk Sterically Hinders Enzymatic Dephosphorylation of the Kinase. *Journal of Molecular Biology*. 364:938-944.

Perrone, S., G. Stazzoni, M.L. Tataranno, and G. Buonocore. 2012. New pharmacologic and therapeutic approaches for hypoxic-ischemic encephalopathy in the newborn. *Journal of Maternal-Fetal and Neonatal Medicine*. 25:83-88.

Perrone, S., L.M. Tataranno, G. Stazzoni, L. Ramenghi, and G. Buonocore. 2013. Brain susceptibility to oxidative stress in the perinatal period. *The journal of maternal-fetal & neonatal medicine : the official journal of the European Association of Perinatal Medicine, the Federation of Asia and Oceania Perinatal Societies, the International Society of Perinatal Obstetricians*. 7058:1-5.

Persons, D.L., E.M. Yazlovitskaya, and J.C. Pelling. 2000. Effect of Extracellular Signal-regulated Kinase on p53 Accumulation in Response to Cisplatin. *Journal of Biological Chemistry*. 275:35778-35785.

Pharoah, P.O.D., T. Cooke, M.A. Johnson, R. King, and L. Mutch. 1998. Epidemiology of cerebral palsy in England and Scotland, 1984–9. *Archives of Disease in Childhood - Fetal and Neonatal Edition*. 79:F21-F25.

Pirianov, G., K.G. Brywe, C. Mallard, a.D. Edwards, R.a. Flavell, H. Hagberg, and H. Mehmet. 2007. Deletion of the c-Jun N-terminal kinase 3 gene protects neonatal mice against cerebral hypoxic-ischaemic injury. *Journal of cerebral blood flow and metabolism : official journal of the International Society of Cerebral Blood Flow and Metabolism*. 27:1022-1032.

Pirianov, G., K.G. Brywe, C. Mallard, D. Edwards, R.A. Flavell, H. Hagberg, and H. Mehmet. 2006a. Deletion of the c-Jun N-terminal kinase 3 gene protects neonatal mice against cerebral hypoxic-ischaemic injury. *J Cereb Blood Flow Metab*. 27:1022-1032.

Pirianov, G., a. Jesurasa, and H. Mehmet. 2006b. Developmentally regulated changes in c-Jun N-terminal kinase signalling determine the apoptotic response of oligodendrocyte lineage cells. *Cell death and differentiation*. 13:531-533.

Plotnikov, A., E. Zehorai, S. Procaccia, and R. Seger. 2011. The MAPK cascades: signaling components, nuclear roles and mechanisms of nuclear translocation. *Biochimica et biophysica acta*. 1813:1619-1633.

Polazzi, E., and B. Monti. 2010. Microglia and neuroprotection: From in vitro studies to therapeutic applications. *Progress in Neurobiology*. 92:293-315.

Pouysségur, J., and P. Lenormand. 2003. Fidelity and spatio-temporal control in MAP kinase (ERKs) signalling. *European journal of biochemistry / FEBS*. 270:3291-3299.

Prins, M.L. 2007. Cerebral metabolic adaptation and ketone metabolism after brain injury. *J Cereb Blood Flow Metab*. 28:1-16.

Pucilowska, J., P.A. Puzerey, J.C. Karlo, R.F. Galán, and G.E. Landreth. 2012. Disrupted ERK Signaling during Cortical Development Leads to Abnormal Progenitor Proliferation, Neuronal and Network Excitability and Behavior, Modeling Human Neuro-Cardio-Facial-Cutaneous and Related Syndromes. *The Journal of Neuroscience*. 32:8663-8677.

Raivich, G. 2005. Like cops on the beat: the active role of resting microglia. *Trends in neurosciences*. 28:571-573.

Raivich, G. 2008. c-Jun Expression, activation and function in neural cell death, inflammation and repair. *Journal of Neurochemistry*. 107:898-906.

Raivich, G., M. Bohatschek, C. Da Costa, O. Iwata, M. Galiano, M. Hristova, A.S. Nateri, M. Makwana, L. Riera-Sans, D.P. Wolfer, H.-P. Lipp, A. Aguzzi, E.F. Wagner, and A. Behrens. 2004. The AP-1 transcription factor c-Jun is required for efficient axonal regeneration. *Neuron*. 43:57-67.

Raivich, G., M. Bohatschek, C.U.A. Kloss, A. Werner, L.L. Jones, and G.W. Kreutzberg. 1999. Neuroglial activation repertoire in the injured brain: graded response, molecular mechanisms and cues to physiological function. *Brain Research Reviews*. 30:77-105.

Repici, M., C. Centeno, S. Tomasi, G. Forloni, C. Bonny, A. Vercelli, and T. Borsello. 2007. Time-course of c-Jun N-terminal kinase activation after cerebral ischemia and effect of D-JNKI1 on c-Jun and caspase-3 activation. *Neuroscience*. 150:40-49.

Repici, M., L. Mare, A. Colombo, C. Ploia, A. Sclip, C. Bonny, P. Nicod, M. Salmona, and T. Borsello. 2009. c-Jun N-terminal kinase binding domain–dependent phosphorylation of mitogen-activated protein kinase kinase 4 and mitogen-activated protein kinase kinase 7 and balancing cross-talk between c-Jun N-terminal kinase and extracellular signal-regulated kinase pathways in cortical neurons. *Neuroscience*. 159:94-103.

Reynolds, A.J., I.A. Hendry, and S.E. Bartlett. 2001. Anterograde and retrograde transport of active extracellular signal-related kinase 1 (ERK1) in the ligated rat sciatic nerve. *Neuroscience*. 105:761-771.

Rezaie, P., and A. Dean. 2002. Periventricular leukomalacia, inflammation and white matter lesions within the developing nervous system. *Neuropathology*. 22:106-132.

Rice, J.E., R.C. Vannucci, and J.B. Brierley. 1981. The influence of immaturity on hypoxic-ischemic brain damage in the rat. *Annals of Neurology*. 9:131-141.

Roberts, P., and C. Der. 2007. Targeting the Raf-MEK-ERK mitogen-activated protein kinase cascade for the treatment of cancer. *Oncogene*. 26:3291-3310.

Robertson, C.M.T., N.N. Finer, and M.G.A. Grace. 1989. School performance of survivors of neonatal encephalopathy associated with birth asphyxia at term. *The Journal of Pediatrics*. 114:753-760.

Robertson, C.T., M. Watt, and Y. Yasui. 2007. Changes in the prevalence of cerebral palsy for children born very prematurely within a population-based program over 30 years. *JAMA*. 297:2733-2740.

Robertson, N.J., I.J. Cox, F.M. Cowan, S.J. Counsell, D. Azzopardi, and A.D. Edwards. 1999. Cerebral Intracellular Lactic Alkalosis Persisting Months after Neonatal Encephalopathy Measured by Magnetic Resonance Spectroscopy. *Pediatr Res*. 46:287-296.

Robertson, N.J., S. Faulkner, B. Fleiss, A. Bainbridge, C. Andorka, D. Price, E. Powell, L. Lecky-Thompson, L. Thei, M. Chandrasekaran, M. Hristova, E.B. Cady, P. Gressens, X. Golay, and G. Raivich. 2013. Melatonin augments hypothermic neuroprotection in a perinatal asphyxia model. *Brain : a journal of neurology*. 136:90-105.

Roohey, T., T.N. Raju, and a.N. Moustogiannis. 1997. Animal models for the study of perinatal hypoxic-ischemic encephalopathy: a critical analysis. *Early human development*. 47:115-146.

Rose, B.A.F.T.W.Y. 2010. Mitogen-Activated Protein Kinase Signaling in the Heart: Angels Versus Demons in a Heart-Breaking Tale. *Physiological Reviews*. 90:1507-1546.

Rosenblum, K., M. Futter, K. Voss, M. Erent, P.A. Skehel, P. French, L. Obosi, M.W. Jones, and T.V.P. Bliss. 2002. The Role of Extracellular Regulated Kinases I/II in Late-Phase Long-Term Potentiation. *The Journal of Neuroscience*. 22:5432-5441.

Roskoski, R. 2012. ERK1/2 MAP kinases: structure, function, and regulation. *Pharmacological research : the official journal of the Italian Pharmacological Society*. 66:105-143.

Rousset, C.I., C. Thornton, H. Hagberg, and A.a. Baburamani. 2012. Mitochondria and perinatal brain injury. *Journal of Maternal-Fetal and Neonatal Medicine*. 25:35-38.

Ruff, C.A., N. Staak, S. Patodia, M. Kaswich, E. Rocha-Ferreira, C. Da Costa, S. Brecht, M. Makwana, X. Fontana, M. Hristova, P. Rumajogee, M. Galiano, M. Bohatschek, T. Herdegen, A. Behrens, and G. Raivich. 2012. Neuronal c-Jun is required for successful axonal regeneration, but the effects of phosphorylation of its N-terminus are moderate. *Journal of Neurochemistry*. 121:607-618.

Runchel, C., A. Matsuzawa, and H. Ichijo. 2011. Mitogen-activated protein kinases in mammalian oxidative stress responses. *Antioxidants & redox signaling*. 15:205-218.

Rutherford, M., L. Srinivasan, L. Dyet, P. Ward, J. Allsop, S. Counsell, and F. Cowan. 2006. Magnetic resonance imaging in perinatal brain injury: clinical presentation, lesions and outcome. *Pediatr Radiol*. 36:582-592.

Sadeghi, K., A. Berger, M. Langgartner, A.-R. Prusa, M. Hayde, K. Herkner, A. Pollak, A. Spittler, and E. Förster-Waldl. 2007. Immaturity of Infection Control in Preterm and Term Newborns Is Associated with Impaired Toll-Like Receptor Signaling. *Journal of Infectious Diseases*. 195:296-302.

Saluja, I., M. O'Regan, D. Song, and J. Phillis. 1999. Activation of cPLA2, PKC, and ERKs in the Rat Cerebral Cortex During Ischemia/Reperfusion. *Neurochem Res*. 24:669-677.

Samuels, I.S., J.C. Karlo, A.N. Faruzzi, K. Pickering, K. Herrup, J.D. Sweatt, S.C. Saitta, and G.E. Landreth. 2008. Deletion of ERK2 Mitogen-Activated Protein Kinase Identifies Its Key Roles in Cortical Neurogenesis and Cognitive Function. *The Journal of Neuroscience*. 28:6983-6995.

Sánchez-Gómez, M., amp, x, V. a, and C. Matute. 1999. AMPA and Kainate Receptors Each Mediate Excitotoxicity in Oligodendroglial Cultures. *Neurobiology of Disease*. 6:475-485.

Sanchez-Niño, M.D., A.B. Sanz, C. Lorz, A. Gnirke, M.P. Rastaldi, V. Nair, J. Egido, M. Ruiz-Ortega, M. Kretzler, and A. Ortiz. 2010. BASP1 Promotes Apoptosis in Diabetic Nephropathy. *Journal of the American Society of Nephrology*. 21:610-621.

Sanders, R.D., H.J. Manning, N.J. Robertson, D. Ma, a.D. Edwards, H. Hagberg, and M. Maze. 2010. Preconditioning and postinsult therapies for perinatal hypoxic-ischemic injury at term. *Anesthesiology*. 113:233-249.

Santarpia, L., S. Lippman, and A. El-Nagger. 2012. Targeting the Mitogen-Activated Protein Kinase RAS-RAF Signaling Pathway in Cancer Therapy. *Expert opinion on therapeutic Targets*. 16:103-119.

Sawe, N., G. Steinberg, and H. Zhao. 2008. Dual roles of the MAPK/ERK1/2 cell signaling pathway after stroke. *Journal of neuroscience research*. 86:1659-1669.

Selcher, J.C., E.J. Weeber, J. Christian, T. Nekrasova, G.E. Landreth, and J.D. Sweatt. 2003. A Role for ERK MAP Kinase in Physiologic Temporal Integration in Hippocampal Area CA1. *Learning & Memory*. 10:26-39.

Sen, E., and S.W. Levison. 2006. Astrocytes and developmental white matter disorders. *Mental Retardation and Developmental Disabilities Research Reviews*. 12:97-104.

Shah, D.K., S. Lavery, L.W. Doyle, C. Wong, P. McDougall, and T.E. Inder. 2006. Use of 2-Channel Bedside Electroencephalogram Monitoring in Term-Born Encephalopathic Infants Related to Cerebral Injury Defined by Magnetic Resonance Imaging. *Pediatrics*. 118:47-55.

Shankaran, S., A.R. Laptook, R.A. Ehrenkranz, J.E. Tyson, S.A. McDonald, E.F. Donovan, A.A. Fanaroff, W.K. Poole, L.L. Wright, R.D. Higgins, N.N. Finer, W.A. Carlo, S. Duara, W. Oh, C.M. Cotten, D.K. Stevenson, B.J. Stoll, J.A. Lemons, R. Guillet, and A.H. Jobe.

2005. Whole-Body Hypothermia for Neonates with Hypoxic–Ischemic Encephalopathy. *New England Journal of Medicine*. 353:1574-1584.

Shaul, Y.D., and R. Seger. 2007. The MEK/ERK cascade: from signaling specificity to diverse functions. *Biochimica et biophysica acta*. 1773:1213-1226.

Sheldon, R.a., C. Sedik, and D.M. Ferriero. 1998. Strain-related brain injury in neonatal mice subjected to hypoxia-ischemia. *Brain research*. 810:114-122.

Shen, Y., H.-M. Yu, T.-M. Yuan, W.-Z. Gu, and Y.-D. Wu. 2009. Erythropoietin attenuates white matter damage, proinflammatory cytokine and chemokine induction in developing rat brain after intra-uterine infection. *Neuropathology : official journal of the Japanese Society of Neuropathology*. 29:528-535.

Shu Zhen, M., and S. Takashima. 1999. Expression of Transforming Growth Factor-β1 in Periventricular Leukomalacia. *Journal of Child Neurology*. 14:377-381.

Sie, L.T.L., M.S. van der Knaap, J. Oosting, L.S. de Vries, H.N. Lafeber, and J. Valk. 2000. MR Patterns of Hypoxic-Ischemic Brain Damage After Prenatal, Perinatal or Postnatal Asphyxia. *Neuropediatrics*. 31:128-136.

Signorini, C., L. Ciccoli, S. Leoncini, S. Carloni, S. Perrone, M. Comporti, W. Balduini, and G. Buonocore. 2009. Free iron, total F2-isoprostanes and total F4-neuroprostanes in a model of neonatal hypoxic–ischemic encephalopathy: neuroprotective effect of melatonin. *Journal of Pineal Research*. 46:148-154.

SilVerstein, F., K. Buchanan, and M.V. Johnston. 1984. Pathogenesis of hypoxic-ischemic brain injury in a perinatal rodent model. *Neuroscience Letters*. 49:271-277.

Skiöld, B., G. Alexandrou, N. Padilla, M. Blennow, B. Vollmer, and U. Ådén. 2014. Sex Differences in Outcome and Associations with Neonatal Brain Morphology in Extremely Preterm Children. *The Journal of pediatrics*.

Skoff, R.P., D.A. Bessert, J.D.E. Barks, D. Song, M. Cerghet, and F.S. Silverstein. 2001. Hypoxic–ischemic injury results in acute disruption of myelin gene expression and death of oligodendroglial precursors in neonatal mice. *International Journal of Developmental Neuroscience*. 19:197-208.

Sommer, C., P. Gass, and M. Kiessling. 1995. Selective c-JUN Expression in CA1 Neurons of the Gerbil Hippocampus during and after Acquisition of an Ischemia-Tolerant State. *Brain Pathology*. 5:135-144.

Stanciu, M. 2000. Persistent Activation of ERK Contributes to Glutamate-induced Oxidative Toxicity in a Neuronal Cell Line and Primary Cortical Neuron Cultures. *Journal of Biological Chemistry*. 275:12200-12206.

Streit, W.J. 1993. Microglial—Neuronal interactions. *Journal of Chemical Neuroanatomy*. 6:261-266.

Streja, E., C. Wu, P. Uldall, J. Grove, O. Arah, and J. Olsen. 2013. Congenital Cerebral Palsy, Child Sex and Parent Cardiovascular Risk. *PLoS ONE*. 8:e79071.

Suzumura, A., M. Sawada, H. Yamamoto, and T. Marunouchi. 1993. Transforming growth factor-beta suppresses activation and proliferation of microglia in vitro. *The Journal of Immunology*. 151:2150-2158.

Szydlowska, K., A. Gozdz, M. Dabrowski, M. Zawadzka, and B. Kaminska. 2010. Prolonged activation of ERK triggers glutamate-induced apoptosis of astrocytes: neuroprotective effect of FK506. *Journal of Neurochemistry*. 113:904-918.

Tanoue, T., M. Adachi, T. Moriguchi, and E. Nishida. 2000. A conserved docking motif in MAP kinases common to substrates, activators and regulators. *Nature cell biology*. 2:110-116.

Ten, V.S., E.X. Wu, H. Tang, M. Bradley-Moore, M.V. Fedarau, V.I. Ratner, R.I. Stark, J.A. Gingrich, and D.J. Pinsky. 2004. Late Measures of Brain Injury After Neonatal Hypoxia–Ischemia in Mice. *Stroke*. 35:2183-2188.

Thornton, C., C.I. Rousset, a. Kichev, Y. Miyakuni, R. Vontell, a.a. Baburamani, B. Fleiss, P. Gressens, and H. Hagberg. 2012. Molecular mechanisms of neonatal brain injury. *Neurol Res Int*. 2012:506320-506320.

Torii, K., H. Uneyama, H. Nishino, and T. Kondoh. 2004. Melatonin suppresses cerebral edema caused by middle cerebral artery occlusion/reperfusion in rats assessed by magnetic resonance imaging. *Journal of Pineal Research*. 36:18-24.

Tran, S.E.F., T.H. Holmström, M. Ahonen, V.-M. Kähäri, and J.E. Eriksson. 2001. MAPK/ERK Overrides the Apoptotic Signaling from Fas, TNF, and TRAIL Receptors. *Journal of Biological Chemistry*. 276:16484-16490.

Trujillo, J.I. 2011. MEK inhibitors: a patent review 2008 - 2010. *Expert opinion on therapeutic patents*. 21:1045-1069.

Uemura, Y., N.W. Kowall, and M.A. Moskowitz. 1991. Focal ischemia in rats causes time-dependent expression of c-fos protein immunoreactivity in widespread regions of ipsilateral cortex. *Brain Research*. 552:99-105.

van den Tweel, E.R.W., A. Kavelaars, M.S. Lombardi, C.H.A. Nijboer, F. Groenendaal, F. van Bel, and C.J. Heijnen. 2006. Bilateral Molecular Changes in a Neonatal Rat Model of Unilateral Hypoxic-Ischemic Brain Damage. *Pediatr Res*. 59:434-439.

van Velthoven, C.T.J., A. Kavelaars, F. van Bel, and C.J. Heijnen. 2010. Mesenchymal stem cell treatment after neonatal hypoxic-ischemic brain injury improves behavioral outcome and induces neuronal and oligodendrocyte regeneration. *Brain, behavior, and immunity*. 24:387-393.

Vannucci, R.C. 1990. Experimental biology of cerebral hypoxia-ischemia: relation to perinatal brain damage. *Pediatric research*. 27:317-326.

Vannucci, R.C., J. Towfighi, R.M. Brucklacher, and S.J. Vannucci. 2001. Effect of Extreme Hypercapnia on Hypoxic-Ischemic Brain Damage in the Immature Rat. *Pediatr Res*. 49:799-803.

Vannucci, R.C., and S.J. Vannucci. 1997. A model of Perinatal Hypoxic-Ischemic Brain Damagea. *Annals of the New York Academy of Sciences*. 835:234-249.

Vannucci, S.J., and H. Hagberg. 2004. Hypoxia–ischemia in the immature brain. *Journal of Experimental Biology*. 207:3149-3154.

Vantaggiato, C., I. Formentini, A. Bondanza, L. Naldini, and R. Brambilla. 2006. ERK1 and ERK2 mitogen-activated protein kinases affect Ras-dependent cell signaling differentially.1-15.

Varner, M.W., and M.S. Esplin. 2005. Current understanding of genetic factors in preterm birth. *BJOG: An International Journal of Obstetrics & Gynaecology*. 112:28-31.

Velier, J.J., J.A. Ellison, K.K. Kikly, P.A. Spera, F.C. Barone, and G.Z. Feuerstein. 1999. Caspase-8 and Caspase-3 Are Expressed by Different Populations of Cortical Neurons Undergoing Delayed Cell Death after Focal Stroke in the Rat. *The Journal of Neuroscience*. 19:5932-5941.

Vexler, Z.S., and D.M. Ferriero. 2001. Molecular and biochemical mechanisms of perinatal brain injury. *Seminars in neonatology : SN*. 6:99-108.

Vincent, P., and C. Mulle. 2009. Kainate receptors in epilepsy and excitotoxicity. *Neuroscience*. 158:309-323.

Vincent, V.A.M., F.J.H. Tilders, and A.M. Van Dam. 1997. Inhibition of endotoxin-induced nitric oxide synthase production in microglial cells by the presence of astroglial cells: A role for transforming growth factor β. *Glia*. 19:190-198.

Vincer, M.J., A.C. Allen, K.S. Joseph, D.A. Stinson, H. Scott, and E. Wood. 2006. Increasing Prevalence of Cerebral Palsy Among Very Preterm Infants: A Population-Based Study. *Pediatrics*. 118:e1621-e1626.

Vivès, E., P. Brodin, and B. Lebleu. 1997. A Truncated HIV-1 Tat Protein Basic Domain Rapidly Translocates through the Plasma Membrane and Accumulates in the Cell Nucleus. *Journal of Biological Chemistry*. 272:16010-16017.

Volpe, J.J. 2001. Neurobiology of Periventricular Leukomalacia in the Premature Infant. *Pediatr Res*. 50:553-562.

Vries, L., and F. Groenendaal. 2010. Patterns of neonatal hypoxic–ischaemic brain injury. *Neuroradiology*. 52:555-566.

Vries, R.G.J., M. Prudenziati, C. Zwartjes, M. Verlaan, E. Kalkhoven, and A. Zantema. 2001. A specific lysine in c-Jun is required for transcriptional repression by E1A and is acetylated by p300. *The EMBO Journal*. 20:6095-6103.

Vukojevic, K., D. Petrovic, and M. Saraga-Babic. 2010. Nestin expression in glial and neuronal progenitors of the developing human spinal ganglia. *Gene Expression Patterns*. 10:144-151.

Waetzig, V., K. Czeloth, U. Hidding, K. Mielke, M. Kanzow, S. Brecht, M. Goetz, R. Lucius, T. Herdegen, and U.-K. Hanisch. 2005. c-Jun N-terminal kinases (JNKs) mediate pro-inflammatory actions of microglia. *Glia*. 50:235-246.

Wagner, E.F., and A.R. Nebreda. 2009. Signal integration by JNK and p38 MAPK pathways in cancer development. *Nature reviews. Cancer*. 9:537-549.

Wakade, C., M.M. Khan, L.M. De Sevilla, Q.-G. Zhang, V.B. Mahesh, and D.W. Brann. 2008. Tamoxifen neuroprotection in cerebral ischemia involves attenuation of kinase activation and superoxide production and potentiation of mitochondrial superoxide dismutase. *Endocrinology*. 149:367-379.

Wallin, C., M. Puka-Sundvall, H. Hagberg, S.G. Weber, and M. Sandberg. 2000. Alterations in glutathione and amino acid concentrations after hypoxia–ischemia in the immature rat brain. *Developmental Brain Research*. 125:51-60.

Wang, G., J. Pan, and S. Chen. 2012a. Kinases and kinase signaling pathways: Potential therapeutic targets in Parkinson's disease. *Progress in Neurobiology*. 98:207-221.

Wang, J., T.R. Van De Water, C. Bonny, F. de Ribaupierre, J.L. Puel, and A. Zine. 2003a. A Peptide Inhibitor of c-Jun N-Terminal Kinase Protects against Both Aminoglycoside and Acoustic Trauma-Induced Auditory Hair Cell Death and Hearing Loss. *The Journal of Neuroscience*. 23:8596-8607.

Wang, L.-W., Y.-F. Tu, C.-C. Huang, and C.-J. Ho. 2012b. JNK signaling is the shared pathway linking neuroinflammation, blood-brain barrier disruption, and oligodendroglial apoptosis in the white matter injury of the immature brain. *Journal of neuroinflammation*. 9:175-175.

Wang, R.-M., Q.-G. Zhang, C.-H. Li, and G.-Y. Zhang. 2005. Activation of extracellular signal-regulated kinase 5 may play a neuroprotective role in hippocampal CA3/DG region after cerebral ischemia. *Journal of Neuroscience Research*. 80:391-399.

Wang, X., B. Nadarajah, A.C. Robinson, B.W. McColl, J.-W. Jin, F. Dajas-Bailador, R.P. Boot-Handford, and C. Tournier. 2007. Targeted Deletion of the Mitogen-Activated Protein Kinase Kinase 4 Gene in the Nervous System Causes Severe Brain Developmental Defects and Premature Death. *Molecular and Cellular Biology*. 27:7935-7946.

Wang, X., L. Stridh, W. Li, J. Dean, A. Elmgren, L. Gan, K. Eriksson, H. Hagberg, and C. Mallard. 2009. Lipopolysaccharide sensitizes neonatal hypoxic-ischemic brain injury in a MyD88-dependent manner. *Journal of immunology (Baltimore, Md. : 1950)*. 183:7471-7477.

Wang, X., H. Wang, L. Xu, D.J. Rozanski, T. Sugawara, P.H. Chan, J.M. Trzaskos, and G.Z. Feuerstein. 2003b. Significant neuroprotection against ischemic brain injury by inhibition of the MEK1 protein kinase in mice: exploration of potential mechanism

associated with apoptosis. *The Journal of pharmacology and experimental therapeutics*. 304:172-178.

Wang, X., C. Zhu, L. Qiu, H. Hagberg, M. Sandberg, and K. Blomgren. 2004a. Activation of ERK1/2 after neonatal rat cerebral hypoxia-ischaemia. *Journal of Neurochemistry*. 86:351-362.

Wang, Y.-N., Y.-J. Chen, and W.-C. Chang. 2006. Activation of Extracellular Signal-Regulated Kinase Signaling by Epidermal Growth Factor Mediates c-Jun Activation and p300 Recruitment in Keratin 16 Gene Expression. *Molecular Pharmacology*. 69:85-98.

Wang, Z.-Q., D.-C. Wu, F.-P. Huang, and G.-Y. Yang. 2004b. Inhibition of MEK/ERK 1/2 pathway reduces pro-inflammatory cytokine interleukin-1 expression in focal cerebral ischemia. *Brain Research*. 996:55-66.

Watts, B.A., T. George, E.R. Sherwood, and D.W. Good. 2011. Basolateral LPS inhibits NHE3 and HCO3− absorption through TLR4/MyD88-dependent ERK activation in medullary thick ascending limb. *American Journal of Physiology - Cell Physiology*. 301:C1296-C1306.

Weber, E.M., B. Algers, H. Würbel, J. Hultgren, and I.A.S. Olsson. 2013. Influence of Strain and Parity on the Risk of Litter Loss in Laboratory Mice. *Reproduction in Domestic Animals*. 48:292-296.

Welin, A.-K., P. Svedin, R. Lapatto, B. Sultan, H. Hagberg, P. Gressens, I. Kjellmer, and C. Mallard. 2007. Melatonin Reduces Inflammation and Cell Death in White Matter in the Mid-Gestation Fetal Sheep Following Umbilical Cord Occlusion. *Pediatr Res*. 61:153-158.

Weston, C.R., and R.J. Davis. 2002. The JNK signal transduction pathway. *Current opinion in genetics & development*. 12:14-21.

Whelan, J.T., S.E. Hollis, D.S. Cha, A.S. Asch, and M.-H. Lee. 2012. Post-transcriptional regulation of the Ras-ERK/MAPK signaling pathway. *Journal of cellular physiology*. 227:1235-1241.

Wu, Y.W., W.M. March, L.A. Croen, J.K. Grether, G.J. Escobar, and T.B. Newman. 2004. Perinatal Stroke in Children With Motor Impairment: A Population-Based Study. *Pediatrics*. 114:612-619.

Xiao, B.-G., X.-F. Bai, G.-X. Zhang, B. Hojeberg, and H. Link. 1996. Shift from anti- to proinflammatory cytokine profiles in microglia through LPS- or IFN-gamma-mediated pathways. *Neuroreport*. 7:1893-1898.

Xu, Z., B.-R. Wang, X. Wang, F. Kuang, X.-L. Duan, X.-Y. Jiao, and G. Ju. 2006. ERK1/2 and p38 mitogen-activated protein kinase mediate iNOS-induced spinal neuron degeneration after acute traumatic spinal cord injury. *Life sciences*. 79:1895-1905.

Yager, J.Y., R.M. Brucklacher, and R.C. Vannucci. 1992. Cerebral energy metabolism during hypoxia-ischemia and early recovery in immature rats. *American Journal of Physiology - Heart and Circulatory Physiology*. 262:H672-H677.

Yamasaki, T., H. Kawasaki, S. Arakawa, K. Shimizu, S. Shimizu, O. Reiner, H. Okano, S. Nishina, N. Azuma, J.M. Penninger, T. Katada, and H. Nishina. 2011. Stress-Activated Protein Kinase MKK7 Regulates Axon Elongation in the Developing Cerebral Cortex. *The Journal of Neuroscience*. 31:16872-16883.

Yang, H., D.W. Young, F. Gusovsky, and J.C. Chow. 2000. Cellular Events Mediated by Lipopolysaccharide-stimulated Toll-like Receptor 4: MD-2 IS REQUIRED FOR ACTIVATION OF MITOGEN-ACTIVATED PROTEIN KINASES AND Elk-1. *Journal of Biological Chemistry*. 275:20861-20866.

Yang, L., H. Sameshima, T. Ikeda, and T. Ikenoue. 2004. Lipopolysaccharide administration enhances hypoxic-ischemic brain damage in newborn rats. *Journal of Obstetrics and Gynaecology Research*. 30:142-147.

Yoo, B.K., J.W. Choi, B.H. Han, W.-K. Kim, H.-C. Kim, and K.H. Ko. 2005. Role of MAPK/ERK1/2 in the glucose deprivation-induced death in immunostimulated astroglia. *Neuroscience Letters*. 376:171-176.

Yoon, B.H., S.H. Yang, J.K. Jun, K.H. Park, C.J. Kim, and R. Romero. 1996. Maternal Blood C-Reactive Protein, White Blood Cell Count, and Temperature in Preterm Labor: A Comparison With Amniotic Fluid White Blood Cell Count. *Obstetrics & Gynecology*. 87.

Zatorre, R.J., R.D. Fields, and H. Johansen-Berg. 2012. Plasticity in gray and white: neuroimaging changes in brain structure during learning. *Nature neuroscience*. 15:528-536.

Zhang, J.-X., Y.-F. Feng, Q. Qi, L. Shen, R. Wang, J.-S. Zhou, H.-Z. Lü, and J.-G. Hu. 2014. JNK Is Necessary for Oligodendrocyte Precursor Cell Proliferation Induced by the Conditioned Medium from B104 Neuroblastoma Cells. *J Mol Neurosci*. 52:269-276.

Zhang, J.-Z., L. Jing, F.-Y. Guo, Y. Ma, and Y.-L. Wang. 2007. Inhibitory effect of ketamine on phosphorylation of the extracellular signal-regulated kinase 1/2 following brain ischemia and reperfusion in rats with hyperglycemia. *Experimental and toxicologic pathology : official journal of the Gesellschaft für Toxikologische Pathologie*. 59:227-235.

Zhang, Q., G. Zhang, F. Meng, and H. Tian. 2003. Biphasic activation of apoptosis signal-regulating kinase 1-stress-activated protein kinase 1-c-Jun N-terminal protein kinase pathway is selectively mediated by Ca2+-permeable alpha-amino-3-hydroxy-5-methyl-4-isoxazolepropionate receptors involving oxidative stress following brain ischemia in rat hippocampus. *Neuroscience Letters*. 337:51-55.

Zhao, Y., and T. Herdegen. 2009. Cerebral ischemia provokes a profound exchange of activated JNK isoforms in brain mitochondria. *Molecular and cellular neurosciences*. 41:186-195.

Zhao, Y., G. Spigolon, C. Bonny, J. Culman, A. Vercelli, and T. Herdegen. 2012. The JNK inhibitor D-JNKI-1 blocks apoptotic JNK signaling in brain mitochondria. *Molecular and Cellular Neuroscience*. 49:300-310.

Zhu, C., X. Wang, F. Xu, B.a. Bahr, M. Shibata, Y. Uchiyama, H. Hagberg, and K. Blomgren. 2005. The influence of age on apoptotic and other mechanisms of cell death after cerebral hypoxia-ischemia. *Cell death and differentiation*. 12:162-176.

Zhuang, Z.-Y., P. Gerner, C.J. Woolf, and R.-R. Ji. 2005. ERK is sequentially activated in neurons, microglia, and astrocytes by spinal nerve ligation and contributes to mechanical allodynia in this neuropathic pain model. *Pain*. 114:149-159.

Zou, J., Y.-W. Pan, Z. Wang, S.-Y. Chang, W. Wang, X. Wang, C. Tournier, D.R. Storm, and Z. Xia. 2012. Targeted Deletion of ERK5 MAP Kinase in the Developing Nervous System Impairs Development of GABAergic Interneurons in the Main Olfactory Bulb and Behavioral Discrimination between Structurally Similar Odorants. *The Journal of Neuroscience*. 32:4118-4132.

Appendix 1

Hypoxia/Ischemia Results in Demyelination of Periventricular White Matter Axons in the Neonatal Mouse Model

Recent studies implicate ERK as a pivotal mediator in axon myelination and Schwann cell development in the neonatal mouse model. Histopathology of the external capsule was studied to examine how myelin is affected by HI injury in our mouse model. Toluidine blue was utilised due to its ability to binds nucleic acid and proteins, allowing cellular structures to be clearly seen in ultrathin tissue sections.

Postnatal day7 C57/Bl6 mice underwent either 30min or 60min HI and allowed to survive to 7days. Croc alone littermates were run alongside HI treated pups as controls. The forebrains were vibrotomed and portions of the external capsule, superior to the ventricles were excised and sliced to four 5µm thick sections per animal. Sections were stained with toluidine blue and optical luminosity used to assess the density of myelinated axons (thickly ringed in dark blue) present.

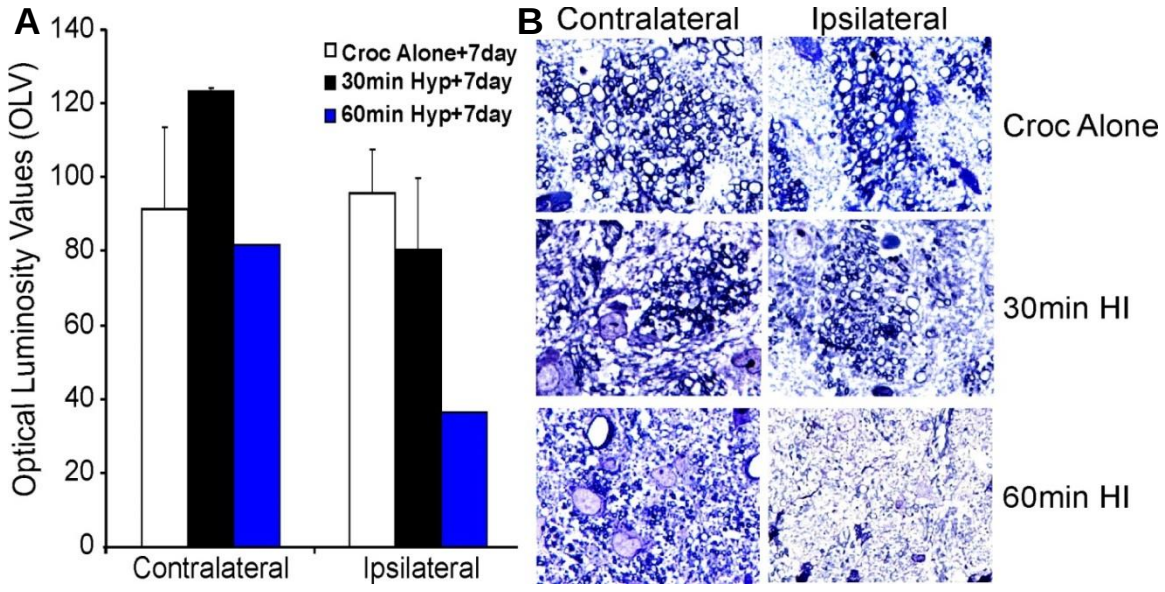

Figure 1 Toluidine-blue histochemistry was used to visualise myelinated axons in periventricular white matter of P7 mice undergoing 30min or 60min HI at 100X magnification. A: Experimental pups were compared to carotid occlusion alone littermates and the density of myelination seen in the ipsilateral hemispheres assessed by optical luminosity (n=7, mean plus SEM over 3 fields). B: Croc alone pups showed no reduction in the number of myelinated axons whereas 30min Hi resulted in a 35% decrease and 60min HI in a 55% decrease compared to the contralateral hemisphere.

30min HI sees a 35% decrease in myelinated axons in the ipsilateral WM (n=2), and a 55% decrease occurs following 60min HI (n=2) compared to contralateral. There is no change in myelination of croc alone littermates.

Appendix 2

Ras overexpression results in increased HI-induced damage whereas MEK1 Dominant Negative reduces it

P7 single allele mutant mice for Ras or for DN MEK1 were subject to 30min HI with a survival time of 48hr. Forebrains were assessed for damage markers including microglial activation (alphaM), Tunel positive cell death, histological tissue loss (cresyl violet/nissl)) and the extent of infarction (nissl).

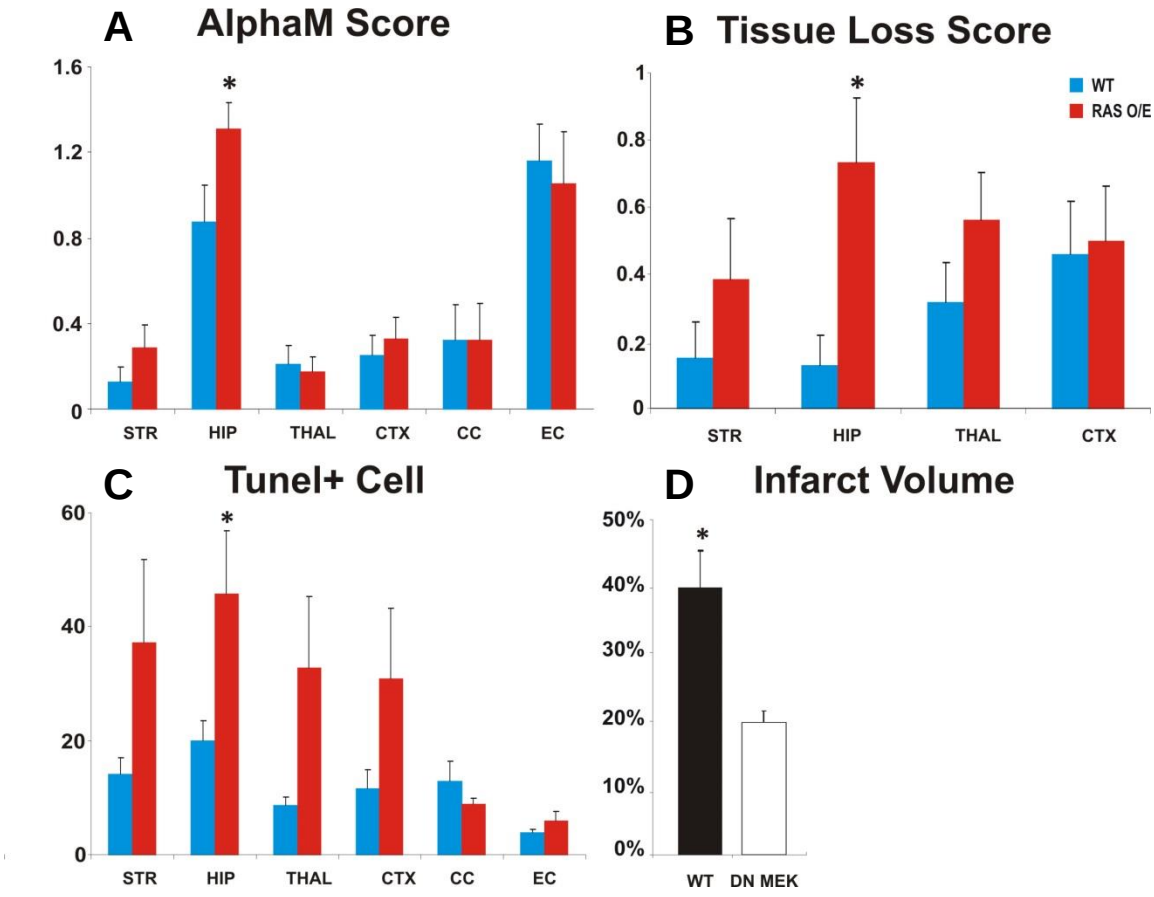

Figure 2 Effects of Ras overexpression and dominant negative Mek1 on damage response following 30min HI. A-C: Ras overexpression resulting in increased microglia activation, histological tissue loss and the number of dying cells within the neonatal mouse forebrain at 48hr post insult. Wildtype littermates were compared as controls. In particular, hippocampus proved highly sensitive to injury. D: Neuronal expression of a dominant negative isoform of MEK1 (MEK1dn) with a neuron-specific tubulin alpha 1 promoter causes considerable reduction in neuronal cell death compared to littermate controls, following severe hypoxic ischemic insult. * P<0.05 by student t-test.

Ras overexpression resulted in a rise in histological tissue loss and Tunel positive dying cells within the ipsilateral grey matter regions of the neonatal mouse brain. In contrast, neuron specific dominant negative isoform of MEK1 gave a reduction in infarct volume but no difference was observed in other damage markers (Not shown).

Appendix 3

Neuronal deletion of CAP23 is protective following severe HI insult to the neonatal mouse brain

Our laboratory has observed CAP23 to be upregulated following HI insult (S. Lange unpublished) suggesting a potential role of this protein in HI brain injury.

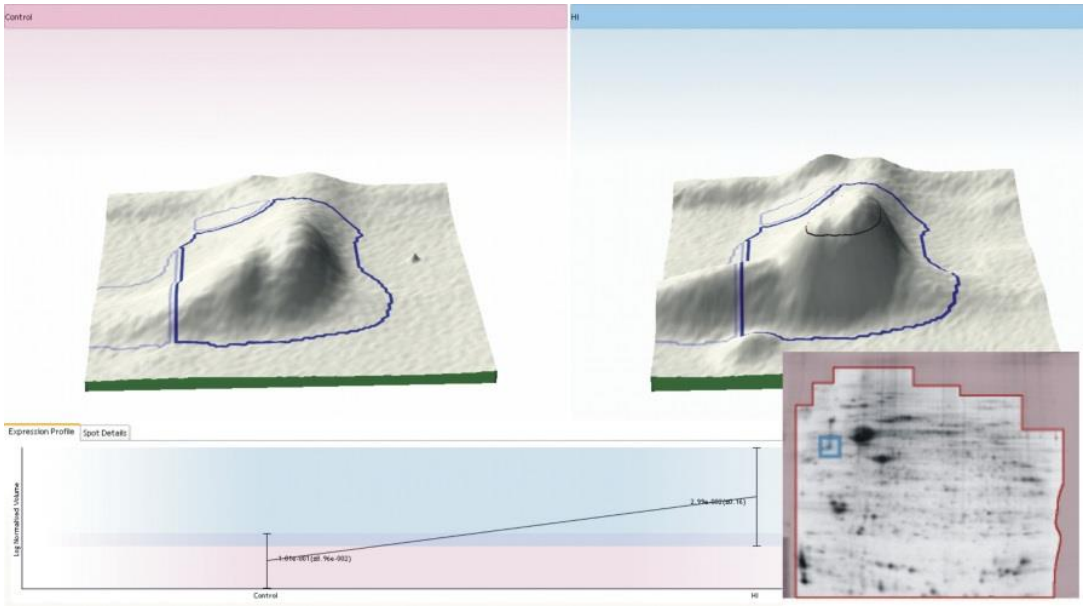

Figure 3 BASP1 up-regulation following hypoxic ischemic insult in the neonatal mouse brain. Images from 2D gel indicating BASP1 up-regulation following 30min HI BASP1 is a 22 kDa neuronal tissue-enriched acidic protein in neuronal axon terminals where it resides at the inner surface of the plasma membrane, predominantly in lipid rafts (S. Lange unpublished).

CAP23, a mouse homologue of BASP1, is widely expressed during development, maintained in selected brain structures in adult, at particularly high levels in the cortex, hippocampus and DRG neurons, and re-induced by nerve injury and during nerve regeneration. CAP23 is a major cytoskeleton-associated and calmodulin (CaM) binding protein belonging to the GMC family which includes GAP43/neuromodulin, Myristoylated Alanine-Rich C Kinase Substrate (MARCKS), and cytoskeleton-associated protein 23 (CAP23). GAP-43 and CAP-23 are among the most abundant proteins in axonal growth cones. In vitro, PC12 cells saw increased neuritogenesis on application of claulansine F, via the upregulation of GAP43/CAP23, which was on par to nerve growth factor stimulation. Neurite outgrown was attenuation, as was GAP43 upregulation, on addition of the MEK inhibitor

PD98059 (Ma et al., 2013). In addition, CAP23 expression is reduced in the absence of neuronal C-Jun (Verhaagen, Mattson and Raivich, unpublished observations). This suggests that both ERK and C-Jun are direct mediators of CAP23 function in neurogenesis. Recent studies identify BASP1, as a pro-apoptotic factor in diabetic neuropathy suggesting this protein acts upstream of caspase activation and mitochondrial injury. Bax antagonist and specific caspase inhibitors prevent its pro-apoptotic effects. Down regulation of the BASP1 did not prevent cytokine-dependent apoptosis (Sanchez-Niño et al., 2010). Lastly, in the adult rat model of stroke, CAP23 is upregulated as a promoter of axonal sprouting near to the infarct region (Carmichael et al., 2005).

Postnatal day 7 mice underwent left side carotid artery occlusion followed by 60min exposure to 8% O_2. They were allowed to recover with dams for 48he at which point they were sacrificed and brains perfused as mentioned in chapter 2. As global knockout of CAP23 mice are born sterile, have pronounced abnormalities at the neuromuscular junction and exhibit high postnatal mortality, the cre recombinase system has been used to generate neuron-specific CAP23 knockout mice.

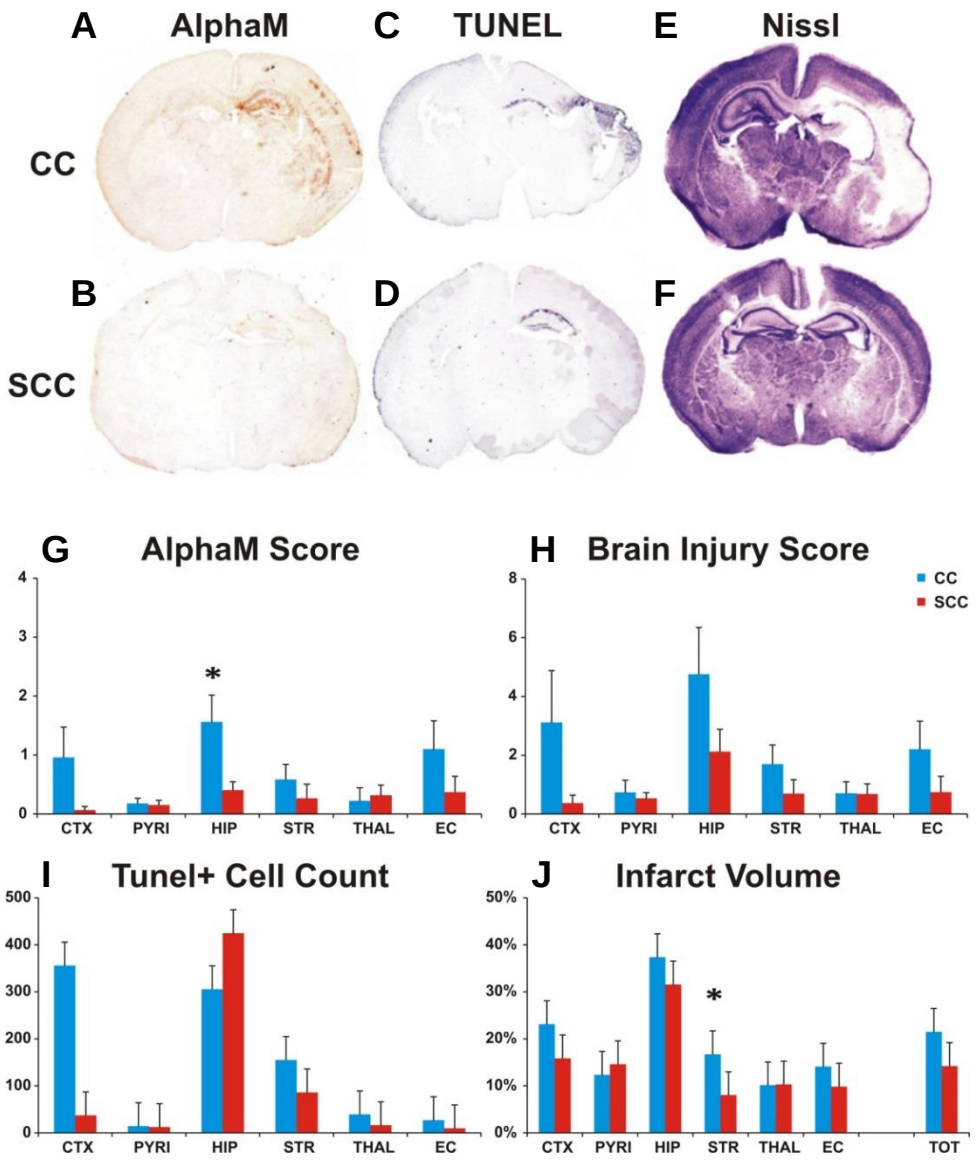

Figure 4 Quantitative analysis of the alpha-M staining of neonate tissue following 60min HI with 48hr survival in CC (CAP23 fl/fl) and SCC (CAP23del). Sections of aM stained neonatal forebrains of CC (A) and SCC (B) animals. Analysis showed a region specific-pattern and degree of microglia activation on the ipsilateral (G) based on a semi-quantitative scoring system (0-4). Microglia activation is decreased across all the 6 forebrain regions, except in thalamus, in the SCC group compare to CC groups. Tunel positive cell death (C-D, I) is decreased in the white matter, striatum, pyriform cortex, cerebral Cortex and thalamus. Hippocampus shows higher levels of Tunel + cells in the SCC group. However, this was insignificantly so. E-F, H: Brain injury score, a combination of activated microglia and histological tissue loss scores, indicate a persistent decrease in injury in all forebrain regions. This was validated by measurement of infarct volume (J) where SCC animals show decrease in white matter, striatum, cortex and hippocampus. Significance occurred in striatum (p=0.0015). The total loss also show lower percentage loss in the SCC group compared to the CC group. *P< 0.05 by student t-test.

Solutions

0.5M Phosphate Buffer (PB)

40ml NaOH, 142g NaH2PO4, made up to 2 litres with double distilled H_2O, pH adjusted to 7.4-7.5 with H_3PO_4.

0.1M PB

200ml 0.5 M PB made up to 1 litre with double distilled H_2O.

10mM PB

50ml 0.1M PB made up to 500ml with double distilled H_2O.

Phosphate buffered saline (PBS)

8.5g NaCl, 20mls 0.5M PB made up to 1 litre with double distilled H_2O, pH adjusted to 7.4 with H_3PO_4.

20% Paraformaldehyde (PFA)

400mg NaOH, 200ml PFA made up to 1 litre with double distilled H_2O, pH adjusted to 7.4 with H3PO4. This was stored at 4ºC.

4% PFA (for perfusion)

200ml 20% PFA, 8.5g NaCl, 20ml 0.5M PB, made up to 1 litre with double distilled

H_2O. This was stored at 4ºC. This was freshly made each time.

4% PFA (for immunohistochemistry and Nissl)

2ml 37% formaldehyde (BDH), made up to 50ml with 0.1M PB

30% Sucrose

30g sucrose (Fluka), 2ml 0.5 M PB made up to 100ml with double distilled H_2O. This was stored at 4ºC. This was freshly made each time.

0.1% Bovine Serum Albumin in PB (PB/BSA)

500mg BSA, made up to 500 ml with 0.1M PB. This was stored at 4ºC.

Cacodylate Buffer

3.64g TRIS in 80ml double distilled H_2O, 29.96g Cacodylate; pH adjusted to 7.5 with

HCl. 0.24g cobalt chloride, pH adjusted to 7.2 with HCl. Made up to 100ml with double distilled H_2O. Stored at 4ºC

TdT solution

1µL TdT (Roche), 1.5µL dUTP-biotinylated (Roche), 100µL cacodylate buffer, 897.5µL double distilled H_2O.

TUNEL stop solution

300mM NaCl (1753.2mg / 100ml double distilled H_2O) 30mM sodium citrate (882.3mg/100ml double distilled H_2O).

Cresyl Violet (BHD)

4g cresyl violet dissolved in 40ml 100% ethanol in a closed 50 ml falcon tube for 15min. Add to 360ml warm double distilled H_2O, and mixed on a warming stirrer plate for 20 minutes. Filter and use.